UNIVERSITY OF SOUTHAMPTON

Faculty of Engineering and Physical Sciences

National Centre for Advanced Tribology (nCATS)

Novel Smart Coatings for Corrosion Protection

by

Anna Crosby

Thesis for the degree of Doctor of Philosophy

June 2021

Academic Thesis: Declaration Of Authorship

I, Anna Frances Rosamond Crosby declare that this thesis and the work presented in it are my own and has been generated by me as the result of my own original research

Novel smart coatings for corrosion protection

I confirm that:

1. This work was done wholly or mainly while in candidature for a research degree at this University;

2. Where any part of this thesis has previously been submitted for a degree or any other qualification at this University or any other institution, this has been clearly stated;

3. Where I have consulted the published work of others, this is always clearly attributed;

4. Where I have quoted from the work of others, the source is always given. With the exception of such quotations, this thesis is entirely my own work;

5. I have acknowledged all main sources of help;

6. Where the thesis is based on work done by myself jointly with others, I have made clear exactly what was done by others and what I have contributed myself;

7. None of this work has been published before submission.

UNIVERSITY OF SOUTHAMPTON

ABSTRACT

FACULTY OF ENGINEERING AND THE ENVIRONMENT

Thesis for the degree of Doctor of Philosophy

NOVEL SMART COATINGS FOR CORROSION PROTECTION

Anna Frances Rosamond Crosby

There is a desire in defence departments throughout the world to decrease the costs associated with corrosion ($2.3 billion in the US alone in 2012-2013) especially in the naval sectors. Using smart coatings that are able to self-heal autonomously is one way of reducing costs. Self-healing capabilities can be induced through the incorporation of healing agents that have been encapsulated in microcapsules which rupture when the coating is damaged, releasing the healing agent and healing the damage to the polymer. If a porous network can be incorporated into the coating then better dispersion of microcapsules can take place.

Polydopamine (PoDA) was identified as a potential coating as a result of its facile auto-oxidative deposition and novelty. PoDA films are highly adherent, can be deposited onto a multitude of substrates and have been used for applications as diverse as DNA patterning and surface functionalization for the production of self-assembled monolayers.

The PoDA coatings were deposited onto structural steel from an alkaline buffered phosphate buffer solution and their corrosion performance after immersion in 3.5% NaCl solution was analysed using electrochemical impedance spectroscopy. The results are presented in the form of Nyquist and Bode plots. The deposition and polymerisation parameters such as temperature, monomer concentration and molar ratio of oxidant to dopamine were examined and optimised. Once the best combination of deposition parameters had been identified the resultant coating was subjected to further testing including X-Ray Photoelectron Spectroscopy and Scanning Kelvin Probe in order to better understand its properties and corrosion protection mechanism.

The EIS results showed that a 0.5:1 molar ratio of *p*-benzoquinone (*p*-BQ) : dopamine monomer with a 2 mg mL^{-1} dopamine monomer concentration and a deposition temperature of 25°C

produced the coating that offered the best protection against corrosion. In addition, when the coating was purposefully damaged, EIS testing showed the presence of an adsorption process and maintained corrosion protection for the *p*-BQ oxidized PoDA coating when compared to the autoxidated coating meaning the presence of *p*-BQ offers some intrinsic protection against corrosion. XPS demonstrated differences in composition between the autoxidated and *p*-BQ oxidized PoDA coatings and indicted that *p*-BQ acts as a more efficient oxidant than atmospheric oxygen. However, the similarities in functional groups between autoxidated and *p*-BQ oxidized PoDA mean that it is not possible to determine what the fate of *p*-BQ oxidant is and so further analysis is required. SKP results revealed that the protection mechanism was found to be different to that of established conducting polymers such as PANi. Overall the results indicate that *p*-BQ itself is acting as a corrosion inhibitor. However the coatings were too thin, even after optimisation of the deposition conditions and so polyaniline deposited from an oxalic acid solution of aniline monomer was identified as a suitable alternative.

A cubic liquid crystal template was developed following examination of mesophases by polarised light microscopy and viscosity measurements. The mesophase was formed from a 50/50 wt% mix of Brij S100 and this was used as the basis of the templating of polyaniline. The presence of the template changed the requirements for the deposition of polyaniline, primarily because the oxidation of aniline monomer is a diffusion controlled reaction. Experiments were undertaken to determine optimum conditions for the deposition of PANi.

Aniline monomer was encapsulated into polydopamine capsules using a procedure published by Cui et al [1] . The filled capsules were then incorporated into the templated polyaniline coating and an epoxy topcoat was applied. The self-healing capabilities of the coating system were evaluated by deliberately inducing a defect into the coating using a scalpel blade. The corrosion behaviour of the coating system in 3.5% NaCl was evaluated using EIS and the coating was found to self-heal. The results of this project represent the formation of a novel-self healing coating which protects steel against corrosion in seawater.

Table of Contents

Table of Tables

Table of Figures

Table of Figures

Acknowledgements

I would like to thank Dr Julian Wharton and Keith Stokes for help and guidance on the experimental aspects of the project and advising how to proceed when some stages of the project were unsuccessful.

Thanks to Dr Mengyan Nie for his help in familiarising me with EIS and polydopamine at the beginning of the project.

Dr Steve Hinder at the University of Surrey's surface analysis lab provided invaluable help with both the obtaining and analysis of XPS spectra.

Many thanks to Dr Andrej Nazarov at the Institut de la Corrosion in Brest for his assistance in conducting the scanning kelvin probe experiments. Thanks also to Dominique Thierry and Nathalie Lebozec for hosting me at the institute and for useful discussion during the CCNS meetings.

Thank you to Jacquie Crosby (Mum) for proofreading and editorial help. I am extremely grateful to both her and my Dad for all their love and support over the years. Dad, will you now accept that I might be a scientist rather than a historian?

Special thanks to Simon Watson for all his time spent accompanying me in the chemistry lab; most of the practical work could not have been done without you agreeing to sit with me.

Thank you to the various residents of 53 Avenue Road (Maria (hugger extraordinaire), Gregor, Tim, Stephen and Pawee) for making my time in Southampton happy and full of laughter as well as the odd whiskey!

Finally thank you to Sean. For everything.

Definitions and Abbreviations

Acronyms

2D 2-Dimensional

3D 3-Dimensional

AC Alternating Current

AFM Atomic Force Microscopy

AP Ammonium Persulfate

BTs Ballast Tanks

CP Cathodic Protection

CPE Constant Phase Element

CPs Conducting Polymers

CSA Chemical Shift Anisotropy

CV Cyclic Voltammetry

DA Dopamine

DC Direct Current

DHI 5,6-dihydroxyindole

D-M Dopamine-Melanin

EDA European Defence Agency

EIS Electrochemical Impedance Spectroscopy

ES-HRMS ElectronSpray Ionisation High Resolution Mass Spectroscopy

EVA Ethylene Vinyl Acetate

FT-IT Fourier Transform Infra Red

HF Hydrogen Fluoride

HPLC-MS High Performance Liquid Chromatography Mass Spectrometry

IDQ 5,6-Indolequinone

ITO Indium Tin Oxide

IUPAC International Union of Pure and Applied Chemistry

LCs Liquid Crystals

L-DOPA L-3,4-dihydroxyphenylalanine

L-MM Levenberg-Marquardt Method

MAS Magic Angle Spinning

MCM Mobil Crystalline Material

MEFP5 Mytilis Edulis Foot Protein 5

MIC Microbiologically Induced Corrosion

MS Mass Spectrometry

MW Molecular Weight

Ni-Cr Nickel-Chrome

NMR Nuclear Magnetic Resonance

PANi Polyaniline

PAQ Poly(aminoquinones)

PEDOT Polyethylenedioxythiophene

PoDA Polydopamine

PPy Polypyrrole

PXRD Powder X-Ray Diffraction

QCM Quartz Crystal Microbalance

RH Relative Humidity

ROMP Ring Opening Metathesis Polymerisation

SBR Styrene-Butadiene Rubber

SCE Standard Calomel Electrode

SEM Scanning Electron Microscopy

SKP Scanning Kelvin Probe

SKPFM Scanning Kelvin Probe Force Microscopy

SOB Sulphur Oxidising Bacteria

SRB Sulphate Reducing Bacteria

TEM Tunnelling Electron Microscopy

TOF-SIMS Time of Flight-Secondary Ion Mass Sprectroscopy

TRIS TRis(hydroxymethyl)aminomethane

Definitions and Abbreviations

UV-Vis Ultra Violet-Visible

WI Warburg Impedance

XPS X-Ray Photoelectron Spectroscopy

Nomenclature

°C Temperature in degrees centigrade (relative to 273.15 K)

A Amperes (unit of measurement for electric current)

Å Angstrom (10^{-10} m)

B_0 Applied magnetic field

C Initial dopamine concentration in mg mL^{-1}

C Capacitor, value measured in Farads

[C_{AO}] Dopamine concentration

C1s Electron extended from the 1s orbital of a carbon atom

d Film thickness

d_{max} Maximal film thickness

E Potential in volts

f Applied frequency

Fe2p Electron extended from the 2p orbital of an iron atom

g 100 mL^{-1} Grams of solute per 100 mL of solvent

g L^{-1} 1 gram of solute dissolved in a litre of solvent

h hour (3600 seconds)

HO Hydroxy

Hz Hertz (unit of frequency) (s^{-1} in SI units)

I Current in Amperes

I_1+I_2 Cubic liquid crystal phase

$j = \sqrt{-1}$

k Consumption rate constant

K^{obs} Observed rate constant

L_1+L_2 Micellar liquid crystal phase

Lα Lamellar liquid crystal phase

M Moles of substance in 1L of solution

mg mL^{-1} Milligrams of solute per mL of solvent

min. Minute (6- seconds

mM millimolar

mVs^{-1} Millivolts per second

N1s Electron extracted from the 1s orbital of a nitrogen atom

Na1s Electron extracted from the 1s orbital of a sodium atom

nm nanometres (10^{-9} m)

O1s Electron extracted from the 1s orbital of an oxygen atom

Definitions and Abbreviations

R Resistance in ohms ($kg.m^2.S^3.A^{-2}$)

rA Rate of dopamine consumption

R_p Polarisation resistance in ohms

R_u Uncompensated (solution resistance) in ohms

s seconds (SI unit of time)

T_g Glass transition temperature

V Volts ($kg.m^2.S^{-3}.A^{-1}$) measure of electric potential

V_1+V_2 Cubic liquid crystal phases

V_m Rate of deposition

Vs^{-1} Volts per second

wt./wt. weight by weight proportion of substance in mixture by mass

Y' Real admittance

Y'' Imaginary admittance

Y_o CPE Value

|Z| Modulus impedance

Z Impedance in ohms cm^2

Z_{imag} or Z'' Imaginary impedance

Z_o Initial impedance

Z_{real} or Z' Real impedance

Greek Nomenclature

α	measure of the extent to which a CPE behaves like a capacitor
α_1	order of reaction
α_2	constant
β	Magic angle (54.74°)
Γ	Mass of deposited polymer per unit area
θ_m	Angle between applied magnetic field and principle z-axis of tensor
θ	phase shift
θ_a	Angle between applied field and spinning axis
μL	microlitre (10^{-6} L)
μm	micrometre (10^{-6} m)
ρ	polymer density
χ^2	goodness of fit between real impedance data and the proposed equivalent circuit model
ω	$2\pi f$ in radians s^{-1}
Ω	ohms (measure of resistance)

Chapter 1 Project Background

1.1 CCNS

"*Novel smart coatings for the corrosion protection of critical marine structures"* forms the novel aspect of the European Defence Agency (EDA) project "*Corrosion Control for Naval Ships"*. The project aims to develop strategies to extend repair intervals for naval ships in order to reduce maintenance costs and improve ship security by exploiting new and emerging technologies. Three main areas of corrosion protection are being focussed on; corrosion and fouling in seawater pipe systems, optimisation of cathodic protection and improving performance of protective coatings.

The aim of the PhD was to produce a novel-anti corrosion coating that is also self-healing and conductive and possesses sensing abilities. It was hoped that polydopamine (PoDA) be a suitable candidate for the conducting polymeric coating. Previous research at the University of Southampton, funded by the Centre for Defence Technology and Enterprise and conducted by Dr Mengyan Nie [2] had indicated that PoDA had the potential to be both conducting and self-healing. However, due to the highly experimental nature of PoDA as a coating, other conducting polymeric systems, such as polyaniline (PANi) have had to be considered as well.

1.2 Aims and objectives

The aim of the PhD is to produce a self-healing coating that offers protection against corrosion. Ideally, the coating should also be conducting so it can be incorporated into an electric circuit. The self-healing capabilities of the coating should be provided by healing agents that have been encapsulated and the capsules themselves will be contained in a 3- dimensional (3-D) porous network that has been incorporated into the deposited polymer using some form of template.

1.3 Thesis outline

This thesis first comprises a literature review of the current state of research into polydopamine and polyaniline coatings as corrosion protection mechanisms as well as the strategies currently used for their deposition. Templated and self-healing coatings are also reviewed. The techniques used to evaluate the coatings developed during this work are discussed along with the methods used for the deposition of the coatings. The experiments conducted are described; results are then presented and

discussed and conclusions drawn. Finally, work which can be conducted to further the project is detailed.

Chapter 2 Corrosion

As has been previously stated, the overall aim of this project is to produce a smart coating that is capable of self-healing and can be applied to “critical marine structures”. This introduction seeks to define the critical marine structures under investigation and the problems associated with their use.

Ballast tanks (BTs) are an essential feature of any vessel and in larger naval vessels are used to control the stability of the ship and to correct its trim (how high the ship sits in the water). For the larger classes of naval vessels ballast tanks can hold upwards of 100,000 m^3 of liquid ballast and have surface areas of over 1,000,000 m^2 [3]. This gives a huge area for corrosive environments to act on. Although ballast tanks are of high importance, their awkward geometries and hard to access locations mean they are often neglected and not always inspected as thoroughly as they might be. In addition, the large surface areas of ballast tanks mean that replacement of coating systems is extremely costly which can lead to a reluctance by ship owners to undertake necessary maintenance. The combination of these factors can have catastrophic consequences for the structural integrity of ship. The bulk crude carrier MV Erika sank off the coast of Brittany in 1999 spilling most of her cargo of 31,000 tonnes of heavy fuel oil into the North Atlantic, resulting in an environmental disaster. The subsequent investigation ruled that the primary cause of the Erika’s sinking was improper maintenance of her ballast tanks; coatings had not been replaced and large cracks had appeared in the tanks [4]. Poor weather conditions resulted in additional stresses being placed on the ballast tanks which made cracks even larger, weakening the internal structure of the tanker and ultimately causing her to break in two. In general, in order to keep building costs down, BTs are constructed from low carbon steels which are considerably more likely to corrode than stainless steels due to the absence of elements, such as chromium, that are capable of forming adherent protective oxide layers. The importance of ballast tanks in the function of a ship means they can be classed as a critical marine structure. In addition, the fact that they can be neglected in terms of inspection and maintenance means they are the perfect environment for a self-healing coating which reduces the need for inspection and lengthens the time periods required between coating maintenance.

2.1 Corrosion theory

Corrosion can be broadly defined as the attack of a metal by its surrounding environment. As discussed above, the coatings investigated here are intended for use in ballast tanks made from low

carbon steel and therefore, the focus will be on the corrosion of iron and steel in a near neutral aqueous environment (seawater).

How full or empty a ballast tank is depends on the cargo loading. A ship fully loaded with cargo will have empty ballast tanks whilst one which has no cargo load will have full ballast tanks. Even when the tanks are ostensibly empty of seawater ballast, the atmosphere within the tanks will be humid and it is highly likely that thin films of electrolyte will adhere to the surfaces of the tanks, making atmospheric corrosion a likely problem.

The corrosion of metal is an electrochemical process and requires five components to be present in order to occur: an anode, a cathode, an electrical contact between the anode and cathode, a solution capable of conducting ions, and one or more reactive species.

The surface of a piece of metal exists as a series of localised anodes and cathodes. This occurs because there are free electrons present in the metal which are capable of movement and this leaves behind metal cations which form localised, positively charged cathodes. There will also be areas of higher electron density which are negatively charged local anodes. The ability of the electrons to move within the metal proves an inherent electrical contact between the anodes and cathodes. Without any moisture present, the metal could exist in this state indefinitely with the relative locations of the anodes and cathodes altering with the movement of the free electrons.

However, the presence of an electrolyte, and reactants contained within, allows the formation of a localised galvanic corrosion cell. The overall corrosion reaction has two half reactions; a reduction reaction which occurs at the cathode and an oxidation reaction which takes place at the anode.

The anodic reaction for iron and steel is shown in Equation 2.1 and results in the dissolution of the iron into solution.

$$Fe_{(s)} \rightarrow Fe^{2+}{}_{(aq)} + 2e^- \qquad \text{Eq. 2.1}$$

The cathodic reaction consumes the electrons produced in the anodic reaction and the exact reaction that takes place is dependent on the nature of the electrolyte as shown by Equations 2.2, 2.3 and 2.4 below:

$$2H^+{}_{(aq)} + 2e^- \rightarrow H_{2(aq)} \qquad \text{Eq. 2.2}$$

$$O_{2(aq)} + 4H^+{}_{(aq)} + 4e^- \rightarrow 2H_2O_{(l)} \qquad \text{Eq. 2.3}$$

$$2H_2O_{(l)} + O_{2(aq)} + 4e^- \rightarrow 4OH^-{}_{(aq)} \qquad \text{Eq. 2.4}$$

The reaction defined in Equation 2.2 occurs in acidic solutions where there is little oxygen present and is known as the hydrogen evolution reaction. If oxygen is present then the reaction in equation 2.3 will take place. In near-neutral and alkaline solutions, the reaction of Equation 2.4 will occur. In seawater, the third reaction, termed the oxygen reduction reaction, is the most likely to occur.

2.1.1 Thermodynamics of corrosion

The likelihood of a given metal to corrode is dependent on the change in Gibbs free energy (ΔG) for the corrosion reaction. The more negative the value of ΔG, then more likely the reaction is to happen. A positive ΔG value indicates that corrosion will not spontaneously occur. For example, the value of ΔG for the corrosion of gold is +65,700 J. This supports the observation that gold does not spontaneously corrode when placed in water.

As corrosion reactions are electrochemical in nature, the Gibbs free energy can be related to the electromotive force, also known as the cell potential, of the corrosion cell by Equation 2.5.

$$\Delta G = -nFE \qquad \text{Eq. 2.5}$$

Here n is the number of moles of electrons, F is the Faraday constant (96485 C mol^{-1}) and E is the cell potential.

When all products and reactants are in their standard states, the following equation can be used.

$$\Delta G^{\circ} = -nFE^{\circ} \qquad \text{Eq. 2.6}$$

Thus, if the electrochemical potential of the cell is known, the Gibbs free energy may be calculated.

2.1.2 Pourbaix diagrams

Pourbaix diagrams, named after their creator, Marcel Pourbaix present thermodynamic data in the form of potential vs pH plots [5]. They show at what potentials and pHs a specific metal will adopt a passivated state, an immune state or an actively corroding state. The Pourbaix diagram for iron in water at 25°C is presented in Figure 2.1 below.

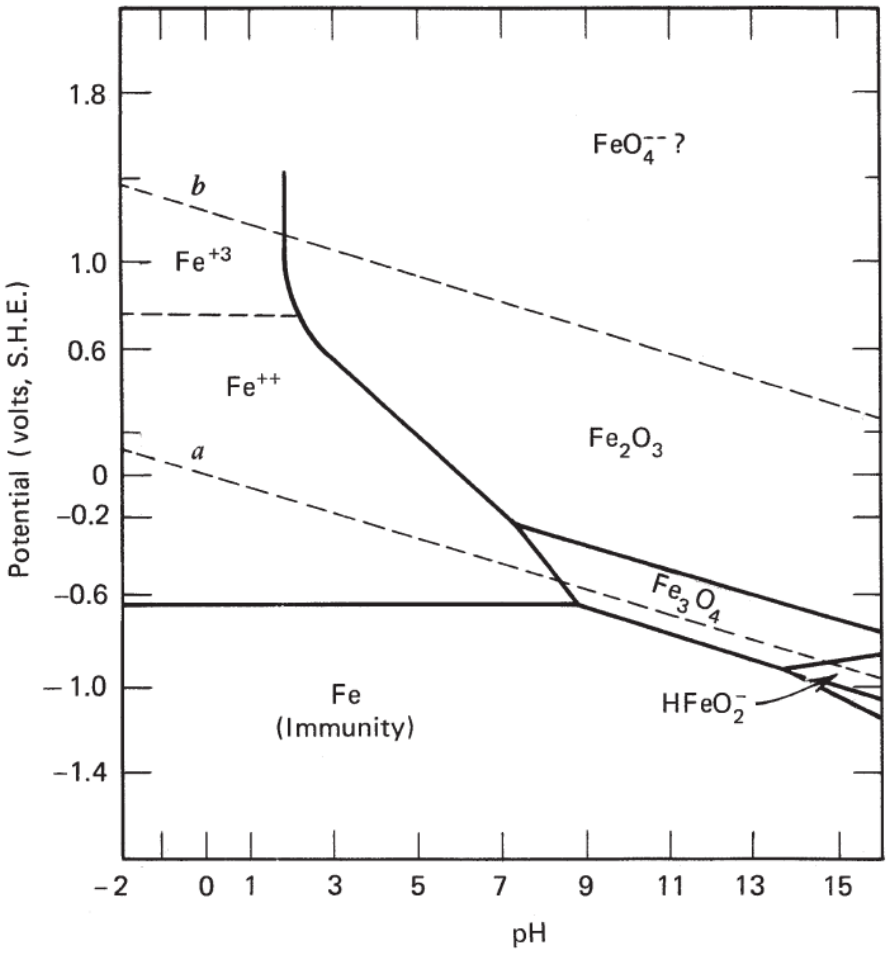

Figure 2.1 Pourbaix diagram for iron in water at 25°C [6]

Horizontal lines represent reactions that do not involve pH affecting species such as OH^- and H^+. The horizontal line at -0.617 V, represents the potential of $Fe^{2+} + 2e^- \rightarrow Fe$. Below the line, elemental iron is stable and is considered to be in an immune state.

Vertical lines represent processes that involve species that affect pH but are not dependent on electrons. The vertical line at pH 1.76 represents the reaction $2Fe^{3+} + 3H_2O \rightarrow Fe_2O_3 + 6H^+$. To the right of the vertical line Fe_2O_3 is the stable species and will offer some protection against corrosion in the form a surface oxide film. To the left of the vertical line, corrosion of the iron will occur as there is no surface oxide film and Fe^{3+} is stable in solution.

Sloping lines represent reactions which involve both pH affecting species and electrons such as $Fe_2O_3 + 6H^+ + 2e^- \rightarrow 2Fe^{2+} + 3H_2O$. To the right of the sloped line, Fe_2O_3 is stable and present as a surface oxide film. To the left, Fe^2 is stable in solution and iron will undergo corrosion.

When they are present, surface oxide films are presumed to offer protection to the underlying elemental iron and so these regions of the Pourbaix diagram are often referred to as passive regions.

2.1.3 Methods of preventing corrosion

There are many methods which can be employed to prevent corrosion from occurring. Cathodic protection relies on forcing the metal requiring protection to become the cathode rather than the anode. There are two main forms of cathodic protection, sacrificial protection and impressed current cathodic protection (ICCP). In ballast tanks, it is common to employ the use of sacrificial anodes. Here, large pieces of zinc are attached to the surface of the tanks. Because the Gibb's free energy of the corrosion of zinc is more negative than that of the corrosion of iron, the zinc will act as the anode rather than the steel ballast tank. ICCP uses an external current and an inert non-metallic anode, such as graphite. The application of the current polarises the metal to be protected and forces it to become the cathode. Both methods of cathodic protection require maintenance and can be expensive.

Coatings may also be employed as means of corrosion prevention. Although some inorganic coatings, such as oxide layers and enamels, can be used, they are rarely used in a marine context. This is especially true of steel and iron in a marine environment because the iron oxides are too friable to offer any protection and the enamel coatings are liable to undergo mechanical damage. Therefore, organic coatings are more commonly used in a marine context.

The primary function of most organic coatings is to act as a barrier against electrolyte and cathodic reactants. This minimises the cathodic reaction which, in turn, prevents the anodic reaction, namely the dissolution of metal. For some coatings, such as the coal-tar and epoxy coatings often used in ballast tanks, the barrier protection is the only form of protection offered. The coal tar coatings may be applied with a thickness of mm rather than μm. Such coatings are used because the tanks are exposed to both immersion and atmospheric corrosion.

Pigments which inhibit corrosion may also be included in the coatings. Such pigments, which include chromates and molybdates, are solubilised as the electrolyte penetrates the coating. Their subsequent transfer to the metal surface allows them to passivate the metal surface and prevent corrosion. However, chromates are highly toxic and their use is being phased out. Indeed, this project came about because of the European Defence Agency's desire to find alternatives to chromate-containing coatings.

Another type of active coating which has seen interest in recent years is the conductive polymers. These include polythiophene, polypyrrole and polyaniline. The mechanism by which these polymers protect against corrosion is discussed in further detail in section 3.2, but it is thought that they protect by passivating the surface of the metal because the polymers are capable of cycling between a reduced and oxidised state which allows the surface of the metal to be oxidised [7].

2.1.4 Coating failure mechanisms

All coatings, regardless of their type, will provide protection to a metal substrate by acting as a barrier. The presence of the coating prevents electrolyte, and cathodic reactants which may be present in the electrolyte, from coming into contact with the metal surface. In an ideal world, the applied coatings would remain intact and impervious to electrolyte but this is rarely the case in real life. Coatings may have defects which arise as a result of poor application or defects may occur as a result of external damage to the coating. Even coatings which do not have any visible damage may still be sufficiently porous to allow the diffusion of electrolyte and oxygen through the coating and eventual contact with the underlying metal substrate. For some coatings, the presence of water alone is sufficient to disrupt the bonding between organic coatings and substrates, leading to the delamination of the coating. In other instances, the delamination of a coating can be initiated and/or increased by the electrochemical cathodic and anodic corrosion reactions and these instances are discussed below.

2.1.4.1 Osmotic blisters

Coatings with defects can act as semi-permeable membranes; this allows electrolyte to permeate through the coating. The presence of water soluble salts, either in the electrolyte or in the coating, can contribute to the rate of coating failure. If a small amount of electrolyte permeates through the coating, the salt concentration of the electrolyte behind or underneath the coating may become greater than the salt concentration of the surrounding electrolyte. When this is the case, an osmotic cell forms. Because of this osmotic cell, more bulk electrolyte from outside the coating is forced into the coating to balance the ion concentrations. This causes liquid-filled blisters to form in the coating. These are termed osmotic blisters.

2.1.4.2 Cathodic delamination

If a defect is present in an organic coating, the electrolyte will be present at the metal/coating interface and this allows a localised corrosion cell to form and oxygen can readily diffuse through the electrolyte to the metal substrate. The resulting cathodic reaction can lead to the delamination of the coating in a process that is usually referred to as cathodic delamination/disbondment. As shown in Equation 2.4 above, the cathodic reaction in near-neutral aqueous solutions, results in the

formation of hydroxyl ions (OH^-). This increases the pH at the area surrounding the defect at the interface between coating and metal substrate and the increased alkalinity degrades the bonds between coating and metal and leads to the delamination of the coating. The exposed metal acts as the anode and, as shown on Equation 2.1 above, the dissolution of the metal occurs and electrons are produced. These electrons feed the cathodic reaction which leads to further delamination.

2.1.4.3 Filiform corrosion

If there is a high level of humidity in the atmosphere and oxygen is present the process of filiform corrosion can occur. This is a form of coating delamination which is driven by the anodic reaction. Filiform corrosion exists in the form of filamentous tracks which consist of a mobile head, filled with electrolyte that contains metal cations and attacking anions, such as chloride; and a tail formed from dry corrosion products.

If the atmosphere is sufficiently humid, as is always the case in a ballast tank, a thin film of electrolyte, such as seawater, will adhere to the organic coating. The presence of a defect in the coating mean the thin electrolyte layer will also adhere to the underlying steel substrate. In seawater, the electrolyte will contain water, oxygen and chloride ions. The initial stage of filiform corrosion is shown in Figure 2.2 below.

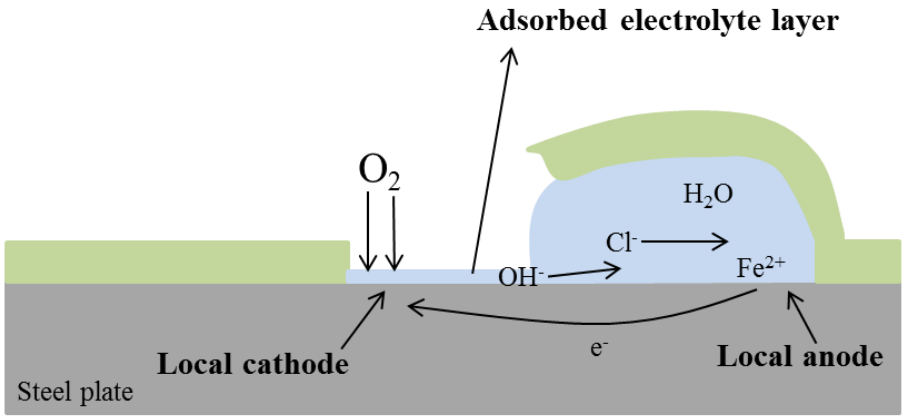

Figure 2.2 Initial stage of filiform corrosion

The presence of the thin film leads to the formation of a differential aeration cell. The thinness of the electrolyte film means that atmospheric oxygen can diffuse far more readily through the electrolyte than it can through the surrounding organic coating. As a result, the preference is for the cathodic oxygen reduction to occur at the defect site on the exposed metal rather than under the coating. The area under the intact coating surrounding the coating is then oxygen deficient relative

to the defect site and so the area under the coating becomes the local anode. The chloride anions present in seawater are drawn to the anodic region and this leads to a corrosion gradient. The electrolyte present at the cathodic region is then drawn forward by osmosis.

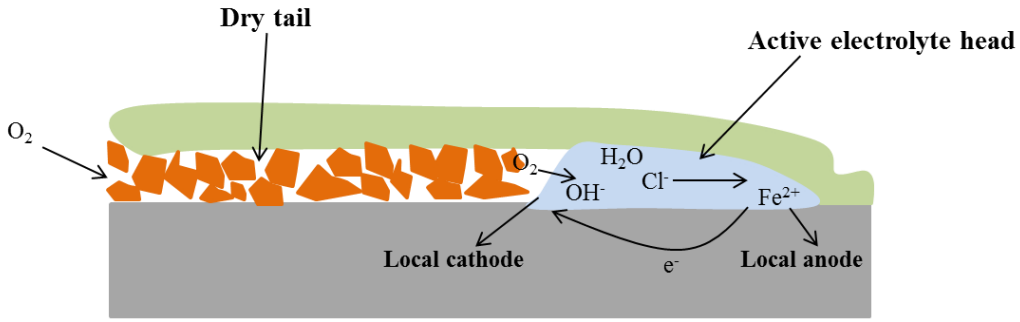

Figure 2.3 - Later stage of filiform corrosion

As shown in Figure 2.3 above, the movement of the electrolyte to the head of the filament leaves behind a dry tail which allows oxygen to readily reach the back of the filament head. The cathodic reaction therefore takes place at the back of the head and the anodic reaction takes place at the front, closest to the intact coating. The metal cations produced during the anodic reaction migrate to the cathodic region where they combine with the hydroxyl ion products of the cathodic reaction to form insoluble corrosion products and the resultant filament tail. The reactions between the anodic reaction products and species present in the electrolyte in an oxygen deficient atmosphere can lead to the formation of acids which lowers the pH of the head of the filament which can destabilise the bonds between coating and substrate.

2.1.5 Microbially induced corrosion in ballast tanks

As well as containing NaCl at an approximate concentration of 3.5%, seawater also contains microorganisms and organic matter. The presence of these microorganisms can result in Microbiologically Induced Corrosion (MIC). MIC is not a specific type of corrosion instead it is the term used to refer to the collection of microorganisms and their activities which result in the inducement of localised corrosion.

When microorganisms come into contact with the metal surface of the ballast tanks they can form biofilms through the adsorption of the macromolecules. Once microorganisms have attached to the metal substrates, they release adhesive substances known as extracellular polymeric substrates (EPS) which allow film formation. These biofilms often have irregular coverage of the metal substrate which can lead to the formation of concentration cells; the area underneath the biofilm becomes a localised anode and the surrounding area becomes a cathode which can result in the initiation of localised corrosion such as pitting [8]. Localised corrosion can be much more severe in terms of material loss than uniform corrosion. If the ballast tanks are not inspected then the pits can

be left to develop further. The action of sea water in ballast tanks sloshing around during sea voyages puts the tanks under further stresses and strains which can cause the pits to develop into large cracks.

In addition to the formation of biofilms, bacteria and microorganisms are capable of accelerating the rates of the partial corrosion reactions or alter the corrosion mechanism. Sulphate reducing bacteria (SRB) reduce the elemental sulphur present in mild steels which results in the formation of hydrogen sulphide (H_2S). The production of H_2S catalyses the penetration of hydrogen into the steel which, in turn, induces cracking of the steel. If the respiration rate of the SRB is greater than the rate of diffusion into the corrosive solution, then the area becomes anaerobic allowing the proliferation of sulphide production [9]. In the case of iron, H_2S accelerates corrosion through the formation of iron sulphide materials [10]. If both SRB and Sulphur oxidising bacteria (SOB) are present, the SOB can oxidise H_2 S to sulphuric acid making the corrosive environment even more aggressive and increasing the rate of corrosion.

The initiation of corrosion is further affected by the way ballast tanks are constructed. In order to prevent against crevice corrosion, BTs are constructed by welding, rather than bolting, sheets of steel plate [11]. Welding can alter the microstructure of the steel resulting in a greater susceptibility to corrosion than un-welded material. These weld zones are particularly susceptible to microbiologically induced corrosion as the roughness and changes in microstructure provide the ideal environment for the adherence of biofilms [12].

However, the coatings themselves can often be affected by the metabolic products of certain bacteria especially if the products are acidic in nature and this process can occur in periods as short as 60 days [13]. In addition, bacteria have been shown to be attracted to defects within the coating [14].

Chapter 3 Literature

3.1 Polydopamine

The vast majority of reported polydopamine (PoDA) research has been undertaken using chemical deposition methods. Conversely, there have only been three papers published [15-17] that relate to the electrochemical deposition of PoDA on substrates such as either gold [15, 17] or amorphous carbon [16]. This can be considered advantageous in that achieving electrochemical deposition would be novel, especially on a more active substrate such as steel. However, there is also the possibility that there has been little published work because prior attempts have been unsuccessful.

3.1.1 The catecholamines

Dopamine (DA), as shown in Figure 3.1, is a neurotransmitter that belongs to the catecholamine family of compounds which also includes noradrenaline (Figure 3.2) and L-DOPA (Figure 3.3). Within all these figures, the catechol moiety is highlighted in red and the amine in blue.

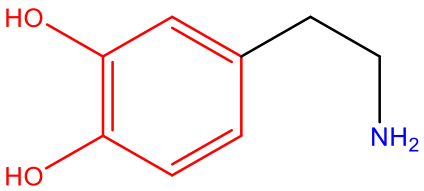

Dopamine

4-(2-aminoethyl)benzene-1,2-diol

Figure 3.1 - Dopamine chemical structure

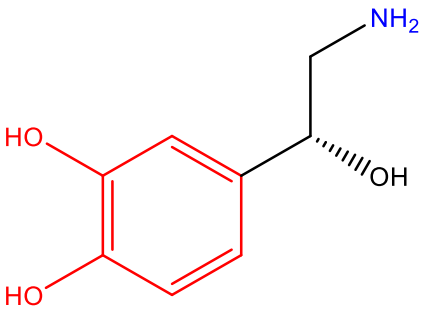

Norepinephrine

4-[(1R)-2-amino-1-hydroxyethyl]benzene-1,2-diol

Figure 3.2- Noradrenaline (norepinephrine) chemical structure

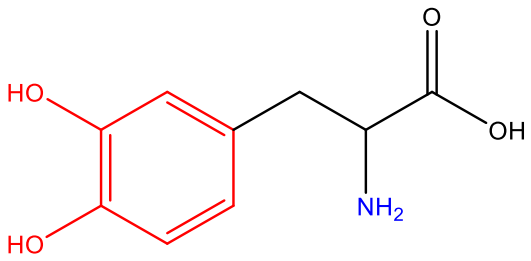

L-DOPA

L-3,4-dihydroxyphenylalanamine

Figure 3.3-L-DOPA chemical structure

All three molecules are interlinked from a biochemical perspective, since L-DOPA is the precursor to dopamine (DA) [18] which is itself the precursor to noradrenaline [19]. Both L-DOPA and noradrenaline are known to form melanins; biological pigments present in most animals and responsible for things such as skin pigmentation and hair colour. This, along with the similarities in structure to DA, has led to the proposition that PoDA may adopt a melanin-like structure. The increased interest in dopamine came about as a result of its similarity to L-DOPA. L-DOPA constitutes approximately 40% of the proteins that mussels use to adhere to rocks (Figure 3.4) [20].

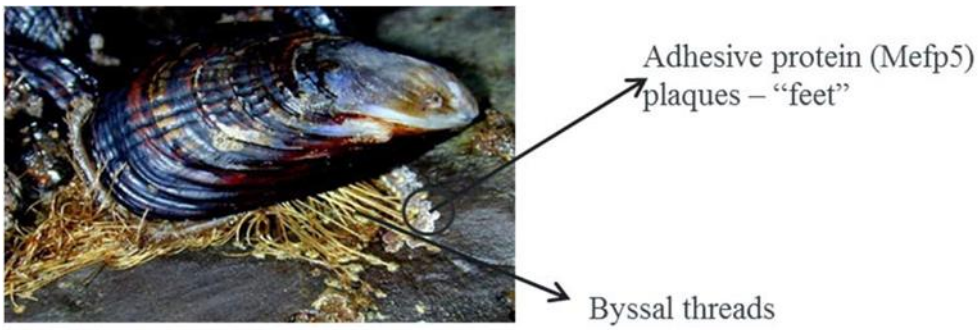

Figure 3.4– Mussel adhering to rocks using byssal threads and adhesive foot plaques [21]

Mussels have been shown to be able to adhere to many surfaces, including Teflon (Figure 3.5) and so it was proposed that a coating produced from dopamine (as an analogue for L-DOPA) would have excellent adhesive properties [22].

Figure 3.5–Mussel adhering to a sheet of Teflon (PTFE) [23]

The combination of catechol and amine groups seems to be critical for adhesion [24, 25] as dopamine incorporates both a catechol and an amine group and has the added benefit that PoDA

is very easy to deposit [26]. Any solid surface that is deposited in an alkaline buffered solution of dopamine will become coated in a thin film of PoDA (Figure 3.6).

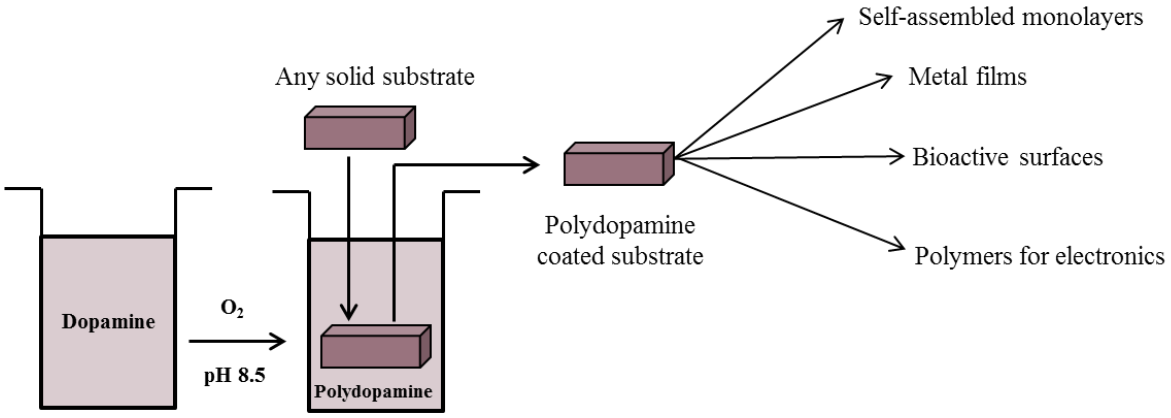

Figure 3.6- Process of spontaneous deposition of PoDA

3.1.2 Mechanism of PoDA formation

The PoDA formation mechanism was initially based on the Raper-Mason reaction sequence [18] for the formation of melanins (Figure 3.7). The mechanism was proposed as a result of similarities in structure of both adrenaline and L-DOPA.

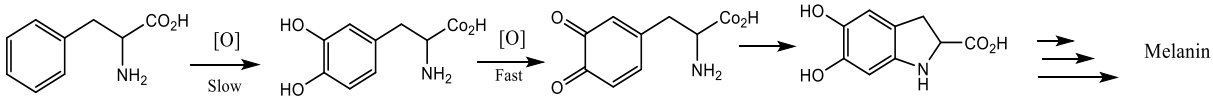

Figure 3.7 - The Raper-Mason mechanism [18]

The PoDA formation mechanism (Figure 3.8) is generally now accepted, although opinion differs as to whether PoDA forms from either 5, 6-dihydroxyindole (DHI), 5, 6-indolequinone (IDQ) or a combination of the two.

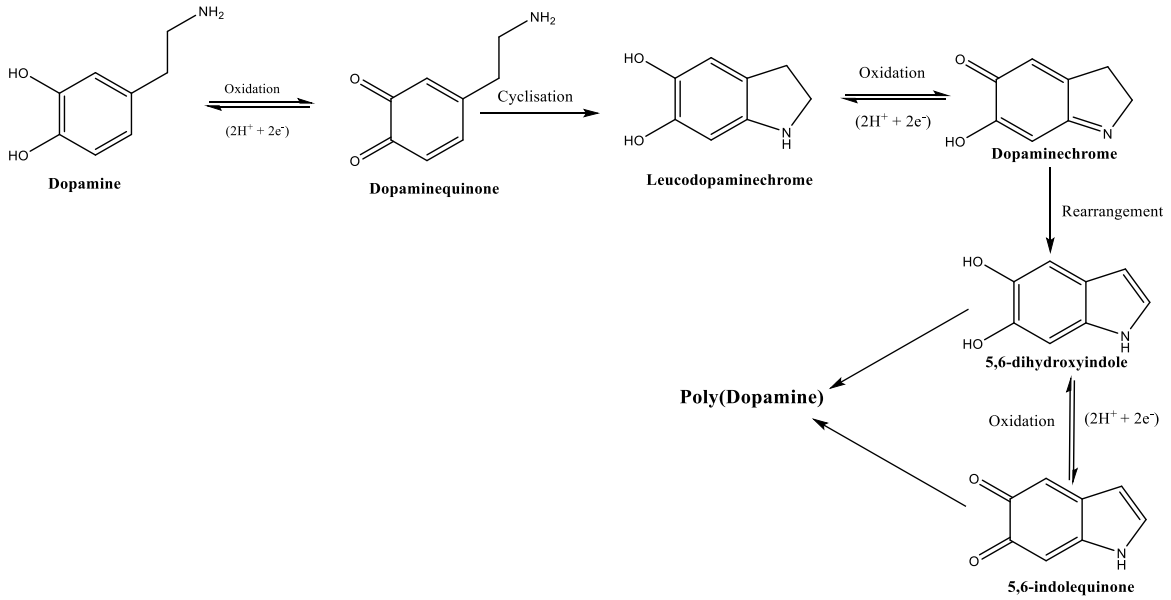

Figure 3.8 - PoDA formation mechanism

However, the possible products of the reaction sequence provide many possibilities for PoDA structures, especially as there are several different tautomers that can form for both DHI and IDQ (Figure 3.9). Consequently, it would be advantageous to determine the exact pathway by which PoDA is formed.

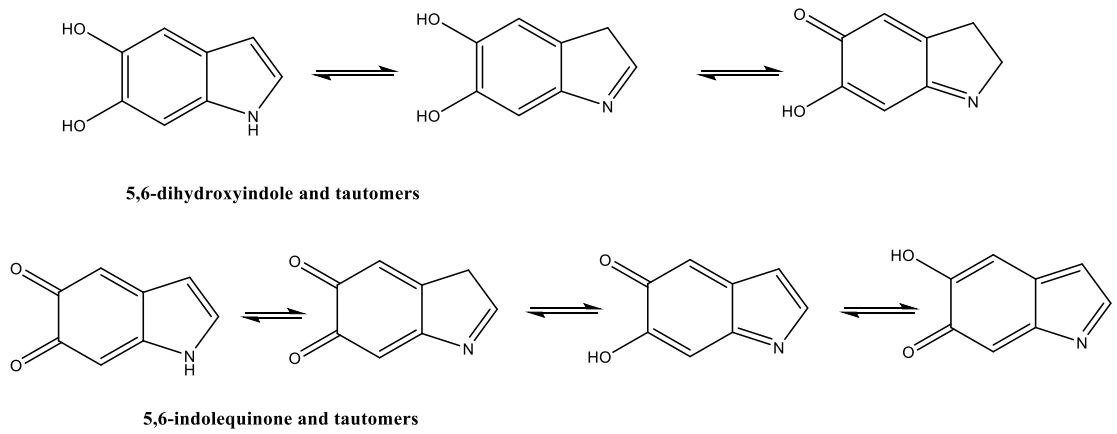

Figure 3.9 - Tautomers of 5,6-dihydroxyindole and 5,6-indolequinone

The reaction steps for polymerisation are agreed to be the same regardless of whether a covalently linked polymer is formed or a supramolecular structure. However, although this simplifies the study of dopamine from a mechanistic point of view, from a structural point of view it equally validates both structural groups. As a result, at least initially, each class of polymeric structures can be considered equally valid.

Yu et al. [27] used Gaussian calculations (density functional theory. DFT) to determine the most likely repeating unit structures. They found that the most favourable transition would be the formation of an indolequinone which would then dimerise to form a suitable repeating unit. This follows the proposed formation mechanism and supports the idea of a covalently linked PoDA. If the formation of the indolequinone can be indeed proven by analytical techniques, it would render those structures which rely on 5,6-dihydroxyindole repeating units invalid (i.e. the majority). Yu et al. also concluded that the rate of the reaction would increase with temperature.

Bernsmann et al. managed to give some indication of the relative timings of the reaction mechanism [28]. Initially, the dopamine solution is colourless but transforms to a brown colour after the oxidation of dopamine. Bernsmann et al. deliberately lowered the pH of the solution after 5 min of oxidation. This caused the solution to turn from brown to colourless and the dopaminequinone peak of the UV- Vis spectrum disappeared. After a 10 min oxidation period, the intensity of the dopaminequinone peak decreased but did not disappear entirely. These observations can be explained by the reversible nature of the dopamine oxidation (Equation 3.1).

$$\text{dopamine} \leftrightarrow \text{dopaminequinone} + 2H^{+} + 2e^{-} \qquad (3.1)$$

Equation (3.1) demonstrates that the application of acid would force the reverse reduction of dopaminequinone to dopamine. Thus, it can be inferred that after a longer oxidation period, dopaminequinone has transformed to a more stable product which is not perturbed by the addition of acid.

3.1.3 Proposed structures

The proposed structures for PoDA can be divided into two main categories: (*i*) those that propose covalent linkages between monomers, producing a polymeric structure akin to melanins; and (*ii*) those that propose non-covalently linked monomers (or small oligomers) resulting in supramolecular systems that are similar to the polymeric structures adopted by quinhydrones and catechols (Figure 3.10) [29]. Here, monomeric units of both the quinhydrone and catechol are held together by hydrogen bonding.

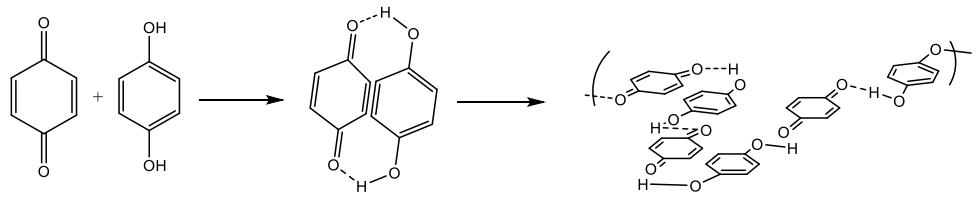

Figure 3.10 - Quinhydrone/catechol polymerisation

The notion of a supramolecular-like structure originates from the fact that quinhydrones are known to readily auto-oxidise, much like dopamine. However, the black colour and adherent properties of PoDA have much in common with melanins and, in addition, both noradrenaline and L-DOPA are known to form melanins.

There are two primary types of melanin: (i) eumelanin with indole precursors and (ii) pheomelanin which originates from benzothiazine (Figure 3.11). Given the almost universally accepted PoDA formation mechanism, it seems apparent that when authors say PoDA is synonymous with melanin they really mean eumelanin, despite very few of them specifically making this distinction.

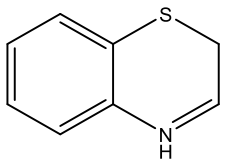

Figure 3.11 – Benzothiazine chemical structure

The primary problem with a structural model based on melanins is that the exact structure of melanin itself is still contested [30, 31], although it is accepted that the polymeric structure relies on covalent linkages between DHI units to some degree [32, 33]. In addition, many groups rely on comparison with natural melanins for structural determination [34] and, as natural melanins are, for the most part, derived from human tissue, no two melanin samples are exactly alike. It is not known to what degree this inhomogeneity of structure is likely to carry over to synthetic melanins.

The process of determining the PoDA structure is complicated further by the fact that PoDA is insoluble in water and in the majority of organic solvents, including those that are readily deuterated for liquid-state nuclear magnetic resonance (NMR) analysis [35].

Most studies hypothesised a structure (often based on observed properties) and then used some combination of analytical technique to support the hypothesis. To overcome the problem of the insolubility of PoDA, solid state NMR has been employed on the final polymer product and liquid state techniques, such as Fourier Transform-Infra Red (FT-IR) and Ultraviolet (UV) spectroscopies, on isolated intermediates. To date, there has been little analysis on PoDA within a film form. The majority of analysis and structure determination has been undertaken on precipitate that has been collected from solutions and dried. The danger with this strategy is the possibility that there may be a difference between the properties of PoDA as a thin film and the bulk polymer.

A schematic summary of the four main classes of proposed PoDA structures is shown in Figure 3.12.

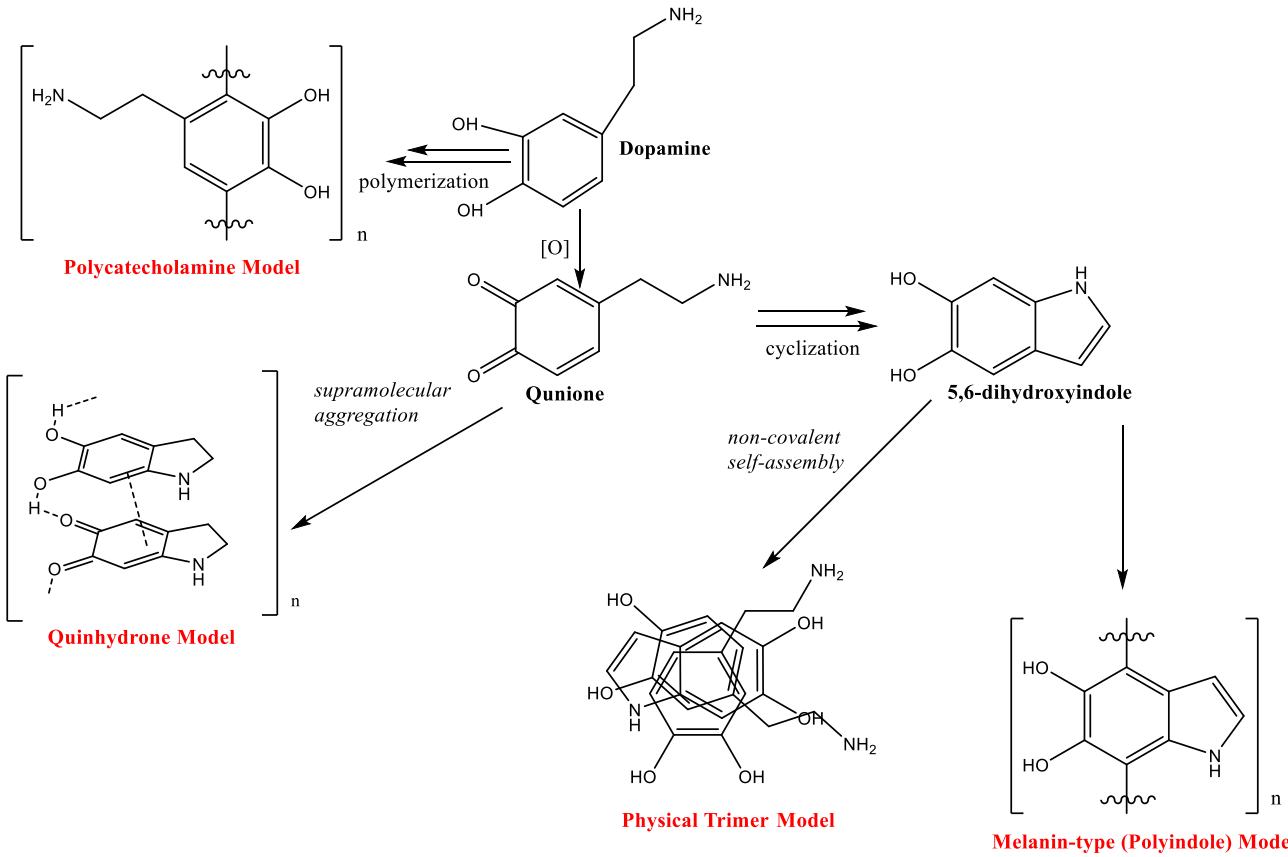

Figure 3.12 - The four classes of proposed PoDA structures (labelled in red)

3.1.3.1 Covalently linked polymers

The first covalently linked structure for PoDA was proposed by Herlinger et al. [36] in 1995 (Figure 3.13). This was 12 years before Lee et al.'s [37] seminal paper on PoDA deposition but the Herlinger study is rarely referenced in the more recent literature. Herlinger et al. proposed the following structure after spectrophotometrically observing the intermediates prior to the soluble low molecular weight (M.W.) melanin precursor. The melanin insolubility meant their proposed PoDA structure was un-confirmed.

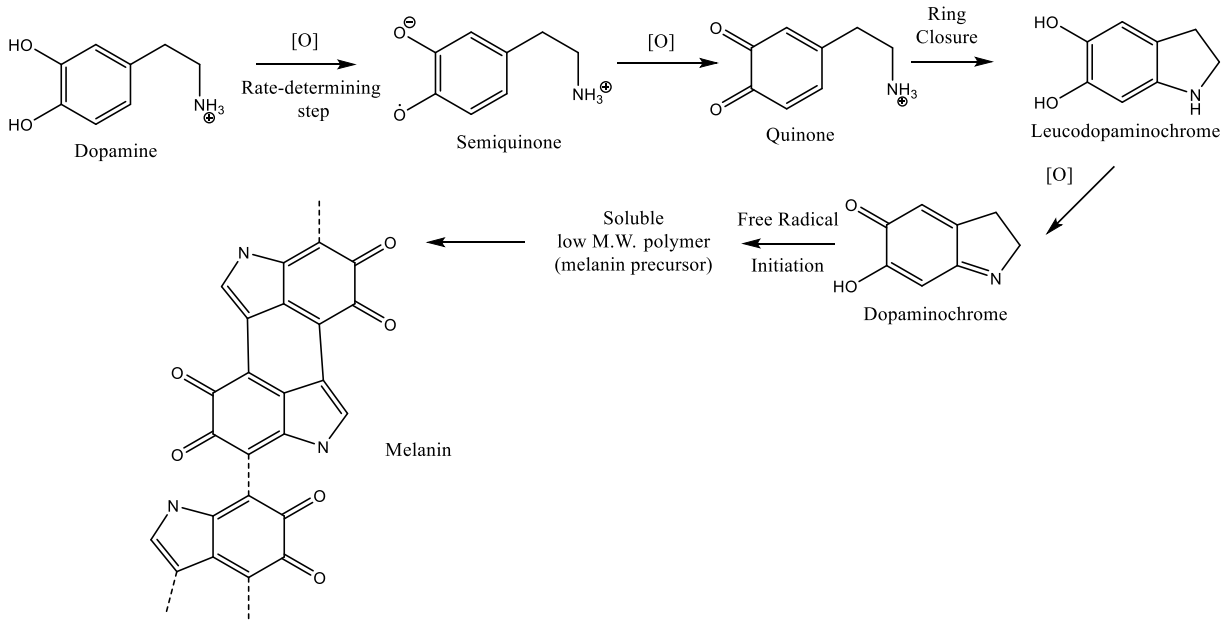

Figure 3.13 - Proposed mechanism of formation and structure of PoDA (Herlinger et. al) [36]

There is one crucial difference between the mechanism proposed by Herlinger and that which is often discussed in the more recent literature; they deduced that polymerisation occurred from dopaminochrome rather than the dihydroxyindole or indolequinone. However, it is possible that the soluble low M.W. polymer they propose as the final precursor to melanin could be some form of quinone, especially as their proposed final structure for melanin is comprised of quinone groups.

Wei et al. [38] proposed a simplified reaction mechanism (Figure 3.14) and subsequent polymeric structure as a result of their work with additional oxidants. It was reported that there would be no difference in either reaction mechanism or final product between polymerisation induced by molecular oxygen (O2) and polymerisation induced by additional oxidant. However, they provide no evidence of structural determination other than observing the change in intensity of the dopamine signal through Ultra Violet-Visible (UV-Vis) spectroscopy. While this shows that the initial

dopamine in solution was depleted, it provides no information about what the dopamine is transformed into. However, the authors were investigating the effect of added oxidants on dopamine polymerisation rather than the structure and so their methods were not focussed towards structural determination.

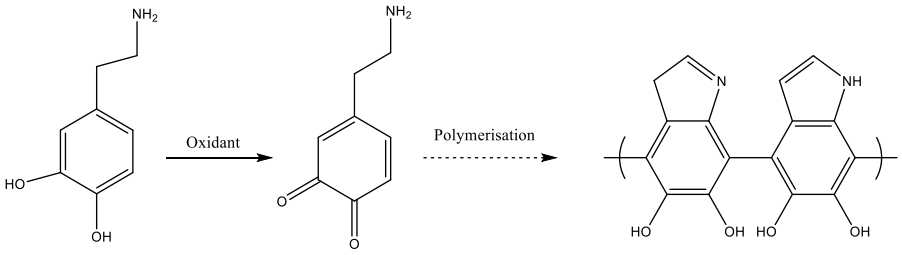

Figure 3.14 - Proposed polymeric structure (Wei et. al.) [38]

Postma et al. [39] present two potential structures with different bonding possibilities (Figure 3.15). However, they provide no analytical evidence to support the proposed structures, nor do they make reference to the origin of the structure: i.e. whether they were proposed by the authors or extracted from another paper.

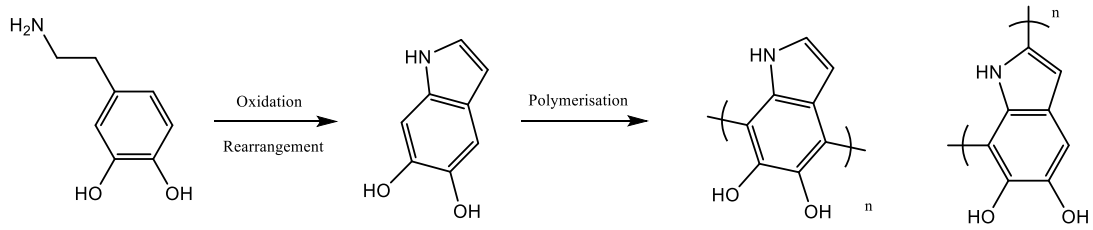

Figure 3.15 - Proposed PoDA structure (Postma et al.) [39]

The structures shown in Figure 3.16 were proposed by Yu et al. [40]. However, as with Postma et al. [39], they did not provide any analytical evidence. Later, as part of their discussion, they attributed the structures to Lee et al. but the Lee study presents no structures. Yu et al. did not seek to determine the structure of PoDA; instead they mention it as an aside in relation to the potential properties of the PoDA microcapsules they were producing. The authors did not provide any conclusions with regards to this relationship. They did however raise an important point -that there is a crucial relationship between polymeric structure and properties and thus that knowing the structure of PoDA is vital if refinement of properties is to take place.

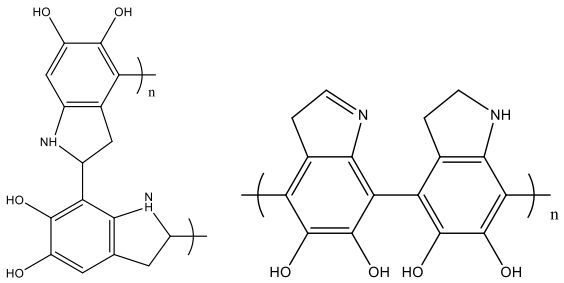

Figure 3.16 - Proposed PoDA structures (Yu et al.) [40]

3.1.3.2 Covalently bonded polymers with a degree of unsaturation

Liebscher et al. [41] proposed the structure shown in Figure 3.17 after undertaking NMR, electronspray ionisation high resolution mass spectrometry (ES-HRMS), X-Ray Photoelectron Spectroscopy (XPS) and FT-IR. They also claimed that the results they obtained prove that a supramolecular model is not possible. They state that "It is possible to give proof of hypothesized structural proposals found in the literature but also renders them unlikely."[41].

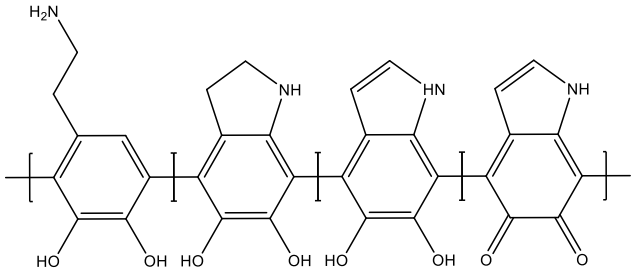

Figure 3.17 - Proposed PoDA structure (Liebscher et al) [41]

An interesting assertion made in this study is that the melanins resulting from L-DOPA, 5,6-DHI and dopamine precursors will not have the same final polymeric structure. Several other authors, especially Bernsmann and Ball [16, 28, 42, 43], use the term melanin indiscriminately for the polymeric structure of all catecholamine precursors and make the assumption that all precursors will result in the same polymeric structure. However, this has been disputed by Binns et al. who have published extensively on melanin chemistry [33].

Liebscher et al. refute the idea of a PoDA structure containing non-covalent interactions both recently in ref. [41], which was solely devoted to the PoDA structure and their earlier work on dopamine coated magnetic nanoparticles [44]. The early work found only one oxygen signal (XPS) for the polymeric shell of PoDA which makes an entirely non-covalent structure such as that proposed by Dreyer [35] unlikely (Figure 3.18). The results of Magic Angle Spinning (MAS) ^{1}H NMR, used to overcome the difficulties of analysing magnetic materials, resulted in the proposition

of a structure akin to that proposed by Herlinger et al. (Figure 3.13) as there were too few aromatic C-H signals (according to ^{1}H NMR) for a completely hydroxyindole derived structure to be valid.

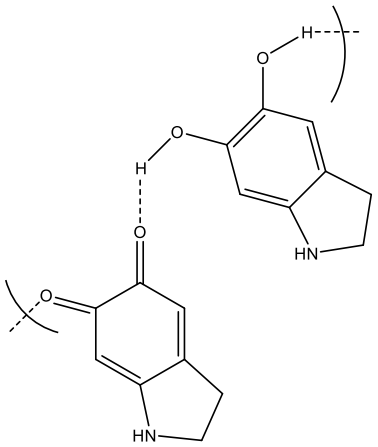

Figure 3.18 - Proposed non-covalent structure (Dreyer et al) [35]

The Liebscher et al. study which studied PoDA coatings formed from both Tris and phosphate buffered processes, found that no structural differences occurred using the two buffers and thus based their work on the possibility of there being several indole monomers (Figure 3.9).

The ^{1}H MAS-NMR indicated that the presence of dihydroxyindoles and indolequinones in the PoDA structure. This would be consistent with the structure required for Dreyer et al.'s non-covalently bonded structure (Figure 3.18). However, the ^{1}H NMR spectrum did not show chemical shift peaks that would be indicative of H atoms at the 4 and 7 positions of the dihydroxyindole (Figure 3.19) which would be a requirement for Dreyer et al.'s proposed structure to be valid. The ^{13}C MAS NMR and XPS indicated that there was a degree of unsaturation with regards to the indole moieties.

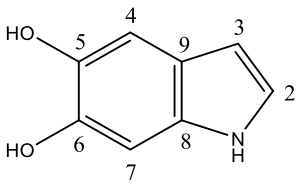

Figure 3.19 - Numbered dihydroxyindole

3.1.3.3 Supramolecular systems

Both of the proposed supramolecular structures consist of repeating units held together by π-π stacking. However, the structure of the repeating units differs greatly between the two proposed systems [35, 45].

3.1.3.3.1 Cyclic tetramers

The structure in Figure 3.20 was proposed by Kaxiras et al. [45] following first-principle calculations (time-dependent DFT and radial-distribution factors), based on the assumption that eumelanin is synonymous with PoDA, which may or may not be accurate. Their work highlights the problem that direct comparisons are being made between eumelanin and PoDA when the structure of eumelanin is not confirmed. They detail the current understanding of the eumelanin structure, as follows:

- small repeating units, e.g., DHI / IDQ tetramers;
- planar stacking of repeating units;
- eumelanin can bind to metal ions without permanent structural changes.

It was concluded that tetramers or pentamers are the most likely repeating units as cyclic hexamers would have a 120° angle between molecules and such steric hindrance would render them unstable. They also found that the only possible repeating units with positive energies of formation were tetramers that contained two or more indolequinone monomers. The radial distribution factors indicated planar π-stacking with inter-tetramer spacings of 3.00 Å which indicates that a porphyrin ring structure could well be adopted, as is shown in Figure 3.20. This would support the notion that melanin can incorporate metal cations without fundamental structural changes. Interestingly, copper was not found to be retained in experiments where it was used as an oxidant [36] , which could possibly indicate that the eumelanin / PoDA analogy is not necessarily valid. However, the retention of copper could depend on the strength of the chelation effect.

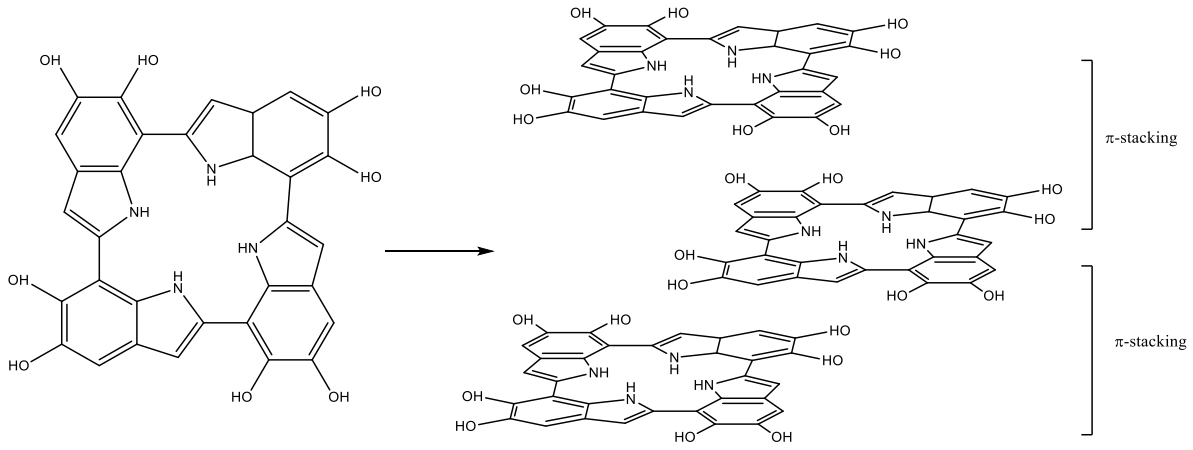

Figure 3.20 - Proposed PoDA structure (Kaxiras et al) [45]

3.1.3.4 Hydrogen bonding between indole units

Dreyer et al. [35] used a combination of NMR, electron paramagnetic resonance (EPR), powder X-Ray Diffraction (PXRD) and FT-IR to investigate the idea that PoDA adopts a quinhydrone-like structure. Their reasoning was that the quinhydrones have several properties in common with PoDA including strong colouring and insolubility, and the fact that catechols and hydroquinones are known to undergo autoxidation.

The authors proposed a model where monomers were linked through non-covalent interactions. Solid state NMR (15N) is consistent with indoline-like structures. Comparison between the liquid state NMR of dopamine and the solid-state PoDA spectrum indicates the oxidation of diol to dione and the formation of an aliphatic indoline formation indicating a cyclisation reaction occurred. This is in broad agreement with the general mechanism of PoDA formation presented in Figure 3.8

EPR data indicated that radicals are involved in the formation of PoDA which would indicate support for Herlinger's proposal that semiquinones are involved (Figure 3.13). The PXRD data indicated that repeating units had spacings of 3.8 Å. They therefore concluded that the repeating units of PoDA are quinoid and catechol indoles connected by hydrogen bonding between the OH and C=O groups (Figure 3.21). These repeating units are then connected by π-π stacking to create a supramolecular PoDA structure.

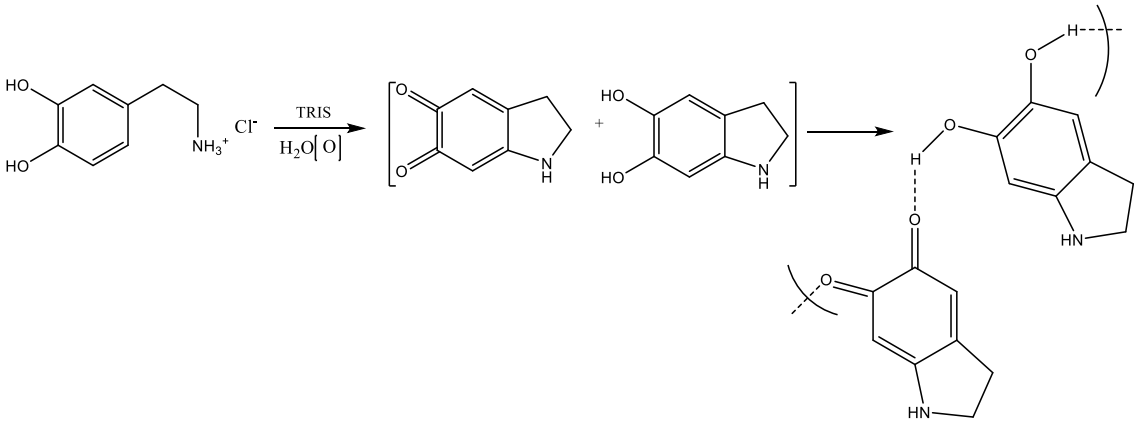

Figure 3.21 - Proposed route of formation and PoDA structure (Dreyer et al) [35]

A similar model to that shown in Figure 3.21 was proposed by Kim et al. [46]. The authors did not seek to define a PoDA structure as they were primarily interested in whether there were differences in morphology between either PoDA coatings deposited under either atmospheric oxygen or an applied pure oxygen atmosphere. FT-IR, UV-Vis, XPS and Scanning Electron Microscopy (SEM) was used to determine that the atmospherically deposited coatings contained large aggregates that were absent in coatings deposited under pure oxygen. They attributed this phenomenon to pure oxygen conditions producing a higher concentration of DHI and IDQ. The conjugated nature of DHI and IDQ would result in inter-molecular stacking as a result of π-π interactions and charge transfer. The higher the concentrations of DHI and IDQ that are produced, the better the stacking between oligomers and the stronger the attractive forces between oligomers. This resulted in smoother surface morphologies.

This seems a reasonable assumption given the oxygen dependent nature of the proposed PoDA formation mechanism and the possibility that atmospheric oxygen alone may be limited in availability, thus leading to higher concentrations of less conjugated products that may not stack so well. This would also explain the formation of aggregates under atmospheric conditions. However, their conclusions are based on the assumption that the supramolecular model is valid but the authors provide no evidence either to support their assumption or to explain how they arrived at their conclusion.

3.1.3.5 Mixed system

Hong et al. [47] reported that they believed PoDA to form through a combination of covalent polymerisation and physical self-assembly. As is shown in Figure 3.22, they proposed that both the self-assembly and covalent polymerisation processes originate from DHI. In the covalent polymerisation pathway, both DHI dimers and DHI and dopamine trimers are formed. In the physical self-assembly pathway, a non-covalently bonded trimer of two dopamine molecules and one DHI molecule forms. The products of both pathways then combine to form a supramolecular

structure, held together by non-covalent interactions, in which the constituent oligomers are held together by both covalent and non-covalent interactions. Hong et al. reached their conclusions by following the reactions through HPLC-MS. They proposed that there may be a difference in the final structure of PoDA depending on whether Tris or phosphate buffer is used although they did not provide reasoning for this assertion. In addition to reaction monitoring through High Performance Liquid Chromatography (HPLC), the authors also undertook theoretical calculations to determine which possible oligomers would be the most stable. This led them to propose the DHI-DHI and trimeric conjugates shown Figure 3.22. As a final note, the authors acknowledged that further analysis of the individual intermediates is required and the kinetics of their formation need to be further investigated.

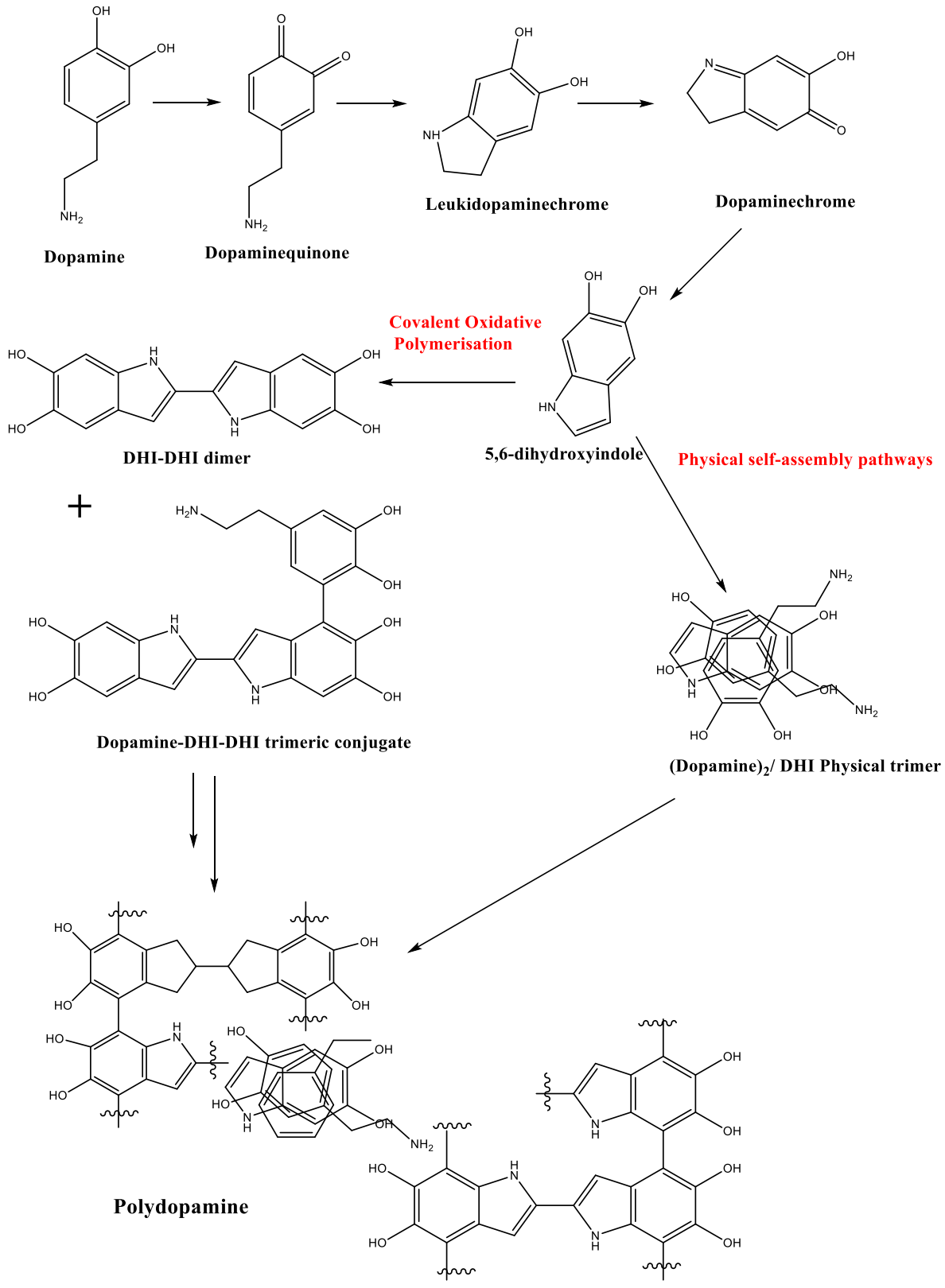

Figure 3.22 - Mixed pathway polymerisation and proposed structure (Hong et al) [47]

3.1.3.6 Inconclusive study

Della Vecchia et al. [48] conducted a study with the stated aims to:

- elucidate the repeating unit of PoDA;
- determine the degree of polymerisation in PoDA;
- rationalise the polymerisation process with respect to the deposition process.

An extensive analysis of the PoDA degradation products concluded that there are several possible repeating units, and multiple possible pathways for PoDA formation and are presented in Figure 3.23. Although they could not define an exact structure or pathway, Della Vecchia et al. concluded that covalent bond formation was crucial to the development of PoDA. They also reported that their MS data supported the hypothesis of Hong et al. that self-assembly trimerisation is involved in PoDA formation as there was strong evidence that the PoDA structure contained small oligomers. HPLC and MS data ruled out structures composed of non-covalently bound monomers in the initial stages of polymerisation, such as those proposed by Dreyer et al. [35]. However, they did not rule out the concept that non-covalent interactions could be possible between covalently bonded small repeating units. The authors concluded that Tris buffer can be incorporated into the structure of PoDA, a previously reported phenomenon [49], and that the incorporation is dependent on dopamine concentration. They attributed this to higher dopamine concentrations resulting in un-cyclised amine containing structures which are more likely to react with Tris. Their final conclusion summed up the state of research into the structure of PoDA: "PoDA should now be represented at best as a collection of oligomeric species in which monomer units are linked through different bonding as no current model is a completely valid explanation of the properties of PoDA."[48].

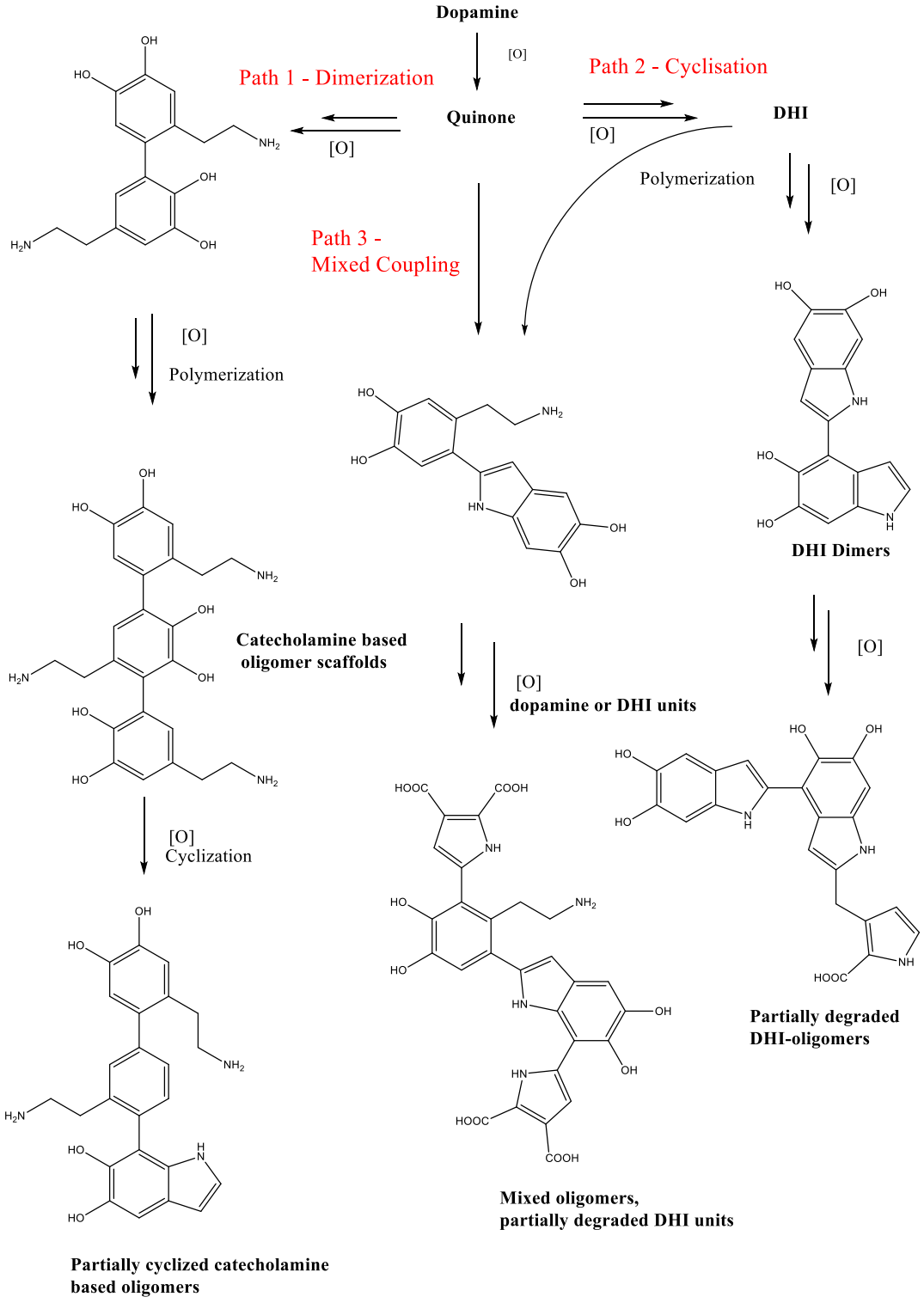

Figure 3.23 - Proposed pathways and oligomers (Della Vecchia et al) [48]

3.1.4 Deposition

There have been a limited number of investigations into the actual PoDA deposition mechanism onto a substrate surface. Only one study has proposed a deposition process for dopamine itself, inspired by Bernsmann et al.'s [28] hypothesis that deposition requires the absorption of monomers

or small oligomers onto the surface through a radical initiated process. Jiang et al. [50] proposed that branching reactions using 5,6-dihydroxyindole and 5,6-diindolequinone will result in oligomers. The oligomers then assemble through π-π stacking and from nanoaggregates which then undergo further aggregation to form a supramolecular structure. It has been proposed that the initial aggregation is triggered by the absorption of dopamine radicals onto the substrate surface. The absorbed radicals then initiate the polymerisation reaction and ultimately form a continuous film. Monomers / small oligomers can be deposited into the original PoDA layer through non-covalent interactions, leading to film thickening with longer deposition time. This assumption is supported by evidence from studies that have observed that supplies of fresh dopamine can lead to the formation of thicker PoDA films (90 nm with additional injection compared to 45 nm for a single deposition [49]). The idea of small DHI or IDQ oligomers forming is supported by both structural analysis and theoretical calculations. Jiang et al. highlighted the need for a fundamental understanding of the interaction between PoDA and substrate to enable comprehension of the deposition mechanism.

3.1.5 Current deposition procedures and refinement

Since Lee et al.[37] published their universal method for deposition of PoDA, there have been several hundred papers published on aspects of PoDA research. However, very few of these papers have sought to examine the structure and formation mechanism of PoDA. The majority of the studies have considered applications of PoDA and most have used the Lee method (2 g L^{-1} in 10 mM Tris buffer at pH 8.5 with 24 h deposition time) with very little or no alteration; many of the applications are electrical or biological in nature so the thin films produced by Lee's method are perfectly adequate.

3.1.5.1 Parameter examination

Attempts have been made to optimise various deposition parameters. The aims of definition have varied; some authors have attempted to decrease the required deposition time, others to increase the thickness of the deposited PoDA coating. Lee et al. [37] reported an achieved thickness limit of 45 nm and the aim has been to overcome this limit.

3.1.5.2 Additional oxidants

Wei et al. [51] used ammonium persulfate (AP) in a 1:2 molar ratio of AP: dopamine at various pHs to investigate the effect of additional oxidants. At pH 5.5 and 7.0 no polymerisation occurred

without the addition of AP. At pH 8.5 polymerisation took place spontaneously but was enhanced (in terms of deposition time) by the addition of AP. Following the findings at pH 8.5, sodium periodate and potassium chlorate were also tested. Stronger oxidants ($NaIO_4$) were found to further enhance deposition. This was determined by UV-Vis spectroscopy monitoring of the polymerisation intermediate peaks.

To date no investigation has been undertaken to compare the performance of different oxidants at acidic conditions. Investigations into PoDA film thickness have all used alkaline media thus it is not known whether thickness could be greater from an acidic solution than from an alkaline one.

Bernsmann et al. [49] undertook a comparison between cupric ions (Cu^{2+}) and dissolved oxygen (O_2) as oxidants as a means of overcoming the thickness barrier. Both experiments used a 2 g L^{-1} dopamine in a pH 8.5, 50 mM Tris buffer solution. In one experiment the solution was continuously aerated whilst in the other, the DA solution was deoxygenated through N_2 bubbling and 30 mmol $CuSO_4$ was added. On $CuSO_4$ addition, the pH dropped to 4.5 and was not adjusted. It was found that although the rate of deposition was slower when Cu^{2+} was the used, the films that deposited ultimately achieved a greater thickness (80 nm) than when O_2 was the oxidant. They hypothesised that a completely different mechanism would apply to oxidation by Cu^{2+} as this occurs under acidic conditions whereas oxidation by O_2 does not.

3.1.5.2.1 Organic oxidants

It has also been found that the *p-B*enzoquinone based polymers that form under alkali conditions can act as oxidation-reduction polymers meaning they may have a similar corrosion protection mechanism to other red-ox polymers such as polyanilines [52].The alkalinity is required because the mechanism requires the incorporation of a hydroxyl moiety [53].

Furlani et al. found that the polymers produced by *p*-BQ had conductivities which were comparable to polyanilines. This renders the second mechanism equally likely [54]. Sadykh-Zade et al. found that the polymerisation products were polymers based on hydroquinones. The OH groups come from the transformation of *p*-BQ to hydroquinones, a transition that is almost instantaneous under certain conditions [55].

Several studies that have used the oxidation of aniline monomer, whether chemical oxidation using peroxydisulfate or electrochemical oxidation by the application of an external potential, to produce polyaniline (PANi) coatings have discovered the existence of p-benzoquinone (p-BQ) as a by-product of the oxidation when it was carried out under both acidic and alkaline conditions. However, the evolution of p-BQ did not take place when electropolymerisation was undertaken under acidic conditions. The aniline coatings used in this project have been electrochemically deposited from an

acidic medium (oxalic acid) without the use of additional oxidants, thus avoiding the formation of p-benzoquinone. The chemical oxidation of aniline under alkaline conditions fails to yield PANi of any form and instead forms small chained oligomers.

As p-BQ was already known as an oxidant, the effects of the by-product on aniline monomer required further investigation. After analysis of reaction products by FT-IR, UV and elemental analysis using a CHNS/O analyser, Stejskal and Trchova [56] concluded that aniline is oxidised by p-BQ to a monoamine or the reduced aminophenol form (see Figure 3.24). These intermediates then facilitate the formation of aniline oligomers and the subsequent joining of oligomers to existing PANi chains under alkaline conditions forming hydroquinones and benzoquinone. Many oxidative polymerisations result in the release of protons which change alkaline environments into acidic ones but the authors do not mention this. However, the incorporation of released protons into the hydroquinone products would prevent the acidification of the reaction solution and ensures the maintenance of an alkaline regime.

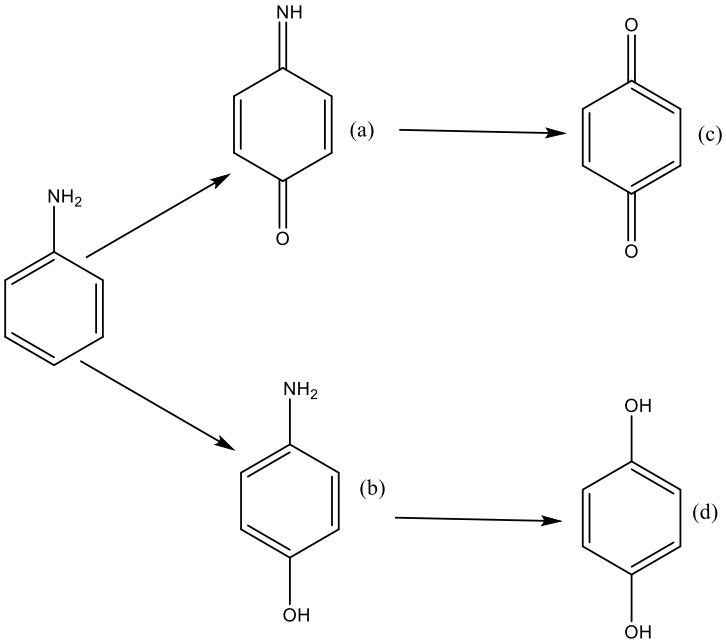

Figure 3.24 - Oxidation of aniline monomer to either (a) benzoquinone monoamine or (b) the reduced analogue *p*-aminophenol.; further oxidation facilitates the joining of aniline oligomers to existing PANi chains resulting in (c) *p*-benzoquinone and (d) the reduced form *p*-hydroquninone

Under acidic conditions, the reaction would result in the incorporation of p-benzoquinone (or associated compound) into the PANi chain. Several authors have proposed variants of the chains which are shown in Figure 3.25.

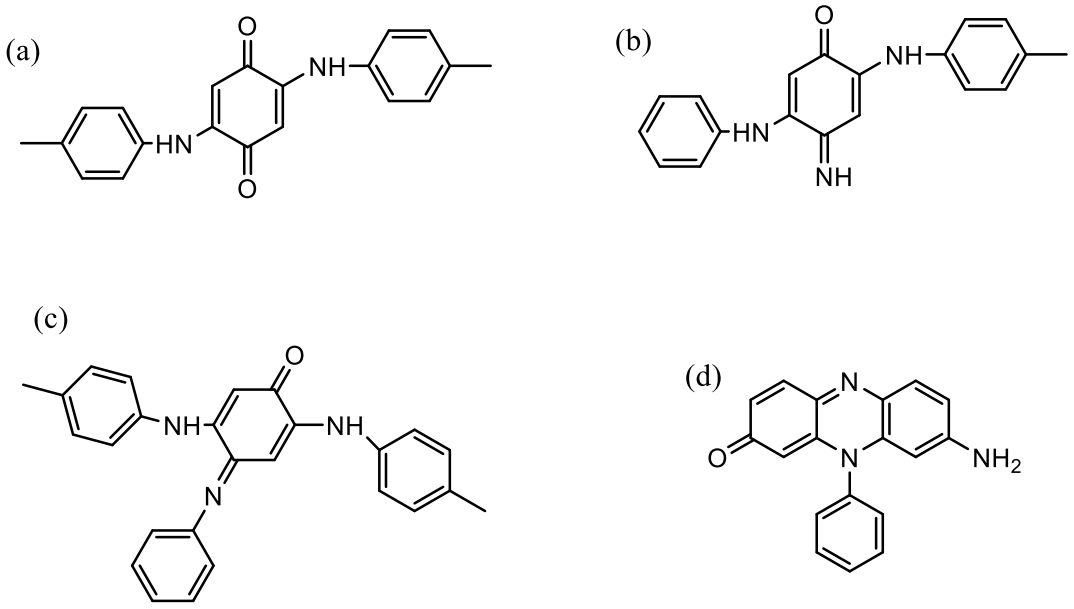

Figure 3.25 -Proposed structures for PANi chains with incorporated *p*-benzoquinone moieties: (a) Venancio et al. [57], (b) Surwade et.al. [58], (c) Kriz et al. [59] and (d) Zujovic et al. [60]

The discovery of these polymers is extremely interesting as previous research has indicated that polymers that contain both amino and benzoquinone entities are capable of inhibiting the corrosion of mild steel [61-63]. Muralidharan et al [61] concluded, using flowing electrochemical measurements and adsorption isotherms, that p-benzoquinone could be incorporated into an electrodeposited poly(phenyldiamine) coating, forming a polymer whose structure is presented in Figure 3.26b and which they termed polyamino-benzoquinone (PAQ) [64].

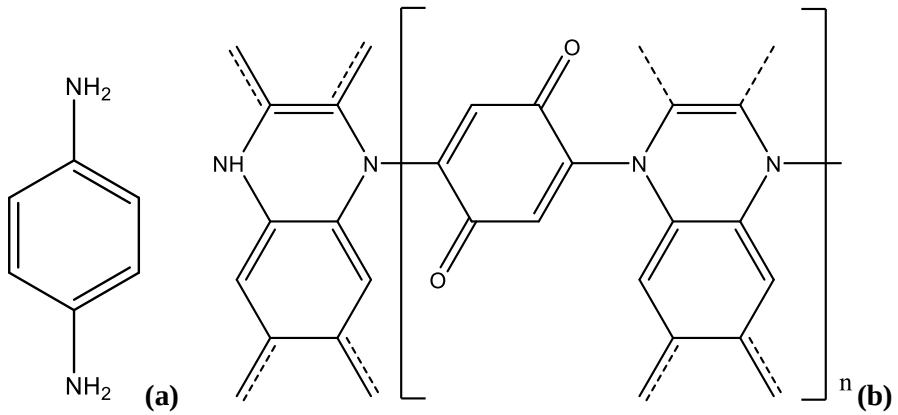

Figure 3.26 - (a) Phenyldiamine monomer and (b) polyamino-benzoquinone capable of protecting against the corrosion of mild steel in 1M H_2SO_4 and 1M HCl solution

The authors concluded that the polymer is capable of inhibiting both anodic and cathodic corrosion reactions in the following ways:

1. Strong adsorption of the PAQ film to the active sites of the metal substrate which suppresses the substrate dissolution as the Fe^{2+} ions are unable to be transported away from the surface and dissolved oxygen is less able to diffuse to the metallic interface;

2. Adsorption of PAQ leads to the formation of a protective film.

Unfortunately the authors do not state the thickness of the deposited protective layer. However, the initial EIS has very low impedances; the presented Nyquist plot has a maximum diameter of 100 Ω and the initial charge transfer resistance (measured after 15 min immersion in 1 M H_2SO_4) was 30 Ωcm^2 indicating that the deposited films are even thinner than the PoDA based coatings deposited in the present project. The PAQ adsorption is attributed to the π-electrons present in the polymeric chain being accepted into the vacant d-orbitals of the iron substrate atoms. The authors proposed that the increasing double layer capacitance values were due to an increased degree of PAQ adsorption until a saturation point was reached.

The CPE values obtained for the *p*-BQ mediated PoDA increase sharply for the first 24 hours and then reach a plateau for the remainder of the immersion test. This indicates that the *p*-BQ / PoDA coating may be undergoing a similar interaction with the substrate. As its name suggests, phenyldiamine possesses two amine groups whilst dopamine is a monoamine. This makes it impossible for the PoDA- based coating to incorporate *p*-BQ in the same way as poly(phenyldiamine) as there is no possibility for a polymeric chain to form solely from amine linkages. The oxidation of aniline (another monoamine) by *p*-benzoquinone has been studied in some detail by Stejskal et al. [65] in an attempt to understand the interactions between the *p*-BQ side products produced during the polymerisation of aniline. Their interest in the reaction also stems from the fact that that the primary industrial route for the production of *p*-BQ is the oxidation of aniline by potassium dichromate in acidic, aqueous conditions. They report that the interactions between *p*-BQ and aniline cannot form a polymer as a result of the lack of amine groups.

The formation of PBQ polymers is known to proceed through a Michael addition reaction [66], the same mechanism by which the cyclisation of dopamine is thought to occur [41] Therefore, the cyclisation of the amine moiety of dopamine cannot take place before the incorporation of *p*-BQ otherwise there are no tertiary amine sites for the Michael addition to take.

Figure 3.23 demonstrates the myriad of possible structures that have been proposed as being representative of PoDA. Path 1 was proposed by Della Veccia et al. [48] and was accompanied by compelling structural analysis. The products of path 1 are oligomers of dopamine that contain two unreacted amine groups which would allow the Michael addition based incorporation of *p*-BQ.

Jeyaprabha et al. [67] present a fairly extensive EIS study of the corrosion protection inhibition properties of PAQ. However, rather than deposit a polymeric film on the substrate as has been done with the PoDA based coatings, they mixed the bulk PAQ polymer that they had previously produced using chemical oxidation into an inert polymeric matrix. A similar study using aniline monomer also failed to produce a coating through chemical oxidation and only bulk polymeric particles could be produced. The highly adherent coating produced by Muralidharan et al. [61] was deposited using electropolymerisation. This indicates that the PoDA-BQ system is potentially unique in the respect that chemical oxidation of dopamine by *p*-BQ is capable of forming an adherent coating.

3.1.5.3 Buffered polymerisation

Herlinger et al. [36] assessed EPPS, phosphate and borax and Tris buffers in their study into the kinetics of dopamine polymerisation. They reported no change in oxygen consumption rate between Tris and phosphate buffers but noted that the EPPS buffer accelerated oxygen consumption whereas the borax buffer inhibited the consumption of oxygen. They attributed the inhibition by borax to a side reaction with the catechol groups of dopamine.

Bernsmann et al. [49] also compared the effect of a buffer on the deposition of what they called dopamine-melanin (D-M). The purpose of their investigation was to overcome the 45 nm thickness barrier experienced by other groups in as few steps as possible. They had previously overcome the limit using 90 repeat immersions. They used a 2 g L^{-1} dopamine in 50 mM Tris buffer solution and compared it with the same concentration of dopamine in a pH 8.5 50 mM phosphate buffer solution. Both solutions were exposed to atmosphere, with agitation, for 24 hours in the presence of a silicon oxide (SiO_2) substrate. The authors found that thicker films produced with the phosphate buffer. After growing to 100 nm, the phosphate produced film detached. However, the authors had previously reported delamination problems with silicon oxide [28, 42, 43] that they did not experience with other substrate. Therefore, it may be possible that the achieved film could be thicker than 100 nm on a substrate other than SiO_2.

3.1.5.4 Short deposition times

Short deposition times can be anything from 10 minutes to 1 hour. This is in contrast to the Lee method which used deposition times of at least 24 hours [37].

Thin films with bulk properties.

Zangmeister et al. [68] did not make any proposals about the PoDA structure; they made the assumption that the structure was eumelanin. The aim of their investigation was to find the minimum deposition time for a continuous PoDA film that retained the properties of a bulk film. They also intended to carry out physicochemical characterisation of films resulting from short deposition times. Their hypothesis was that a vertical substrate orientation and short deposition times would result in thin, reproducible films. Atomic Force Microscopy (AFM), XPS, FT-IR and cyclic voltammetry (CV) measurements were made on films deposited on gold substrates at times from 2 min to 60 min.

AFM revealed a granular topography (with grain size 25±5 nm) that was continuous across the substrate after 10 min. This indicated to the authors that a 10 min deposition is sufficient to form a topologically continuous PoDA film with minimal surface roughness. The CV was performed between –0.500 and + 0.700 V versus Ag/AgCl at 0.025 V s^{-1} for dopamine in a deoxygenated phosphate buffer solution and PoDA deposited on a gold electrode. The two voltammogram peaks observed for dopamine monomer were assigned to leucodopaminochrome / dopaminochrome and dopamine / dopaminequinone (all structures shown in Figure 3.8). There were also two peaks present in the voltammogram for the PoDA film, one which was assigned to the oxidation of 5,6-dihydroxyindole to 5,6-indolequinone and the other to dopamine-dopaminequinone. The presence of the latter peak for the polymer concurs with Hong et al.'s proposal of a mixed reaction pathway involving a self-assembled trimer incorporating dopamine monomer [47]. FT-IR results revealed that carbonyl species are a minor component of the final structure which would lend support to a model that is based on DHI units and is not reliant on non-covalent interactions. However, this is counter to Yu et al.'s [27] proposal (section 3.1.3.5) that an indolequinone based model of PoDA structure would be more energetically favourable. FT-IR also revealed that an aromatic amine is present but this does not differentiate between the dihydroxyindole and the indolequinone. Either way, this supports the general reaction mechanism for the bulk polymer. The structural conclusions made from FT-IR were supported by XPS data. In addition, XPS was able to differentiate between the tertiary amine present in dopamine monomer and the primary amine present in PoDA. With

time, the concentration of primary amine increases whilst the concentration of the tertiary amine decreases.

This is indicative of dopamine being consumed and PoDA being formed. The authors' final conclusion was that a minimum deposition time of 10 min was required to achieve thin films that retain bulk properties. Whilst this has implications for deposition in that it may be possible to coat samples in a shorter time than previously anticipated, the focus was on thin films which, unless grafted onto a bulk polymer, are not much use as a support for a sensing and self-healing coating.

3.1.5.5 Oxygen provision

Kim et al. [46] found that the colour of dopamine solution becomes much darker in a shorter time Oxygen period under a pure O_2 atmosphere than under atmospheric conditions. From this they infer that O_2 concentration affects the reaction kinetics. This is not entirely surprising given the number of oxidation steps that occur in the proposed PoDA formation mechanism. In addition, no reaction occurs if a closed deposition vessel has been purged with N_2. UV-VIS spectroscopy was used to monitor the consumption of dopamine throughout a deposition reaction (Lee et al.'s protocol) and thus determine the rate of reaction using Equation 3.2

$$-r_A = k[C_{AO}]^{\alpha_1} = \frac{dC_{AO}}{dt} \quad \text{(Eq. 3.2)}$$

Where r_A is the rate of dopamine consumption; k is the consumption rate constant; C_{AO} is the concentration of dopamine and $\alpha 1$ is the order of reaction. Kim et al. found that the rate of dopamine consumption was greater in pure O_2 atmosphere than in atmospheric conditions by two orders of magnitude. This confirms the theory that oxygen concentration is essential to the kinetics of deposition. The oxygen reduction reaction is presented in Equation 3.3; the protons and electrons come from dopamine monomer: each molecule gives up two protons and two electrons.

$$1/2O_2 + 2H^+ + 2e^- \leftrightarrow H_2O \quad \text{(Eq. 3.3)}$$

The reaction in Equation (3.3) would imply that when more oxygen is present, the rate of consumption of protons and electrons increases thus also increasing the rate of consumption of dopamine and, one could reasonably assume, the rate of formation of PoDA. In this context, when considering the number of probable oxidation steps in the proposed PoDA formation mechanism, it is easy to see how lack of oxygen can quickly become a limiting factor, especially when the solubility of oxygen is limited to begin with; typical values at 20°C are 284 μmol L^{-1} [69].

However, the authors do not compare either set of conditions with oxidant induced deposition. As this can occur at acidic pH, it implies that the kinetics are more complex than a dependence on oxygen concentration.

3.1.5.6 Deposition solvent

Ball [70] noted that there has been no investigation into whether PoDA can be deposited from solvents other than water. In an earlier paper Ball, along with Bernsmann [28], proposed that PoDA's physical deposition mechanism is akin to that of polyaniline (PANi) which is often deposited from organic solvents [71, 72]. If this is the case, then there are potentially important ramifications for electrochemical deposition as it may be easier to deposit PoDA from an organic solvent than an aqueous solution. The PANi mechanism was believed to proceed by aniline radical absorption onto the substrate followed by radical polymerisation. Herlinger et al. [36] proposed that one of the intermediates in the PoDA deposition process would be a semiquinone (Figure 3.13) so the theory is not without precedent.

3.1.5.7 Effect of pH on deposited film

Bernsmann et al. [28] submerged silicon slides coated with dopamine-melanin (D-M) (their terminology) into solutions with pH 1, 3, 11 and 13 for 24 hours. After this period the films deposited into solutions with pH less than 13 remained adhered to the substrate, but the film in a solution of pH 13 disintegrated after 15 min. However, Bernsmann has noted in other studies that the interaction between D-M and silicon oxide may be particularly weak and thus liable to delamination [16, 49].

3.1.5.8 Kinetic investigations

Aspects of the deposition kinetics have been investigated predominantly by the Bernsmann group [43, 49] with an additional, much earlier, study by Herlinger et al.

3.1.5.8.1 Measuring rate through oxygen consumption

Herlinger et al. [36] measured oxygen consumption throughout the dopamine polymerisation reaction in a closed cell. No substrate was used so only bulk polymerisation was observed. Following their investigations, Herlinger et al. have proposed the following rate law Equation (3.4) and the dependency of the observed rate constant (k_{obs}) Equation (3.5) for the consumption of oxygen (for which Herlinger et al. reported a value of 15×10^{-4} s^{-1} for a pH of 8.5), as they had

calculated that the rate constant would be inversely proportional to the proton concentration and proportional to the initial dopamine concentration.

$$-d_{O_2}/dt = k^{obs}[O_2] \quad \text{Eq. (3.4)}$$

$$k^{obs} = A\,[DH]/[H^+] \quad \text{Eq. (3.5)}$$

However, this was not sufficient evidence for them to propose a mechanism of polymerisation. In an attempt to understand the mechanism, they added methanol to the reaction. This had the result of reducing k^{obs} by 30% even at 1% by volume of methanol. As methanol is known to trap radicals, it would appear that radicals are involved in the polymerisation and/or deposition process. As a result, they proposed an intermediate with a semi-quinone structure (Figure 3.13). The authors decided that the rate determining step was the formation of the quinone following hydrogen abstraction from dopamine. The reasoning behind this assumption was the dependence of the rate constant on the proton concentration Equation (3.5). The authors believed that all other steps in their proposed reaction scheme (Figure 3.13) would be fast. The oxygen consumption studies led Herlinger et al. to conclude that there would be insufficient oxygen for any transformation of dopaminochrome to involve either protons or oxygen unless hydroxyl ions could be produced in a side reaction. If this is the case, then it would extremely difficult for DHI or IDQ to form. In a way, this conclusion undermines their own reaction scheme as their presented structure contains quinone groups that would be impossible to produce without an oxidation reaction, even if the 5,6-dihydroxyindole could be produced through a radical reaction. In addition, they term their final product melanin and, although the structure of eumelanin has yet to be fully elucidated, there is overwhelming experimental and theoretical calculation evidence that it is based on some combination of DHI monomers and/or oligomers.

3.1.5.8.2 Determining deposition rate using quartz crystal microbalance

The purpose of the QCM experiments undertaken by Bernsmann et al. was to define the optimum contact time between dopamine solution and substrate and the effects of the provision of fresh dopamine solution [28]. However, the volume under investigation was only 100 μL which potentially limits the usefulness of the data as it may not be indicative of bulk polymerisation. A dopamine solution (2 g L^{-1}) was injected and allowed to polymerise for 15 min after which the resultant film was dried. The QCM resonances reached a steady state, indicating the formation of a film of constant thickness, after 6 injections of fresh dopamine solution. The films appeared to be thin and rigid and according to the Subrey Equation (3.6) the film thickness was determined to be almost proportional to the number of dopamine injections. Where, Γ is the mass of deposited polymer per unit area, ρ is the polymer density and d is film thickness.

$$\alpha = \frac{\Gamma}{\rho} \qquad \text{Eq. (3.6)}$$

Ellipsometry was used to confirm that thickness was variable between injections; this was attributed to the drying stage between depositions. Hence, the drying stage was removed and exact proportionality between the number of dopamine injections and thickness of the deposit was achieved.

When concentration of dopamine solution was varied, multiple deposition steps were also used. For every initial dopamine concentration tested, the thickness of the D-M deposit increased with time. To determine the D-M growth rate, the thickness vs time was plotted to give a slope and thus a rate (*Vm*). *Vm* was then plotted against the initial dopamine concentration. It was found that above starting concentrations of 0.5 g L^{-1}, *Vm* was constant for all concentrations, using a 15 minute deposition time.

However, when the deposition time was reduced to 5 min Vm increased with increasing concentration. This appears to indicate that the rate determining step involves dopamine and is dependent on the initial dopamine concentration. This supports the conclusions of Herlinger et al.

3.1.5.9 The effect of pH on PoDA deposition kinetics

After realising that redox reactions (e.g., the oxidation of dopamine to dopamine quinone) are independent from pH in thermodynamic terms but highly pH dependent in kinetic terms, Ball et al. investigated the effects of pH on the deposition of PoDA [43]. They kept the initial concentration of dopamine constant at 2 g L^{-1} and tested pHs of 6.0, 8.5 and 10.2. Higher pHs than 10.2 were not investigated as the authors had previously experienced delamination under more alkaline conditions. However, they have postulated that this may be due to specific interactions between PoDA and silicon oxide so the same problem may not occur with steel. Thus, it is possible that higher pHs may result in thicker films on a mild steel substrate. The formation of dopamine was found to slow at pH 6.0 but increased in rate between pH 8.5 and pH 10.2.

3.1.5.10 The effect of dopamine concentration in PoDA deposition kinetics

Ball et al.'s second study with varied dopamine concentrations revealed that the initial concentration of dopamine markedly influences several aspects of the deposition process. Using ellipsometry they discovered that maximal film thickness increases almost linearly with initial dopamine concentration. However, the overall rate constant increases non- linearly, implying that

deposition is not first order. The initial deposition rate was found to follow a similar pattern to that of the overall deposition rate.

The film roughness was found utilising AFM to increase with increasing initial dopamine concentration. The roughness was attributed to nano-scale aggregates that could not be removed with rinsing. This led Ball et al. to conclude that the aggregates were intrinsic to the deposited films. Root mean squared roughness was assessed against film thickness for dopamine concentrations of 1 g L^{-1} and 5 g L^{-1} and the resultant slope had a value of 1 for both concentrations. This indicated that the aggregates incorporate into the film as it grows and that the effect of concentration follows a scaling law.

The surface energy of the deposited film appeared to be unaffected by the initial dopamine concentration and was deemed to be dependent on the initial substrate after a comparison between the silicon substrate results and Bernsmann et al.'s previous work with deposition onto PLA and PVDF [73].

The authors tried to derive a kinetic model for the deposition of PoDA that took into account their findings:

- increased film thickness with increased initial dopamine concentration;
- increased film roughness with increasing film thickness;
- surface energy independent of concentration.

The rate was based on Equation (3.8) and took into account Equation (3.7) which showed that deposition kinetics could be fitted with an exponential decay function. The results implied that Equation (3.9) was also valid.

$$d(t) = d_o + d_{max}\left(1 - e^{-kt}\right) \quad \text{Eq. (3.7)}$$

$$dd(t)/dt = d_{max} k e^{(-kt)} \quad \text{Eq. (3.8)}$$

W here $d_{\max}$ = maximal film thickness and k = rate constant

$$d_{max} = \alpha_2 C \quad \text{Eq. (3.9)}$$

Where α_2 = constant and C = initial concentration of dopamine.

These were then combined to give a final rate equation, Equation (3.10) which implies that the rate is proportional to both the initial dopamine concentration and some function of reaction time.

$$dd(t)/dt = \alpha_2 k C e^{(-kt)} \quad \text{Eq. (3.10)}$$

The relationship between the roughness of the films and their thickness was attributed to smoother films having a smaller surface area in contact with the solution and therefore fewer possible sites

for interaction with the precursors to polymerisation, thus producing a thinner film. A lack of variation in surface energy was explained by assuming the composition of the film is independent of the examined variables.

3.1.6 Electrochemical deposition of PoDA

There are very few papers relating to the electropolymerisation of dopamine and only one which seeks to understand the deposition process. Li et. al. [17] sought to investigate the polymerisation reaction that poisons the working electrode when dopamine is investigated with cyclic voltammetry. The study was published before PoDA had gained recognition as a surface modification method and so the quality of deposition was not taken into account. Li et al. polymerised dopamine from 50 mM dopamine in phosphate buffer solution onto gold electrodes using CV at 20 mV s^{-1} from 0 V to 1.0 V versus SCE for a 2 hour period to produce a rigid film on the electrode surface. The deposition was monitored by electrochemical quartz crystal microbalance throughout. They observed that with every successive deposition cycle, the current peak heights decreased from which they inferred that the deposited film must be insulating in the phosphate buffer.

Further investigation revealed that the reaction did not proceed at pH 5 but that polymerisation occurred at pH 7.0, 9.1 and 11.1. They do not however make any differentiation between the effectiveness of those three pHs. The authors also varied the dopamine concentration and found that increasing the concentration of dopamine meant an increased amount of PoDA was deposited. However, the highest concentration tested was 2×10^{-4} M which is below that used in the experiments already attempted at Southampton. The concentration of electrolyte was also deemed important; the level of deposition was reduced when the buffer concentration was increased. The buffer used at Southampton for electropolymerisation was 0.1 M phosphate so it is possible that lowering the buffer concentration may improve deposition [17].

The mechanism of formation proposed was identical to that presented in Figure 3.8. However, they did not propose a structure for the final polymer other than to note that an FT-IR spectrum of the final product was very similar to that which was obtained from a polyindole. From this they inferred that the polymer was probably covalently linked 5,6-indolequinone units. Several studies in support of a covalently-linked structure believe polymerisation occurs from 5,6-hydroxyquinone but this is from chemical deposition. It may be possible that the reaction mechanisms for chemical and electrochemical depositions are different. However if polyaniline is as analogous to dopamine

as some authors think [28, 49] then this is unlikely, as the oxidative polymerisation mechanism of polyaniline formation has been subjected to a lengthy and rigorous review and was found to be the same for both chemical and electropolymerisation.

On a final note, the authors suggested using a sweep rate of greater than 1 V s^{-1} as this seemed to prevent polymer deposits at the working electrode. Thus we can infer that, for successful deposition of PoDA, a scan rate of less than 1 V s^{-1} is required.

Bernsmann et al. [16] deposited PoDA onto amorphous carbon using a potential scan of –0.4 V to 0.3 V versus Ag/AgCl and a scan rate of 0.01 V s^{-1} from a 10 mM Tris buffered solution at pH 7.5 containing 0.5 g L^{-1} of dopamine hydrochloride. The dopamine solution was deoxygenated before use. They used a low scan rate as higher ones prevented deposition which supports Li et al.'s observations. AFM revealed that after 50 cycles, a homogenous film had formed which was also found to be impermeable to iron complexes. The electrodeposition work was undertaken as part of an investigation into tuning the permeability sensors to electrochemical probes through different PoDA deposition methods.

Loget et al. [15] approached the electropolymerisation of dopamine from an application perspective. They sought to use PoDA as a means of immobilizing single strands of DNA since dopamine has been found to immobilise biomolecules. They aimed to deposit very thin films on a gold substrate, so their findings, such as they are, are less useful to this project. Their finding concurred with those of Bernsmann et al. namely that 50 scans produce a continuous film of PoDA [16]. They confirmed this as a result of a complete absence of any solution electrochemistry being visible by CV.

3.2 Polyaniline

Polyaniline (PANi) is a non-toxic and intrinsically conducting polymer that has a conducting property of up to 5 Ω-cm^{-1} [74]. These high conductivity levels have led to PANi being termed [75] an organic metal and this, coupled with low toxicity, makes PANi an ideal candidate for the smart coating. In addition, PANi has a significant advantage over PoDA in relation to this project as the field of PANi coating research is 20 years more advanced than that of PoDA coatings and as a result, deposition parameters are much better defined so the incorporation of a 3D porous network and incorporation of self-healing agents should be more straightforward. Additionally, PANi has been extensively studied for its corrosion prevention properties. As a result, there is a substantial volume of published literature relating to the deposition and properties of PANi and its corrosion protection capabilities. The focus of this current review will be to critically assess the deposition strategies which use PANi as an anti-corrosion coating.

However, the suitability of PANi as a medium of protection against corrosion in a marine environment is under debate. Some authors suggest that PANi is able to protect against chloride containing media [76, 77] while others dispute this [78].

3.2.1 Polyaniline structure

Unlike PoDA, PANi has multiple oxidation states. These are termed leucoemeraldine (PANi-LE), emeraldine (PANi-EM) and pernigraniline (PANi-PE). The most stable is emeraldine which can exist in neutral base form (PANi-EB) or the doped salt form (PANi-ES). PANi-ES has been found to offer superior corrosion resistance over PANi-EB which means some form of dopant will be required (Na_2SO_4 is the most commonly used dopant) for a successful PANi coating. Despite these multiple oxidation states, the structure of PANi is well-defined and accepted across all the literature that relates to PANi's anti-corrosion properties. Figure 3.27 shows the electronic relationship between the three forms of polyaniline:

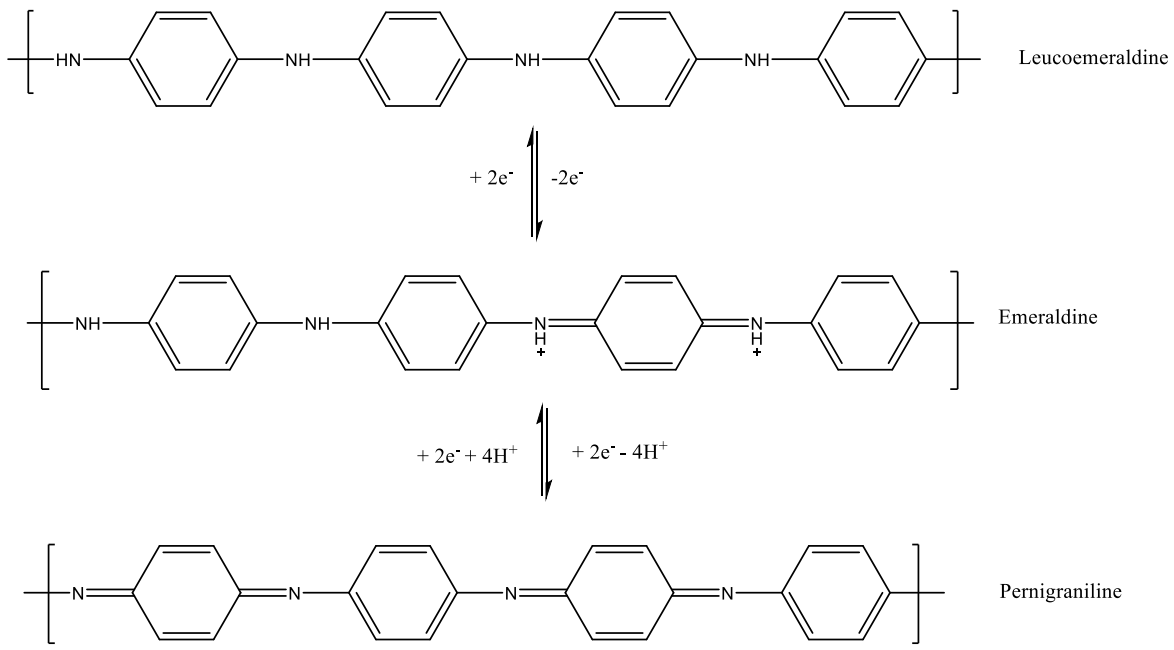

Figure 3.27 - Relationship between the forms of polyaniline

The structure of PANi is much simpler than some proposed PoDA structures and relies heavily on polyconjugation. In a similar manner to PoDA, the nitrogen atoms of PANi are the oxidation centre for aniline polymerisation. Both aniline and dopamine polymerisations are preceded by oxidative

polymerisation which requires a monomer with electron donating groups. For both dopamine and aniline this is the nitrogen -containing secondary amine group (NH_2).

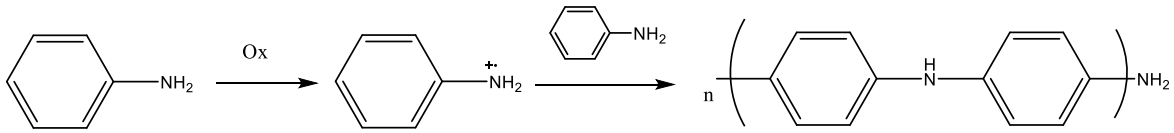

Figure 3.28 - Reaction scheme for the oxidative polymerisation of aniline

The polymerisation mechanism (Figure 3.28) proceeds by the creation of radical sites in the monomer through reaction with an oxidising agent (chemical polymerisation) or the application of a potential (electropolymerisation), and subsequently these radical sites initiate polymeric growth. The applied potential, or the oxidation potential of an added oxidant, needs to be above 1.05 V versus Ag/AgCl [79] for polymerisation to occur. As a result, persulphates are the most commonly added oxidant used in the polymerisation of aniline. However, these may be unsuitable for deposition onto carbon steel as sulphates are known to accelerate the corrosion of mild steel. Iodates have been proposed as a suitable alternative oxidant for deposition of PANi onto mild steel [80]. Much like dopamine, the polymerisation conditions that will be required for aniline are very specific. Whilst PANi will form at pHs from 1-14, it is only conducting when formed in acidic conditions, at pH 1-4. Unfortunately, this has implications for the deposition by mild methods aspect of this project because relatively strong acids are required to form low pH conditions.

3.2.2 Deposition of polyaniline

Polyaniline can be produced through the oxidative polymerisation of aniline in a manner similar to the formation of PoDA. The oxidative polymerisation can be undertaken through either chemical or electrochemical methods. In order to produce a film of PANi directly onto the desired substrate, in a way that is analogous to the PoDA films we are depositing, electrodeposition is required. The literature indicates that chemically polymerised PANi films induce corrosion potential shifts to more noble potentials than those achieved by electropolymerised films [81]. However electrochemically polymerised PANi offers a greater degree of control over the polymerisation process.

3.2.2.1 Chemical polymerisation and deposition

The powder products of oxidation can still be used as a method of protecting against corrosion. Pan and Wang [82] developed a two part PANi based protective coating The base coat (Part I) was PANi powder dispersed in poly-acrylic acid whilst part II consisted of polyethylene and TiO_2 (sacrificial pigment for UV degradation). Salt fog tests were conducted and the coating was found

to have superior corrosion resistance over 30 days when compared with an existing zinc-based system (containing zinc tetroxy chromate). Rout et al. combined PANi powder with alkyld resins and cobalt octate as a dispersing agent [71].

An alternative method of applying chemically produced PANi as a protective coating is to disperse PANi powder into N-methyl-2-pyrrolidinone (NMP) to produce a solvent borne dispersion that can be easily spread onto the desired substrate. The NMP solvent is then evaporated off either at room temperature over a period of several days [83] or over a shorter time period using applied heat [84].

Rout et al. [71]examined a range of chemically produced PANi contents (wt.%) in an alkyld resin binder and found, by EIS, that the conductivity of coatings increased with increasing PANi content up to a maximum of 15% polyaniline.

3.2.2.2 Electropolymerisation and electrodeposition

Polyaniline can be electrodeposited from any aqueous solution with a low pH [85]. For the majority of conducting polymers, the electropolymerisation mechanism is complicated, and is often dependent on polymerisation parameters such as applied potential and temperature [86]. Moraes et al. found that an applied voltage of –0.6 V to 1.5 V versus SCE was required to ensure sufficient adherence to the substrate [81]. Electropolymerisation is further complicated by the choice of underlying substrate. The carbon steel used in shipbuilding is liable to undergo dissolution or passivation with the former more likely to occur when polymerisation is undertaken from an aqueous solution. Therefore, undertaking electropolymerisation of conducting polymers from a non-aqueous organic solution would be advantageous.

Polyaniline has been successfully electrodeposited from neutral aqueous solutions. Dung Nyguyen et al. [87] investigated such a deposition in an attempt to try and deploy the corrosion protection properties of PANi which had previously been observed on stainless steel for the protection of a mild steel, a more active substrate. The authors also sought to contradict the generally accepted view that successful films could not be produced from a neutral solution. In addition, they wanted to compare the effect that deposition solution pH has on metal passivation. The authors succeeded in producing a reproducible coating that they claimed offered good adherence and corrosion protection. However, they did not provide quantitative values to support these assertions, which render their results somewhat incomparable with other systems that have been better quantified in terms of adhesion and corrosion protections. Camlet et al. [88] concluded that electrodeposition of PANi, using cyclic voltammetry, from a neutral $LiClO_4$ solution was possible as long as the current density was above 3 mA cm^{-2}.

Whilst the use of non-aqueous solutions as the deposition media for aniline may be less likely to induce dissolution of the substrate, there are implications for both the conducting nature and proposed templating of the coating. The most conducting form of PANi is Emeraldine which requires acid doping and an acidic deposition medium will therefore be required. The liquid templating of polyaniline to produce a porous coating requires a lyotropic liquid crystal mesophase which is formed from the mixing of an amphiphilic component and an aqueous solution. Therefore depositing a conducting and porous PANi coating will require deposition from an acidic aqueous solution. Studies have previously been undertaken using oxalic acid as a deposition medium with iron and steels as substrates [89-92]. Successful coatings were deposited with an oxalic acid medium, using cyclic voltammetry to deposit the thickest coatings. Such conditions have been further investigated for the incorporation of templating; they required further refinement as the liquid crystal template is considerably more viscous than the aqueous deposition media of the current prior art.

3.2.3 How polyaniline protects against corrosion

The majority of corrosion prevention methods can be divided into three categories [93]:

(i) cathodic protection where electrons are donated from the metal requiring protection to a sacrificial material that is corroded preferentially;

(ii) anodic protection where a process causes charge (either ions or electrons) to be withdrawn from the metal requiring protection;

(iii) barrier protection where the underlying metal substrate is protected from the corrosive environment by another material such as an applied coating or a passivating layer of metal oxide.

The mechanisms by which polyaniline protects against corrosion are under debate. Some authors believe that PANi induces the formation of an oxide layer on the underlying substrate [94]. Others have proposed that the applied PANi coating merely forms an impermeable barrier against the corrosive species [78]. However it has been found that coating holidays (gaps in the deposited coating) can still be protected by the PANi coating that surrounds them [95] indicating that the protection mechanism is more complex than simple barrier protection.

There are also authors who describe how PANi coatings, in their experiments at least, failed to protect against corrosion. Araujo et al. [96] demonstrated that PANi with an epoxy topcoat failed to protect against the corrosion of carbon steel in 0.1 M Na_2SO_4 as the coating was insufficiently adherent.

However, they used the undoped neutral EB form of PANi whereas all the other examined literature has used the doped ES form, indicating that dopants play an active part in corrosion protection.

3.2.3.1 Anodic protection

Electrochemically, the anodic protection mechanism of PANi works by PANi-ES acting as an electrocatalyst mediator for electron transfer between the underlying steel substrate and dissolved oxygen [7]. This requires PANi to cycle between its oxidised and reduced phases, PANi-ES and PANi-LB, respectively [97].

This is possibly as a result of the highly conjugated nature of PANi. Cook et al. concluded that the proposed cycling would only occur in acidic solutions as the current experienced by PANi in 3.5% NaCl solution (near neutral solution) would be too low to force PANi to adopt its reduced form [7].

Talo et al. [76] used XPS to investigate the underlying mild steel substrate after application of an epoxy/PANi coating and 30 days immersion (open circuit potential) in 3.5% NaCl and subsequent removal of the PANi containing coating. The authors sought to improve the understanding of the mechanism by which PANi prevents against corrosion. They wished to prove or disprove the notion that the presence of a PANi containing layer results in the formation of an oxide layer between the PANi coating and the metal substrate. This phenomenon had previously been proposed by other groups [83, 93]. XPS revealed that iron, carbon and oxide were present and that iron was primarily present as Fe^{2+}. The authors concluded that Fe_3O_4 and $Fe(OH)_2$ were the most likely compounds present. Potentiodynamic polarisations showed that the corrosion potential of the epoxy/PANi coated samples had from -0.600 V for a bare mild steel to +0.101 vs Ag/AgCl when subjected to a 3.5% NaCl immersion. As a result, the formation of an ennobling oxide layer was considered the most likely method of corrosion protection. However, there was no mention of the mechanism by which the oxide layer would form underneath the PANi coating or what role PANi would play in the formation of the layer. A further XPS study, including XPS depth profiling was undertaken by Fahlman et al. with chemically formed PANi (both neutral EB and HCl doped ES) deposited with NMP onto cold rolled steel and the samples exposed to a 70-80°C humidity chamber for 7 days. Bare cold rolled steel was subjected to the same conditions as a control. XPS depth profiling involved the layer-by-layer removal of PANi and oxidation products until pure iron was detected and was undertaken to further the understanding of the oxide layer compositions. Both control and coated samples were found after 24 hours, to have a top layer of Fe_2O_3 that was approximately the same thickness (15 Å) for all samples.

This is in contrast to the study done by Talo et al. which concluded that only Fe_3O_4 and $Fe(OH)_2$ was present. Fahlman et al. found that below the Fe_2O_3 layer, again for all samples, an Fe_3O_4 layer was formed. The authors then used this as a measure of corrosion protection; the thinner the Fe_3O_4 layer, the better the corrosion protection abilities. Unsurprisingly, bare carbon steel had undergone severe corrosion and an Fe_3O_4 layer of thicker than 200 Å had formed. In contrast, the samples coated with PANi had undergone no visible corrosion and their Fe_3O_4 layers were only 35 Å thick. At the time of the study, the proposed mechanism for the formation of sub-surface Fe_3O_4 relied on grain boundaries [83]. Water molecules were believed to diffuse through nanometre pores in the Fe_2O_3 layer down to the surface of the bulk un-oxidised steel, forming Fe_3O_4. This would induce Fe^{2+} formation and these iron ions could diffuse through grain boundaries and react with O_2 or H_2O at the Fe_2O_3 / Fe_3O_4 interface to form more Fe_3O_4 layer. This requires the dissolution of the bulk steel. Fahlman et al. extended the mechanism to explain how the ES form of PANi could protect

against corrosion. They proposed that electrons from the steel are donated into the lowest unoccupied molecular orbital (LUMO) of ES. This results in a positive charge on the steel surface which then spreads resulting in a charged Fe_2O_3 layer. The Fe_3O_4 layer is then stabilised and prevented from growing thicker and thus reduces the dissolution of the bulk steel as there is an electron deficiency resulting in a shift in corrosion potential to that of a more noble metal. This proposed mechanism supports the idea that PANi is required to adopt a reduced form in order to provide protection against corrosion.

Wessling [75]. supported the above discussed and proposed the mechanism in diagram form (Figure 3.29), highlighting the requirement of PANi to cycle between its oxidised and reduced forms.

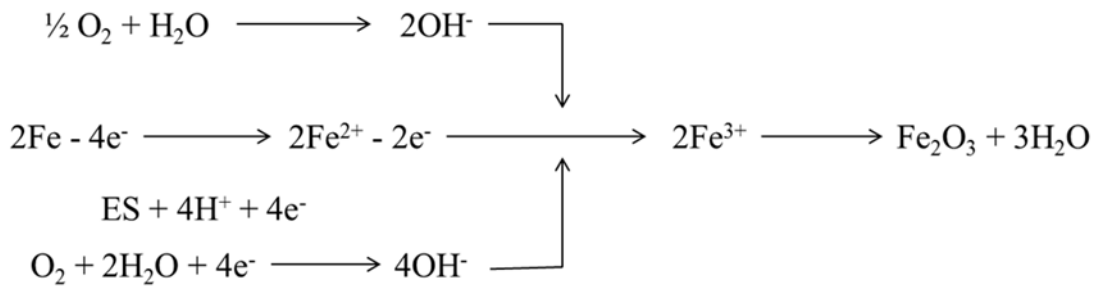

Figure 3.29 - Diagrammatic representation of oxide layer formation

Rout et al. [71] undertook EIS to determine the effect of PANi on the surface of mild steel. A flaky iron oxide layer was identified (Fe_2O_3) and the authors hypothesised that the presence of PANi forces the formation of ferric rather than ferrous oxide. The ferrous iron was reported to be more soluble in water. Thus it can be concluded that, if ferrous iron is present, oxidation, and therefore dissolution, of the bulk steel will proceed at a greater rate. Pan et al., using Scanning Kelvin Probe Force Microscopy (SKPFM), studied PANi coatings and concluded that their findings supported the proposed mechanism, namely that PANi prevents corrosion by enabling the formation of a passivating film of iron oxide [82].

There have been several scanning kelvin probe (SKP) studies undertaken on coatings formed from PANi-ES dispersed in a binder. Here the authors induced a defect into the coating and then used SKP to study the potentials around the defect site [98, 99]. This allowed the authors to study the effect of polyaniline on cathodic delamination. The studies concur that PANI-ES polarizes iron to the extent that an oxide film begins to form which protects the iron substrate. When cathodic

delamination takes place, the alkaline conditions eventually leads to all the doped polyaniline salts being converted to non-conducting PANi-LB which does not offer protection [100]. Therefore, PANI-ES can only delay cathodic delamination rather than prevent it [99]. Further SKP work by Rohwerder et al. concluded that PANi may be better at protecting in an immersive environment rather than an atmospheric environment because under immersion the entirety of the PANi coating is available to contribute to the passivation of the defect. Under atmospheric conditions, only the coating area in contact with the electrolyte film is active and passivation is unable to occur ass the current density required for passivation cannot be overcome[101].

There is evidence to suggest that the deposition solution plays a part in PANi's protective capabilities. This is unsurprising given that the solution anions will act as dopants for the effective salt form of polyaniline. Kraljic et al. [102] electropolymerised PANi from both sulphuric and phosphoric acid (both 0.5 M) on low alloy steel and found that phosphate deposited PANi provided better protection in acidic solutions, than PANi deposited from sulphuric acid. Ahmad attributed the improved protection capabilities of phosphate-based PANi to the formation of $FeHPO_4$ which improved the passivation and adhesion of the PANi film [103]. Similar results were reported by Moraes et al. for deposition from phosphate buffer solutions [81]. It was concluded that high concentrations of phosphates were required to produce a strong passivation layer and that phosphates are incorporated into the PANi film to counter the charge that builds up when PANi is oxidised. They concurred with Ahmad that $FeHPO_4$ would form at high phosphate concentrations but also deduced that at low phosphate concentrations, $Fe(H_2PO_4)$ would form. The lower solubility of $Fe(H_2PO_4)$ would result in the formation of a poorer phosphate layer. However, the authors did not take into account the fact that both these proposed compounds require ferrous iron rather than ferric and thus their research in some way contradicts the view that PANi protects against corrosion by forcing the formation of ferrous iron. Holness et al, following an SKP study on the cathodic delamination of PANi-ES coatings, concluded that the salt used to dope the polyaniline is extremely important to the protection capabilities. [99] Moraes' proposed mechanism is very similar to that proposed by Yagan et al. [104] as a result of their work with deposition from oxalic acid solution, which led them to conclude that iron oxalate contributed to corrosion protection .

3.2.3.2 PANi's ability to protect against corrosion in chloride containing media

It seems apparent that those authors who have reported good corrosion protection in chloride containing media have electrodeposited their PANi coatings from oxalic acid [91] or phosphate [102] [81, 105] containing deposition solutions with the exception of Vera who obtained AFM results that suggested a PANi film alone (deposited from nitric acid) was sufficient to prevent chloride movement [84]. Those who have found poor performance in chloride media have deposited from sulphuric acid [106]. Chemical deposition of PANi has also produced effective

corrosion protection in chloride containing media when doped with a suitable material [83, 107, 108]

In summary the literature demonstrates that, in terms of ease of deposition and demonstrable corrosion protection, as long as the correct deposition conditions are chosen, PANi is a plausible alternative conducting coating to PoDA.

3.3 Templating of porous polymers

Previous work undertaken at nCATS identified that if a coating were to be made porous then channels would be created within the coating [2]. This would potentially allow healing agents to be more evenly distributed through the coating rather than sit near the surface as is the case with most current self-healing systems. Therefore, one of the primary aims of the project is to produce a porous polymer coating which incorporates a self-healing mechanism. An idealised coating and its mechanism of healing is shown below.

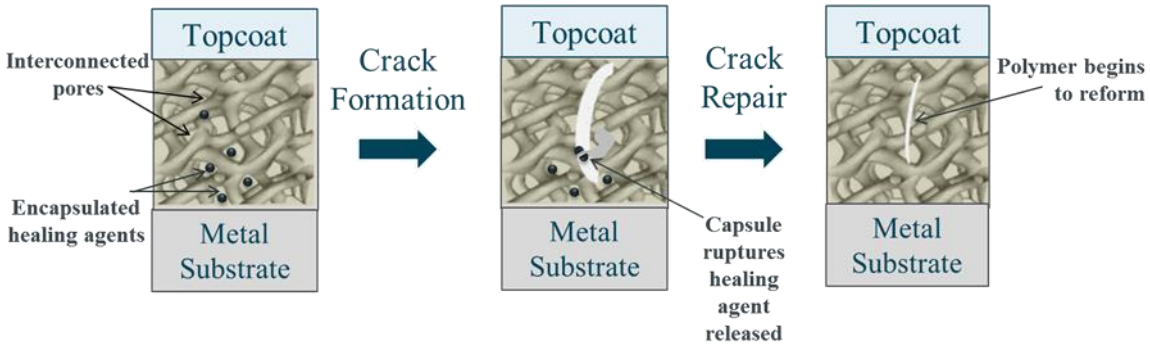

Figure 3.30 - Schematic of self-healing coating function

There are two primary methods currently used to obtain a porous material through templating; liquid crystal templating and solid templates using silica. Both methods work on the premise that a template that contains pores will cause the templated material to be porous as well. There are several pore sizes that can be achieved, varying from a few angstroms to several nanometres.

The International Union of Pure and Applied Chemistry (IUPAC) conventions on mesoporous materials defines a mesoporous material as one which contains pores of an intermediate size (between 2 nm and 50 nm) [109]. Pores that are greater than 50 nm are macropores and those with diameters of less than 2 nm are classed as micropores, despite this being somewhat of a misnomer.

The aim of this project is to produce a conductive polymer that incorporates a porous network capable of storing healing agents. A macroporous network might disrupt the conductivity of a conducting polymer [110] and a microporous network may well be too narrow to store sufficient healing agents, especially if microcapsules rather than nanocapsules are used. Therefore, a mesoporous netwrk appears to be the most viable option for this project. The storage requirement for the polymer means that a 3D porous structure is preferable to a two-dimensional (2D) structure. Mesoporous materials have extremely large surface areas as a result of an open framework structure with a narrow distribution of pore sizes.

3.3.1 Hard templating methods

Hard templating of mesoporous materials was made possible by the development of MCM (Mobil Crystalline Materials) in the 1980s. MCM-41 has 2D-hexagonal pores whilst KIT-6 contains 3D cubic pores.

Since then, the mesoporous MCM materials have been used as templates for a variety of materials from metals [111] to carbon structures [112]. More difficult, is the templating of polymers as polymers are considerably less rigid than metals and therefore the pores have a tendency to collapse [113]. Hard templating proceeds in three stages: (i) the precursor infiltrates the template's mesochannels; (ii) the conversion of the precursor into its final form takes place within the channel and (iii) the template is removed either thermally or chemically [112]. In order for the templated network to be regular the following requirements must be met. The template itself must be pre-formed, well-ordered and contains small mesotunnels inside the template boundaries [114]. If this is not the case then the replicated network will not be able to maintain its structure once the template is removed which will result in low symmetry products [115].

Johnson et al [116] succeeded in producing mesoporous polymers by using colloidal silica with a particle size of 150 – 300 nm. In this case the silica particles themselves caused defects (holidays) in the polymer film, resulting in a porous structure. They found (via TEM images) that sintering was crucial to reproducing the porous structure onto a polymer template and that pore size was dependent on the initial concentration of monomer; the higher the initial concentration of monomer, the smaller the pore size that resulted. If this phenomenon is replicated in liquid crystal templating it raises the possibility that pore size can potentially be tuned by changing the initial dopamine concentration. This also has implications for potential film thickness since higher concentrations of dopamine monomer result in thicker PoDA films. However, the most significant problem with using a hard templating method is that, typically, an aqueous solution of 48% HF is required for the removal of the silica template.

Hard templating has also been used successfully to produce a mesoporous conducting polymer [117]. More importantly, the polymer in question was PANi which has been identified as an alternative polymer for this project if the coating thickness of PoDA cannot be sufficiently improved. It also offers encouragement that it is indeed possible to template conducting polymers. However, the template was based on MCM-41 mesoporous silica resulting in the PANi coating having 2D- hexagonal pores. In order to incorporate healing agents, the pores of the coating used in this project need to be 3D and cubic. In addition, 48vol.% aqueous HF solution was needed to remove the silica template which hardly qualifies as deposition under mild conditions

3.3.2 Soft templating methods

A soft templating method is one in which the template can be removed using either alcohol or water, as opposed to the much harsher chemicals, such as HF, that are required for the removal of hard silica templates [113]. Generally speaking, the soft templating methods rely on the use of liquid crystals.

3.3.2.1 Liquid crystals

A solid (crystalline material) possesses long-range positional order. Liquid materials possess no long- range order, either periodic or orientational. In between the classes of ordered crystals and disordered liquids fall liquid crystals with partial atomic disorder. They possess no long-range positional ordering but do possess a degree of long-range orientational order [118].

There are two broad categories of liquid crystals (LCs) which are distinguished by how they change phase [119]. Thermotropic liquid crystals occur on the melting of solid surfactants while lyotropic liquid crystals form on the combination of solvents and amphiphillic materials [120]. There are three possible outcomes when water and amphiphillic materials (in this case a surfactant) are combined.

1. The surfactant is insoluble and remains as a solid with some surfactant monomer forming an aqueous solution. This is a similar process to adding water to solidified bacon fat. Such surfactants are more likely to form thermotropic rather than lyotropic liquid crystals.

2. Some surfactant dissolves forming a micellar solution such as when a bar of solid soap is placed in water.

3. A lyotropic liquid crystal forms. This is a fine balance; if more water is added, the liquid crystal collapses to a micellar solution.

Both the thermotropic and lyotropic classes contain several sub-categories of structures known as mesophases. The mesophases of thermotropic liquid crystals are solely dependent on temperature, making it relatively facile to obtain a desired mesophase .The mesophases of lyotropic liquid crystals have much more complicated structures, which are dependent on the ratio of surfactant to solvent as well as temperature. The deposition of PANi and PoDA occurs from aqueous solution which is not compatible with the use of thermotropic LCs and therefore, the more complex lyotropic liquid crystal mesophases must be used.

3.3.2.2 Lyotropic mesophases

Lyotropic LCs can take several forms (mesophases) depending on the ratio of surfactant to solvent [121]. Figure 3.31 shows the idealist change in mesophase structure as the amphiphile (surfactant) concentration is increased. However, not all surfactants will be able to form all mesophases, and the mesophases do not always form in the order presented in Figure 3.31. Therefore, the mesophase evolution of each surfactant must be considered on an individual basis. In addition to surfactant concentration the mesophase can be affected by the shape of the surfactants. Those surfactants with large hydrophilic elements and small hydrophobic elements tend to form normal mesophases more readily. In this particular case, the use of deposition solutions that contain an organic element such as oxalic acid, means the micelle packing may be disturbed by the hydrocarbon chains. This will affect the surfactant concentrations at which a given mesophase will occur.

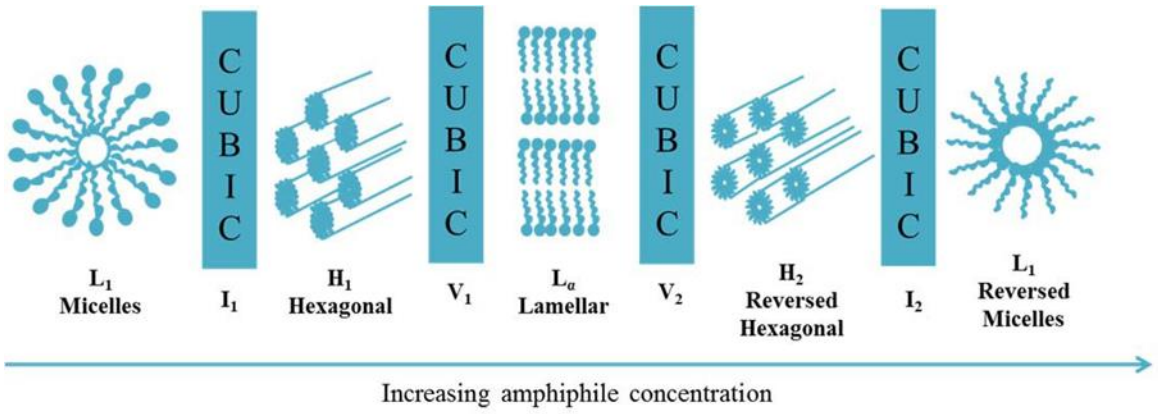

Figure 3.31 - Effect of increasing amphiphile concentration on the shape of the lyotropic mesophase

The I_1 and I_2 phases refer to cubic micellar structures which are unstable [122]. Instead the cubic phases of interest are V_1 and V_2 which are bi-continuous, more stable and are discussed in greater detail further on.

The structures of the lyotropic mesophases can also be considered in terms of mean interfacial curvature (Figure 3.32) where the interface in question is the polar or apolar/water interface. In normal mesophases the polar/apolar interface curves away from the aqueous element. The lamellar phase has no degree of curvature as it is completely planar. In reverse phases, the polar/apolar interface curves towards the aqueous phase.

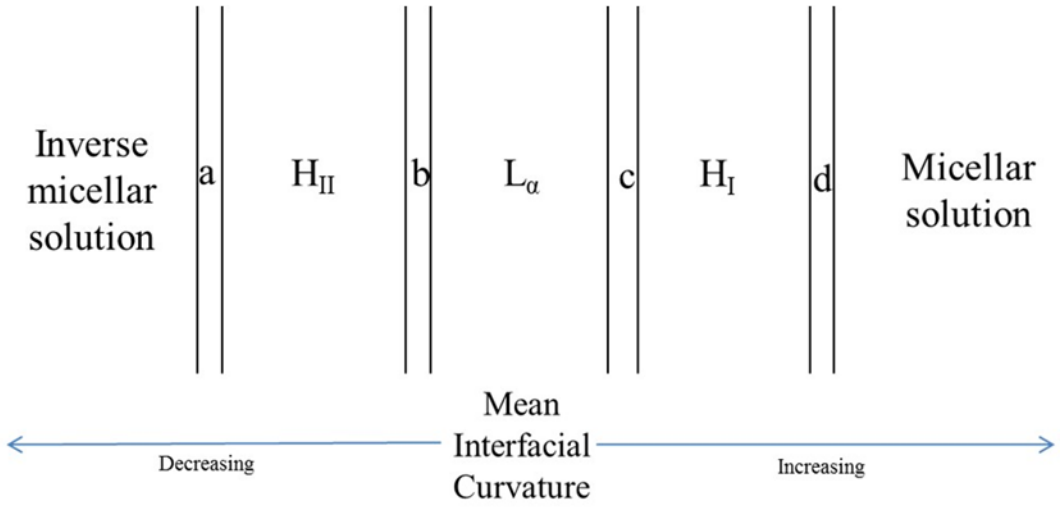

Figure 3.32 - Dependence of mesophase structure on surfactant to solvent ratio. (a) and (d) are unstable micellar cubic mesophases. (b) and (c) are stable bi-continuous cubic mesophases, H_I is the normal hexagonal mesophase and H_{II} is the reverse hexagonal mesophase

Lamellar phases have a 1-dimensional (1-D) arrangement of surfactant molecule bilayers that are separated by water layers (Figure 3.33). They have can have diameters of several microns with the separating water layers of between 8 and 100 Å, and are considered the most simple mesophase.

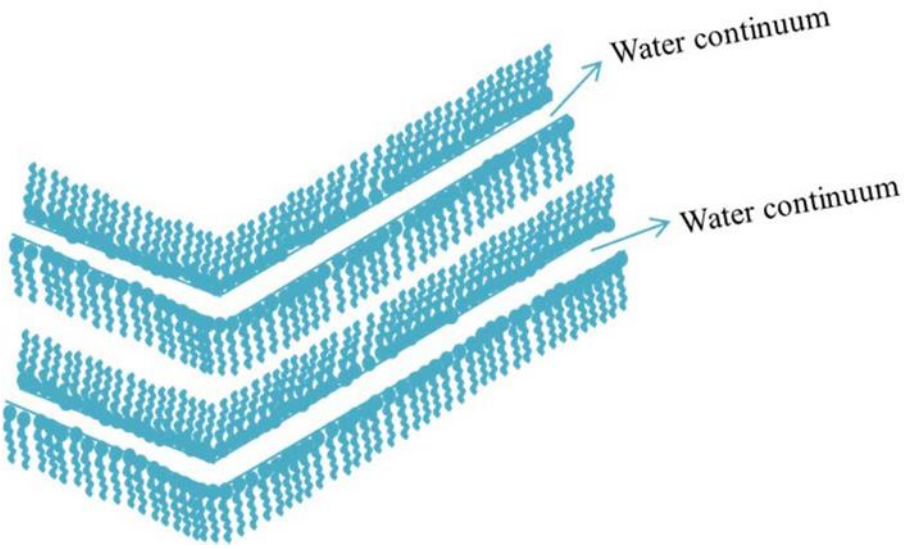

Figure 3.33 - Lyotropic lamellar mesophase: alternating amphiphillic bilayers and water continuum interlayers; the bilayers can be of infinite length

The hexagonal phase is 2-dimensional (2-D) and has two possible phase structures

- normal hexagonal (H_I) which consists of amphiphillic surfactant micelles arranged in rods of an indeterminate length in a hexagonal array surrounded by a water continuum (Figure 3.34a).

- reverse hexagonal (H_{II}) where it is the H_2O solvent that is arranged into hexagonal rods with the surfactant micelles arranged in the space surrounding the rods (Figure 3.34b).

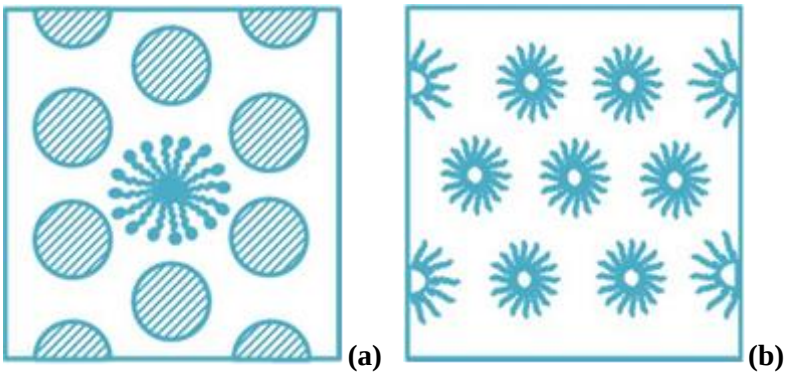

Figure 3.34 - (a) The normal hexagonal phase: hexagonally packed amphiphillic cylinders surrounded by a water continuum. (b) the reverse hexagonal phase: cylinders of water surrounded by an alkyl continuum

The micelle packed cubic phase can also exist in normal and reverse phases and consists of either normal (I_1) or reverse micelles (I_2) in a cubic packed arrangement with body centred cubic (BCC) packing being the most common [121]. In the case of cubic liquid crystals, a normal LC has cubic packing of surfactant micelles with an aqueous continuum (Figure 3.35a) and the reverse mesophase consists of a micelle continuum (Figure 3.35b). These are the unstable I_1 and I_2 phases.

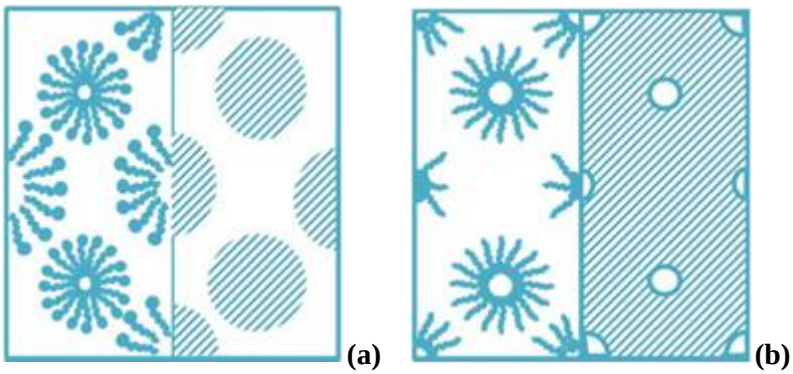

Figure 3.35 - Cubic phase showing cubic packing of (a) normal micelles and (b) reverse micelles

The V_1 and V_2 cubic phases consist of a bi-continuum of either two surfactant layers that intertwine, but never meet, surrounded by water (the normal phase), or two water layers that intertwine, but never meet, and are surrounded by surfactant micelles (the reverse phase).

As the aim of this study is to produce a polymer with a 3-D structure, a cubic phase liquid crystal will need to be used as the template. The V_1 and V_2 are more stable and so these are preferable as templates over I_1 and I_2 phases. As has been previously stated, both polydopamine and polyaniline are formed from aqueous solutions so the position of the aqueous solution within the liquid crystal will need to be carefully considered. In practical terms this means the determination of whether a normal or inverse liquid crystal is required. The polymer needs to possess pores that can contain the microcapsules required to hold healing agents and/or corrosion inhibitors and therefore the normal cubic mesophase is required (see Figure 3.36). This makes determining the optimum surfactant to aqueous solution range even more critical: whilst reverse mesophases are stable in excess solvent, normal mesophases rapidly collapse to a structure-less micellar solution.

Figure 3.36 - Cubic mesophase showing channel network (white areas) and pores (blue areas)

The monomer that is contained in the water continuum (the blank area of Figure 3.36) will be polymerised by electrochemical oxidation around the amphiphillic arrangement (blue area of Figure 3.36). Once the polymer has formed, the surfactant template can be removed with a water/ethanol wash leaving behind an empty channel network of interconnected pores where the surfactant template once was. These channels can then be filled with pre-prepared micro- or nanocapsules which contain healing agents and/or corrosion inhibitors.

3.3.2.3 Liquid crystal templating

There have been numerous instances of using liquid crystal templating to create mesoporous materials in a wide variety of pore sizes and shapes. However, the overwhelming majority of these have been templates for silica-based materials or metallic oxides which have then been used as molecular sieves. Few instances of templating for polymers have been recorded, and even fewer for conducting polymers.

Two main synthetic strategies for liquid crystal templating have emerged in recent years. One strategy is co-operative self-assembly, where inorganic species are forced to interact with surfactants through coulombic forces. The inorganic species polymerise at the inorganic/surfactant interface and cross-link with the surfactants. A charge density builds up between the surfactant and the inorganic species and this charge density must be equal between the inorganic and organic (surfactant) species for assembly to occur. As a result of the charge density phase separation occurs, and the subsequent reorganisation into an ordered 3D arrangement will always be that of the lowest energy. The second strategy, also referred to as true liquid crystal templating, requires high concentrations of surfactants in order to form micelles. This results in improved condensation of the inorganic precursor which leads to more confined growth of the porous species around the surfactant micelles. After condensation, the surfactant template can be easily removed with water, leaving a highly symmetric mesoporous network of the inorganic material behind.

Very little research has been undertaken that has been application focussed or that has tried to develop a templating procedure for a specific polymer, as we are attempting to do for PANi. In addition, much of the little application-focussed research that has been undertaken has been directed in the fields of biological membranes [123] and electronics [124] so the resultant polymer films have been thin, either by design or as a limitation of deposition technique. Where the technique was limiting, this was not considered an issue as only thin films were required for the applications.

However, there are great difficulties with the electrochemical deposition of coatings onto mild steel. Bender et al. [125] used Indium Tin Oxide (ITO) glass as their substrate which is considerably less active than the mild steel used in our experiments.

Poly(oxyethylene) alkyl ethers, such as Brij 56, are commonly used as the amphiphillic mesogen component of a lyotropic liquid crystal template. In such cases, water serves as the solvent. There is evidence to suggest that varying the length of the alkyl chain will vary the diameter of the pore size [126]. In addition, larger pore sizes can be achieved if a hydrophobic element, such as heptane, is added to the template. The hydrophobic additive dissolved the interior of the ordered liquid crystal phase which widens the pores. However, the ratio of polar additive to surfactant must be carefully controlled (no more than 1% w/w of hydrophobic component) otherwise too much of the template structure will be dissolved and the ordered micelles will begin to collapse, rendering the template unusable [127].

There has only been one recorded instance of using liquid crystal templating to produce conducting polymer films [128]. Hulvat et al. used electropolymerisation in the hydrophobic domain to produce PEDOT (polyethylenedioxythiophene) films. No films were formed when the template was heated to above the isotroperisation temperature. The authors investigated electropolymerised liquid crystal templating as ethylenedioxythiophene is insoluble in water and cannot be easily chemically oxidised. They managed to achieve a film thickness of 1.5 μm after only 250 s using a 1 A current; having identified that charge density is the most important parameter affecting electrochemical liquid crystal templating. However, Hulvat et al. used ITO glass as their substrate and this is considerably less active than the carbon steel required for this project. This is the greatest limitation to using an electrochemical mediated templating method, as severe pitting corrosion occurs during the deposition.

Bender et al. [125] identified that using a lyotropic liquid crystal template in conjunction with electropolymerisation imparts a high degree of control over both the templating and the polymerisation process. This is especially true of control over the film thickness which, considering encapsulated healing agents need to be incorporated into the coating, is an important consideration for this project.

Jang and Bae found, when templating polyacetonitrile, that the ratio of polymeric precursor to surfactant was crucial [129]. If the ratio was too small then there was insufficient surfactant to form micelles but excess polymeric precursor meant the solution was too viscous to successfully template the polymer. The authors sought an alternative method having identified that conventional liquid crystal templates are unsuitable for some polymers as phase separation between the monomer and surfactant can occur and destroy the developing polymeric network. Instead the authors used reverse microemulsion. This consists of a surfactant, water, dissolved salt and stabilising oil. The microemulsion is termed reverse because the water is dissolved in oil rather than the other way round. The surfactant water mix forms a miceller structure in the same manner as a liquid crystal and the polymerisation takes place around the micelles [130]. As far as PoDA is concerned, this work is very interesting as it demonstrates that as long as the polymer is soluble in aqueous solutions (which PoDA is), there is an alternative to the electrochemical liquid crystal templating demonstrated by Hulvat et al. However, as PANI is to be used for templating, such a method would be unsuitable. In agreement with other researchers, [116, 131] Jang and Bae identified that surfactant chain length and surfactant concentration are crucial in tuning the resultant pore size of the templated material.

If the mesopores are approaching 50 nm diameter (the maximum size as defined by IUPAC), then they are potentially wider than the thickness of the deposited PoDA coating and so the liquid crystal templating was carried out on polyaniline only.

In order to successfully incorporate a 3-D porous network into polyaniline, the aniline monomer will have to be incorporated into the aqueous component of a soft-templating system with the non-aqueous component being some form of surfactant. Within a defined temperature range and narrow range of surfactant: water ratios, a 3-D liquid crystal will form and act as template. The application of an external potential will force the polymerisation of the aniline monomer around the 3-D template meaning the polymer will take on the 3-D structure with pores where the liquid crystal was prior to removal with an ethanol/water mix. However, oxalic acid (is an organic acid which means it may interfere with the assembly of the liquid crystals as the incorporation of hydrophobic or hydrophilic elements can affect resultant pore size [124] and the ratio of surfactant: aqueous component required for successful assembly of 3-D structures [121].

Therefore, the standard phase and mesophase structure diagrams that have previously been calculated and produced for individual surfactants and shown the relationships between temperature and surfactant: aqueous component ratio and the resultant mesophase can no longer be used. Therefore, the correct ratio of surfactant: aqueous component will have to be re-determined for each surfactant that is tested to account for the incorporation of oxalic acid into the aqueous component. Fortunately, this can be done with relative ease by examining the gel that forms when the surfactant and aqueous components are mixed using polarized light microscopy. It is through this method that the established phase diagrams have been constructed [132].

3.4 Self-healing materials

Self-healing materials can be classified into two categories, either autonomic or non-autonomic [133]. Those materials which are autonomic will heal themselves with no external intervention, whilst non- autonomic materials will require some form of external intervention or trigger, such as UV radiation or heat [134] in order to initiate healing. The use of microcapsules containing healing agents would constitute an autonomic self-healing process, being initiated solely by damage which occurs to the surrounding polymeric matrix while the healing agent is released by the simultaneous rupture of a microcapsule containing healing agents.

There are multiple mechanisms by which self-healing materials can operate, including reversible cross-linking and nanoparticle migration. However, the focus in this report will be on a method of storing healing agent, namely microcapsules. Microcapsules work on the basis that they are incorporated into the polymer coating itself, usually by being dispersed into the matrix. Whilst the majority of existing work has incorporated the microcapsules directly into the coating, as opposed to inside a porous network, the added benefit of a network is that, in theory at least, it should be much easier to replace the microcapsules once their contents has been used in a healing reaction. Microcapsules work on the premise that when a crack or defect forms in the polymer network, the microcapsule is ruptured, and the healing agent(s) is/are released and drawn into the crack by capillary action. The healing agents then undergo a chemical reaction, be it a catalysed polymerisation or the covalent bonding to another material, which heals the crack.

3.4.1 Use of microcapsules

Smart coatings used for anti-corrosion are generally designed to respond to some sort of environmental change associated with a corrosion process, such as a change in pH or potential. The coating system consists of a passive barrier coating, such as an epoxy, with an even dispersion of nano-or microcapsules that contain healing agents or corrosion inhibitors. Change in pH is the most favoured stimuli as the formation of localised anodes and cathodes during the initiation of the corrosion process are accompanied by pH changes. Bernsmann et al. [28] found that PoDA films deposited on silicon oxide began to disintegrate within 1 hour when exposed to high pHs (12-14). This is interesting, as the presence of cathodic corrosion reactions at the metal substrate often results in the increase of localised pH to very elevated levels. Therefore, it is possible that PoDA microcapsules would be suitable for use in a pH-controlled healing agent release system.

Microcapsules are droplets of liquid or micron-sized particles of solid that have been enclosed in an inert shell, such as polyethylene [135]. The very first practical example of using microencapsulation as a method of self-healing was developed by White et al. in 2001 [136]. The authors used Grubbs' catalyst (Figure 3.37) to initiate the healing of an epoxy resin with

dicyclopentadiene with both the catalyst and monomer encapsulated. The polymerisation of dicyclopentadiene is a Ring-Opening- Metathesis polymerisation (ROMP) used to produce olefins [137]. Dicyclopentadiene was chosen as the healing material as a result of its strength and ease of integration with existing epoxy.

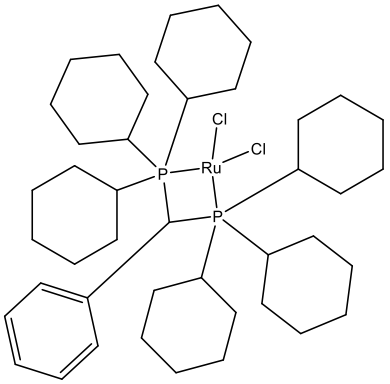

benzylidene-bis(tricyclohexylphosphino)-dichlororuthenium

Figure 3.37 - Grubb's catalyst

Further work by White led to the incorporation of non-encapsulated monomers with the catalyst captured in polyethylene shells [138]. This approach was to make replenishing the supply of both monomer and catalyst much easier as significant problems were encountered with successfully encapsulating the dicyclopentadiene monomer. Whilst a similar strategy would overcome the problem of dopamine monomer and additional oxygen reacting before they are required, the free-flowing monomer solution is unsuitable here as dopamine undergoes autoxidation and would polymerise on its own before it would be required for healing purposes.

The vast majority of self-healing work that has been undertaken using the microencapsulation concept has involved ROMP. This could potentially be applied to dopamine if a material other than PoDA is used to heal defects but this approach may interrupt the conductivity of the PoDA coating. The approach is unsuitable if dopamine is used as the primary healing agent as dopamine cannot undergo ROMP.

At the current moment in time, the PoDA coating is in the region of tens of nanometres thick [42, 49]. Thus, incorporating microcapsules into the coating will be very difficult and may cause the disruption of polymer properties, especially conductivity. Therefore, the healing agents would have to be incorporated into nanocapsules rather than microcapsules. Fortunately there has been recent research into the development of PoDA nanoparticles which showed promise towards being developed into hollow nanoparticles through a self-assembly method. The challenging aspect of using PoDA to encapsulate dopamine is that dopamine is known to polymerise and deposit onto

existing PoDA coatings [28]. However, this is not an issue when PANi is used as the coating matrix because of the much greater thickness of the PANi coating compared to the PoDA coating. Because aniline monomer is hydrophobic, it is relatively facile to use the emulsion templating methods [139-141]. The fact that PANi coatings are much thicker also means that microcapsules can be used.

The presence of the microcapsules is crucial to the successful performance of the smart coating and therefore their design and function must be taken into careful consideration. The most significant requirements for the design of suitable microcapsules are:

- The microcapsule should be chemically compatible with the surrounding polymer matrix and the size of the microcapsule should be carefully considered to ensure the stability of the overall coating. For example: autoxidated PoDA films are about 45 nm thick and adding a container that is a few μm in diameter will disrupt the barrier properties of the coating which is likely to increase the rate of substrate corrosion rather than decreasing it;

- The microcapsule should contain as much inhibitor or healing agent as possible without the contents leaking out under normal conditions;

- The healing contents of the microcapsule should be fast acting to minimise exposure of the underlying substrate to the corrosive environment.

Some polymerised hollow nanocapsules with porous walls have been created which allow easy diffusion of the capsule content out of the hollow interior. If the molecular size of the contents is larger than the pore size then the contents will remain in the capsule interior. However molecules that are smaller can freely diffuse in and out of the capsule. This has been used to trap porphyrin rings within a polymeric capsule [142]. The porphyrin ring was formed within the capsule itself after the constituent parts had been transported into the capsule through small pores.

Because the smaller capsules hold less healing agent than their larger counterparts, a larger weight fraction of the capsules will be required in order for self-healing to be of the same efficacy. Rule et al. [143] found that the total mass of healing agent available for delivery per crack area is dependent on both microcapsule weight fraction and the diameter of the microcapsule.

$$n = pN \qquad \text{Eq. (3.11)}$$

Here n is the number of capsules that rupture, p is the probability that a capsule lies within the crack area and N is the total number of capsules present in the crack area.

$$p = \frac{r_S A d_C}{M_S} \qquad \text{Eq (3.12)}$$

The probability (p) is dependent on r_S (sample density), A is the crack area, d_C is the capsule diameter and M_S is the total mass of the polymer sample

The mechanical properties of the capsule are one of the primary means of the control of release of microcapsule contents. In the case of spherical microcapsules, the radius of the inner core and the outer shell thickness are the most crucial parameters. In self-healing concrete, cylindrical capsules have been found to be more effective at releasing healing agents [144] than their spherical counterparts, but they are far more difficult to synthesise. Using nano-carriers, rather than capsules in the micrometre domain, increases the absorption of the shell contents as they have a larger effective surface area combined with a greater ease of dispersion throughout the polymeric matrix [145].

However, it should be noted that the majority of work involving nano-carriers has bio-focussed applications, whereas self-healing applications have tended to use smaller microcapsules. For self-healing polymers, microcapsules are required as nanocapsules do not provide a great enough probability that a capsule will be present in the damaged area and thus rupture at the same point in time as damage occurs to the polymeric matrix (Equation 3.12). This limits the self-healing capabilities and allows time for corrosion reactions to be initiated at the surface of the underlying substrate.

The use of templated capsule formation procedures allows greater control over the thickness of the shell wall and capsule diameter. There have been several instances of templated formation of PoDA microcapsules [39, 40, 141, 146], including the incorporation of liquid healing agents [140, 147] which is crucial if the capsules are to contain aniline monomer as a healing agent. Hilloulin et al. found that monitoring the compatibility of the encapsulated healing agent with the shell material was essential as the compatibility of some materials differed greatly with time [148].

Traditionally capsules were formed from organic solvents. However such methods often require sonication or heating to force the formation of capsules, which can be extremely damaging to the contents of the capsule. Therefore, layer-by-layer construction based on emulsion polymerisation is a more suitable method [145].

There have been several patents filed for the use of microcapsules in the use of smart coatings [149-152] including for the construction of a self-healing golf ball [153]. Whilst all the patents are very general and far-reaching, and list many combinations of polymer matrices and capsule materials, none of them relates to the use of conducting polymers as the polymeric matrix, or to the use of PoDA as the material used in the construction of the microcapsule.

An alternative to looking at dopamine or aniline monomer as the healing agent is to use another type of polymer. Hurley and Huston [154] have been successful with using Ethylene Vinyl Acetate (EVA) in conjunction with a feedback system that used an electrical current to heat solid EVA that had been incorporated into the polymer coating. Being a thermosetting plastic, EVA melts easily and the readily flows into the defect area where it cools as it returns to a solid form to heal the defect. This highlights the importance of the glass transition temperature (the temperature at which the polymer enters into the glass state (Tg)). If the Tg is too low, the polymer can potentially be melted at atmospheric temperature, particularly in equatorial regions of the globe. If Tg is too high, then a very high current will need to be applied to melt the healing polymer. If the host polymer is not a thermosetting plastic then the application of a current and subsequent generation of heat has the potential to induce further damage to the coating.

There has been some success with incorporating the concept of self-healing into electrically conductive materials [155]. Williams et al. worked on the basis that a disruption of the conducting polymer through a microcrack would increase the resistance of the coating as conductivity would be disrupted. If the coating were to form part of a circuit that also incorporated a voltmeter and ammeter, if measured resistance increased as a result of a crack, then the system could feedback to increase the applied voltage. The increased voltage, coupled with increased resistance, would result in heat generation which would cause the polymer to heal. This work was undertaken on N-heterocyclic carbenes and the effect is similar to that of Hurley and Huston [154] as discussed. However, the additional benefit of using a conducting polymer is that no additional sensing network is required which is extremely beneficial as they are difficult to design and incorporate [156]. Instead, the simple inclusion of a voltmeter and ammeter is sufficient.

In summary, the use of capsules filled with healing agents is well known in the art and will be the most straightforward means of incorporating self-healing capabilities to the 3-Dimensional coating. Polydopamine has successfully been used to create microcapsules and, in some instances, these have been used to hold liquids. Furthermore, one of the reasons for the current popularity of polydopamine as a material is its ability to remain unaffected by its external environment, making it an ideal choice for microcapsules which will be placed in a matrix formed from another polymer. Therefore, polydopamine capsules will be used in the work which attempts to impart self-healing functionality to the 3-Dimensional coating.

Chapter 4 Techniques

4.1 Electrochemical Impedance Spectroscopy (EIS)

Electrochemical impedance spectroscopy (EIS) is used to describe how a circuit responds to the application of an alternating current (AC). For a direct current (DC) circuit, resistance, to the flow of electrons, can be described by Ohm's law (Equation 4.1).

$$E = IR \qquad \text{Eq. (4.1)}$$

Where E = potential, I = current and R = resistance. Hence, in the DC circuit, only one type of electrical component satisfies this relationship; the resistor. However, the resistor is idealised in that it obeys Ohm's law at all current and voltages and is unaffected by frequency.

Systems that are not idealised (i.e., real life AC circuits) have more complex behaviour. They behave differently depending on the applied AC frequency and often have different behaviour if the current or voltage changes. In addition, AC circuits have additional elements that can also resist the current, namely inductors and capacitors. As a result, a much more complex description of resistance to electrons is required and this is provided by impedance.

Impedance, like resistance, refers to the ability of a component to reduce the flow of electrons (Equation 4.2) but it impedes the flow of electrons rather than resists current. The total impedance of an AC circuit is the combined opposition of all resistors, inductors and capacitors to the flow of electrons.

$$Z = \frac{E}{I} \qquad \text{Eq. (4.2)}$$

However, as AC is cyclic, impedance must also describe how voltage and current are variable with time. A phase angle is usually used to depict the time shift. Thus, impedance actually comprises two parts; the ratio of voltage to current which gives the magnitude of the impedance and the phase. In addition, the frequency must also be taken into account. This information can all be depicted on a Bode plot.

Impedance needs to be represented as a complex quantity. Two expressions are required, one for the potential (Equation 4.3) and one for current (Equation 4.4).

$$E(t) = E_O \exp(j\omega t) \qquad \text{Eq.(4.3)}$$

$$I(t) = Z_O \exp(j\omega t - j\phi) \qquad \text{Eq (4.4)}$$

Where Z_0 is initial impedance, j is $\sqrt{-1}$, ω is $2\pi f$ (where f is the applied frequency), t is time and ø is the phase shift in degrees.

The two equations (4.3 and 4.4) can then be combined to give a complex number expression for impedance (Equation 4.5)

$$Z = \frac{E}{I} = Z_O \exp(j\emptyset) \qquad \text{Eq. (4.5)}$$

Equation 4.5 demonstrates that impedance is actually composed of real and imaginary parts. Plotting of the real part (*x*-axis) against the imaginary part (*y*-axis) gives a Nyquist plot. Figure 4.1(a) shows, Nyquist plots allow the modulus impedance, |*Z*|, to be established as a vector quantity. The grey box represents a point on the Nyquist plot (the impedance at a given frequency) and the vector length is the value of the impedance modulus. The angle between the vector shows the phase shift. Figure 4.1(b) demonstrates the same point (grey box) in terms of Cartesian coordinates. It should be noted that the major downside of the Nyquist plot is that it does not show at which frequency the impedance was obtained. Therefore, Bode plots which plot |*Z*| and the phase shift angle against frequency are used as well.

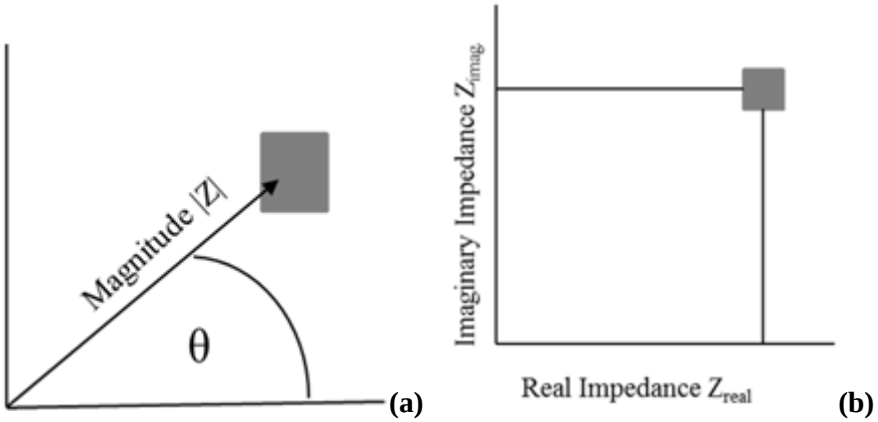

Figure 4.1 - Representation of the same impedance by (a) Vector Polar coordinates and (b) Complex plane Cartesian coordinates.

|Z| can be more easily determined through Equation 4.6

$$|Z| = \sqrt{\left({Z_{real}}^2 + {Z_{imag.}}^2\right)} \qquad \text{Eq. (4.6)}$$

4.1.1 Experimental set-up

The EIS set-up used in the current work is shown in Figure 4.2 below. The working electrode is the sample under investigation. The solution used as electrolyte was 3.5% NaCl in order to replicate the seawater encountered in ballast tanks.

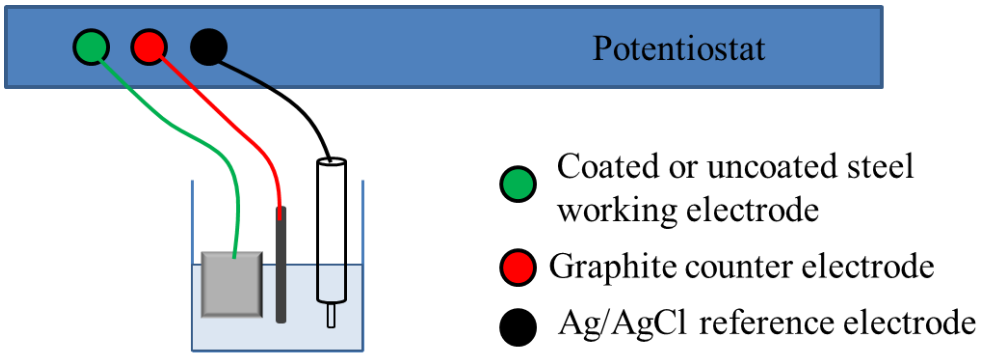

Figure 4.2 Experimental set-up for EIS

In order to minimise noise interference, the beaker containing the immersed electrodes is placed in a grounded Faraday cage.

4.1.2 Equivalent circuits and circuit elements

Coating systems and their associated electrochemical processes can be considered as behaving like electrical circuits. Therefore, aspects of the system can be likened to electrical circuit elements such as resistors and capacitors. Usually, a theoretical model of the processes occurring at the polymer/metal interface and the polymer solution is devised. The processes involved are then assigned an equivalent electrical circuit element. The electrical elements are then combined, in series or parallel, to produce an idealised electrical circuit. The fit between the proposed electrical circuit and the obtained data is compared using a non-linear least squares regression method (see section 4.1.3).

Each circuit element has a relationship between impedance and phase shift which can be written in terms of complex numbers. A resistor reacts immediately to a change in voltage hence the voltage and current waves are exactly in phase meaning there is no phase shift ($\theta = 0°$). Therefore, it can be said that, for a resistor element, impedance is only dependent on resistance and frequency plays no part. This, along with the fact that resistors have only a real component, is demonstrated by Equation 4.7 below.

$$Z_{resistor} = Z_{real} + jZ_{imag} = R + j0 = R \qquad \text{Eq.(4.7)}$$

Capacitors, however, have a phase shift of –90° so the measured current wave will always be 90° behind the applied voltage wave. As a result, the current is at its maximum when the voltage is changing fastest and passes through zero. This also affects the capacitor's frequency dependence; when the frequency is high, voltage changes rapidly which results in a larger current. The relationship demonstrated in Equation 4.8 indicates that the higher the current, the smaller the resultant impedance. Hence at high frequencies, the impedance of a capacitor is small. At very low frequencies, the current begins to approach zero and so impedance becomes massive. Equation 4.8 demonstrates the frequency dependence of a capacitor and that capacitors have only an imaginary component. .

$$Z_{capacitor} = Z' + jZ'' = 0 + j[-1/(2\pi fC)] = j[-1/(2\pi fC)] \qquad \text{Eq. (4.8)}$$

In rare cases, elements known as inductors can be present. Such elements have a behaviour that is opposite to that of a capacitor except for the fact that they too have only an imaginary impedance component. The phase shift of an inductor is +90° and their impedance increases with increasing frequency. However, the inductor is a theoretical concept and does not represent a physical process.

$$Z_{total} = Z_1 + Z_2 = R_1 + R_2 \qquad \text{Eq (4.9)}$$

If elements are coupled in series then their impedances are summed together. However, if the elements are coupled in parallel then the inverse total impedance at a particular frequency will be

the sum of the inverse impedances of the components. Equation 4.10 shows an example of a resistor (R_3) and capacitor (C_4) in parallel taking into account the impedance relationships in Equations 4.8 and 4.9.

$$\frac{1}{Z_{total}} = \frac{1}{Z_3} + \frac{1}{Z_4} + \frac{1}{R_3} + \frac{1}{j\omega C_4} \quad \text{Eq (4.10)}$$

In real electrochemical cells, capacitors do not usually behave in an ideal way. Instead, their behaviour can be described as a constant phase element (CPE) as shown in Equation 4.11.

$$Z = 1/Y^0(j\omega)^\alpha \quad \text{Eq (4.11)}$$

Y^0 is the value of the CPE and α is a measure of the extent to which a CPE behaves like a capacitor. If α has a value of 1.0 then the CPE is acting as a perfect capacitor. An α value of 0.0 means the CPE is behaving as a perfect resistor. The value of α usually falls between these two extremes [157].

If a diffusion process affects the electrochemical reaction under observation, then the resultant impedance is termed Warburg impedance (WI). The diffusion can be either reactant to surface or product away from the electrode's surface. The Warburg impedance is often prevalent if the surface is coated. This can be a deliberately deposited coating, reaction products from surface reactions or species that have been adsorbed onto electrode surface from solution. The WI is expected to have a phase shift angle of 45° in an ideal case and is frequency dependent. At high frequencies, the diffusing species do not move much which results in a small impedance. At low frequencies, on the other hand, the diffusing species move much further from the electrode surface which increases the impedance.

4.1.2.1 Equivalent circuits representing coated metals

The same equivalent circuit, shown in Figure 4.3, is used to represent the situation of a bare metal in electrolyte as well as representing a relatively intact coating applied to a metal substrate in electrolyte. The interpretation of Q2 and R2 is different for coated and uncoated metals. Q has been used to represent a constant phase element.

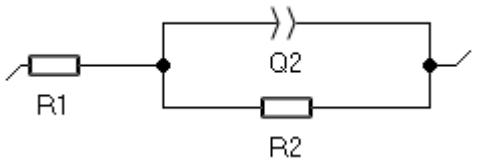

Figure 4.3 Randles equivalent circuit

R1, in both cases, is known as the uncompensated resistance (R_u). The uncompensated resistance is attributed to the resistance of the solution the EIS test is taking place in and the wires connecting the working electrode to the potentiostat. In the case of a bare metal in electrolyte, Q2 represents the double layer capacitance (C_{DL}) which forms at the metal/electrolyte interface and R2 is the polarization resistance (R_p). When the metal is coated, R2 represents the resistance of the coating (R_{coat}) which is sometimes also called the pore resistance as it is generally considered to be an indication of the extent to which electrolyte has penetrated the pores of the coating. The magnitude of R_{coat} may be used a means of indicating the level of coating degradation because the resistance decreases with increased permeation of the electrolyte. Q2 represents the capacitance of the coating. The capacitance of the coating is partially dependent on the dielectric constant of the coating and is also dependent on the thickness of the applied coating.

The Randles circuit would be expected to produce the following plots. Figure 4.4 a shows the typical semi-circular Nyquist plot which is expected for data which fits to a Randles circuit whilst b and c show the Bode magnitude of impedance and phase angle plots respectively.

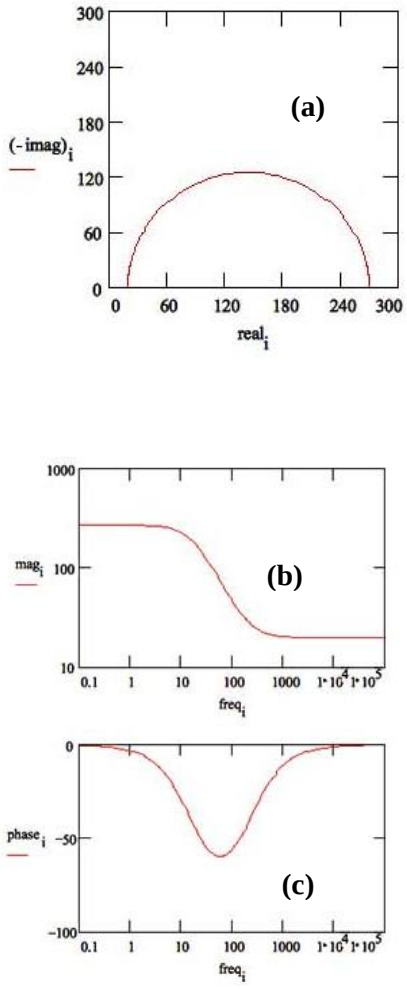

Figure 4.4 - (a) Nyquist (b) Bode impedance and (c) Bode phase angle plots for data that fits to a Randles circuit [158]

When the coating has begun to fail, the circuit shown in Figure 4.5 below is used. The failure of the coating means that the underlying substrate is sufficiently exposed to the electrolyte to allow the processes occurring at the electrolyte/substrate interface to be observed. R1 is the uncompensated resistance, Q1 is the coating capacitance, R2 is the coating resistance, Q3 is the double layer capacitance and R3 is the polarisation resistance.

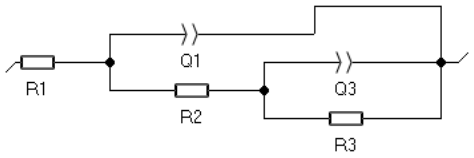

Figure 4.5 Equivalent circuit for a failed coating

The equivalent circuit in Figure 4.5 would be expected to produce the following plots. Figure 4.6a shows the typical semi-circular Nyquist plot which is expected for data which fits to a failed coating circuit whilst b and c show the Bode magnitude of impedance and phase angle plots respectively.

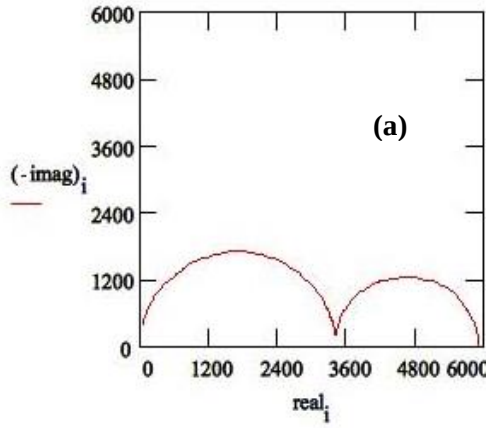

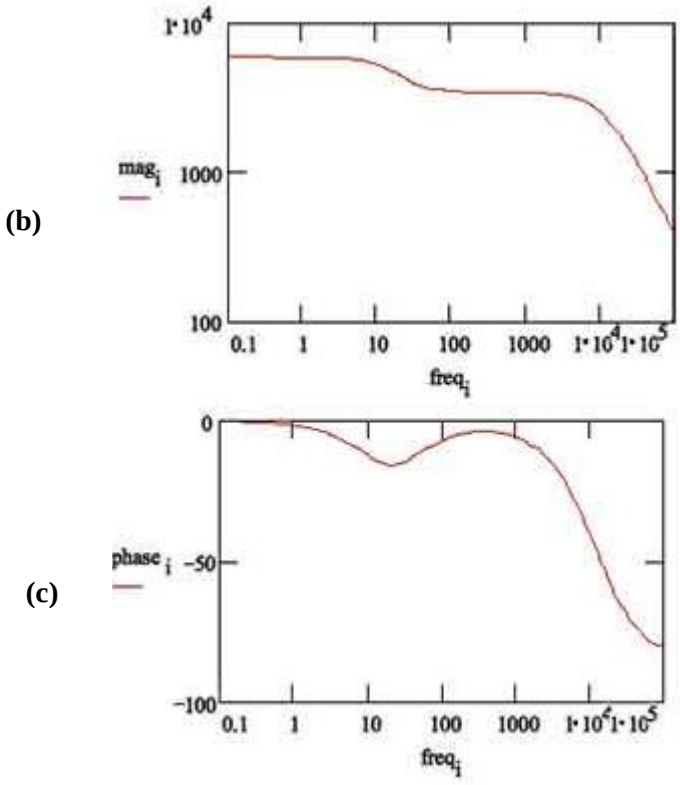

Figure 4.6 - (a) Nyquist (b) Bode impedance and (c) Bode phase angle plots for data that represents a failed coating [158]

If the reaction taking place at the solution/surface interface involves a diffusion process the W2 element, known as a Warburg impedance, is incorporated into the circuit, as per Figure 4.7 below

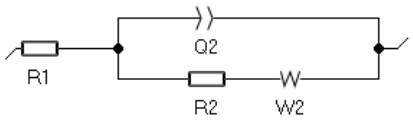

Figure 4.7 Equivalent circuit for a coating with a diffusive element

The line at 45 degrees to the semi-circle of the Nyquist plot is typical for a diffusive process. The phase angles of the Bode plot at the low frequency end will also be very close to 45 degrees. This is shown in Figure 4.8 below.

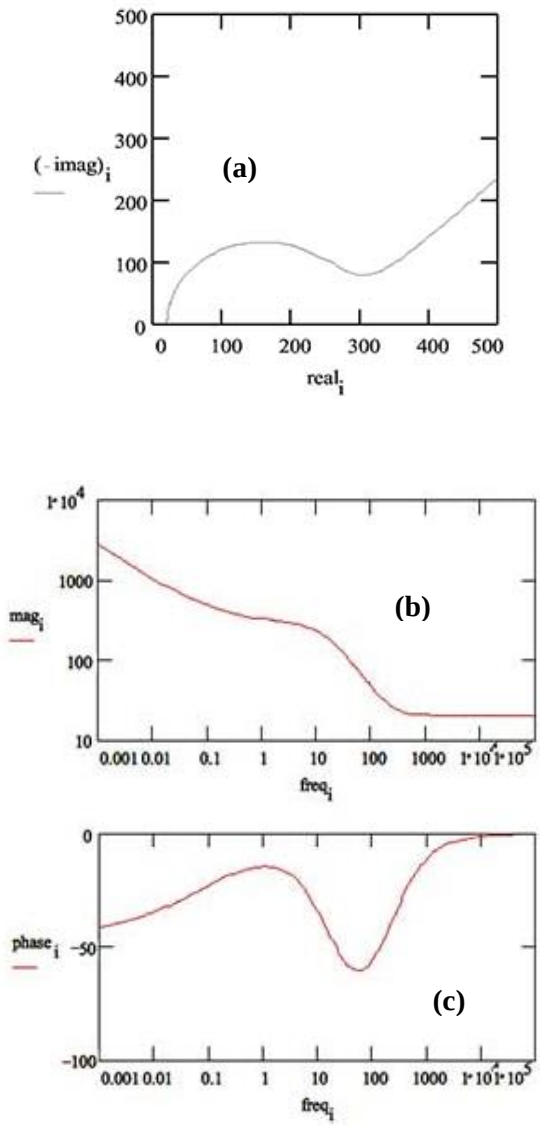

Figure 4.8 - (a) Nyquist (b) Bode impedance and (c) Bode phase angle plots for data that represents a process which involves diffusion or mass transport [158].

4.1.3 Levenberg-Marquardt method

The Levenberg-Marquardt method (L-MM) is a non-linear least squares regression method. This is necessary as EIS data has parameter values that are non-linear compared to the function. For EIS, the parameters are the individual equivalent circuit components and the function is the overall equivalent circuit. The L-MM works by minimising the sum of the squares of the errors between the real data points and the proposed function. In the case of EIS, this is how much the real data differs from the idealised values of the proposed equivalent circuit. Minimisation is undertaken through iterations of parameter values to reduce the sum of the squares of the errors.

In actual fact, the Levenberg-Marquardt method comprises two methods [159]. The Gauss-Newton method which minimises the sum of the squared errors by assuming that at a local level, the function is quadratic and that the local minimum can be found. In addition, the gradient descent method updates parameters depending on whether or not iterations reduce the sum of the least squares. Which of the two methods is used depends on how close the initial parameters are to the optimal parameter values [160]. If the initial parameters are far from optimum then the gradient descent method is used whereas initial parameters close to the optimum results in the deployment of the Gauss-Newton.

The Levenberg-Marquardt method requires initial parameter values within two decades of the actual values before proper fitting can occur [161]. Therefore, estimates for at least some of the proposed circuit elements must be made and inputted into the method. If the contribution of a particular element to the impedance is not significant, then the parameter's fit value will be poor with a large uncertainty value.

4.2 Scanning Kelvin Probe (SKP)

Stratmann proposed that the Volta potential of a metal surface coated with polymer can be related to the corrosion potential of the metal substrate. This would allow the kinetics of the corrosion potential to be examined [162]. To do this the scanning kelvin probe is used. The scanning aspect allows the Kelvin probe to be moved over the sample surface allowing potentials to be recorded for different points on the surface. Figure 4.9 shows the set-up of the SKP.

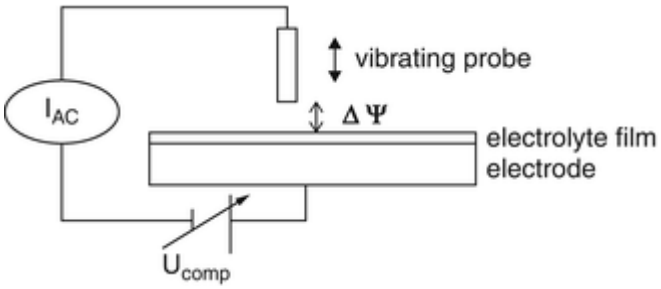

Figure 4.9 - Set-up of the Scanning Kelvin Probe [163]

The SKP setup is made up of a working electrode (the sample under investigation) and a reference electrode (the Kelvin probe) which are connected by an external circuit means that the Fermi levels of both materials are the same and the work function for both are the same. The work function is defined as the work required to remove an electron from the working electrode, through any interfaces that are present, to the reference electrode.

The energy of the electron in the metal working electrode may be defined in terms of electrochemical potential. The electrochemical potential itself ($\bar{\mu}_e{}^{Me}$) is the sum of the chemical ($\mu_e{}^{Me}$) and Galvani potentials ($\varphi_e{}^{Me}$). *F* is the Faraday constant.

$$\bar{\mu}_e{}^{Me} = \mu_e{}^{Me} - F\varphi^{Me} \qquad \text{Eq. 4.13}$$

The work function of the reference electrode ($\alpha_e{}^{Ref}$) can be defined as follows:

$$\alpha_e{}^{Ref} = -\left(\mu_e{}^{Ref} - F\chi^{Ref}\right) \qquad \text{Eq. 4.14}$$

Here $\mu_e{}^{Ref}$ is the chemical potential of the metal of the reference electrode and χ^{Ref} is the dipole potential of the reference electrode.

When a metal substrate is coated with a polymer, the energy (ΔE_1) required to transfer an electron from the metal substrate (Me), through the metal/polymer interface, to the polymer (*Pol)* can be defined as:

$$\Delta E_1 = (\mu_e{}^{Me} - F\varphi^{Me}) + \left(\mu_e{}^{Pol} - F\varphi^{Pol}\right) \qquad \text{Eq.4.15}$$

Where $\mu_e{}^{Me}$ and $\mu_e{}^{Pol}$ are the chemical potentials of the electrons in the metal substrate and the polymer coating respectively. φ^{Me} and φ^{Pol} are the Volta potentials of the metal and polymer.

Once the electron from the metal substrate has been extracted into the polymer it will be extracted through the polymer/air interface to the atmosphere. The energy required to do this (ΔE_2) is defined below s the gas phase is the reference standard.

$$\Delta E_2 = -\left(\mu_e{}^{Pol} - F\varphi^{Pol}\right) \qquad \text{Eq. 4.16}$$

The Galvani potential (φ) may be considered as the result of the Volta-potential and the surface potential (χ) and so Equation 4.17 may be derived: from equation 4.16.

$$\Delta E_2 = -\left(\mu_e{}^{Pol} - F\chi\frac{Pol}{Gas} + F\psi^{Pol}\right) \qquad \text{Eq. 4.17}$$

$\chi\frac{Pol}{Gas}$ is the dipole potential of the polymer/gas interface and ψ^{Pol} is the Volta potential of te polymer surface.

The final transfer of the electron is from the gas to the reference electrode metal (Ref). The energy required for this (ΔE_3) is defined below.

$$\Delta E_3 = +\left(\mu_e{}^{Ref} - F\varphi^{Ref}\right) \quad \text{Eq. 4.18}$$

Combining Equations 4.14 and 4.18 gives ΔE_3 in terms of Volta potential and work function.

$$\Delta E_3 = -\alpha_e{}^{Ref} - F\psi^{Ref} \quad \text{Eq. 4.19}$$

The sum of $\Delta E_1, \Delta E_2$ and ΔE_3 must be zero. As a result, the following is true:

$$\frac{-\mu_e{}^{Me}}{F} + \Delta\varphi\frac{Pol}{Me} = \frac{\alpha_e{}^{Ref}}{F} = \chi\frac{Pol}{Gas} + \Delta\psi\frac{Ref}{Pol} \quad \text{Eq. 4.20}$$

The left hand side of Equation 4.20 is the same as the half -cell potential of the metal/polymer interface and so can be represented by Equation 4.21.

$$E_{1/2}\frac{\alpha_e{}^{Ref}}{F} - \chi\frac{Pol}{Gas} + \Delta\psi\frac{Ref}{Pol} \quad \text{Eq. 4.21}$$

This indicates a linear relationship between the half-cell potential and the Volta potential difference between polymer and reference electrode ($\Delta\psi\frac{Ref}{Pol}$) as long as the other aspects are kept constant. The work function of the reference metal ($\alpha_e{}^{Ref}$) is constant if the gas phase does not change during the experiment and the dipole potential ($\chi\frac{Pol}{Gas}$) should also remain constant.

The corrosion potential of the investigated interface may be given in terms of the half-cell potential and the half-cell potential of the reference electrode ($E\frac{Ref}{1/2}$)

$$E_{corr} = E_{1/2} + E\frac{Ref}{1/2} \quad \text{Eq. 4.22}$$

$$E_{corr} = const + \Delta\psi\frac{Ref}{Pol} \quad \text{Eq. 4.23}$$

Equation 4.23 above defines the corrosion potential of the investigated interface in terms of a constant and the Volta potential difference between polymer and reference electrode ($\Delta\psi\frac{Ref}{Pol}$). The constant is obtained by simultaneously measuring the electrode potential of the polymer coated metal with a standard reference electrode and the Volta potential difference between the polymer surface and the reference metal probe using the Kelvinprobe.

Because the SKP does not require immersion of the sample under investigation, it has been extremely useful in the investigation of atmospheric corrosion phenomena [162] [164] . The ability to map potentials across a surface has permitted the investigation of localised corrosion phenomena, especially cathodic delamination [165, 166].

Several investigations into the protective capabilities and the protective mechanism of Polyaniline [98, 99, 167-170], and other conducting polymers [101, 171-174] have used SKP to examine the corrosion potentials at the metal polymer interfaces.

4.3 X-Ray Photoelectron Spectroscopy (XPS)

When atoms or molecules absorb X-ray photons, electrons can be emitted and therefore XPS can be described as a single photon in, single electron out process. The energy of the applied photon (hv) is defined by the Einstein relation (E=hv), where h = Planck's constant (6.62 x 10^{-34} J s) and v = frequency in Hz of the radiation. Figure 4.10 is a graphical representation of the absorption and emission process.

XPS uses monochromatic radiation, i.e. radiation of a very narrow band of frequencies, and as a result, the photons emitted by the X-ray source have a fixed energy.

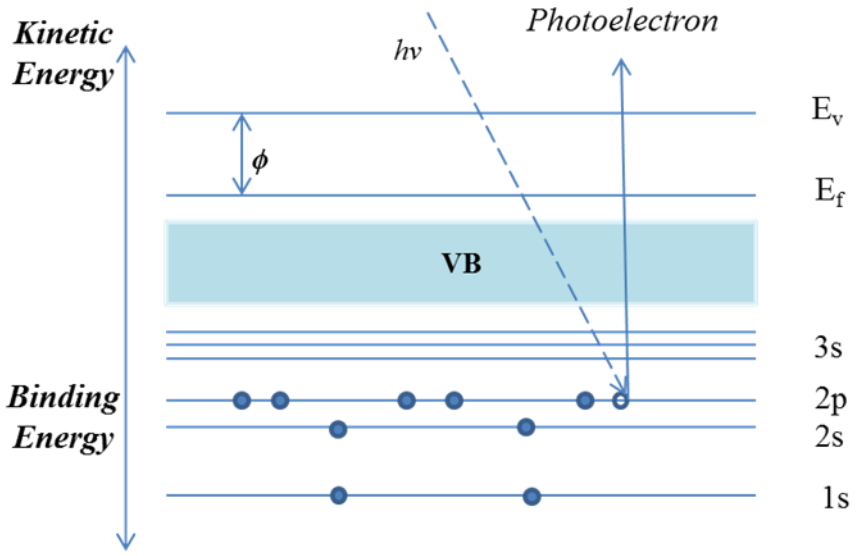

Figure 4.10 – Absorption of a photon and emission of an electron

The binding energy is the energy required to remove an electron from the surface of the sample under investigation. The removed electron will be emitted as a photon and it has a specific kinetic

energy. If the kinetic energy of the emitted electrons is measured by an energy analyser, then the binding energy of the electron can be determined using Equation 4.24;

$$KE=hv- EB\varphi_{spec} \quad \text{Eq. 4.24}$$

Where KE is the kinetic energy of the photoelectron, hv is the photon energy, EB is the binding energy and φspec is the work function of the spectrometer. The work function of the spectrometer is compensated for artificially and can therefore be eliminated resulting in: Equation 4.25:

$$EB=hv-EK \quad \text{Eq. 4.25}$$

XPS spectra are produced by plotting the measured photon intensity against the binding energy.

One of the most important considerations when undertaking XPS measurements on polymers is the effect of chemical shift. This can be defined as the change in binding energy of a core electron of a particular element as a result of the chemical bonding of the element.

The binding energy of a particular electron is determined by the electrostatic interaction between the electron and the nucleus. The electrostatic shielding of the nuclear charge from all the other electrons in the atom is altered by the removal or addition of the electronic charge as a result of bonding. A withdrawal of valence electron charge results in an increase in binding energy whilst the addition of valence electron charge results in a decrease in binding energy. Hence the measured binding energy of carbon is different for different attached functional groups. This allows the identification of chemical environments.

4.4 Scanning electron microscopy

A scanning electron microscope scans a highly focused beam of electrons over the surface of the sample to create an image. Electrons are used because they have wavelengths shorter than white light enabling better resolution.

The sample is scanned with a high energy beam. The beam of electrons is formed by heating a tungsten source at the top of a column and is then accelerated to a voltage of 1-40 kV. The beam is passed through a series of lenses as it travels down the column. The more the beam is condensed, the narrower the beam becomes and the smaller the spot that is focussed onto the sample surface. A scanning coil is used to deflect the beam along the X and Y axes so that a raster scan over the sample surface is achieved. The electrons interact with the sample and secondary electrons are

produced along with backscattered electrons and characteristic X-rays. Multiple detectors are used to collect the various signals and images are formed.

Images are usually derived from secondary electrons and backscattered electrons. Secondary electrons (SE) are low energy electrons that are emitted from the k-orbitals of sample atoms upon interaction with the imaging beam. Backscattered electrons (BSE) are higher energy electrons that are elastically backscattered by the sample atoms. The BSE and SE electrons are accelerated towards a scintillator (a material which fluoresces when struck by a charged particle) and a current is produced that is then passed through a photomultiplier. The amplified signal is then used to construct the image.

4.5 Polarized light microscopy

A polarizer is a filter which allows only light orientated with respect to the polariser to pass through. A polarising optical microscope (POM) uses two polarisers which are placed at right angles to one another; this is termed cross-polar.

The first polariser is orientated vertically to the incident beam so only waves with a vertical direction can pass through the filter. The second polariser is orientated horizontally to the incident wave and so the passed wave is blocked; the plane of polarisation has been rotated from vertical to horizontal and no light will be transmitted.

POM can be used to identify liquid crystal mesophases by firstly identifying the isotropy of the mesophase, i.e. whether the sample further rotates the plane of polarisation. If a sample placed between cross polars allows transmission of light then the sample is deemed anisotropic as it has resulted in the rotation of the plane of polarisation. If the presence of the sample prevents light from being transmitted then it is isotropic and the sample will appear dark.

The only lyotropic liquid crystal phases which possess a micellar arrangement with a geometry that cannot rotate the plane of polarisation is the cubic phases. There are, as discussed in section 3.3.2.2, two possible types of cubic phase. Firstly, if the concentration of micelles in a sample becomes sufficiently large, then they self-assemble into a 3-Dimensional cubic lattice. The most common arrangement is a body centred cubic lattice. The alternative cubic arrangement is the more complex bi-continuous mesophase. They are generally considered to be formed from a single lamellar bilayer that has folded and curved at multiple points. Although both types of cubic phase are isotropic under crossed polars and so appear dark, the bi-continuous cubic phase is considerably more viscous than the cubic packing of micelles. Therefore, viscosity measurements can be

undertaken in order to differentiate between the mesophases formed form the cubic packing of micelles and the bi-continuous cubic phases that are nearly solid at room temperature.

Chapter 5 Methodology

5.1 Polydopamine

5.1.1 Coating deposition procedure

S275 structural steel, obtained from Metals Supermarket UK (Southampton) (composition in Table 5.1) was cut into 15 mm diameter discs and polished with 4000 grit SiC paper. The discs were degreased with ethanol and then acetone and sonication. All chemical reagents, apart from distilled water, were obtained from Sigma Aldrich UK (Gillingham, Dorset) and were used as supplied. A 0.1M sodium phosphate buffer solution was made up (and sufficient dopamine and left exposed to the atmosphere. After 24 h exposure, the now coated disc was monomer was added to make a 2 mg mL^{-1} dopamine solution. A polished S275 disc was placed in 30 mL of the dopamine solution removed from solution, rinsed with distilled water to remove any excess dopamine monomer and solution polymerisation products and then dried under nitrogen flow.

Table 5.1- Elemental composition of S275 steel

Element	% Composition S275 mild structural steel
Carbon	0.25
Iron	97.56
Manganese	0.16
Phosphorous	0.04
Sulphur	0.05
Silicon	0.5

When additional oxidants were used, the deposition procedure was modified as follows. 0.1M sodium phosphate buffer was made up but the solution was degassed through nitrogen bubbling for an hour, resulting in a dissolved oxygen content was less than 2 ppm. The oxygen content was confirmed by a dissolved oxygen meter (Hanna instruments HI9142, Italy) that had been calibrated with a zero-oxygen sodium metabisulfate solution. The bottle of buffer was then transferred to a glovebox. The dopamine monomer was mixed in powder form with the appropriate quantity of additional oxidant. A polished disc was placed with the dry reagents and the beaker was topped up with nitrogen gas before being covered with parafilm. The beaker was transferred to a glovebox and the glovebox was filled with nitrogen gas. The appropriate quantity of phosphate buffer was

added to the dry reagents and the reaction left to proceed under nitrogen atmosphere for 24 hours. The disc was then removed from solution, rinsed with distilled water and dried under nitrogen flow

5.2 Liquid crystal templating

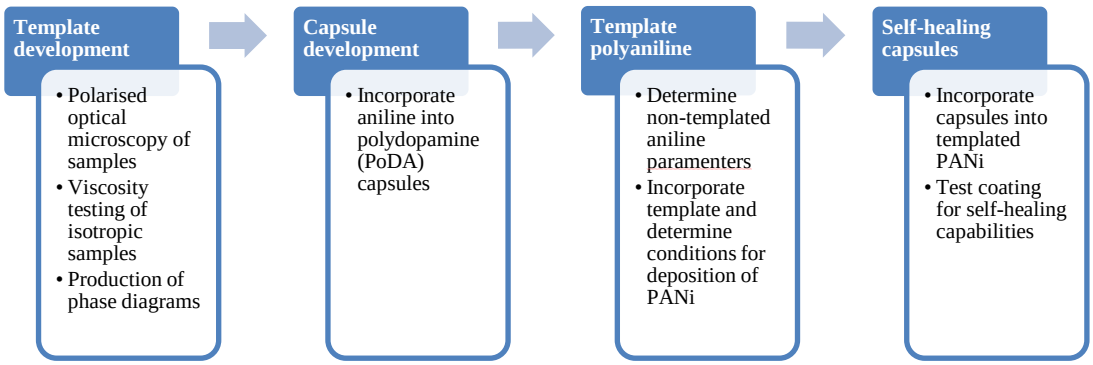

Figure 5.1 - Experiments performed to produce self-healing coatings

The flowchart above (Figure 5.1) shows the process of experiments which were undertaken in order to develop the 3-dimensional porous coating which incorporated capsules in order to impart self-healing functionality to the coating.

In order to produce a mesoporous polymer through liquid crystal templating, a template must be created. As has been identified in section 3.3.2.3, the mesoporous network should be 3-Dimensional (3D). Therefore, a cubic lyotropic liquid crystal mesophase is required. Lyotropic mesophases are dependent on the ratios of aqueous phase to surfactant as well as temperature; mesophase diagrams are produced to show the ratios and temperatures required for the various phases.

There are existing mesophase diagrams for a large number of surfactants and water. However, the deposition of aniline requires an acidic media. As discussed in section 3.2.3.2, the chosen acid is

oxalic acid as the results from the existing literature demonstrate that oxalic acid provides coatings of good thickness without using the harsh conditions of sulphuric or hydrochloric acid. Hydrogen bonding will occur between the oxalic acid and water within the aqueous phase and will disrupt the formation of the micelles and their subsequent self-assembly into mesophases. As a result, mesophase diagrams needed to be constructed for surfactant and oxalic binary mixtures. Four non-ionic Polyoxyethylene surfactants were chosen Brij® L4, Brij® O20, Brij® S100 and Brij® C10. These represent a wide range of chain lengths and head groups, the two aspects of the surfactant which most affect the size of the micelles and the tightness of their packing upon self-assembly.

5.2.1 Production of phase diagrams

Brij® L4, Brij® O20, Brij® C10 and Brij® S100 were all obtained from Sigma Aldrich and used as obtained. Brij® L4 is liquid at 20°C, Brij® O20 and Brij®C10 are waxy solids and Brij® S100 is a crystalline solid. This reflects their relative chain lengths.

In order to produce the mesophases, the surfactants were mixed at weight percentages from 0 to 100 wt % with a 0.1M oxalic acid solution (hereafter the aqueous phase) with the weight percent of surfactant increasing by 10% for each sample. The overall mass of each sample was 30 g. in order to provide a sufficient volume of mesophase for testing.

Those surfactants which were solid at room temperature were melted prior to use and the surfactant and aqueous phase were mixed for 1 minute by hand. Sample beakers were sealed with parafilm to ensure the aqueous phase did not evaporate and thus that the relative wt% of surfactant to aqueous phase did not change.

The mixtures were then placed in a 20°C temperature water bath and incubated for two hours to allow sufficient time for the formation and stabilisation of the mesophase. After two hours, a quantity of each sample was taken and applied to a glass slide and then studied using an Alicona Infinite Focus microscope using the polarised light filter to determine whether the phase was anisotropic.

A further sub-sample was subjected to viscosity testing using a Brookfield High Shear CAP-2000+ viscometer which incorporates a heated stage; the viscosity of the mesophases is one of the features that allows for successful identification of their type.

After sampling, the temperature of the water bath was raised by 10°C. The heating, sampling and testing procedures were repeated until the temperature of the water bath had been raised to 80°C. The upper temperature limit of 80°C was chosen as above 85°C, aniline begins to degrade.

The collected microscopy images were analysed visually and compared to previously identified characteristic textures for the mesophases [118, 120]. This enabled the partial identification of the mesophases. Identification was confirmed by the viscosity results.

24 hours after the first analysis, samples that were identified as being the appropriate cubic mesophases were re-analysed in order to determine the stability of the mesophases. This was necessary as the length of time required for templated polymerisation to occur was not yet known and it was possible that the phases would need to remain stable for several hours.

The results were then plotted using SigmaPlot 12.5 to produce binary phase diagrams.

5.3 Templating of polyaniline

After the phase diagrams had been created, a 50wt% Brij S100/50wt% 0.3M Oxalic acid mixture that had been incubated at 50°C was identified as the preferred mesophase.

Aniline monomer had to be incorporated into the aqueous portion of the mesophase so that it could be polymerised by electrochemical oxidation in order to produce the porous network.

Prior to the production of the lyotropic liquid crystal phase diagrams, the best procedure for the electrodeposition of polyaniline (PANi) had to be determined. A 0.3M oxalic acid solution was made up by dissolving 37.821 g of oxalic acid in 1 litre of deionised water. Aniline monomer is volatile and liable to undergo oxidation upon atmospheric exposure and so aniline solutions are unstable. Therefore, the aniline solution had to be freshly prepared each time deposition of PANi was attempted. The 0.3M oxalic acid solution was used to produce 150 mL of a 0.1M aniline solution by rapidly stirring 1.397 g of aniline into 150 mL of the 0.3M oxalic acid solution. When the aniline was added to the acid solution, a white precipitate (aniline oxalate) formed. The precipitate dissolved with stirring. Because the aniline monomer is hydrophobic, it did not dissolve in the oxalic acid solution and so the monomer was stirred into the oxalic acid for half an hour to ensure an even distribution of the monomer.

A 10cm x 5cm piece of S275 steel obtained as a 30 cm x 30 cm x 5cm plate and cut using a diamond tipped blade, was polished with a 120 grit silicon carbide (SiC) paper and then degreased with ethanol and dried with hot air.

A three-electrode electrochemical set-up was created in order to perform the electrodeposition of the polyaniline. The steel plate was used as the working electrode, Ag/AgCl in saturated KCl (from ABM) was used as the reference electrode and 200 mm x 0.5 mm length of platinum wire was used as the counter electrode.

The electrochemical cell was attached to a CompactStat electrochemical interface (potentiostat) from Ivium Technologies. The proprietary software IviumSoft was used to control the conditions for deposition. A cyclic voltammetry experiment was used, scanning between -1.0V and +1.0V (vs Ag/AgCl) with a scan rate of 50 mVs^{-1}. 25 cycles were performed, as per the procedure defined by Breslin et al. [89] and a bright green deposit, believed to be the Emeraldine-salt form of polyaniline, was present after 25 cycles.

The production of porous templated PANi was then attempted. The 0.1M aniline in oxalic acid solution was made up as before and was stirred for half an hour. The solution was weighed and an equivalent mass of Brij S100 was weighed out and sliced into flakes using a scalpel blade. The white waxy flakes were then melted with stirring until a transparent colourless liquid was formed. The surfactant was maintained at a temperature of 50°C. The aniline solution was then stirred into the melted surfactant to form a yellow gel with 50 wt% Brij S100 and 50 wt% aniline solution. The beaker was sealed with Parafilm and transferred to a 50°C water bath where the gel was conditioned for an hour.

After conditioning of the gel, a steel plate (prepared as previously described) was wrapped in insulating polytetrafluoroethylene (PTFE) leaving one face uncovered. The steel plate was inserted into the gel leaving a 1 cm strip at the top of the plate uncovered. The same electrochemical set-up was used as for the deposition of non-templated PANi. The mass of the steel sample was determined and recorded.

Initially, the same electrochemical parameters used for the deposition of non-templated PANi were used. However, this resulted in the formation of a grey film, thought to be a film of iron oxalate, instead of the bright green Emeraldine salt. Therefore, it became necessary to vary the deposition parameters in order to deposit Emeraldine salt. The scan rate, scan range, number of cycles and concentration of aniline monomer were varied. Following deposition, the template was removed by washing with ethanol and the sample was dried with warm air. After drying, the sample was weighed, and the mass recorded. The surface area of the steel that had been coated was also measured and recorded.

The success of the experiments were judged firstly by whether or not an Emeraldine salt coating was deposited and secondly, by the thickness of the deposited coating.

Coating thickness can be determined by ellipsometry, electrochemical quartz crystal microbalance or the difference in mass between coated and uncoated substrates. The steel substrate used for this project is unsuitable for use with a quartz crystal microbalance because the roughness of the surface is too great to enable successful piezoelectric measurements. In addition, the steel surface, even when polished to a mirror finish with 4000 grit SiC is too rough to perform ellipsometry measurements. As a result, the thickness of the deposited PANi layer was determined by difference in weight using the following equation (Eq. 5.1):

$$t = \frac{(m_{substrate\ after\ coating} - m_{uncoated\ substrate})}{A_1 m_{substrate\ uncoated} \rho} \qquad \text{Eq. (5.1)}$$

Here t = thickness of deposited coating, m = mass, A_1 = the surface area covered by the coating and ρ is the density of the deposited coating.

The deposition conditions which produced the thickest Emeraldine films were deemed to be the optimum conditions. The templated PANi coating produced by the optimum conditions was subjected to further characterisation; SEM images were taken, electrochemical characterisation was performed and corrosion performance testing was undertaken using electrochemical impedance spectroscopy (EIS).

5.4 Production of microcapsules

Preparation of the DiMethylDiEthoxySilane (DMDES) emulsion templates:

5 mg of aniline monomer was dispersed in 400 mL of DMDES by sonication for 10 minutes. Sufficient aniline in DMDES dispersion was added to an ammonia solution (2% v/v) in a 50 mL centrifuge tube so that a 2% v/v solution of the dispersion was created. The contents of the centrifuge tube were shaken manually for 2 minutes. The emulsion was then left undisturbed for 24 hours to allow the condensation reaction to take place.

Preparation of Polydopamine (PoDA) capsules:

Dopamine (4 mg) was dissolved in 1.2 mL of 10 mM TRIS buffer (pH 8.5). 0.8 mL of the prepared DMDES emulsion template was dispersed in the dopamine solution. The polymerization was allowed to proceed for 24 h with constant shaking. Following this, 2 mL of ethanol was added into the brown suspension. The mixture was centrifuged (8500 g for 5 min) and the supernatant was removed. To ensure complete removal of the templates, additional washings with ethanol were performed. Finally, the hollow capsules were washed three times with water and then centrifuged for 5 minutes (5000g).

5.5 Evaluation of coatings

5.5.1 Electrochemical Impedance Spectroscopy

For the polydopamine experiments, a 3.5% NaCl solution was made up by dissolving 35 g of NaCl (Fisher Scientific) in 1 L of distilled water. The coated disc was secured into a PTFE sample holder (made in house) after being deposited there using tweezers.

For the polyaniline experiments, the sample was tested as coated without use of a sample holder.

A BioLogic VSP potentiostat (supplied by EC-Lab UK), connected to a Windows 7 PC was used to perform Electrochemical Impedance Spectroscopy measurements. A three electrode set-up was used. The working electrode was the sample under examination, the reference electrode was Ag/AgCl and the counter electrode was a graphite rod. All three electrodes were immersed in 3.5% NaCl solution. The applied sinusoidal potential was 10 mV and the examined frequency range was 100,000 Hertz to 0.1 Hz. A sequence was set up which took EIS measurements at the required time points. For the polydopamine samples this was immediately after immersion, and then after 1 hour, 4 hours, 12 hours, 24 hours and then every 24 hours until 120 hours or 240 hours. For polyaniline samples, the time points were immediately after immersion, and then every hour for 12 hours and then every 12 hours until 768 hours.

Following data collection, the data was fitted to an equivalent circuit model using the Z-Fit software supplied by BioLogic with the potentiostat. The Levenberg-Marquardt method was used to perform the fit with seed values being provided by estimation from the Bode $|Z|$ plots. 5000 iterations of the fitting method were used. The values obtained for the individual circuit elements were recorded along with the χ^2 goodness of fits.

Both the raw data and the fits were copied into SigmaPlot software and Nyquist and Bode ($|Z|$ and phase angle) plots were produced. Plots were also produced to show the variation of circuit element values with time, again using SigmaPlot.

5.5.2 X-Ray Photoelectron Spectroscopy (XPS)

XPS testing was performed at the University of Surrey using an ESCALAB Mk II (VG Scientific, Germany) with an XR4 twin anode (Mg-Al) and a hemispherical electron energy analyser (Alpha 110). The samples used were prepared in an identical manner to those used for EIS testing. Firstly

abroad spectrum survey scan was taken to identify the most prominent peaks (core level electrons) and their associated binding energies and then detailed elemental scans were taken.

Following analysis, the collected data was analysed using ThermoFisher Advange software. Peak fitting of the elemental peaks was undertaken using a Shirley background and the fitted peaks were compared to a database of previously tested polymers [175] in order to determine the functional groups present.

5.5.3 Scanning Kelvin Probe (SKP testing)

40 mm x 40 mm S275 steel samples and polydopamine coated samples were prepared by polishing with 120 grit SiC and then 1200 grit SiC and coated using the polyaniline deposition procedure described in section 4.11. A 1 mL drop of 3.5% NaCl solution was placed on the centre of a blank S275 sample. Potential profiles were then obtained using a Scanning Kelvin Probe (SKP) from UBM Messtechnik that was fitted with a climatic chamber. The probe was used to trace the potential across a defined area of the sample. The air gap between the Ni-Cr probe tip (which also acted as the reference electrode) was 50 µm and the lateral resolution of the probe tip was 100 µm.

The probe and system were calibrated in humid air (95% relative humidity) with a saturated $Cu/CuSO_4$ electrode prior to use. However, the in-house developed software (Institut de la Corrosion, Brest) converts the potential measured relative to $Cu/CuSO_4$ to a potential relative to the Standard Hydrogen Electrode (SHE). Samples were periodically scanned to produce potential maps of a defined area of the sample.

The same procedure was then repeated for samples that had been coated with either autoxidated PoDA or PoDA that had been produced using a 0.5:1 p-benzoquinone: dopamine ratio and a 2 mg mL^{-1} dopamine solution and a deposition temperature of 35°C.

Chapter 6 Investigations into Polydopamine coatings

6.1 Attempts to produce thicker coatings

As described in the methodology (section 5.1.1), additional oxidants were used in order to try and produce thicker coatings. The chosen oxidants, along with a justification for their selection are presented in Table 6.1.

Table 6.1 - Justification for oxidant choices

Oxidant	**Reason for choice**
Copper acetate ($Cu(OAc)_2$)	Copper sulphate has been used successfully in the literature to produce thicker coatings [49, 176, 177]. However, sulphates are known to have detrimental corrosive interactions with mild steel [178]. It is the Cu^{2+} ion that is responsible for successful oxidation [49] so copper acetate was used as a means of providing the Cu^{2+} without the detrimental anion. Copper (II) oxide is known to be insoluble in cold water [179] and chloride anions are also known to accelerate the corrosion of mild steel [180], rendering copper (II) chloride unsuitable.
Sodium molybdate (Na_2MoO_4)	Sodium molybdate is a known corrosion inhibitor [181]and has been proposed as an alternative to chromate conversion coatings [182]. Therefore, it does not matter and indeed, would be advantageous, if the oxidant was to be incorporated into the deposited coating.
Potassium permanganate ($KMnO_4$)	A very strong oxidant [183] that is included in the list to ensure that a wide range of oxidation potentials is evaluated.
Sodium periodate ($NaIO_4$)	Sodium perchlorate [38] has been investigated in the dopamine literature. However, the use of chlorates as an oxidant for a coating of mild steel is not advantageous. Hence, sodium periodate is presented as an alternative. Periodates are also known oxidants for the oxidation of catechols to quinones [33]; the first oxidation step of the polydopamine formation mechanism (see Figure 3.8 which shows the oxidation of dopamine and subsequent polymerisation).

1,4-benzoquinone	Benzoquinone is well known in organic chemistry as a good oxidizing agent [184]. It is also similar in structure to the oxidised form of dopamine (dopaquinone) so incorporation into the PoDA may well be possible. Whether such incorporation would be advantageous or not remains to be seen. However, it may help to narrow the field of proposed structures after investigation with solid-state NMR.

Certain polymerisation parameters, including the oxidant: monomer ratio, temperature and monomer concentration were varied in order to establish the most effective coating formulation. The outcomes of these variations are detailed in the following sections.

6.1.1 Ratio of oxidant to dopamine monomer

The first parameter to be examined was the ratio of oxidant-to-dopamine monomer. A range of ratios was tested: 3:1, 1.5:1, 1:1 and 0.5:1 to establish which would provide the thickest possible coatings. The rationale for a 3:1 ratio was the three possible oxidation steps in the polymerisation of dopamine (see section 6.1.2). A 1:1 ratio of oxidant to monomer is generally used in the chemical polymerisation of aniline. Ball et al. found a 1.5:1 ratio of ammonium persulphate to be the most effective at oxidising dopamine [177] whilst Herlinger found a 0.5:1 molar ratio of $KMnO_4$ to dopamine to be the most effective [36] at increasing the rate of dopamine polymerisation although the author was not investigating polydopamine as a coating. The deposited coatings were subjected to EIS testing as described in the Methodology (section 5.1.1). The tables of fitted EIS data are presented below along with plots comparing the variation of values obtained for equivalent circuit elements with time.

For the present study, evaluation of the corrosion performance, has been based on the determination of the pore resistances that are observed for each coating as this can be used as a qualitative measure of how well a coating protects against corrosion [185, 186]. Resistance generally degrades with time as a result of ionic species (from the dissolution of the underlying substrate as well as the test electrolyte) and water penetrating through into the coating [158, 186, 187].

For good, intact and inert coatings, the double layer capacitance attributed to the substrate generally remains constant over an extended period (up to 1 month in some studies [187-189]).Variation in capacitance would arise from changes in coating capacitance as a result of changes occurring in the coating such as water up-take and delamination. It would also be anticipated that the uncompensated resistance would remain constant and that there would be an additional resistance

attributed to both the polarisation of the metallic substrate and the coating itself. Such coatings are sufficiently thick that their degradation results in equivalent circuits consisting of two clearly defined time constants; their initial impedance results can be fitted to an almost perfect capacitor. However, the behaviour of coatings that are not inert, such as conducting coatings, is very different [83, 190, 191] and this is also the case for thin polymeric films [192-194]. The polymeric films deposited in this project are both conducting and very thin which will potentially lead to varied and non-standard EIS behaviour.

The vast majority of the literature relating to EIS refers to thick coatings, especially that which considers the failure of coatings as a result of corrosion. It is therefore difficult to relate the accepted literature definitions of EIS parameters to those observed for the PoDA coatings. This is especially true for thin conducting coatings as it can be difficult to separate double layer capacitance of the underlying substrate from the double layer capacitance that can result from conducting coatings. The CPE values are measured as an admittance rather than an effective capacitance as the alpha (α) values suggest that the CPE is not always behaving as a true capacitor i.e. the alpha value is less than 1 and therefore, a simple conversion to effective capacitance is inappropriate. The measured CPE values (approximately 10^{-4} s^{α} Ω^{-1} cm^{-2}) for the PoDA-based samples are indicative of a double layer capacitance. A coating capacitance, even for a thin coating, would be expected to be in the region of 10^{-6} farads (or F which is equivalent to A s V^{-1}) as the relationship between capacitance and impedance is an inverse one and coatings have higher impedances than the substrates they coat [157].

Blank steel data

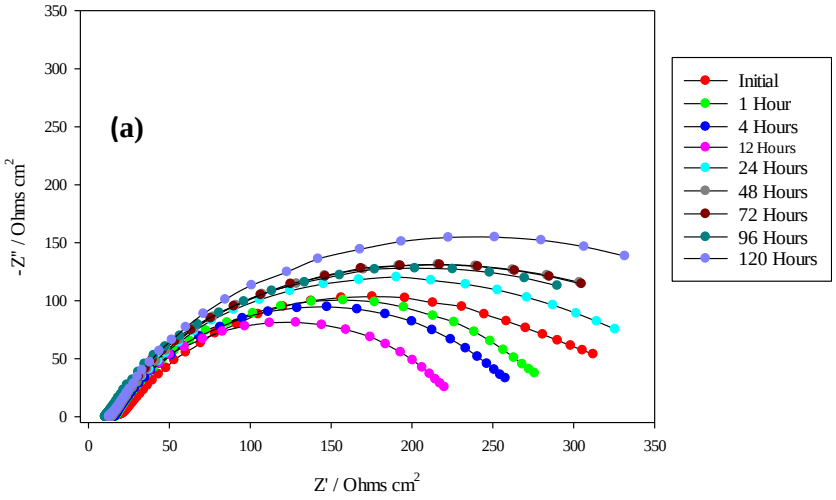

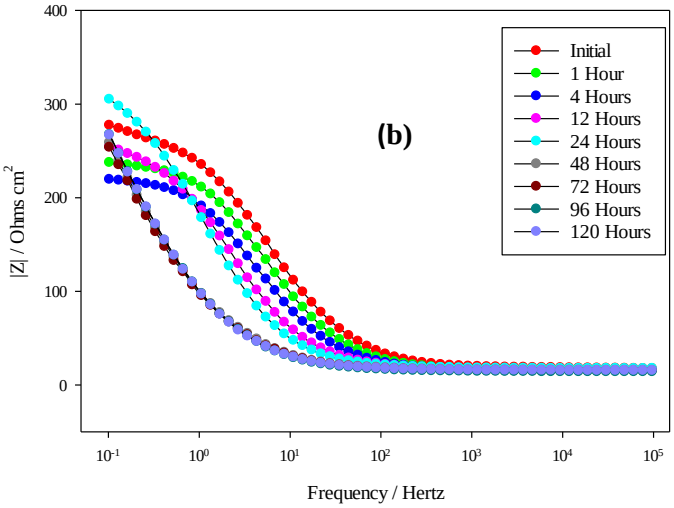

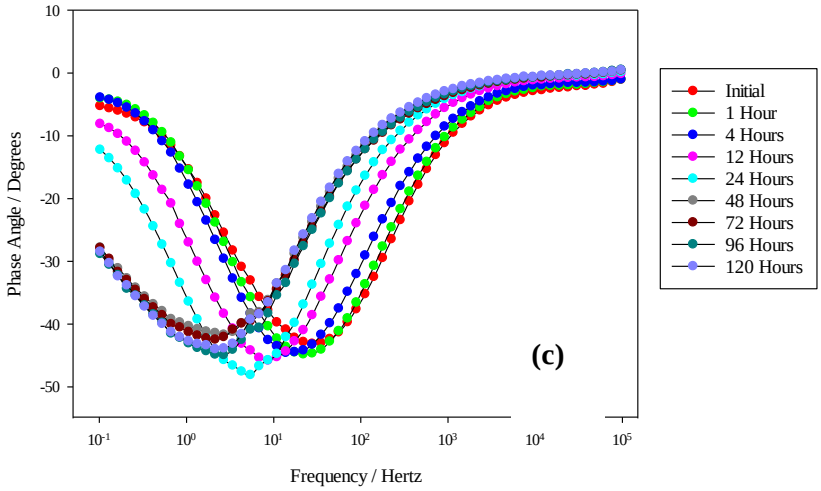

Figure 6.1 - (a) Nyquist, (b) Bode |Z| and (c) Bode phase angle plot overlays for blank steel in a 3.5% NaCl solution

The initial Nyquist plots for bare steel in 3.5% NaCl are, as expected for a bare metal in electrolyte, representative of a Randles circuit. After 72 hours immersion, a diffusive process becomes apparent as emphasised by the 45 degree phase angle at the mid-point frequency range and the 45 degree slope of the bode magnitude plot. Because the primary parameter under consideration is the initial coating impedance, the comparisons between the bare steel and coated samples is presented in the form of plotted, fitted coating impedance value comparisons rather than on the Nyquist and bode plots.

3:1 ratio of oxidant to dopamine monomer

To test the initial efficacy of the chosen oxidants, a molar ratio of oxidant to dopamine of 3:1 was used because there are three oxidation steps in the polymerisation of dopamine (Figure 6.2). The reaction of the final stage of polymerisation is not yet fully determined. However, the first two oxidation steps have been proven by FTIR [35], UV-VIS [28] and solid-state Nuclear Magnetic Resonance (ss-NMR) [35] and so a 3:1 ratio was used in order to provide an excess.

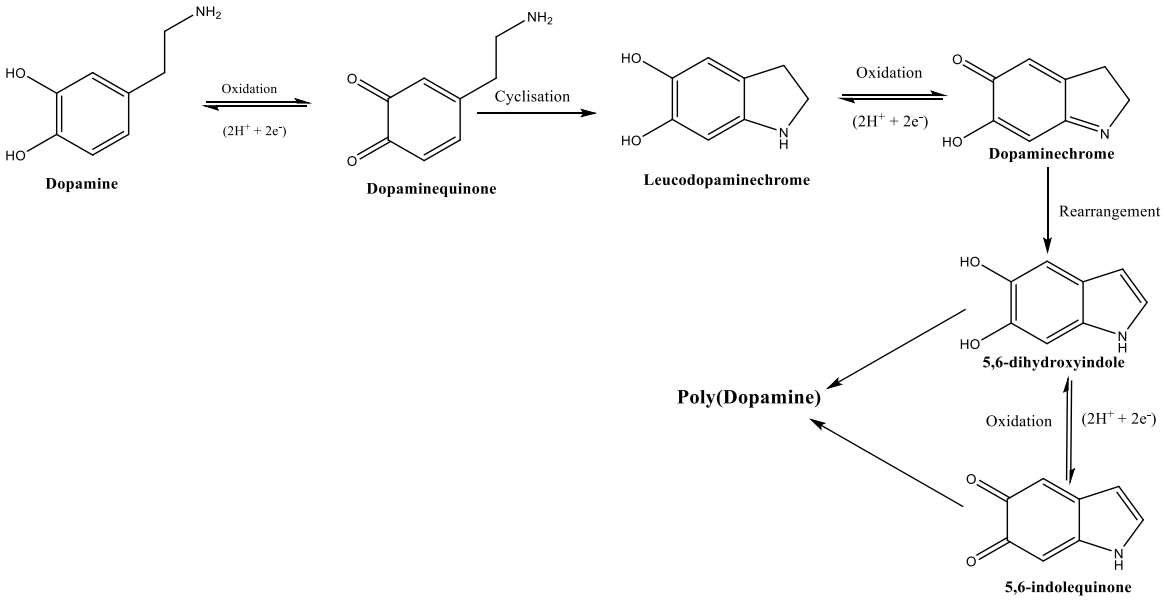

Figure 6.2 - PoDA formation mechanism

Copper acetate

The solubility of $Cu(OAc)_2$ in 20°C water is 7.2 g 100 mL^{-1} [179], which is well above the levels required for even a 3:1 ratio of $Cu(OAc)_2$ to dopamine. When copper acetate was first dissolved in the phosphate buffer, it was soluble. However after 8 hours, a pale blue precipitate had begun to form and adhere to the substrate as is shown in Figure 6.3.

Figure 6.3 - Precipitation of copper (II) phosphate from a 2 mg mL^{-1} dopamine in 0.1M phosphate buffer solution containing a 3:1 molar ratio of $Cu(OAc)_2$ to dopamine at 25°C: the S275 steel disc is 15 mm in diameter

The precipitate colour was indicative of copper phosphate, which is known to be insoluble, therefore it can be inferred that phosphate groups have been substituted for acetate groups. No polydopamine formed either in solution or on the substrate surface from which it can be assumed that the substitution of the acetate cation for a phosphate cation is preferential to the oxidation of dopamine monomer.

Although different ratios of oxidant to monomer were tested to try and improve solubility, similar problems still persisted and $Cu(OAc)_2$ was abandoned as an oxidant.

Potassium permanganate

Figure 6.4 - Coating produced from a 3:1 ratio of $KMnO_4$ to dopamine using a 2 mg mL^{-1} dopamine in 0.1M phosphate buffer solution and a 25°C deposition temperature: the S275 steel disc is 15 mm in diameter. The EIS is carried out in 3.5%NaCl.

Figure 6.4 shows that a 3:1 ratio of $KMnO_4$ to dopamine monomer failed to produce an intact coating. Polydopamine is brown in colour and it is not clear whether the brown colour round the edge of the disc is PoDA or staining from the potassium permanganate. The fact that there is a thin film of PoDA (the iridescent area in the centre of the disc) indicates that a complete film of PoDA formed but then peeled off. As an intact coating was not produced, EIS testing was not carried out.

After the failure of the 3:1 ratio, a lower ratio of 1.5:1 was tested and this proved more successful; the EIS data are shown in section 6.1.1.1.1

Sodium molybdate

A successful coating was produced from a 3:1 ratio of Na_2MoO_4 to dopamine (see Figure 6.5); EIS results are shown in Figure 6.6.

Figure 6.5 - Coating produced from a 3:1 ratio of Na_2MoO_4 to dopamine using a 2 mg mL^{-1} dopamine in 0.1M phosphate buffer solution and a 25°C deposition temperature: the S275 steel disc is 15 mm in diameter. The EIS is carried out in 3.5%NaCl.

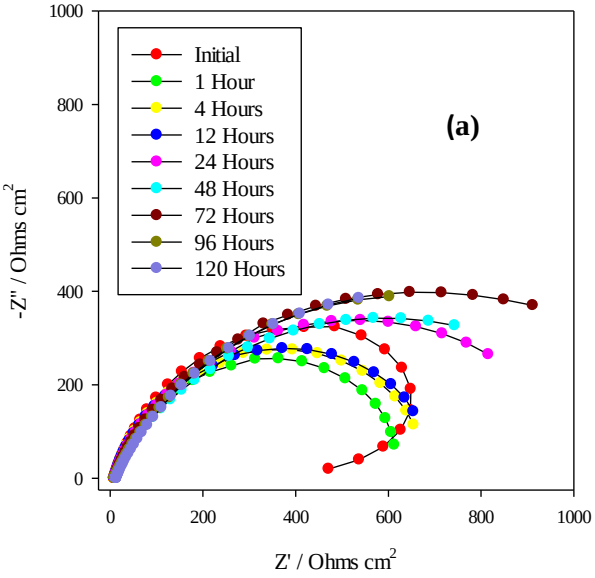
Initial
1 Hour
4 Hours
12 Hours
24 Hours
48 Hours
72 Hours
96 Hours
120 Hours
(a)
-Z'' / Ohms cm2
Z' / Ohms cm2
0
200
400
600
800
1000

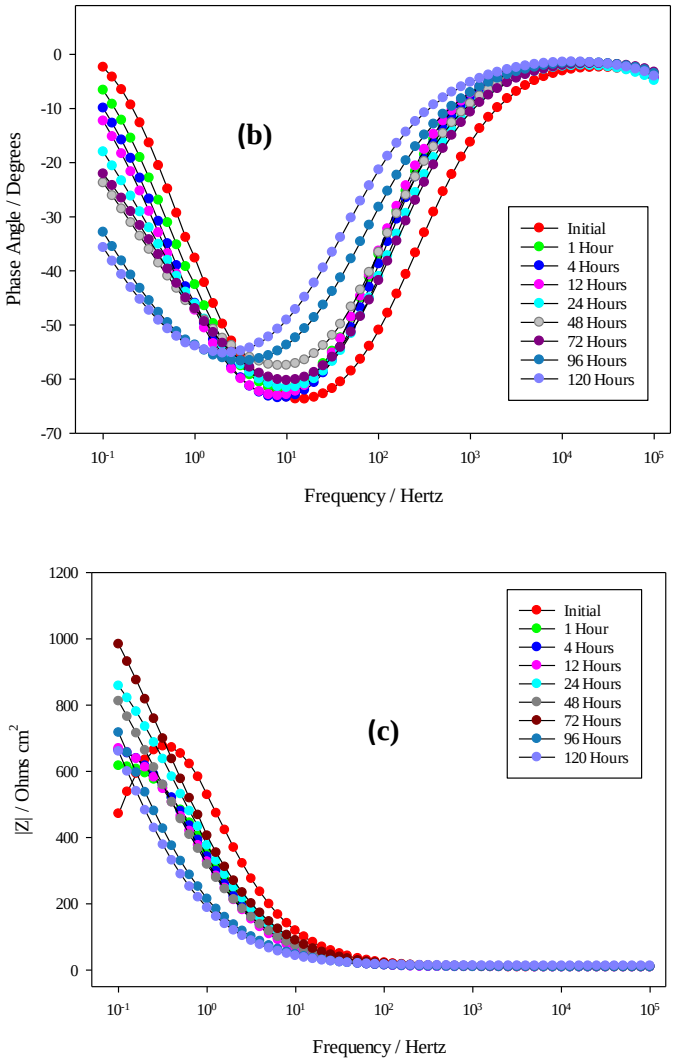

Figure 6.6 - (a) Nyquist, (b) Bode |Z| and (c) Bode phase angle plot overlays for a 3:1 Na_2MoO_4 to dopamine ratio using a 2 mg mL^{-1} dopamine solution (deposited at 25°C).

Both the Nyquist and Bode |Z| plots, (Figure 6.6a and Figure 6.6b), show the presence of an inductive loop. In the Nyquist plot this manifests itself as an obvious loop at the initial time point. The same loop is shown on the Bode |Z| plot in the low frequency region as a decrease in |Z| with decreasing frequency. A similar phenomenon has been observed in other instances where sodium molybdate has been used as a corrosion inhibitor [195, 196]. The loop is indicative of an inductance which is confirmed by the decrease in impedance modulus (|Z|) with increasing frequency. In general, when the system is at steady-state, the incorporation of an inductive element in the equivalent circuit is indicative of a short-circuit [197]. However, the inclusion of sodium molybdate as a corrosion inhibitor will result in the formation of iron molybdate complexes [181] indicating that the system is not at a steady-state and the inductive loop can be interpreted as

representing reactions that are happening in a shorter timescale than the frequency response time [198, 199] (which can be up to 1000 s for frequencies of 0.01 Hz [199]).

Table 6.2 - EIS fitted parameters for a 3:1 Na_2MoO_4 to dopamine ratio using a 2 mg mL^{-1} dopamine solution and a 25°C deposition temperature. The EIS is carried out in 3.5%NaCl solution and the steel disk is 15mm in diameter.

Time / h	R_u / Ω	± / Ω	CPE / $s^{\alpha}\ \Omega^{-1}\ cm^{-2}$ ($\times 10^{-4}$)	± / $s^{\alpha}\ \Omega^{-1}\ cm^{-2}$ ($\times 10^{-6}$)	α	R_p / Ω	± / Ω	χ^2	Circuit
0	13.3	0.2	2.06	1.09	0.90	669.	0.36	0.95	Randles
1	11.6	0.2	4.08	1.37	0.87	634	1.08	0.04	Randles
4	9.4	0.2	4.70	0.549	0.85	706	1.48	0.02	Randles
12	8.9	0.2	5.32	0.996	0.82	730	1.83	0.08	Randles
24	7.6	0.2	5.52	1.58	0.75	1032	3.06	0.01	Randles
48	8.1	0.2	7.61	3.18	0.69	1136	5.59	0.01	Randles
72	6.9	0.2	5.69	1.75	0.71	1302	4.44	0.02	Randles
96	9.2	0.2	11.7	7.82	0.72	1211	11.0	0.02	Randles
120	12.3	0.2	13.8	10.8	0.72	1222	14.4	0.03	Randles

In Table 6.2 above, and the tables which follow, Ru is the uncompensated resistance, the CPE is the constant phase element used to represent the capacitance of the coating , Rp is the pore resistance (the coating resistance) and W, when it occurs, is the Warburg impedance which represents a diffusive process.

Resistors and capacitors both represent a physical process on the surface of the substrate and/or the deposited coating. The inductance does not, however, have such a clear physical representation and therefore no inductive phase elements have been used in the equivalent circuit fitting of the sodium molybdate. The effect on the goodness-of-fit between real data and theoretical data from the equivalent circuit can be seen from the $\chi 2$ values in Table 6.2. The initial time point when the inductive loop was present has a goodness-of-fit of 0.95 compared to the <0.1 values achieved by all other time points. The increase in Rp with time indicates that a thicker oxide layer is gradually building up on the surface. The fact that there is no initial drop in Rp indicates that the NaCl electrolyte has no difficulty in permeating the coating and this is supported by the patchy appearance of the coating (Figure 6.5). This demonstrates that the 3:1 Na_2MoO_4 to dopamine coating has poor barrier properties.

Sodium periodate

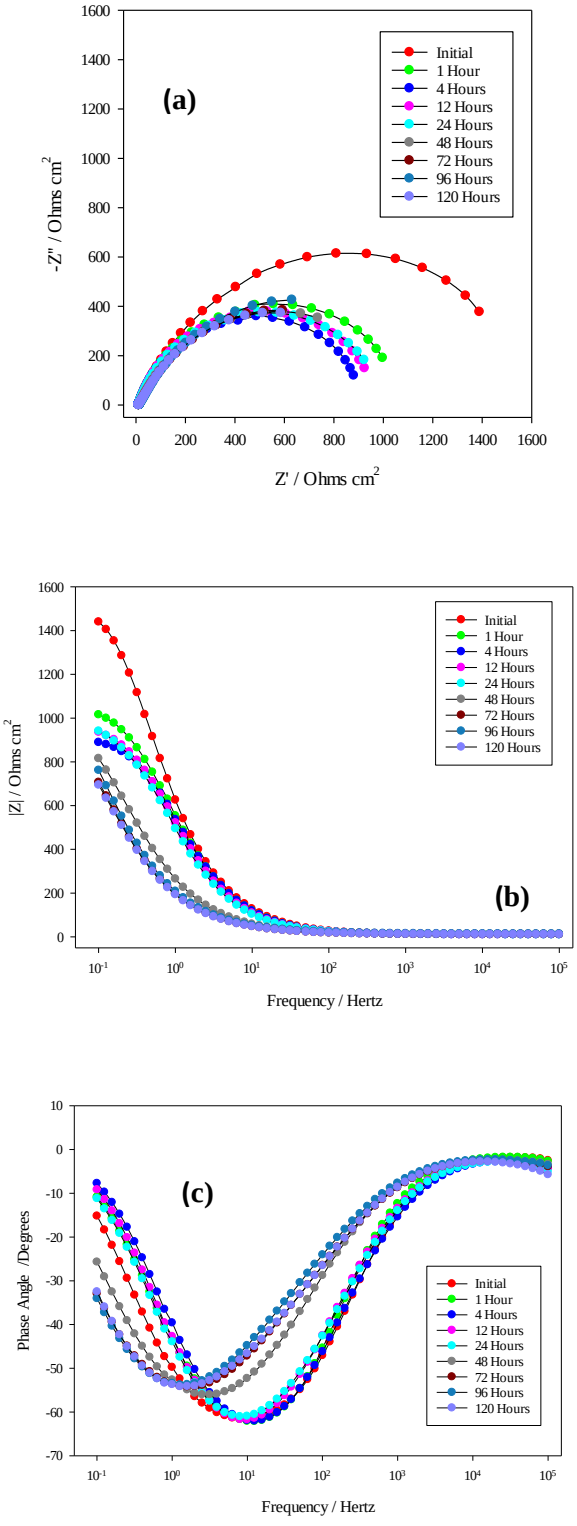

Figure 6.7 - (a) Nyquist, (b) Bode $|Z|$ and (c) Bode phase angle plot overlays for a 3:1 $NaIO_4$ to dopamine ratio using a 2 mg mL^{-1} dopamine solution and 25°C deposition temperature. The EIS is carried out in 3.5%NaCl.

The Nyquist (Figure 6.7a) and Bode |Z| (Figure 6.7b) plots both show a significant drop in impedance between the initial and 1 hour time points, This can be attributed to the penetration of the coating by NaCl electrolyte.

Table 6.3 shows a further decrease in Rp until 12 hours when the trend begins to reverse. This can be attributed to the formation of an iron oxide layer and the build-up of corrosion products at the substrate surface.

Table 6.3 - EIS fitted parameters for a 3:1 $NaIO_4$ to dopamine ratio using a 2 mg mL^{-1} dopamine solution and a 25°C deposition temperature. The EIS is carried out in 3.5%NaCl.

Time / h	R_u /Ω	± / Ω	CPE / s^{α} Ω^{-1} cm^{-2}	± / s^{α} Ω^{-1} cm^{-2}	α	R_p / Ω	± / Ω	χ^2	Circuit
0	11.6	0.2	3.03	4.91	0.79	1667	2.59	0.06	Randles
1	10.7	0.2	2.99	3.92	0.81	1101	1.46	0.10	Randles
4	10.9	0.2	2.70	7.02	0.84	927	1.00	0.24	Randles
12	12.3	0.2	2.97	5.46	0.84	983	1.25	0.36	Randles
24	11.3	0.2	3.38	3.46	0.81	1012	1.54	0.20	Randles
48	12.7	0.2	5.80	44.4	0.76	1128	6.24	0.22	Randles
72	11.8	0.2	12.6	90.8	0.72	1252	13.1	0.26	Randles
96	14.9	0.2	12.1	83.1	0.72	1386	14.3	0.30	Randles
120	11.9	0.2	12.8	93.8	0.72	1217	12.7	0.35	Randles

<u>*p*-Benzoquinone</u>

Table 6.4 shows that the 3:1 p-BQ to dopamine coating has a decrease in Rp within the first hour of exposure to 3.5% NaCl but Rp then increases with increasing exposure time as a result of the formation of a stable layer of corrosion products.

Table 6.4 - EIS fitted parameters for a 3:1 *p*-benzoquinone to dopamine ratio using a 2 mg mL^{-1} dopamine solution and a 25°C deposition temperature. The EIS is carried out in 3.5%NaCl.

Time / h	R_u / Ω	± / Ω	CPE / s^{α} Ω^{-1} cm^{-2} ($\times 10^{-4}$)	± / s^{α} Ω^{-1} cm^{-2} ($\times 10^{-6}$)	α	R_p / Ω	± / Ω	χ^2	Circuit
0	9.5	0.2	4.79	2.57	0.60	619	0.67	0.08	Randles
1	11.9	0.2	3.35	2.73	0.72	459	0.29	0.01	Randles
4	11.3	0.2	3.36	2.80	0.73	448	0.25	0.08	Randles
12	12.2	0.2	6.89	3.05	0.67	575	0.50	0.08	Randles
24	14.6	0.2	11.7	7.45	0.69	745	0.65	0.02	Randles
48	16.5	0.2	15.9	14.2	0.69	838	10.66	0.01	Randles
72	14.8	0.2	16.7	15.3	0.67	1004	15.37	0.02	Randles
96	11.5	0.2	5.64	0.759	0.64	1106	6.09	0.01	Randles
120	9.5	0.2	4.78	2.57	0.60	619	0.67	0.08	Randles

6.1.1.1.1 Lower ratios of oxidant to dopamine

Potassium permanganate

1.5:1

Table 6.5 - EIS fitted parameters for a 1.5:1 $KMnO_4$ to dopamine ratio using a 2 mg mL^{-1} dopamine solution and a 25°C deposition temperature. The EIS is carried out in 3.5%NaCl.

Time / h	R_u / Ω	± / Ω	CPE / $s^{\alpha}\ \Omega^{-1}\ cm^{-2}$ ($\times 10^{-3}$)	± / $s^{\alpha}\ \Omega^{-1}\ cm^{-2}$ ($\times 10^{-5}$)	α	R_p / Ω	± / Ω	χ^2	Circuit
0	21.0	0.2	2.62	0.770	0.84	886	0.92	0.21	Randles
1	18.7	0.2	2.90	0.781	0.81	898	1.06	0.08	Randles
4	16.8	0.2	3.59	0.461	0.81	1120	1.92	0.08	Randles
12	16.0	0.2	4.58	0.926	0.77	1019	2.34	0.02	Randles
24	15.2	0.2	6.99	2.73	0.75	486	1.48	0.08	Randles
48	14.8	0.2	9.01	4.02	0.72	657	3.26	0.04	Randles
72	15.5	0.2	11.2	7.42	0.74	838	6.14	0.06	Randles
96	15.2	0.2	11.5	7.92	0.75	923	7.13	0.02	Randles
120	14.4	0.2	12.1	8.85	0.75	863	6.96	0.02	Randles

1:1

Table 6.6 EIS fitted parameters. for a 1:1 $KMnO_4$ to dopamine ratio using a 2 mg mL^{-1} dopamine solution and a 25°C deposition temperature. The EIS is carried out in 3.5%NaCl.

Time / h	R_u / Ω	± / Ω	CPE / $s^{\alpha}\ \Omega^{-1}\ cm^{-2}$ ($\times 10^{-3}$)	± / $s^{\alpha}\ \Omega^{-1}\ cm^{-2}$ ($\times 10^{-5}$)	α	R_p / Ω	± / Ω	χ^2	Circuit
0	10.8	0.2	0.298	0.208	0.74	529	0.10	0.03	Randes
1	10.3	0.2	0.362	0.323	0.72	423	0.28	0.06	Randles
4	10.2	0.2	0.767	0.775	0.66	325	0.64	0.05	Randles
12	10.0	0.2	1.28	0.931	0.61	333	1.74	0.07	Randles
24	9.9	0.2	1.57	1.42	0.61	217	1.73	0.05	Randles
48	10.4	0.2	1.77	1.42	0.63	253	1.96	0.04	Randles
72	10.8	0.2	1.83	1.47	0.65	234	1.91	0.20	Randles
96	11.4	0.2	2.21	1.50	0.67	246	2.83	0.07	Randles
120	10.6	0.2	2.88	3.66	0.66	231	3.82	0.02	Randles

0.5:1

Table 6.7 - EIS fitted parameters for a 0.5 $KMnO_4$ to dopamine ratio using a 2 mg mL^{-1} dopamine solution and a 25°C deposition temperature. The EIS is carried out in 3.5%NaCl.

Time / h	*R*u / Ω	± / Ω	CPE / $s^{\alpha}\ \Omega^{-1}\ cm^{-2}$ ($\times10^{-3}$)	± / $s^{\alpha}\ \Omega^{-1}\ cm^{-2}$ ($\times10^{-6}$)	α	*R*p / Ω	± /Ω	χ^2	Circuit
0	13.5	0.2	0.234	0.403	0.76	1299	1.27	2.50e-3	Randles
1	12.6	0.2	0.260	0.641	0.76	1053	1.07	0.04	Randles
4	12.9	0.2	0.400	1.91	0.77	602	0.86	0.03	Randles
12	13.4	0.2	0.931	4.82	0.70	396	1.59	0.02	Randles
24	14.0	0.2	1.12	10.2	0.72	275	1.22	0.01	Randles
48	14.3	0.2	1.01	8.89	0.74	288	1.13	0.02	Randles
72	13.8	0.2	1.30	8.61	0.71	286	1.63	0.02	Randles
96	14.8	0.2	1.61	9.42	0.72	304	2.49	0.04	Randles
120	14.0	0.2	1.90	12.9	0.73	252	2.42	0.05	Randles

Comparisons

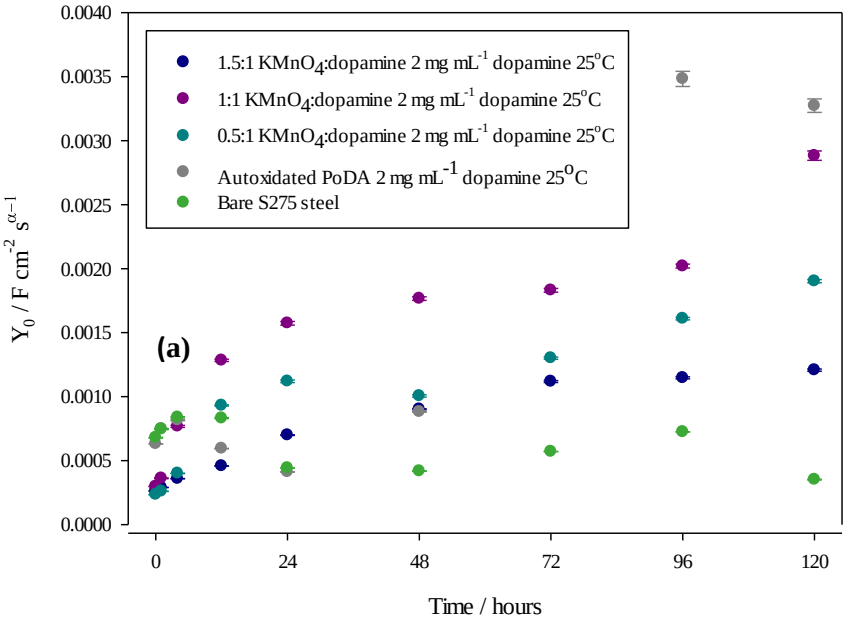

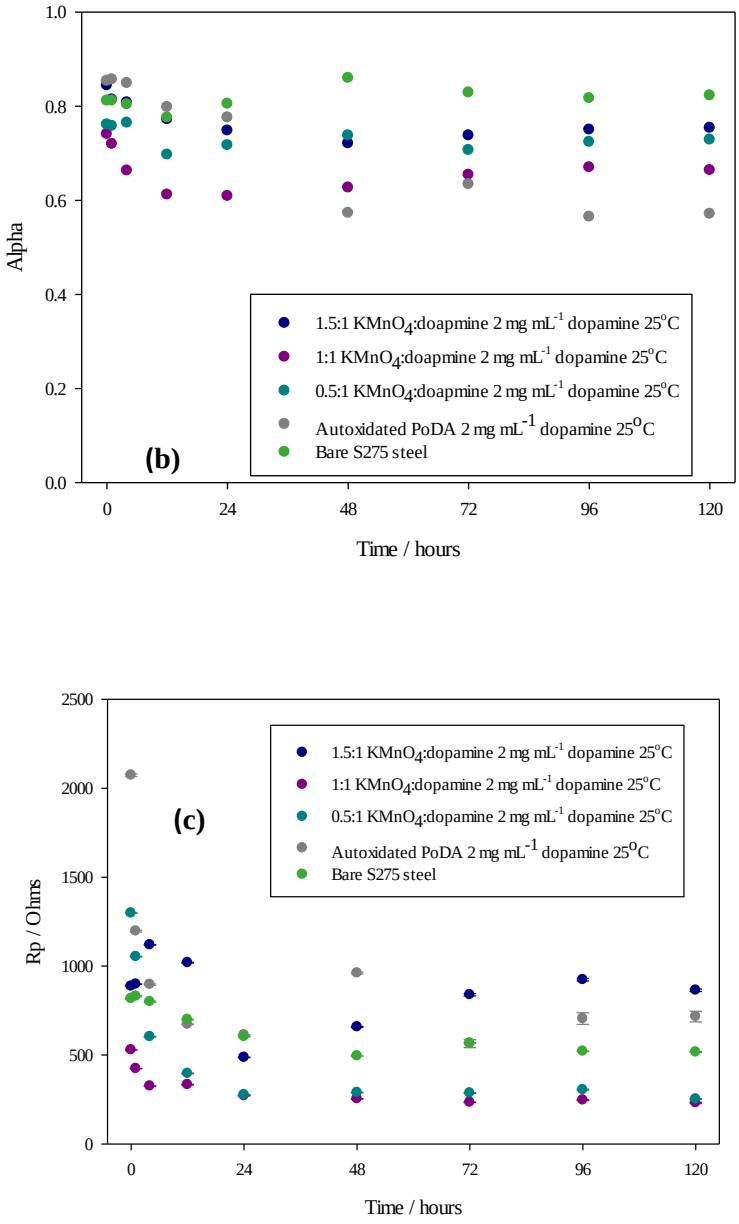

Figure 6.8 - EIS fitted parameters for varied $KMnO_4$ to dopamine ratios using a 2 mg mL^{-1} dopamine solution and a 25°C deposition temperature: (a) CPE, (b) alpha and (c) *R*p values. The EIS is carried out in 3.5%NaCl.

Table 6.5, Table 6.6, Table 6.7 and Figure 6.8 all demonstrate that using $KMnO_4$ as an oxidant in the polymerisation of dopamine does not improve coating performance in terms of barrier properties. This is because $KMnO_4$ is such a powerful oxidant that it immediately begins to polymerise dopamine in solution, and this occurs preferentially over the polymerisation of dopamine and subsequent deposition of a PoDA film onto the steel substrate.

Sodium molybdate

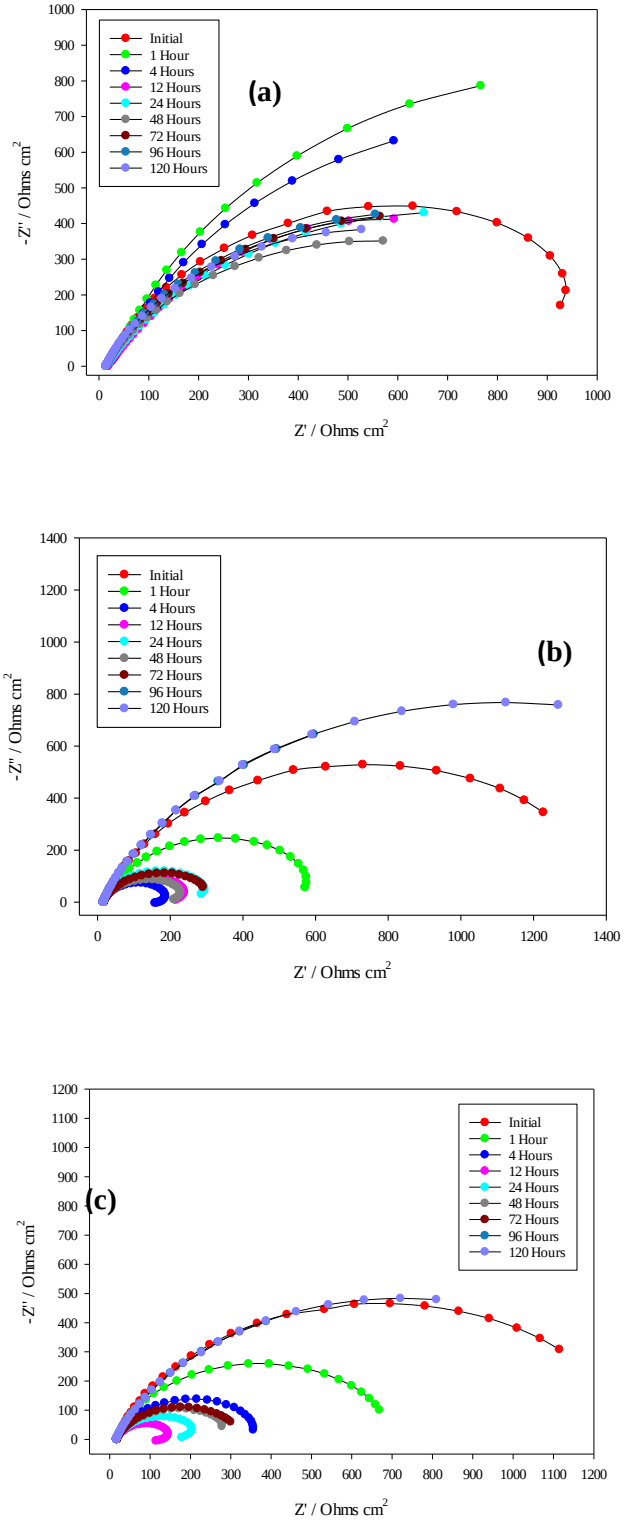

Figure 6.9 - Nyquist plots: (a) 1.5:1 Na_2MoO_4 to dopamine and (b) 1:1 Na_2MoO_4 to dopamine and (c) 0.5:1 Na_2MoO_4 to dopamine :all deposited from 2 mg mL^{-1} dopamine solution at 25°C. The EIS is carried out in 3.5%NaCl.

In a similar manner to the 3:1 ratio coating above, the smaller ratios of Na_2MoO_4 to dopamine all have inductive loops in their Nyquist plots. For the 1:1 and 0.5:1 ratios, the loop appears at a later time point than the 3:1 and 1.5:1 ratios, indicating that the molybdate was further from the substrate than for the higher ratios and leading to a delayed complex formation between molybdate and the steel substrate.

1.5:1

Table 6.8 - EIS fitted parameters for a 1.5:1 Na_2MoO_4 to dopamine ratio using a 2 mg mL^{-1} dopamine solution and a 25°C deposition temperature. The EIS is carried out in 3.5%NaCl.

Time / h	R_u / Ω	± / Ω	CPE / s^{α} Ω^{-1} cm^{-2} ($x10^{-3}$)	± / s^{α} Ω^{-1} cm^{-2} ($x10^{-5}$)	α	R_p / Ω	± / Ω	W / Ω cm^2 $s^{-1/2}$	± / Ω cm^2 $s^{-1/2}$	χ^2	Circuit
0	16.9	0.2	0.29	0.04	0.84	1047	1.32	115	2.37	0.01	RIW
1	15.7	0.2	1.24	2.25	0.92	1504	22.06	112	3.80	0.04	RIW
4	16.9	0.2	1.82	4.97	0.90	1184	30.98	119	3.78	0.05	R+W
12	19.2	0.2	1.53	4.13	0.82	913	27.96	56	7.87	0.03	R+W
24	16.2	0.2	1.11	0.716	0.74	1249	10.40			0.03	Randles
48	14.8	0.2	1.25	0.917	0.75	1054	9.63			0.02	Randles
72	13.9	0.2	1.33	1.02	0.76	1233	12.64			0.04	Randles
96	15.4	0.2	1.36	1.07	0.78	1223	12.35			0.03	Randles
120	14.0	0.2	1.41	1.16	0.78	1083	10.84			0.03	Randles

1:1

Table 6.9 - EIS fitted parameters for a 1:1 Na_2MoO4 to dopamine ratio using a 2 mg mL–1 dopamine solution and a 25°C deposition temperature. The EIS is carried out in 3.5%NaCl.

Time/ h	R_u / Ω	± / Ω	CPE / s^{α} Ω^{-1} cm^{-2} ($x10^{-4}$)	± / s^{α} Ω^{-1} cm^{-2} ($x10^{-6}$)	α	R_p / Ω	± / Ω	χ^2	Circuit
0	16.6	0.2	3.31	0.557	0.80	1446	2.41	0.01	Randles
1	14.3	0.2	3.19	1.68	0.81	604	0.62	0.01	Randles
4	17.8	0.2	3.87	10.3	0.80	171	0.48	0.04	Randles
12	14.7	0.2	2.84	5.70	0.84	227	0.40	0.01	Randles
24	15.1	0.2	4.05	5.37	0.83	293	0.22	0.07	Randles
48	16.8	0.2	4.77	8.88	0.82	219	0.35	0.08	Randles
72	15.8	0.2	8.44	7.17	0.75	318	1.01	0.05	Randles
96	15.1	0.2	5.20	0.525	0.78	212	2.35	0.07	Randles
120	14.4	0.2	5.34	1.73	0.77	620	7.92	0.02	Randles

0.5:1

Table 6.10 - EIS fitted parameters for a 0.5:1 Na_2MoO_4 to dopamine ratio using a 2 mg mL^{1-} dopamine solution and a 25°C deposition temperature. The EIS is carried out in 3.5%NaCl.

Time / h	Ru / Ω	± / Ω	CPE/ s^{α} Ω^{-1} cm^{-2} ($x10^{-4}$)	± / s^{α} Ω^{-1} cm^{-2} ($x10^{-6}$)	α	Rp / Ω	± / Ω	χ^2	Circuit
0	16.2	0.2	3.46	0.521	0.78	1311	2.26	0.04	Randles
1	16.8	0.2	3.38	1.29	0.81	703	6.91	0.02	Randles
4	16.5	0.2	4.18	4.16	0.81	360	0.30	0.18	Randles
12	19.8	0.2	4.39	18.6	0.85	114	0.45	0.05	Randles
24	14.8	0.2	5.44	11.6	0.75	204	0.39	0.01	Randles
48	16.5	0.2	6.15	7.16	0.82	285	0.52	0.04	Randles
72	16.9	0.22	9.54	6.61	0.74	327	1.29	0.06	Randles
96	16.3	0.2	8.18	12.8	0.78	1340	24.2	0.02	Randles
120	15.7	0.2	8.44	4.29	0.76	1421	8.32	0.01	Randles

Table 6.8, Table 6.9 and Table 6.10 all show that the R_p values are greatly reduced and the point of the greatest reduction coincides with the appearance of the inductive loop in the Nyquist plot. After the inductive loop ceases to be present, the R_p values increase once more as a result of the formation of a stable oxide layer.

Comparisons

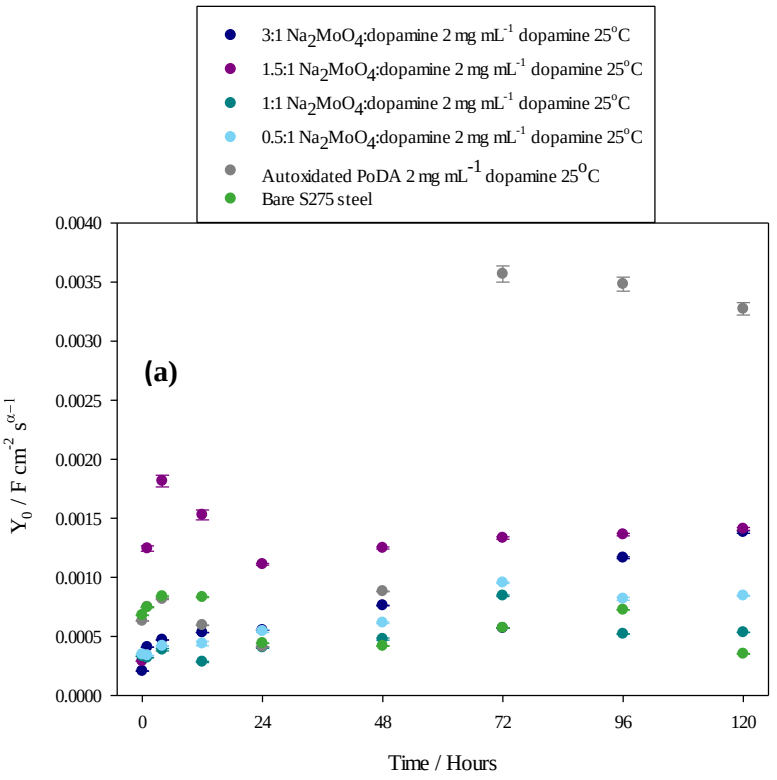

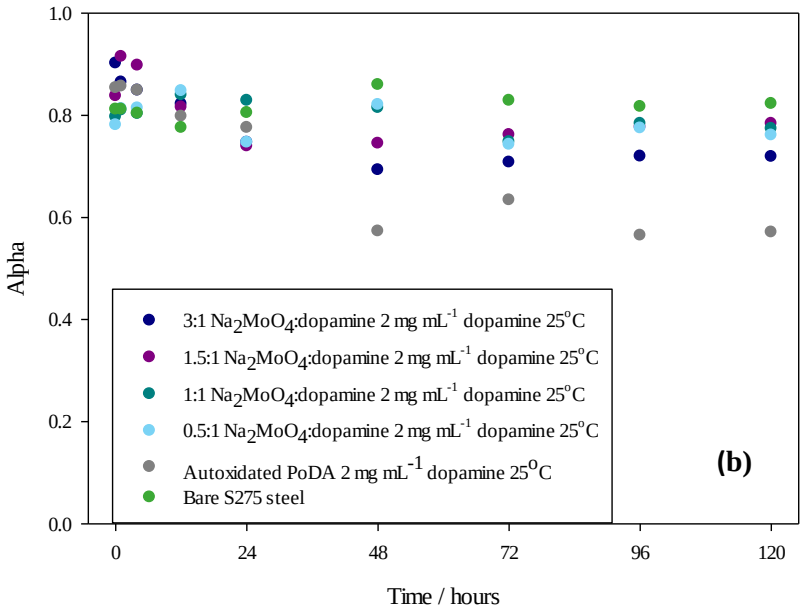

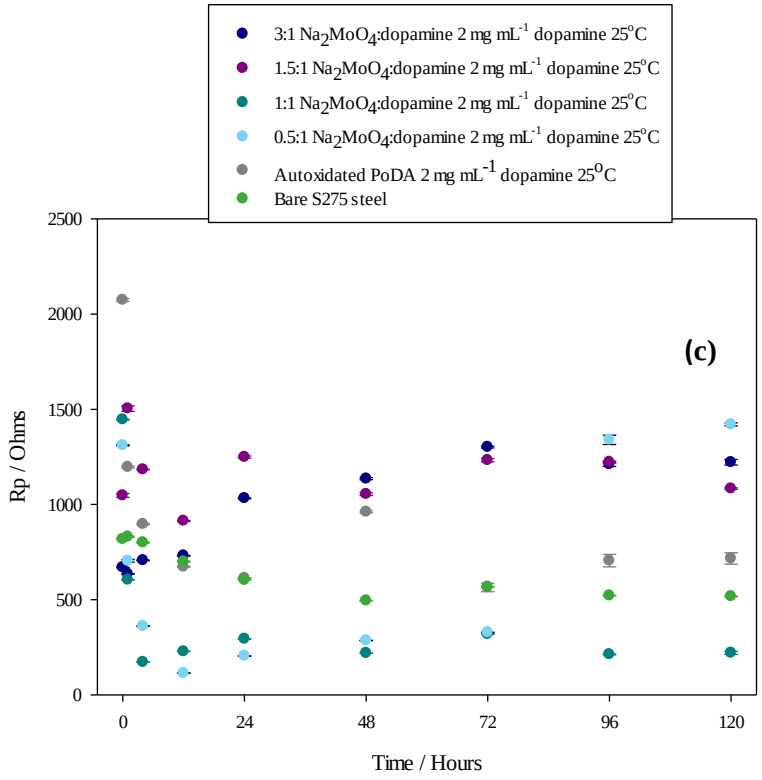

Figure 6.10 - EIS fitted parameters using varied Na_2MoO_4 to dopamine ratio using a 2 mg mL^{-1} dopamine solution and a 25°C deposition temperature: (a) CPE, (b) alpha and (c) *R*p values

Molybdates act as anodic corrosion inhibitors. Such inhibitors act by inducing the formation of an oxide film on the surface of the metal or the formation of a poorly soluble salt film. This increases the polarisation of the metal and pushes it into the passive state. The inductive loops observed in the Nyquist plots indicate the formation of complexes between the molybdate that has been incorporated into the coating and iron in the steel substrate. These complexes should protect the substrate from corrosion. However, the concentration of anodic inhibitors is critical. If the concentration is too low, then the formation of the passivating layer may be incomplete which results in small areas of unpassivated metal. This will result in localised corrosion, such as pitting. The poor performance of the lower sodium molybdate to dopamine ratio coatings can be attributed to this (see

Figure **6.10**c). At the higher concentrations of sodium molybdate, there is sufficient excess molybdate present to form the protective oxide film which will contribute to the perceived better performance of these coatings over the autoxidated PoDA coatings. Thus, the coatings produced with 3:1 and 1.5:1 ratios of Na_2MoO_4 to dopamine perform better than autoxidated PoDA. As the .5:1 ratio of Na_2MoO_4 to dopamine slightly outperformed the 3:1 ratio, the 1.5:1 ratio will be used in all further experiments involving Na_2MoO_4

Sodium periodate

1.5:1

Table 6.11 - EIS fitted parameters for a 1.5:1 $NaIO_4$ to dopamine ratio using a 2 mg mL^{-1} dopamine solution and a 25°C deposition temperature. The EIS is carried out in 3.5%NaCl.

Time / h	R_u /Ω	± / Ω	CPE / $s^{\alpha}\ \Omega^{-1}\ cm^{-2}$ ($x10^{-3}$)	± / $s^{\alpha}\ \Omega^{-1}\ cm^{-2}$ ($x10^{-5}$)	α	R_p / Ω	± / Ω	χ^2	Circuit
0	7.9	0.2	0.412	0.241	0.73	544	0.67	0.09	Randles
1	9.6	0.2	0.398	0.484	0.81	373	0.22	0.02	Randles
4	9.4	0.2	0.711	1.22	0.73	219	0.24	0.02	Randles
12	10.0	0.2	1.03	2.18	0.71	171	0.07	0.08	Randles
24	9.9	0.2	1.07	2.48	0.75	121	0.36	0.07	Randles
48	10.5	0.2	1.52	3.69	0.73	137	0.54	0.04	Randles
72	10.1	0.2	2.22	3.28	0.72	151	1.39	0.06	Randles
96	9.4	0.2	2.93	3.03	0.70	176	2.67	0.08	Randles

1:1

Table 6.12 - EIS fitted parameters for a 1:1 $NaIO_4$ to dopamine ratio using a 2 mg mL^{-1} dopamine solution and a 25°C deposition temperature. The EIS is carried out in 3.5%NaCl.

Time / h	R_u /Ω	± / Ω	CPE / $s^{\alpha}\ \Omega^{-1}\ cm^{-2}$ ($x10^{-4}$)	± / $s^{\alpha}\ \Omega^{-1}\ cm^{-2}$ ($x10^{-5}$)	α	R_p / Ω	± / Ω	χ^2	Circuit
0	14.2	0.2	2.05	0.0281	0.82	1428	1.25	0.01	Randles
1	11.8	0.2	2.14	0.0604	0.83	1013	0.80	0.08	Randles
4	12.2	0.2	2.49	0.127	0.81	672	0.44	0.07	Randles
12	12.7	0.2	2.93	0.253	0.81	441	0.16	0.04	Randles
24	13.4	0.2	5.87	1.44	0.77	169	0.43	0.08	Randles
48	13.8	0.2	8.83	2.42	0.76	143	0.33	0.05	Randles
72	13.9	0.2	8.11	3.14	0.81	110	0.41	0.01	Randles
96	13.5	0.2	11.6	4.41	0.75	105	0.39	0.07	Randles
120	17.9	0.2	7.62	0.380	0.83	71.44	2.88	0.07	Randles

0.5:1

Table 6.13 - EIS fitted parameters. for a 0.5:1 $NaIO_4$ to dopamine ratio using a 2 mg mL^{-1} dopamine solution and a 25°C deposition temperature. The EIS is carried out in 3.5%NaCl.

Time / h	R_u / Ω	± / Ω	CPE / $s^{\alpha}\ \Omega^{-1}\ cm^{-2}$ ($x10^{-4}$)	± / $s^{\alpha}\ \Omega^{-1}\ cm^{-2}$ ($x10^{-6}$)	α	R_p / Ω	± / Ω	χ^2	Circuit
0	17.3	0.2	2.30	0.308	0.74	3161	4.30	0.03	Randles
1	14.1	0.2	2.16	0.538	0.76	1143	0.89	0.01	Randles
4	14.8	0.2	2.98	2.23	0.76	497	0.13	0.05	Randles
12	16.6	0.2	3.59	6.63	0.80	234	0.43	0.08	Randles
24	16.8	0.2	4.17	22.6	0.82	93	0.47	0.04	Randles
48	17.0	0.2	9.30	44.7	0.74	90	0.50	0.05	Randles
72	17.3	0.2	9.54	80.4	0.79	56	0.48	0.06	Randles
96	17.8	0.2	19.7	1.18	0.71	66	0.43	0.04	Randles
120	23.3	0.2	12.8	10.6	0.76	70	6.27	0.03	Randles

Table 6.11, Table 6.12 and Table 6.13 all show a very similar trend in Rp values namely that, as the length of exposure time to NaCl increases for each coating, the Rp value decreases. Whilst the 1:1 and 0.5:1 ratios produce better coatings to begin with, their protective capabilities last for at most four hours before a large drop in Rp occurs. This indicates that the coatings possess barrier properties that are easily overcome.

Comparisons

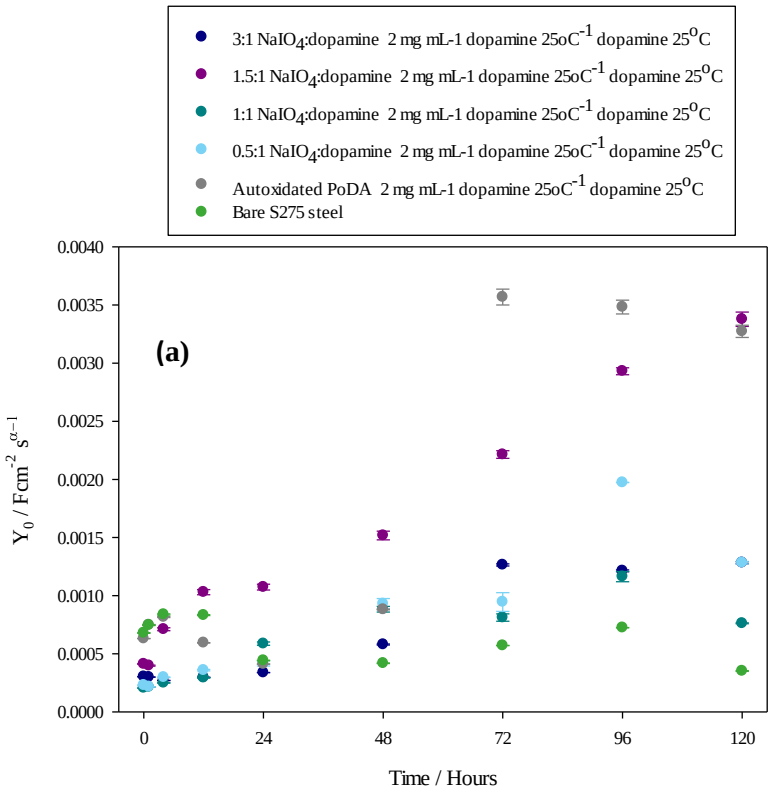

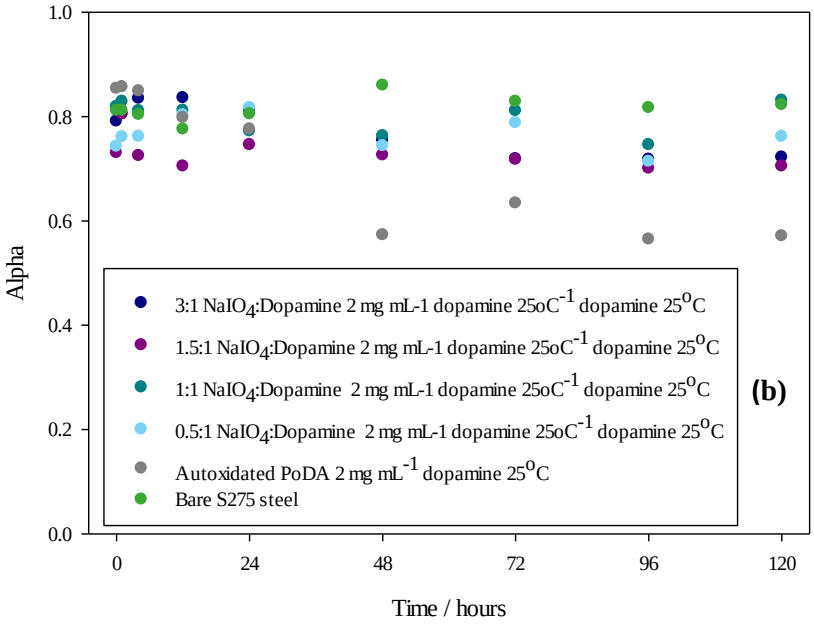

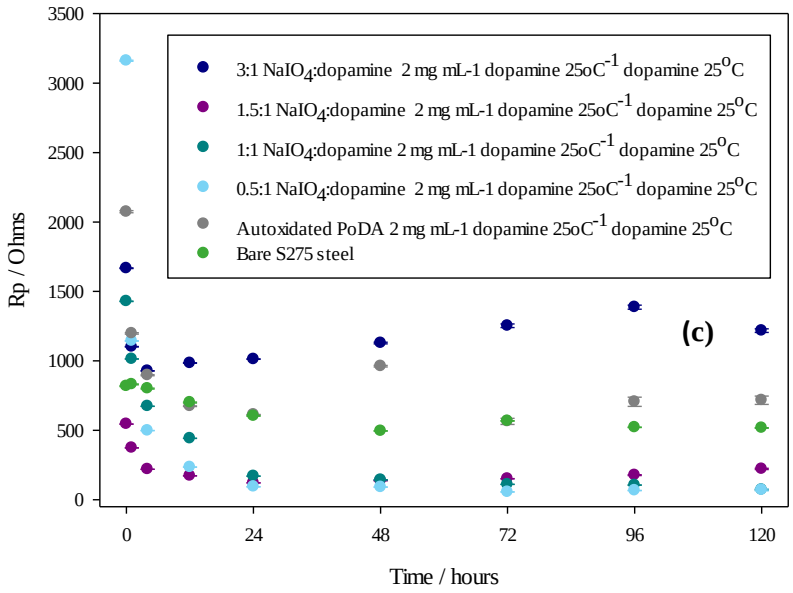

Figure 6.11 - EIS fitted parameters for varied $NaIO_4$ to dopamine ratio using a 2 mg mL^{-1} dopamine solution and a 25°C deposition temperature: (a) CPE (b) alpha and (c) *R*p

As can be seen from the fitted parameters in Figure 6.11, only the 3:1 $NaIO_4$ ratio managed to outperform autoxidated PoDA. The three other ratios performed worse than bare S275 steel indicating that not only did the use of $NaIO_4$ as an oxidant fail to improve the corrosion performance of PoDA, that it actually accelerated the corrosion process. Mild steel is known to perform poorly in corrosion tests when sodium perchlorate is present [200]. The similarity in chemical reactivity between chlorates and iodates indicates that the same can be said for sodium periodate. If $NaIO_4$ has been incorporated into the coating then the corrosive species is in close proximity to the underlying steel which may induce corrosion to a greater degree than if $NaIO_4$ were merely present in solution as there is no barrier present between corrosive species and substrate. Following these results, sodium periodate was not used as an oxidant in any further experiments. As $NaIO_4$ is a powerful oxidant, PoDA will form more readily as particles in solution or as a film on the solution surface than as a film on a supplied substrate. This will be especially true for the higher oxidant ratios, which explains why the initial impedances and Rp values are not as high for the 3:1 and 1.5:1 ratios as they are for the 1:1 and 0.5:1 ratios. Bernsmann et al. reported similar results with their work using $CuSO_4$ as an oxidant [201] and their investigations into the solution interface during the polymerisation of dopamine [202].

p-Benzoquinone

1.5:1

Table 6.14 - EIS fitted parameters for a 1.5:1 *p*-BQ to dopamine ratio using a 2 mg mL^{-1} dopamine solution and a 25°C deposition temperature. The EIS is carried out in 3.5%NaCl.

Time / h	R_u / Ω	± /Ω	CPE/$_s^{\alpha}$ Ω^{-1} cm^{-2} (x10^{-4})	± / $_s^{\alpha}$ Ω^{-1} cm^{-2} (x10^{-6})	α	R_p / Ω	± / Ω	χ^2	Circuit
0	15.5	0.2	4.74	1.37	0.77	2357	7.49	0.053	Randles
1	13.9	0.2	4.73	1.38	0.78	2031	6.06	0.012	Randles
4	13.1	0.2	3.90	1.17	0.79	1960	5.35	0.046	Randles
12	12.3	0.2	4.70	1.39	0.79	1786	5.02	0.047	Randles
24	12.1	0.2	6.98	3.05	0.79	1396	6.04	0.031	Randles
48	15.6	0.2	11.8	8.08	0.76	1391	12.75	0.010	Randles
72	14.1	0.2	19.9	20.9	0.75	1513	30.13	0.095	Randles
96	13.5	0.2	23.4	34.4	0.76	1474	42.91	0.054	Randles
120	13.2	0.2	23.3	28.1	0.75	1506	37.25	0.011	Randles

1:1

Table 6.15 - Fitted parameters for a 1:1 *p*-BQ to dopamine ratio using a 2 mg mL^{-1} dopamine solution and a 25°C deposition temperature. The EIS is carried out in 3.5%NaCl.

Time / h	R_u / Ω	± / Ω	CPE / $_s^{\alpha}$ Ω^{-1} ^{2}	± / $_s^{\alpha}$ Ω^{-1} ^{2}	α	R_p / Ω	± / Ω	χ^2	Circuit
0	14.0	0.2	4.80	1.26	0.66	2789	10.98	0.03	Randles
1	11.7	0.2	5.28	1.52	0.67	2038	7.87	0.08	Randles
4	11.2	0.3	6.21	2.53	0.66	1628	8.75	0.08	Randles
12	13.6	0.2	6.33	2.19	0.69	1376	5.69	0.05	Randles
24	13.2	0.2	7.88	3.37	0.69	1057	5.23	0.03	Randles
48	14.3	0.2	10.8	6.39	0.67	1189	10.22	0.02	Randles
72	14.8	0.2	17.2	15.6	0.66	1528	32.33	0.01	Randles
96	14.6	0.3	19.9	26.0	0.68	1477	45.31	0.01	Randles
120	15.6	0.2	19.0	19.3	0.69	1607	38.42	0.02	Randles

Both Table 6.14 and Table 6.15 show that although there is a slight drop in corrosion protection over the immersion time, the Rp values are maintained at levels above those of both bare S275 steel and autoxidated PoDA. This indicates that the p-BQ mediated coatings have superior barrier properties over PoDA coatings produced using other oxidants.

0.5:1

Table 6.16 - EIS fitted parameters for a 0.5:1 *p*-BQ to dopamine ratio using a 2 mg mL^{-1} dopamine solution and a 25°C deposition temperature. The EIS is carried out in 3.5%NaCl.

Time/ h	*R*u /Ω	± /Ω	CPE / s^{α} Ω^{-1} cm^{-2} ($x10^{-4}$)	± / s^{α} Ω^{-1} cm^{-2} ($x10^{-6}$)	α	*R*p /Ω	± / Ω	W / Ω cm^2 $s^{-1/2}$	±/ Ω cm^2 $s^{-1/2}$	χ^2	Circuit
0	20.3	0.2	1.93	2.47	0.85	3300	16.07	1662	6.59	0.05	R+W
1	20.8	0.2	2.14	0.53	0.86	1809	7.01	1400	3.29	0.10	R+W
4	14.1	0.2	2.87	1.21	0.81	1808	10.74	1289	0.46	0.05	R+W
12	16.3	0.3	0.342	0.51	0.68	1748	2.53	1185	0.19	0.08	R+W
24	13.8	0.2	8.13	1.09	0.77	1830	4.19	1022	0.97	0.08	R+W
48	11.3	0.2	4.59	5.39	0.70	1951	20.97	603	3.72	0.09	R+W
72	10.6	0.2	4.32	2.36	0.70	1632	40.42	488	5.98	0.07	R+W
96	15.5	0.2	2.96	1.88	0.82	1034	23.09	643	3.30	0.02	R+W
120	16.5	0.2	4.35	0.29	0.71	1044	59.30	570	5.00	0.04	R+W

Table 6.16 shows the presence of a diffusive element across the entire immersion period for the 0.5:1 p-BQ : dopamine ratio. The fact that the diffusion process is present even at the initial time point and that the diffusive element is in a separate time constant to the CPE and Rp values indicate that the diffusion element is as a result of a species travelling within the deposited coating itself rather than ions diffusing in from electrolyte or out through the coating from the substrate. This has been observed previously in EIS studies of PANi where a dopant has been added to the polymer during deposition. As this behaviour is not observed in the auto-oxidated PoDA the diffusive element has to be as a result of some reaction involving p-BQ.

Comparisons

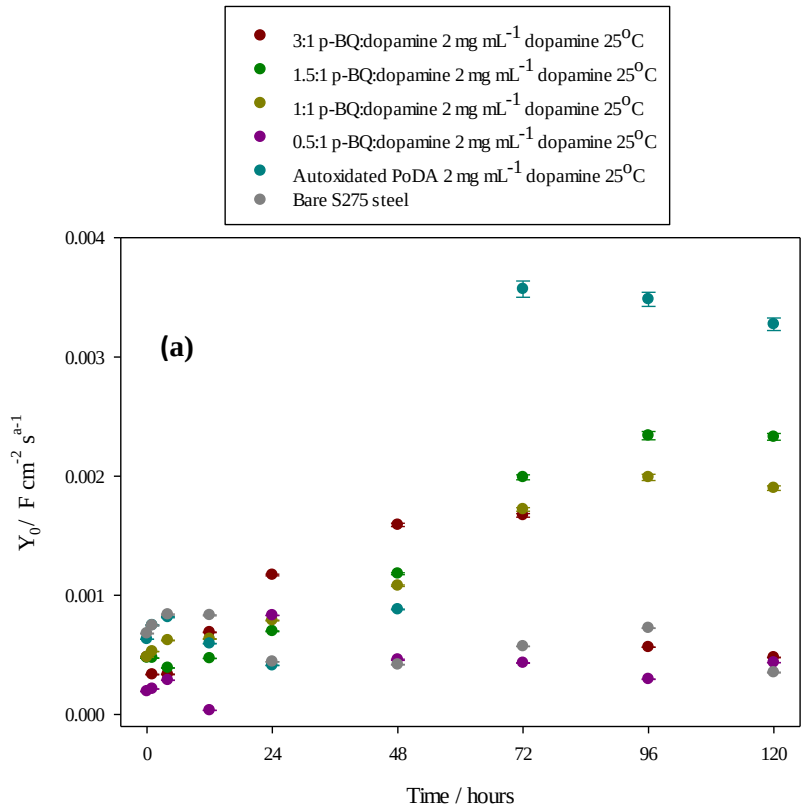

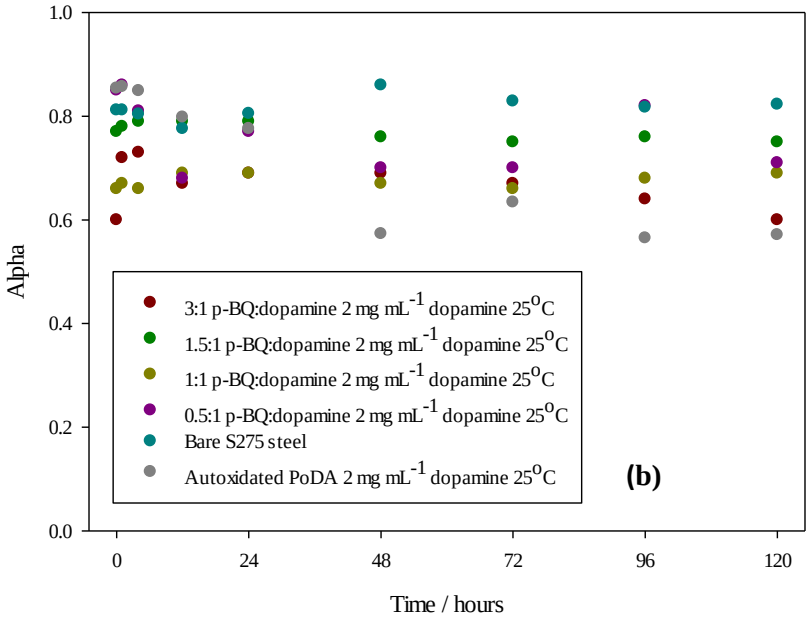

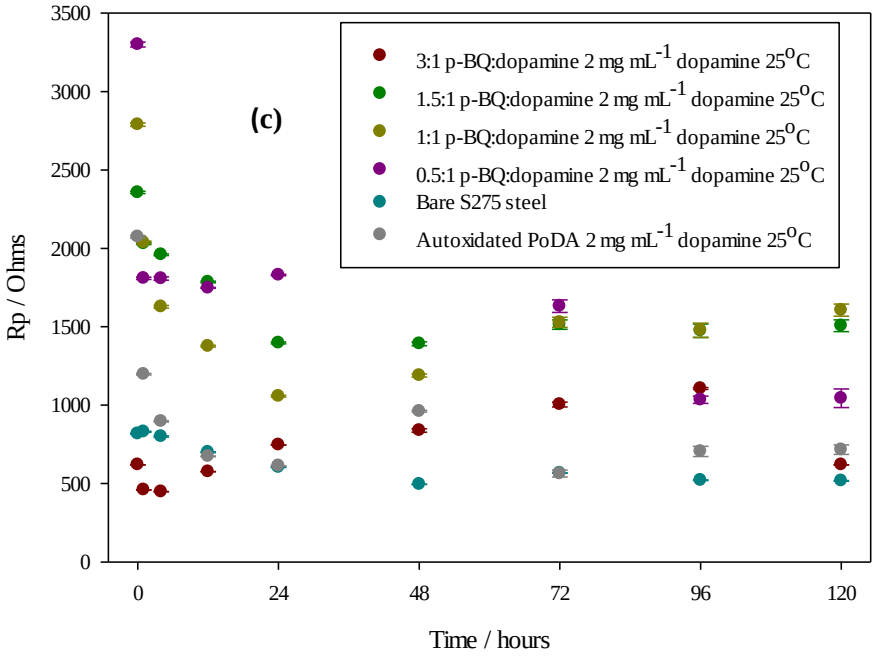

Figure 6.12 - EIS fitted parameters varied p-BQ to dopamine ratio using a 2 mg mL^{-1} dopamine solution and a 25°C deposition temperature: (a) CPE, (b) alpha and (c) Rp

The failure of the higher molar ratios of p-BQ to dopamine to produce coatings that were any improvement over the autoxidated PoDA can be attributed to the ease with which p-BQ forms polyhydroxyhydroquinones. The polymerisation is more likely to occur in solution, especially the alkaline ones used in the polymerisation of dopamine. The greater ratios mean an excess of p-BQ which will form polyhydroxyhydroquinones preferentially in solution rather than the p-BQ acting as an oxidant in the oxidation and subsequent polymerisation of dopamine onto the included substrate [167]. Ragimov et al. found that the initial concentration of p-BQ was the most important factor in determining the rate of polymerisation [168] with higher concentrations having almost instantaneous polymerisation rates. The best performing ratio of p-BQ to dopamine was the 0.5:1 ratio (Figure 6.12) therefore this ratio was used in all further work requiring p-BQ as an oxidant.

6.1.2 Dopamine monomer concentration

Lee et al. used a dopamine concentration of 2 mg mL^{-1} in their initial publication on the formation of coatings from the autoxidation of dopamine [37] and this has been the most commonly used dopamine concentration since. However, previous studies had sought to optimise the O_2-mediated dopamine polymerisation in order to increase the thickness of the deposited PoDA coating [43] by increasing the initial dopamine concentration. Ball et al. reported that this relationship was linear up to a maximum concentration of 20 mg mL^{-1}. Therefore, dopamine concentrations of 5, 10 and 20 mg mL^{-1} were tested in conjunction with the best performing dopamine to oxidant ratios as defined in the previous section.

$KMnO_4$

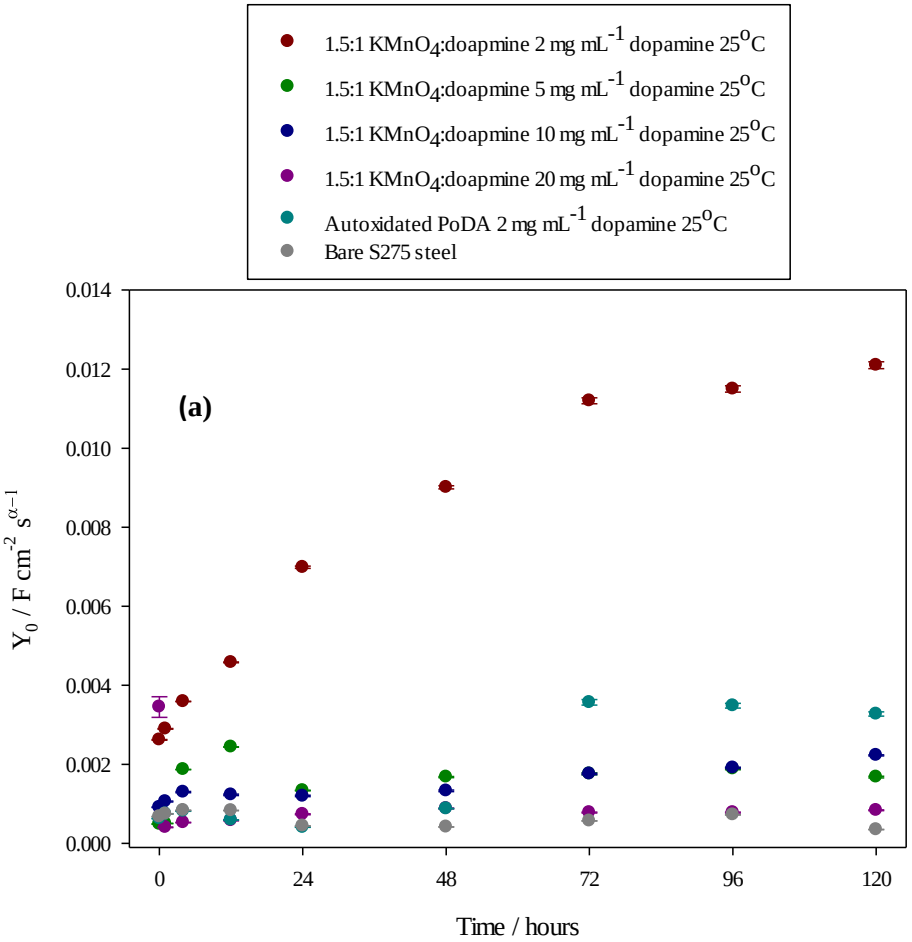

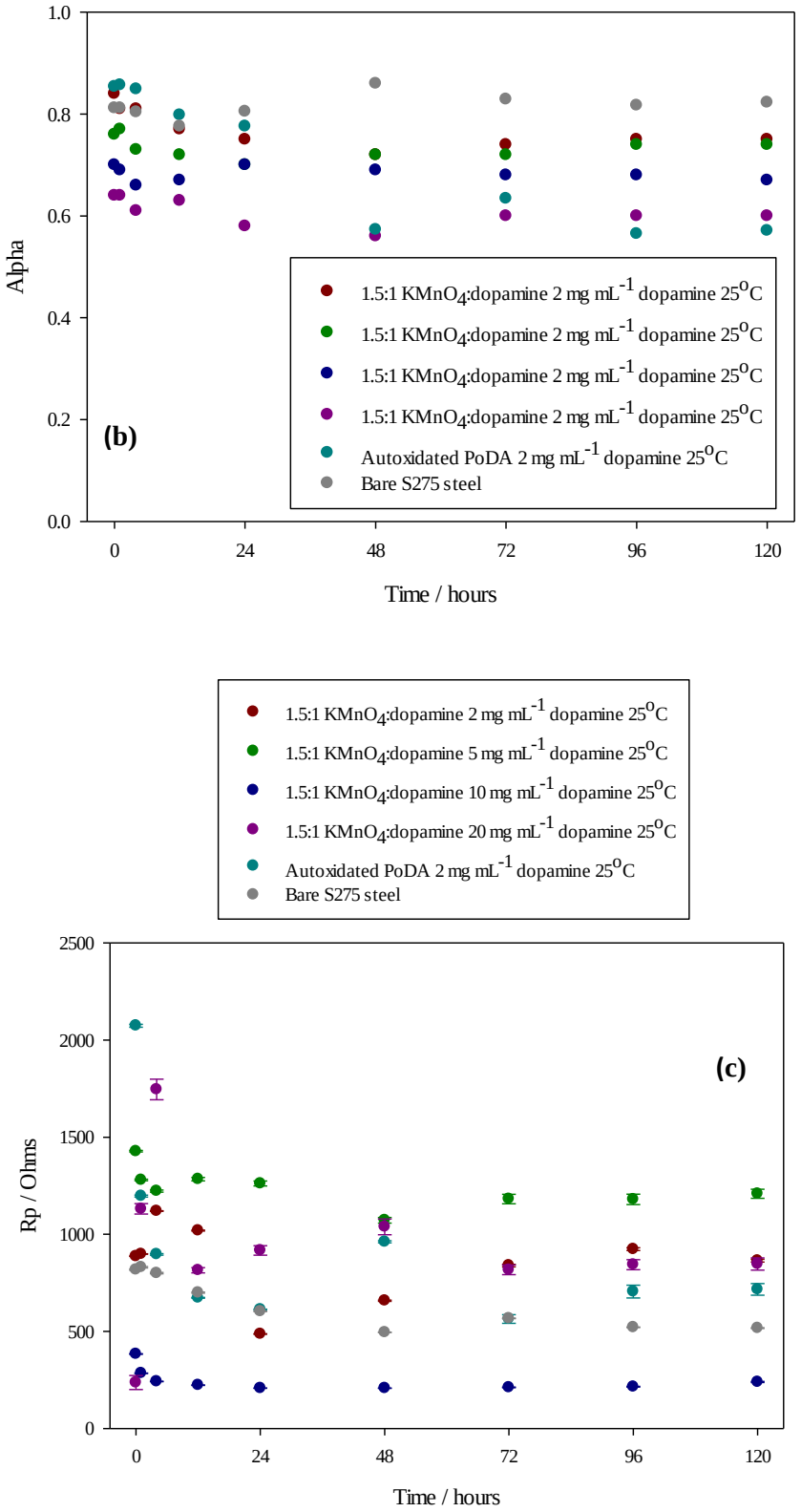

Figure 6.13 - EIS fitted parameters for a 1.5:1 $KMnO_4$ to dopamine ratio using a varied dopamine concentration and a 25°C deposition temperature: (a) CPE, (b) alpha and (c) *R*p values

Na_2MoO_4

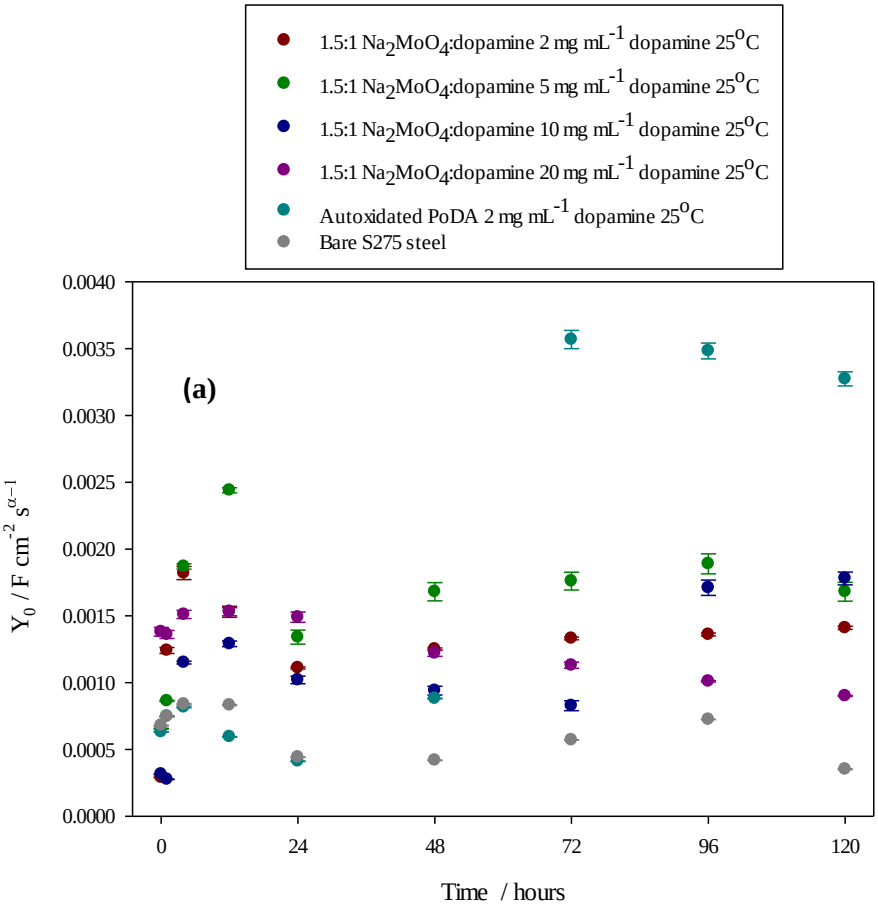
1.5:1 Na2MoO4:dopamine 2 mg mL-1 dopamine 25oC
1.5:1 Na2MoO4:dopamine 5 mg mL-1 dopamine 25oC
1.5:1 Na2MoO4:dopamine 10 mg mL-1 dopamine 25oC
1.5:1 Na2MoO4:dopamine 20 mg mL-1 dopamine 25oC
Autoxidated PoDA 2 mg mL-1 dopamine 25oC
Bare S275 steel
(a)
Y0 / F cm-2 s α−1
Time / hours
0.0040
0.0035
0.0030
0.0025
0.0020
0.0015
0.0010
0.0005
0.0000
0
24
48
72
96
120

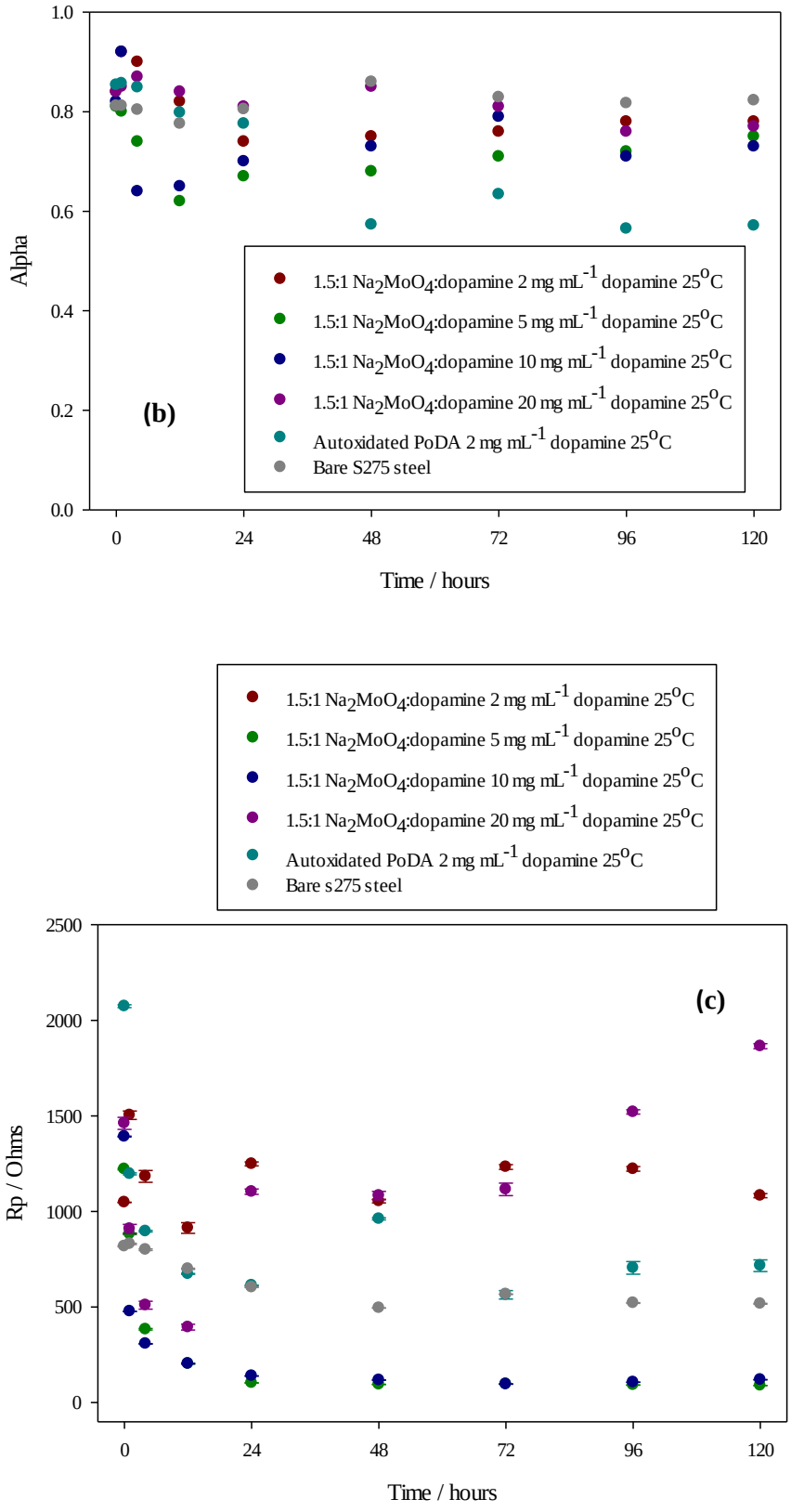

Figure 6.14 - EIS fitted parameters for a 1.5:1 Na_2MoO_4 to dopamine ratio using a varied dopamine concentration and a 25°C deposition temperature: (a) CPE, (b) alpha and (c) *R*p values

p-Benzoquinone

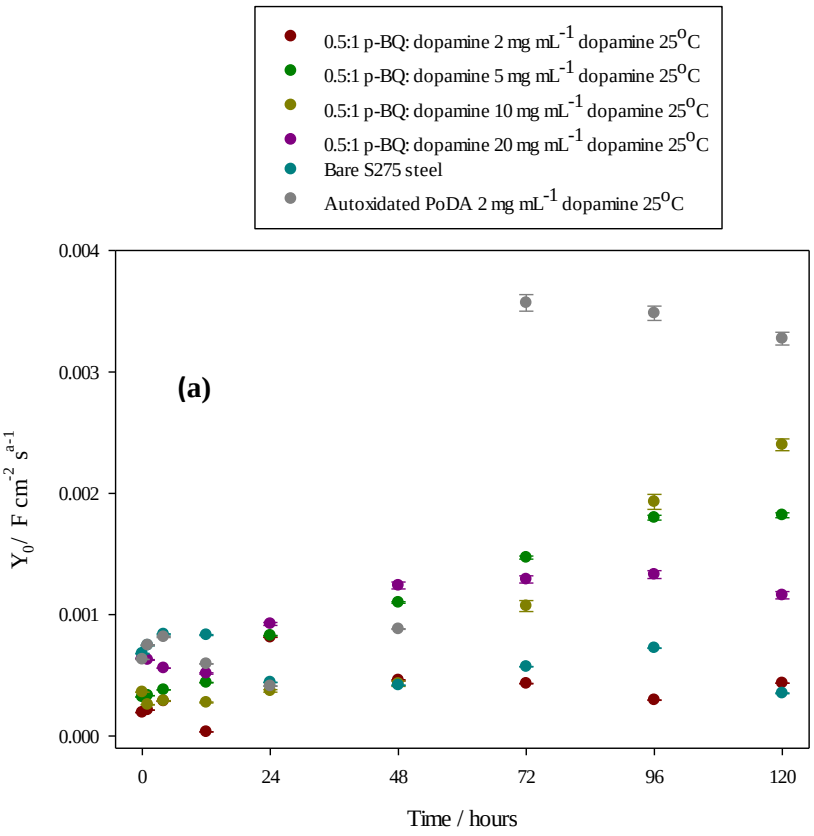

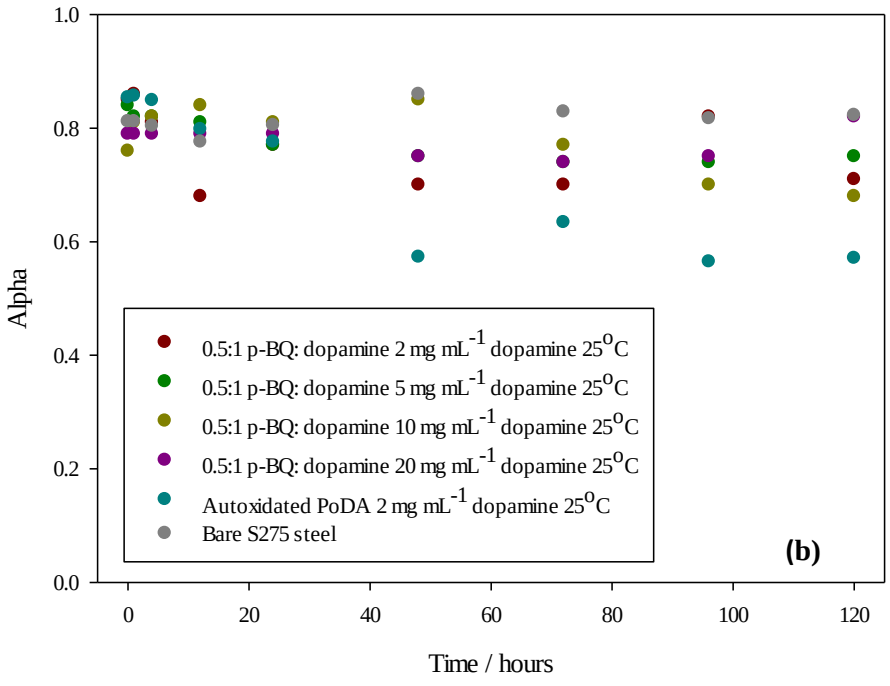

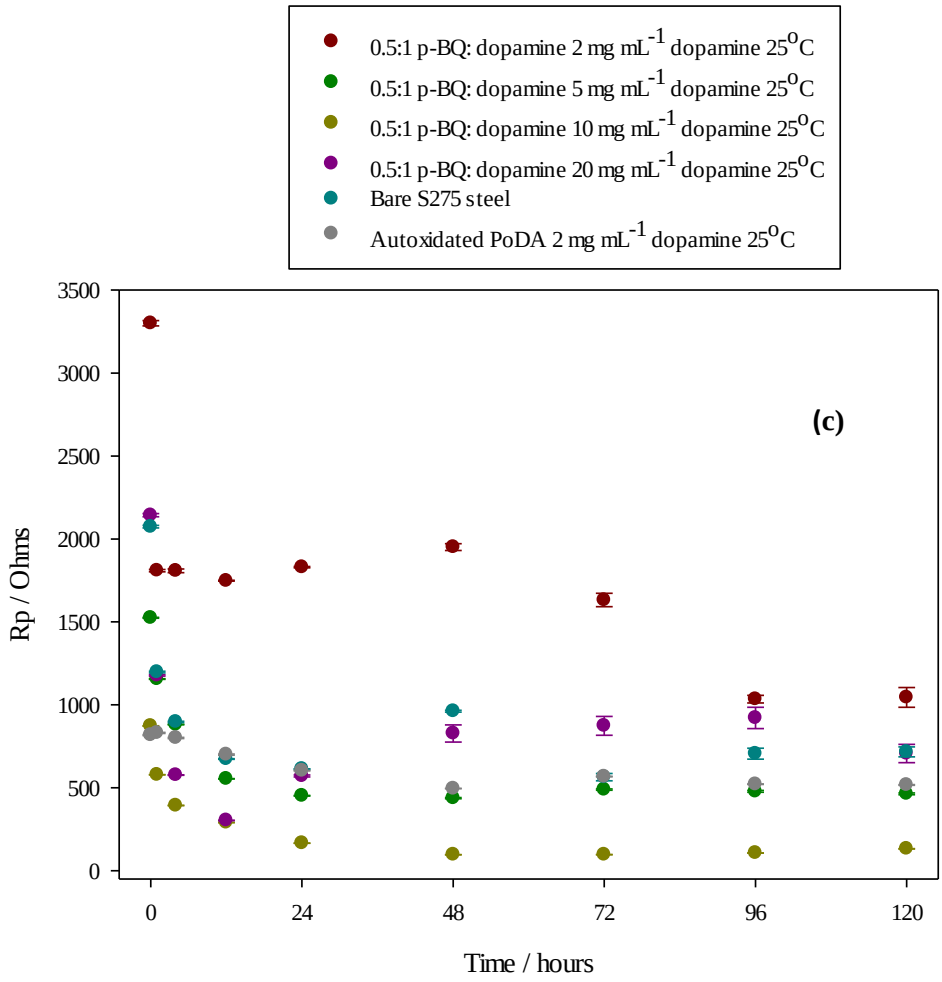

Figure 6.15 – EIS Fitted parameters 0.5:1 *p*-BQ to dopamine ratio using a varied dopamine concentration and a 25°C deposition temperature: (a) CPE, (b) alpha and (c) *R*p values.

As can be seen from Figure 6.13,

Figure **6.14** and Figure 6.15, increasing the dopamine monomer concentration does not equate to an improvement in coating thickness regardless of the oxidant used. This is due to the more favourable polymerisation of dopamine in solution rather than on the substrate surface. As dopamine can deposit onto itself, the presence of PoDA particles in the deposition solution discourages deposition onto the substrate present in the deposition solution. The increased concentration of dopamine leads to increased polymerisation in solution and therefore thinner films on the introduced substrate. This has been observed by several authors working with PoDA [49],[36],[203] despite the findings of Ball et al. [43] which showed that an increase in dopamine concentration of up to 20 mg mL^{-1} resulted in thicker films. Therefore, all future work will be undertaken using 2 mg mL^{-1} dopamine solutions.

6.1.3 Variable deposition temperature

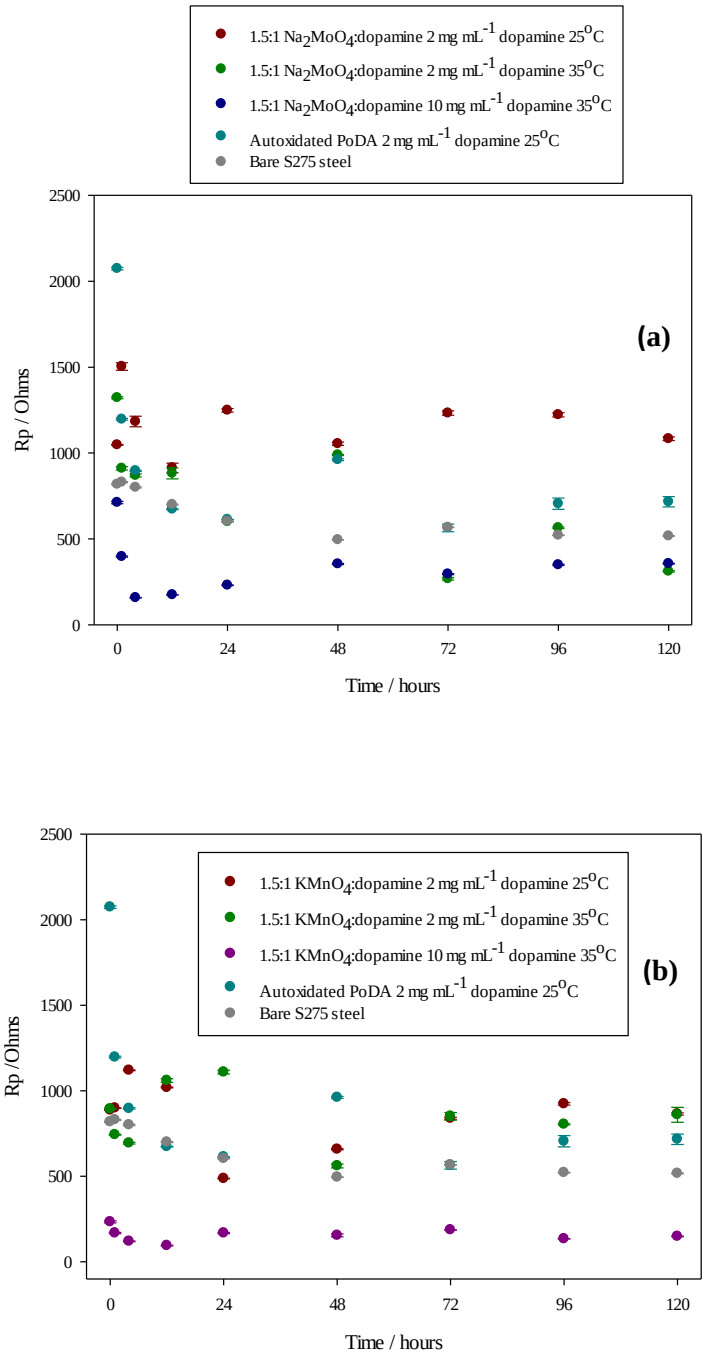

Figure 6.16 - Variation of *R*p values with time for (a) 1.5:1 Na_2MoO_4 to dopamine using a 2 mg mL^{-1} dopamine at 35°C and (b) 1.5:1 $KMnO_4$ to dopamine 2 mg mL^{-1} dopamine at 35°C

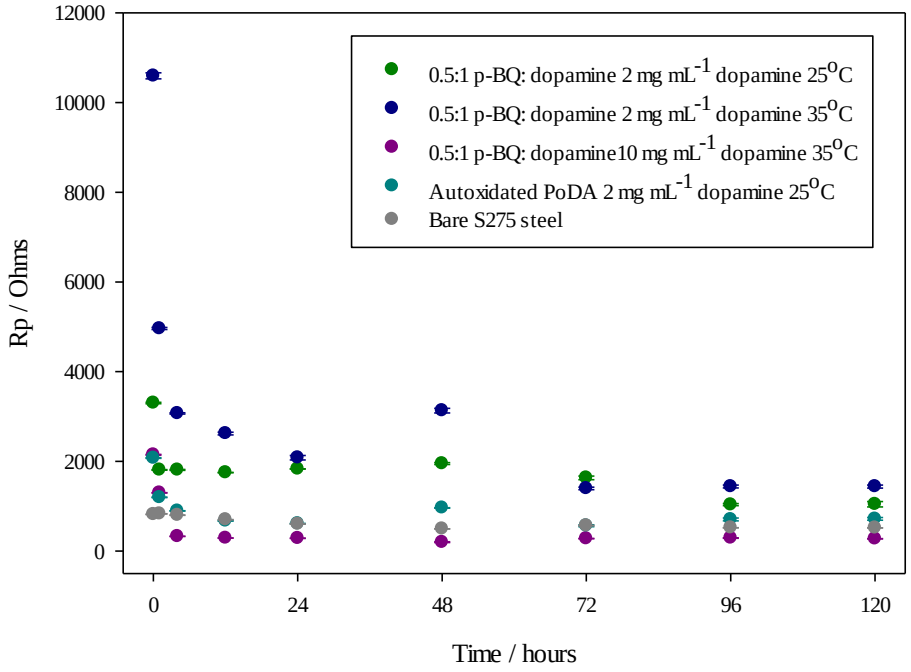

Figure 6.17 - Variation of *R*p values with time for 0.5:1 *p*-BQ to dopamine using a 2 mg mL^{-1} dopamine solution at 35°C

Figure 6.16(a) and (b) both indicate that an increase in temperature does not produce a coating with corrosion prevention properties that are superior to autoxidated PoDA when either KMnO4 or Na_2MoO_4 is used as the oxidant. However, Figure 6.17 shows that when p-BQ is used as the oxidant at elevated temperatures, the barrier initial protection is six times that of steel and that even though this protection begins to decrease with time, it is still maintained at levels above that of both autoxidated PoDA and bare S275 steel.

After the deposition parameter refinement was complete, it became apparent that the best combination of parameters was a 0.5:1 ratio of p-benzoquinone to dopamine monomer using a 2 mg mL^{-1} dopamine monomer solution and a deposition temperature of 35°C. Further testing was required to understand the behaviour and properties of the coating. Hereafter, the initial polydopamine coating produced through autoxidation of dopamine monomer solution will be referred to as O_2-mediated PoDA and the coating deposited using a 0.5:1 ratio of p-BQ to dopamine monomer and a 2 mg mL^{-1} dopamine solution at 35°C will be termed p-BQ mediated PoDA.

6.1.4 Properties and behaviour of *p*-Benzoquinone mediated PoDA coating

The following aspects of this study were carried out in order to try and ascertain the mechanism of corrosion protection of the *p*-BQ mediated PoDA and whether this was the same as that of the O_2^- mediated PoDA. It was hoped that the results would make it possible to ascertain whether:

a) Dopamine and *p*-BQ monomers combine to form a co-polymer that has improved barrier properties over an O_2 mediated PoDA coating and is thicker, thus accounting for the higher impedances achieved.

b) *p*-BQ undergoes autoxidation to form protective polymers (the polyhydroxyquinones discussed previously).

c) *p*-BQ monomer is incorporated into the deposited PoDA coating allowing it to act as a corrosion inhibitor.

d) *p*-BQ is not incorporated into the coating at all and merely acts as a more effective and/or efficient oxidant resulting in the production of a thicker coating that possesses better barrier properties and subsequently offers improved protection against corrosion. This would also account for the higher impedances achieved during EIS testing.

e) BQ is known to undergo polymerisation in the presence of alkali by autoxidation, in a process that is almost identical to that of the autoxidation of PoDA. Such polymeric products have been used as antioxidants in the production of styrene-butadiene rubber (SBR) [204, 205]. Therefore, it is possible that if *p*-BQ is forming polymeric products and these are being incorporated into the coating they will act as an antioxidant and thus inhibit the corrosion processes through a similar mechanism.

However, it has also been found that the *p*-BQ based polymers that form under alkali conditions can act as oxidation-reduction polymers meaning they may have a similar corrosion protection mechanism to other red-ox polymers such as polyanilines [52].The alkalinity is required because the mechanism requires the incorporation of a hydroxyl moiety [53].

6.1.4.1 X-Ray Photoelectron Spectroscopy (XPS)

The XPS studies were carried out on both O_2-mediated PoDA and p-BQ-mediated PoDA with bare uncoated S275 steel used as a reference background. The aim was to determine any differences in composition between the two coatings. Figure 6.18 shows the peaks observed during a survey scan of the bare S275 substrate. The Fe2p peak is attributed to elemental iron and the C1s peak to elemental carbon, both of which are found in a structural steel such as S275 steel. The O1s peak can be attributed to iron oxide formation on the surface of the steel.

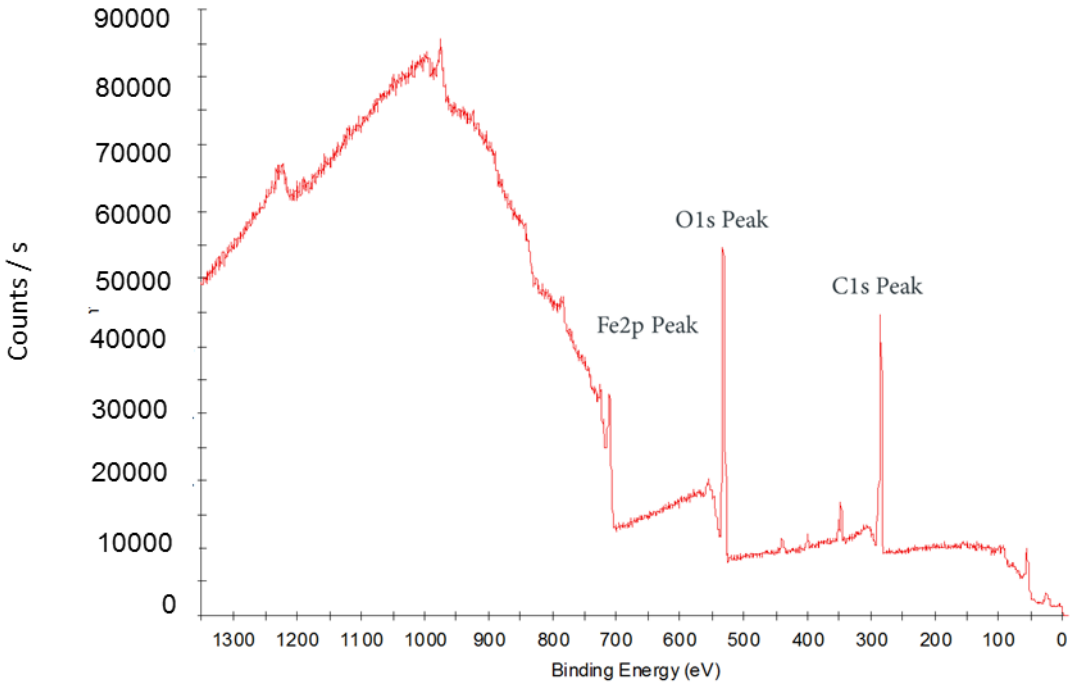

Figure 6.18 – XPS survey scan bare S275 steel

Figure 6.19 shows the peaks of the survey scan of an O_2-mediated PoDA coating deposited at atmospheric temperature. The Fe2p peak present in the bare S275 steel is no longer visible on the coated scan. This indicates that the deposited coating is intact enough to completely mask the underlying substrate. The survey scan contains O1s, N1s and C1s peaks which would be expected for a nitrogen containing polymer such as polydopamine [175].

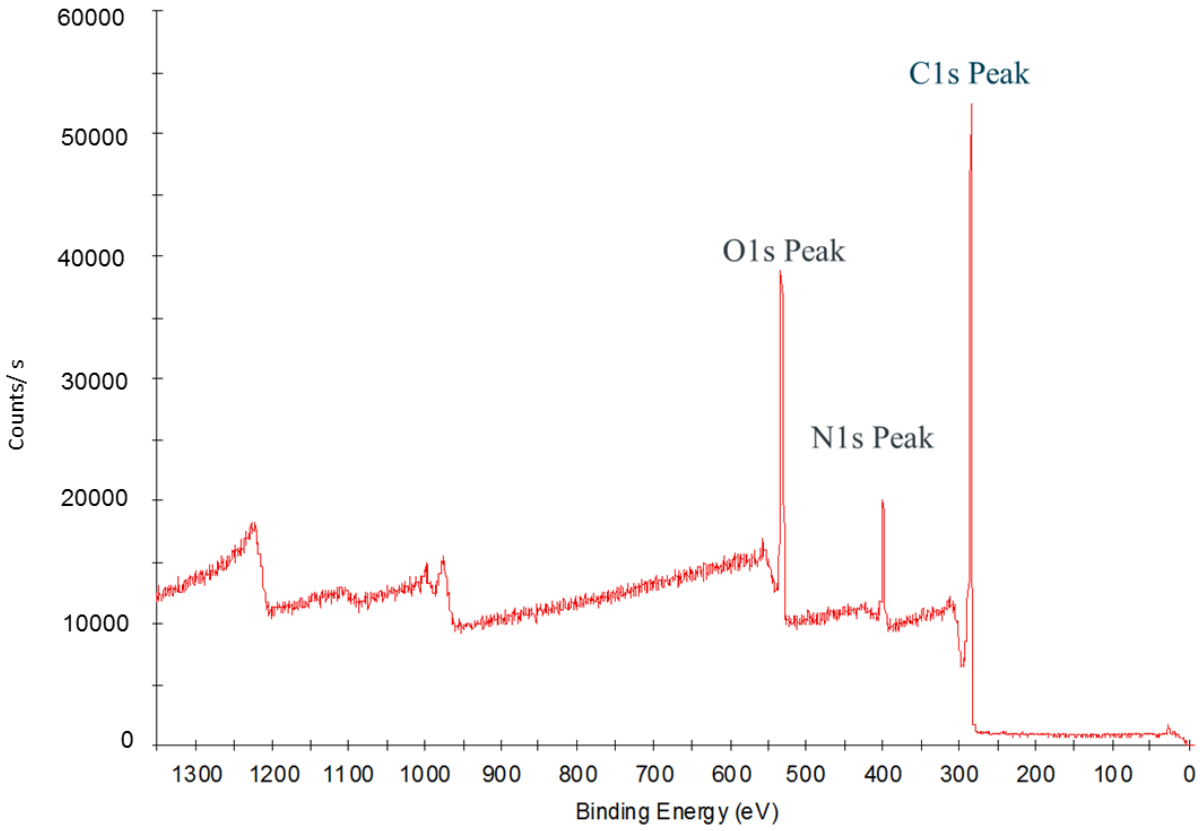

Figure 6.19 –XPS survey scan O_2 mediated PoDA coating deposited at 25°C

To try and determine which functional groups are present in the polymer, detailed scans of the identified survey peaks were undertaken; these are shown in Figure 6.20, Figure 6.21 and Figure 6.22. The peak fittings were compared to a database of XPS scans carried out on polymeric materials [175] in order to identify the functional groups present in the coating.

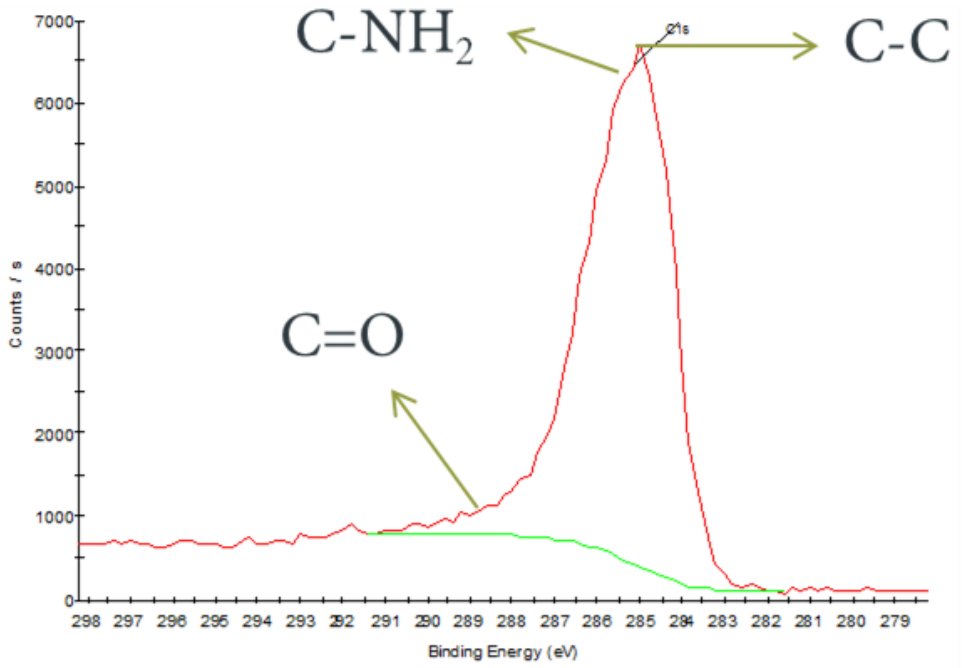

Figure 6.20 – XPS detailed C1s scan, O_2 mediated coating

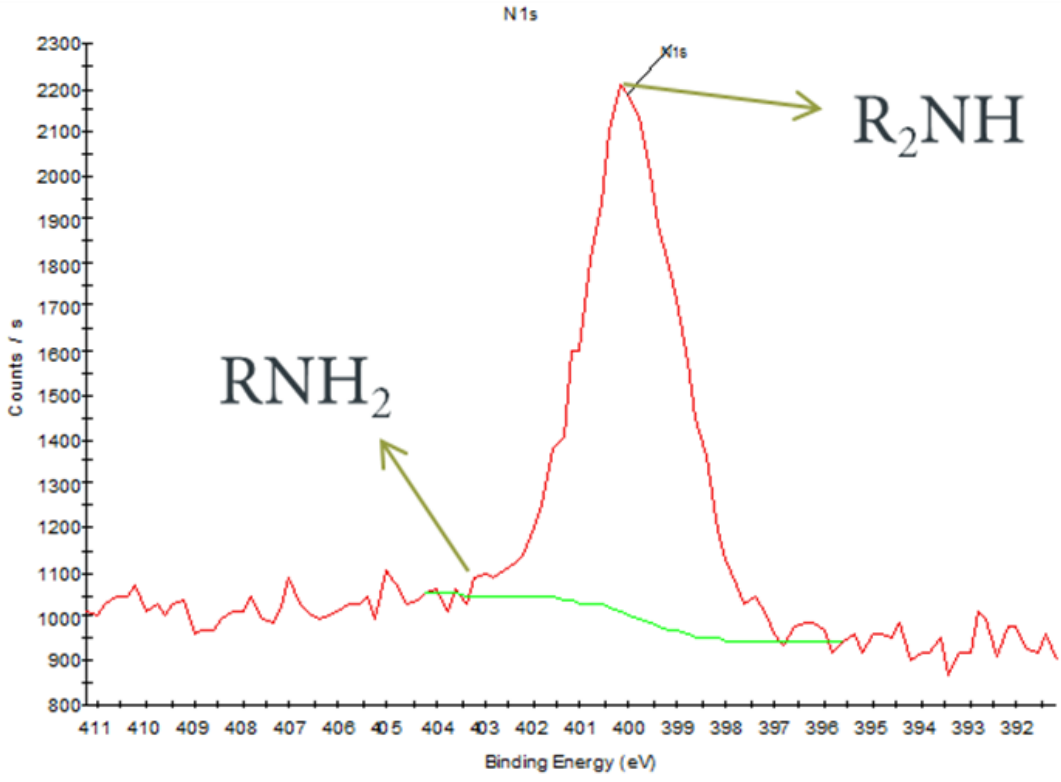

Figure 6.21 - XPS detailed N1s scan; O_2 mediated PoDA coating

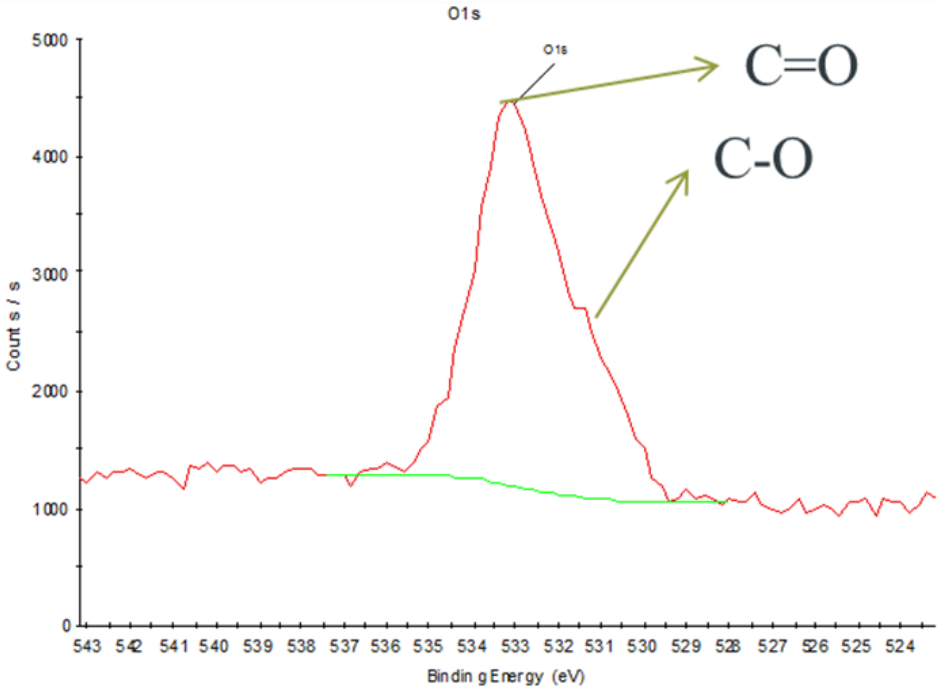

Figure 6.22 – XPS detailed O1s scan, O_2 mediated PoDA coating

The detailed C1s and N1s scans, Figure 6.20 and Figure 6.21, respectively, both show the presence of an NH_2 group in the deposited coating. This indicates that dopamine monomer (Figure 6.23) is present in the deposited coating. Consequently, this suggests that atmospheric oxygen is not acting as the most effective oxidant.

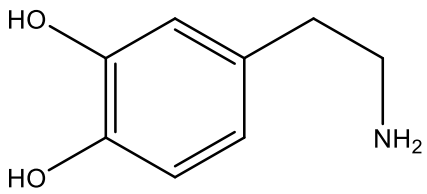

Dopamine

4-(2-aminoethyl)benzene-1,2-diol

Figure 6.23 – Dopamine monomer

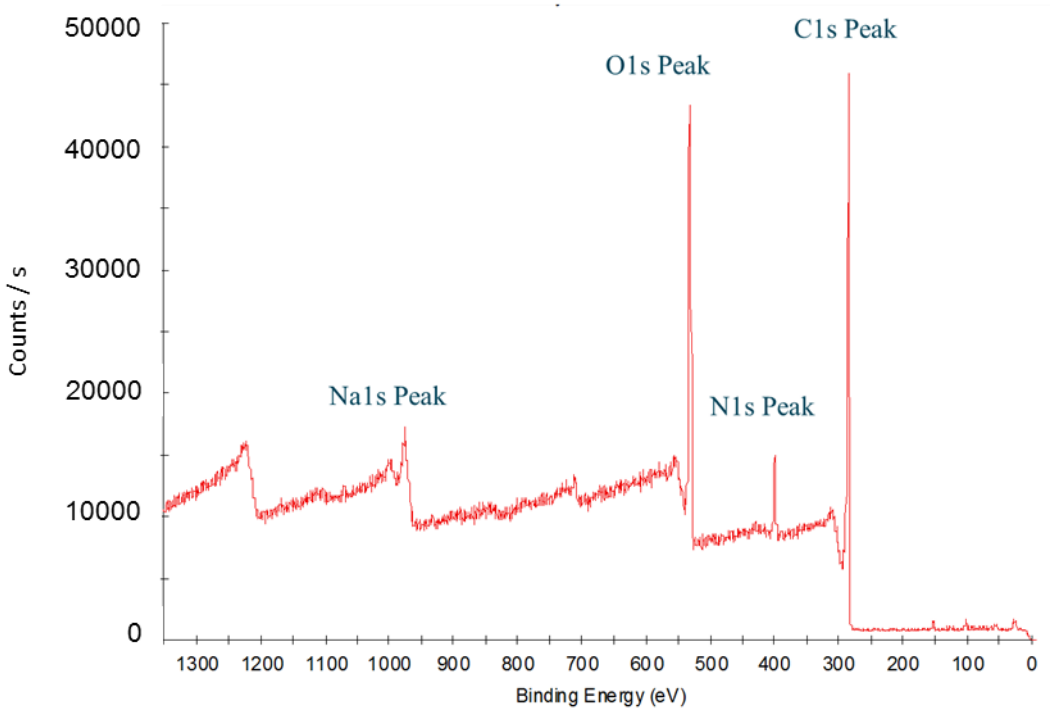

Figure 6.24 - XPS survey scan *p*-Benzoquinone mediated PoDA coating deposited at 35°C

Figure 6.24 shows the survey scan of a p-BQ mediated PoDA coating. As with the O_2-mediated coating, there is no Fe peak present in the survey scan which again indicates that the deposited coating is sufficiently intact to completely mask the underlying mild steel substrate. In addition to the O1s, N1s and C1s peaks seen in the O_2-mediated PoDA scan, there is a Na1s peak present. This has been seen in previous XPS surveys of O_2-mediated PoDA [68]. During the polymerisation reaction, the very thin deposited film is kept in sodium phosphate buffer solution for a 24-hour period which results in sodium ions from the buffer leaching into the PoDA film.

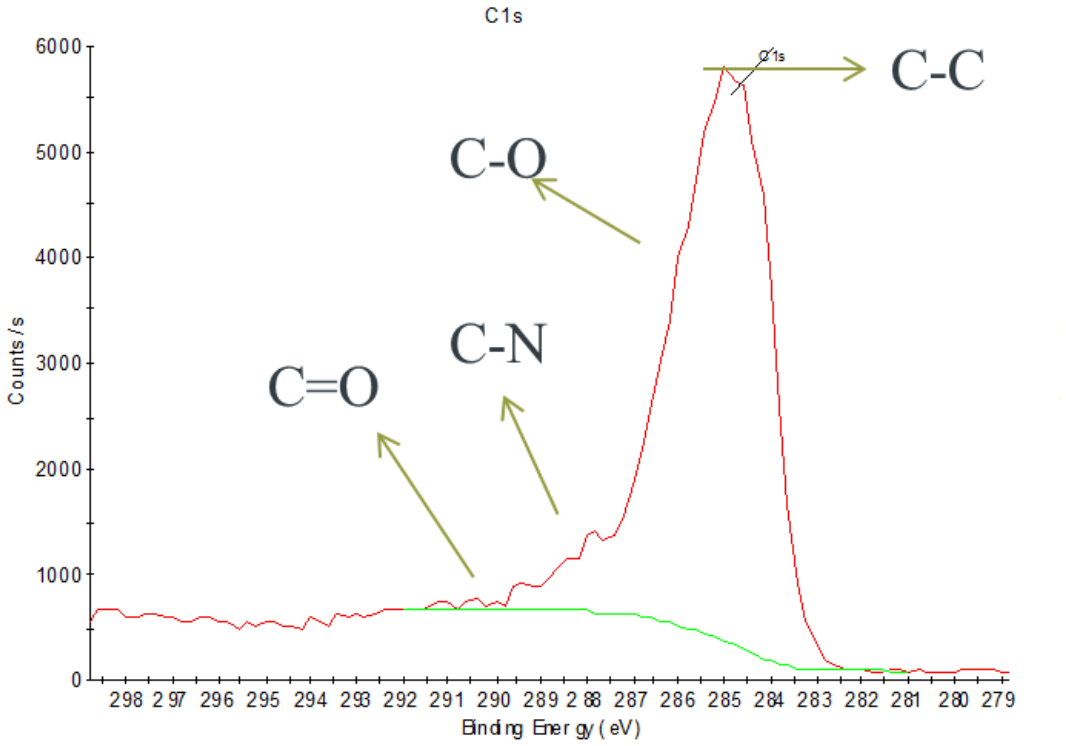

Figure 6.25 - XPS detailed C1s scan, *p*-BQ- mediated PoDA coating

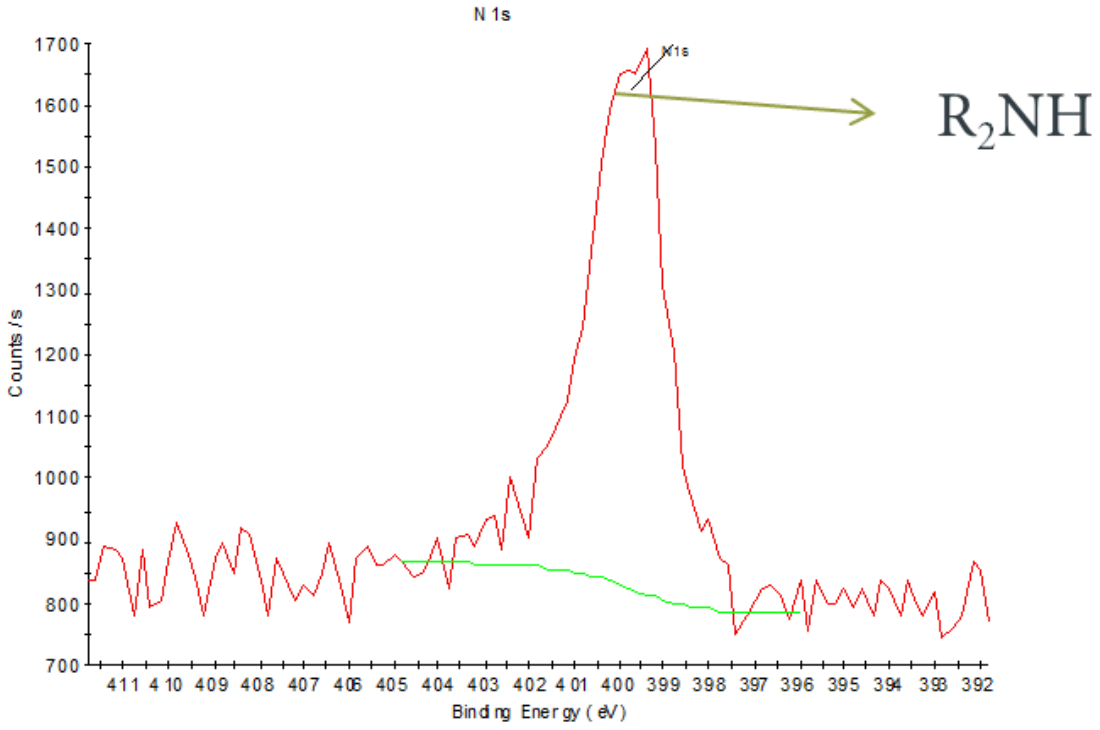

Figure 6.26 - XPS detailed N1s scan, *p*-BQ- mediated PoDA coating

The detailed C1s and N1s scans in Figure 6.25 and Figure 6.26 respectively, show that the NH_2 group present in the O_2-mediated PoDA film is not present in the *p*-BQ-mediated PoDA coating which indicates that *p*-BQ is acting as a more efficient oxidant than atmospheric oxygen [55]. If the greater oxidant efficacy results in thicker coatings then this would account, in part, for the increased impedance observed in the EIS tests. When Bernsmann et al. [49] and latterly Ball et al. [177] used copper sulphate or ammonium persulphate as an additional oxidant to atmospheric oxygen, they also observed the formation of a thicker polymeric film which was attributed to a more efficient oxidation reaction [43]. However, they did not test their deposited films for corrosion performance.

Whilst the XPS results give some indication as to how the structures of the compared coatings differ, they do not provide sufficient structural information to make any great distinction between the two polymers. Figure 6.22 and Figure 6.25 show the presence of C=O functional groups in both the autoxidated and p-BQ mediated PoDA. The most likely copolymer to form between p-benzoquinone and the amine containing dopamine would be some form of poly(amino) quinone. Previous investigations into such polymers have demonstrated that such materials would contain C=O bonds [189]. As is described in the literature review (Chapter 2.1.4), all the proposed forms of PoDA would also contain C=O bonds, regardless of oxidant used. In addition, p-benzoquinone itself contains two C=O functional groups. Therefore, it can be concluded that XPS alone provides insufficient structural information to determine whether a copolymer has formed, a thicker PoDA coating has formed or if p-benzoquinone has been incorporated in monomeric form. However, the lack of OH groups in the p- BQ mediated PoDA indicates a lack of polyhyoxyhydroquinone moieties, indicating that p-BQ has not undergone polymerisation solely with itself; each unit of the polyhydroxyhydroqinones would be expected to contain three OH groups.

Further structural analysis is therefore required. Methods that are easy in the practical sense, such as FT-IR, are difficult with the deposited films as they are so thin. In the case of FT-IR, the polymeric films deposited onto the mild steel substrate are thin enough that there is reflectance from the steel making successful analysis impossible. Other methods that have previously been used to analyse PoDA such as ss-NMR [35] and UV-VIS [177], have been undertaken on the solid precipitates that form in solution during the polymerisation process, however, these precipitates are not necessarily representative of the deposited films and a technique that is capable of providing structural information from deposited films is required.

6.1.4.2 Scanning Kelvin Probe

The distances shown in Figure 6.28, Figure 6.29 and

Figure **6.30** are the *x*- and *y*-radii of the corroded areas of the tested samples and so the plotted areas represent a quarter of the total corroded sample area. SKP tests were undertaken in order to improve the understanding of the corrosion kinetics and how these relate to the mechanism of corrosion protection of *p*-benzoquinone mediated PoDA.

When a hemispherical droplet of electrolyte is placed onto the surface of a piece of metal, it forms a differential aeration cell. The anodic reaction is confined to the middle of the droplet where the oxygen concentration is lower whilst the cathodic reaction will take place at the edge where the oxygen concentration is higher because oxygen can readily diffuse through the edges of the droplet (Figure 6.27). As the relative humidity in the testing chamber is maintained at 95% RH for the duration of the test, the droplet does not dry out.

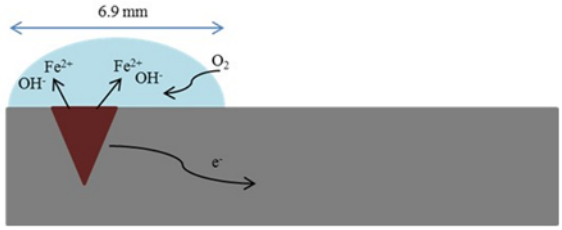

Figure 6.27 - Schematic of the differential aeration cell

Neufeld et al. proposed the concept of secondary spreading following investigations into the initiation of corrosion on zinc surfaces by particles of NaCl [164]. They found that when the hemispherical droplet of NaCl was present, a thin layer of electrolyte spread out from the droplet. The authors found that the anodic reaction remains at the original droplet site and the cathodic reaction spreads with the spread of electrolyte. Later studies found that, as a result of the reactions in the differential aeration cell, the liquid that spreads is highly alkaline [206]. It has been proposed that, under a >90% relative humidity, the secondary spreading effect, at least on an unprotected metal, would ultimately be stopped by the formation of insoluble carbonates [207].

When secondary spreading is present, the rate of the cathodic reduction reaction is dependent on the charge transfer of electrons produced during the anodic dissolution of the metal to the cathodic region. If the surface is insulated, the charge transfer process is inhibited and so is metal dissolution [164].

The physical spreading of the electrolyte results from the disruption of the surface tension of the hemispherical droplet in a Marangoni effect [208]. This occurs because a diffusion gradient is

created when ion transport occurs in order to neutralise charges which build up during the electrochemical corrosion processes. Positive sodium ions (Na^+) migrate outwards to neutralise the OH^- ions produced during the cathodic reduction reaction, whilst the negative chloride ions migrate to the anodic original droplet site to neutralise Fe^{2+}.

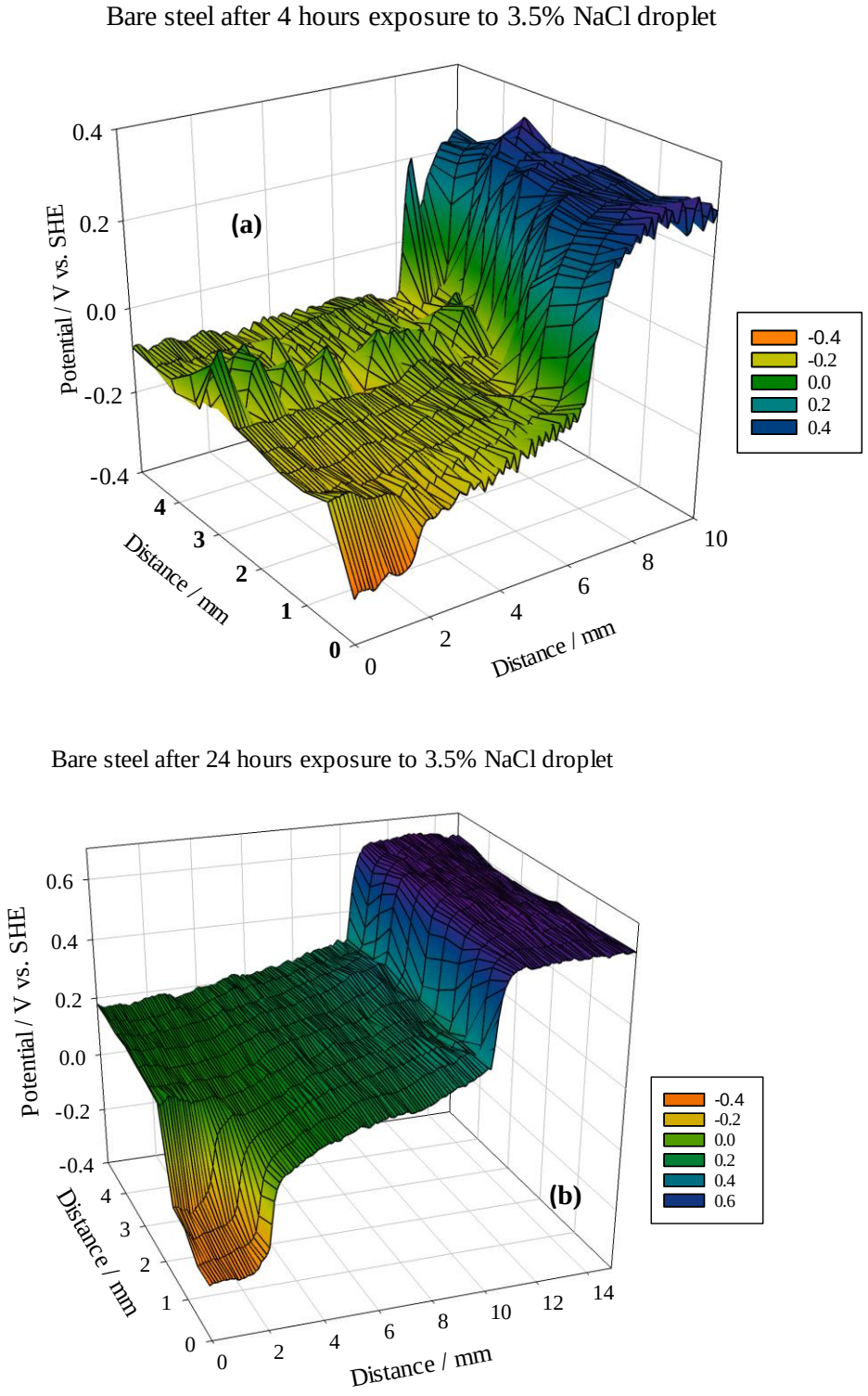

Figure 6.28 - Potential vs. SHE scan of bare S275 steel after: (a) 4 h exposure to 3.5% NaCl droplet and (b) 24 h exposure

Applying a droplet of 3.5% NaCl solution induces the initiation of the anodic reaction[209] . This is seen in Figure 6.28a; the darkest orange areas are the location of the 3.5% NaCl droplet and the anodic reaction. The sharp increase in potential indicates the edge of the hemispherical drop and

initiation of secondary spreading [164]. The lighter orange and yellow areas of the plots show the effect of secondary spread after 4 hours.

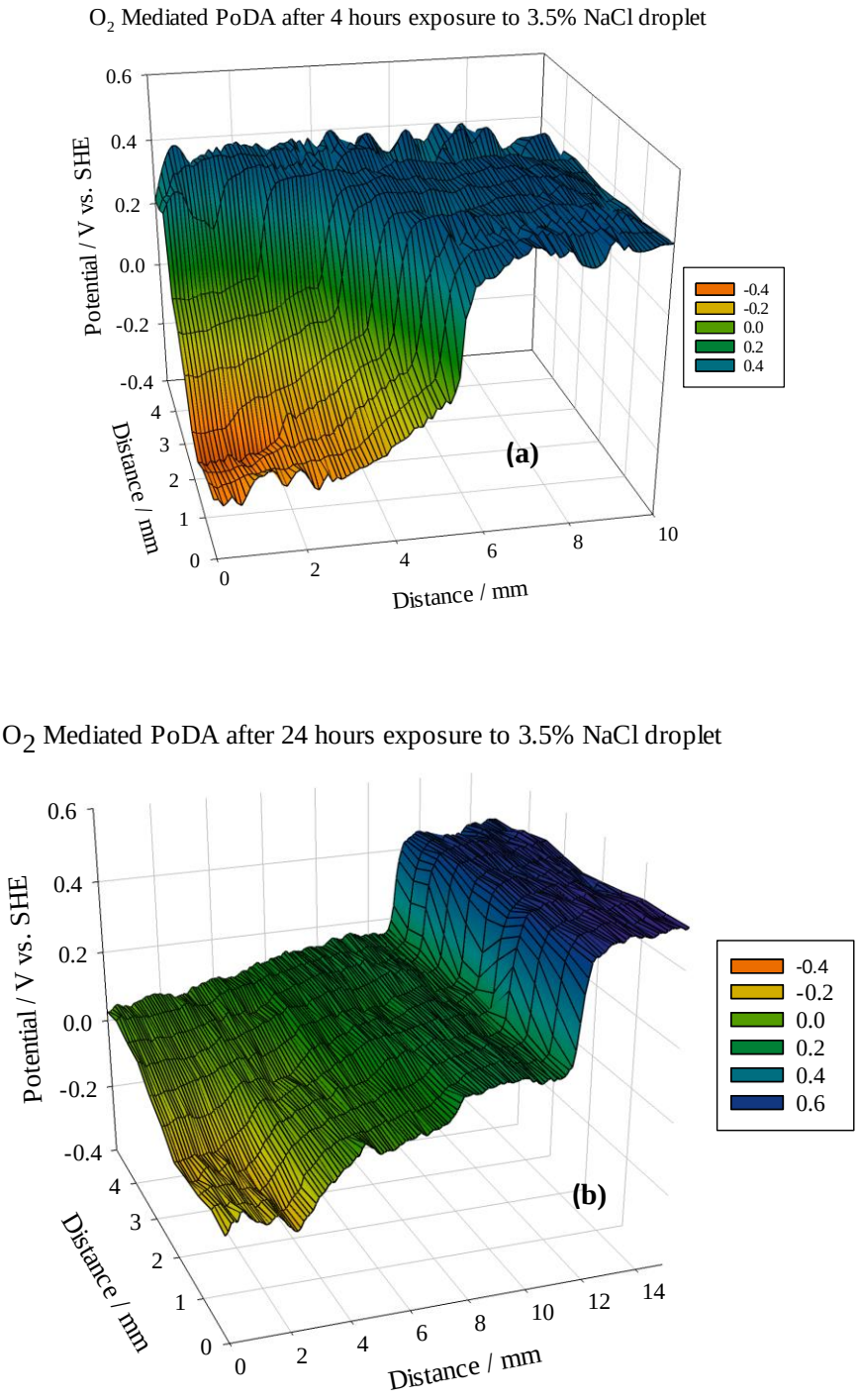

Figure 6.29 -Potential vs. SHE scan of O_2 mediated PoDA surface after: (a) 4 h exposure to 3.5% NaCl droplet and (b) 24 h exposure to 3.5% Na Cl droplet

When an O_2-mediated PoDA coating is present, the anodic reaction is initiated as with the bare steel (Figure 6.29a) but after 4 hours exposure, the secondary spreading is 2 mm less than for bare steel indicating that the charge transfer process has been hindered and therefore, the presence of the

PoDA coating is preventing corrosion occurring. However, after 24 hours, the secondary spread is the same (Figure 6.29b) indicating that the protective capabilities of the PoDA coating have been lost. This concurs with the EIS results (section 6.1.1) which indicate that O_2-mediated PoDA offered protection for only the first 24 hours that the O_2-mediated PoDA coating was immersed in 3.5% NaCl solution.

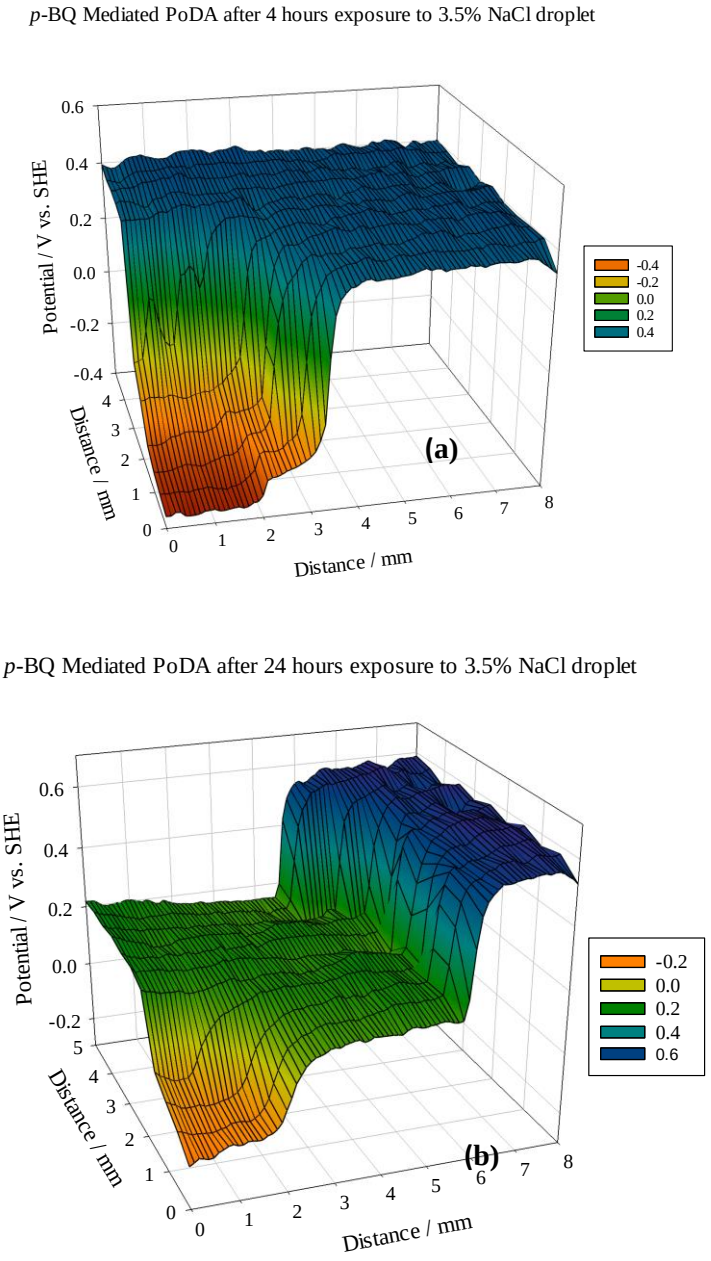

Figure 6.30 - Potential *vs.* SHE scan of *p*-BQ- mediated PoDA surface after: (a) 4 h exposure to 3.5% NaCl droplet and (b) 24 h exposure

After 4 hours exposure, secondary spreading has occurred (Figure 6.30a). However, the spread is less than for both O_2 mediated PoDA and bare S275 steel. The trend continues even after 24 hours

exposure (Figure 6.30b). The secondary spread is only 6.5 mm compared with the 13 mm for bare steel and 11 mm for O_2-mediated PoDA. This demonstrates that *p*-BQ mediated PoDA is capable of inhibiting corrosion to a greater extent than O_2-mediated PoDA. As with O_2-mediated PoDA, this concurs with the EIS results measurements which show that the protective capabilities of *p*-BQ mediated PoDA are maintained over a period of up to 218 hours.

As discussed in the literature review (section 3.2), PANi and other conducting polymers such as polythiophene and polypyrrole protect against metallic corrosion through redox processes with the underlying steel substrate. This results in the inhibition of the cathodic partial reaction which limits the overall corrosion reaction [96, 102]. Previous studies that have used SKP to study the protective mechanism of conducting polymers by examining the corrosion reaction kinetics exposed their samples to a corrosive environment after inducing damage into the deposited coating; these studies found that as the corrosion protection mechanism involved electron transfer, in the form of oxidation and reduction reactions the protection was offered to the damaged area even when the coating had been completely removed. The same studies found that even after 24 hours, the cathodic reaction was still inhibited. [76, 82, 210]. Because of the dependence of secondary spreading on electron transfer, it would be expected that a polymer that involved constant reduction and oxidation as its protective mechanism would completely inhibit secondary spreading. This is not the case with the polydopamine-based polymers.

The fact that the secondary spreading cannot be inhibited completely even for only 24 hours, indicates that the p-BQ mediated PoDA coating does not possess the same corrosion protection mechanism as the red-ox based protection mechanism of PANi and polypyrrole. This effectively rules out the possibility that the polymer that forms is a poly(aminoquinone) or derived solely from p-BQ monomer as such a polymer would be able to undergo redox reactions with the substrate and would have a corrosion protection mechanism that inhibits the corrosion reaction.

6.1.4.3 EIS scratch test results

The p-BQ mediated PoDA coating produced with a 0.5:1 ratio of p-BQ to dopamine at 35°C does not, in its current form, contain specific self-healing capabilities such as the inclusion of encapsulated healing agents or corrosion inhibitors. However, some intrinsically conducting polymers, such as PANi, are capable of imparting protection to an exposed substrate through their redox properties alone and, as PoDA is believed to be a conducting polymer, scratch tests were conducted on the deposited PoDA coatings to determine if they were capable of imparting a similar manner of protection. An O_2-mediated and a p-BQ mediated PoDA coating was deposited on two S275 steel discs. After drying, the coatings were scratched with a glass rod and then exposed to a 3.5% NaCl solution and periodic EIS testing. The resultant scratches had dimensions of 0.5 mm by 3mm. The procedure was then repeated with a metal rod making a larger scratch (1 mm x 4mm).

6.1.4.3.1 O_2 mediated PoDA

Glass rod induced scratch

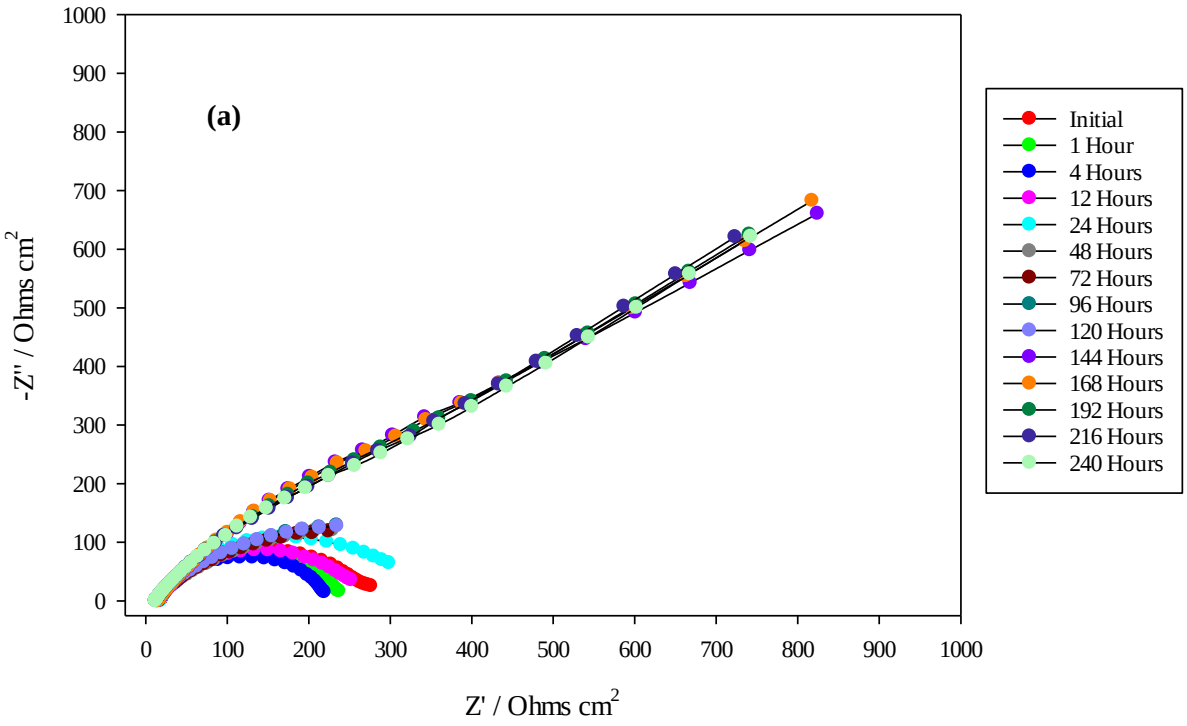

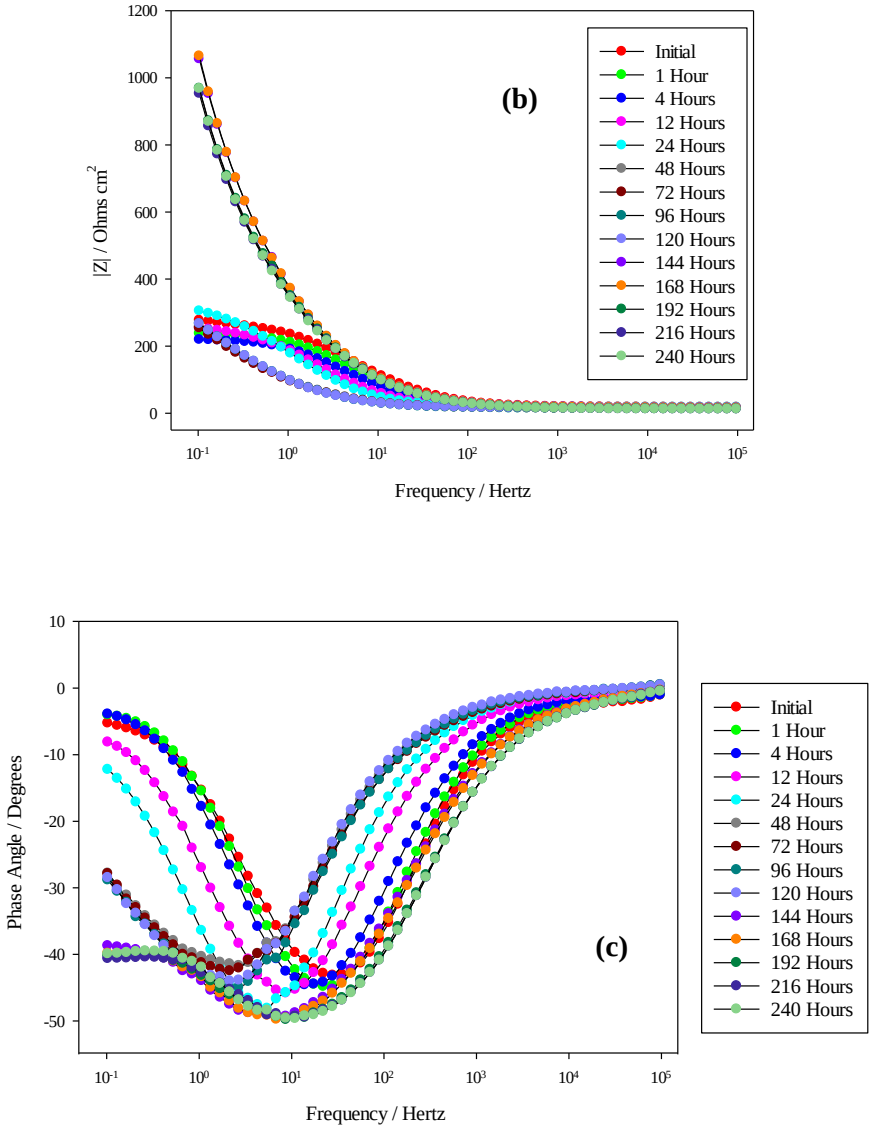

Figure 6.31 - (a) Nyquist, (b) Bode |Z| and (c) Bode phase angle plots for a scratch induced using a glass rod into an autoxidated PoDA coating deposited from a 2 mg mL^{-1} dopamine solution at 25°C.

Intact O_2-mediated PoDA coatings produce |Z| impedance of 1600 Ω cm2 at the initial time point. When a scratch was induced, this is lowered to 350 Ω cm^2 as a result of the barrier properties of the applied PoDA coating being disrupted. As NaCl permeates through the defect, the impedance of the coating drops further until 12 hours when the passivating oxide layer has formed to a sufficient extent that the impedance modulus begins to increase. After 24 hours a diffusive element is incorporated into the impedance as is demonstrated by the shape of the Nyquist plots, and the phase angles of 45° in the Bode phase angle plots. This is a result of iron ions from the oxide layer and ions from the NaCl solution diffusing through a very small opening in the coating (the scratch).

Metal rod induced scratch

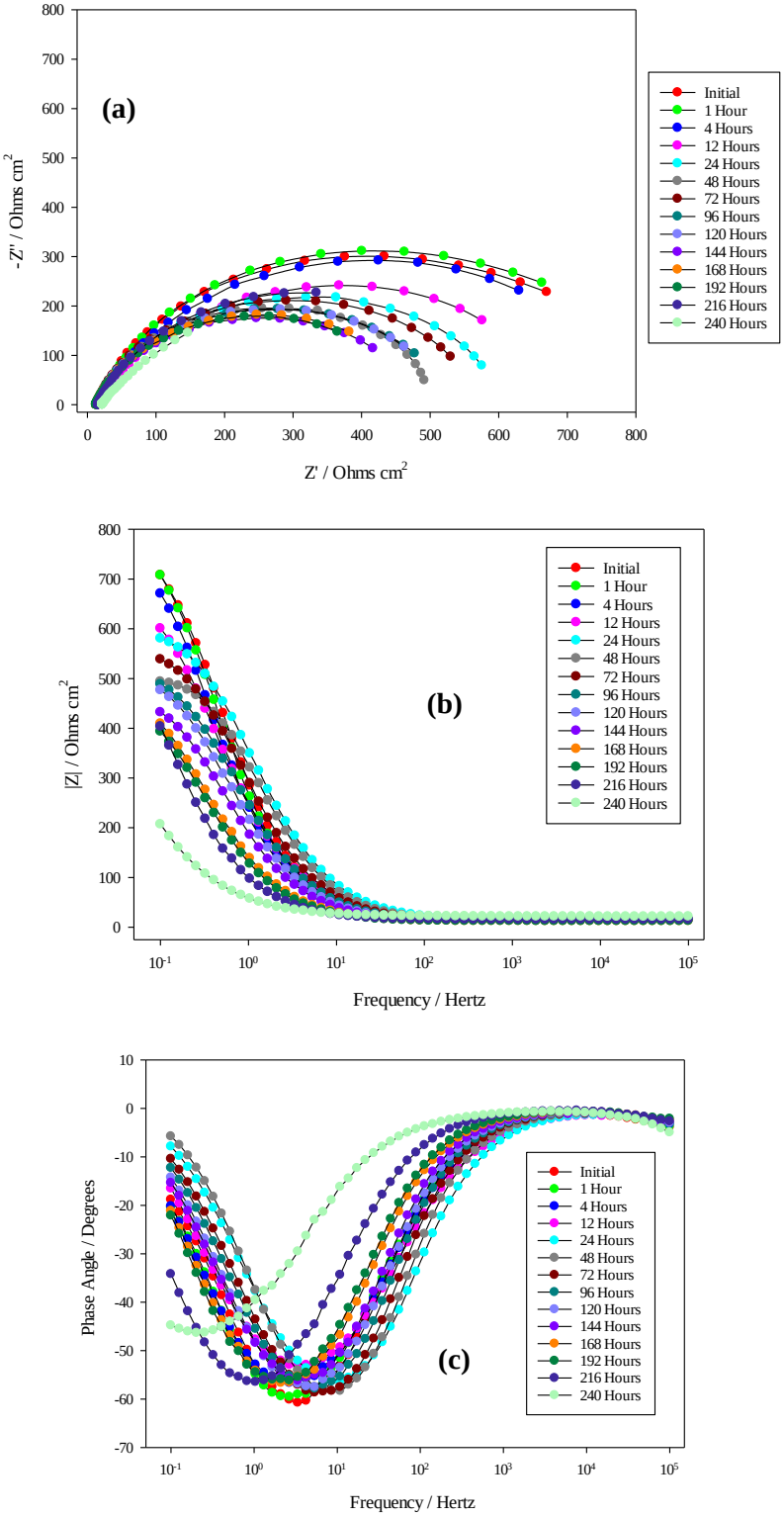

Figure 6.32 - (a) Nyquist, (b) Bode |Z| and (c) Bode phase angle plots for a scratch induced using a metal rod into an autoxidated PoDA coating deposited from a 2 mg mL^{-1} dopamine solution at 25°C.

The scratches induced by the metal rod were larger than those produced by the glass rod which accounts for the lower impedances observed in Figure 6.32 and Figure 6.34 when compared to Figure 6.31 and Figure 6.33. As with the glass scratch, there is an initial decrease in impedance as NaCl permeates through the coating followed by an increase in impedance after 12 hours when the passivating iron oxide layer increases in thickness. Whilst some of the later time points display diffusive behaviour (see Nyquist plot shapes in Figure 6.32a and phase angles in Figure 6.32c, again as a result of ions diffusing from the oxide layer and from solution, the contribution to impedance is much less, as the scratched area, through which the ions will diffuse is greater and therefore the diffusive effect is much less pronounced.

6.1.4.3.2 *P*BQ mediated PoDA

Glass rod induced scratch

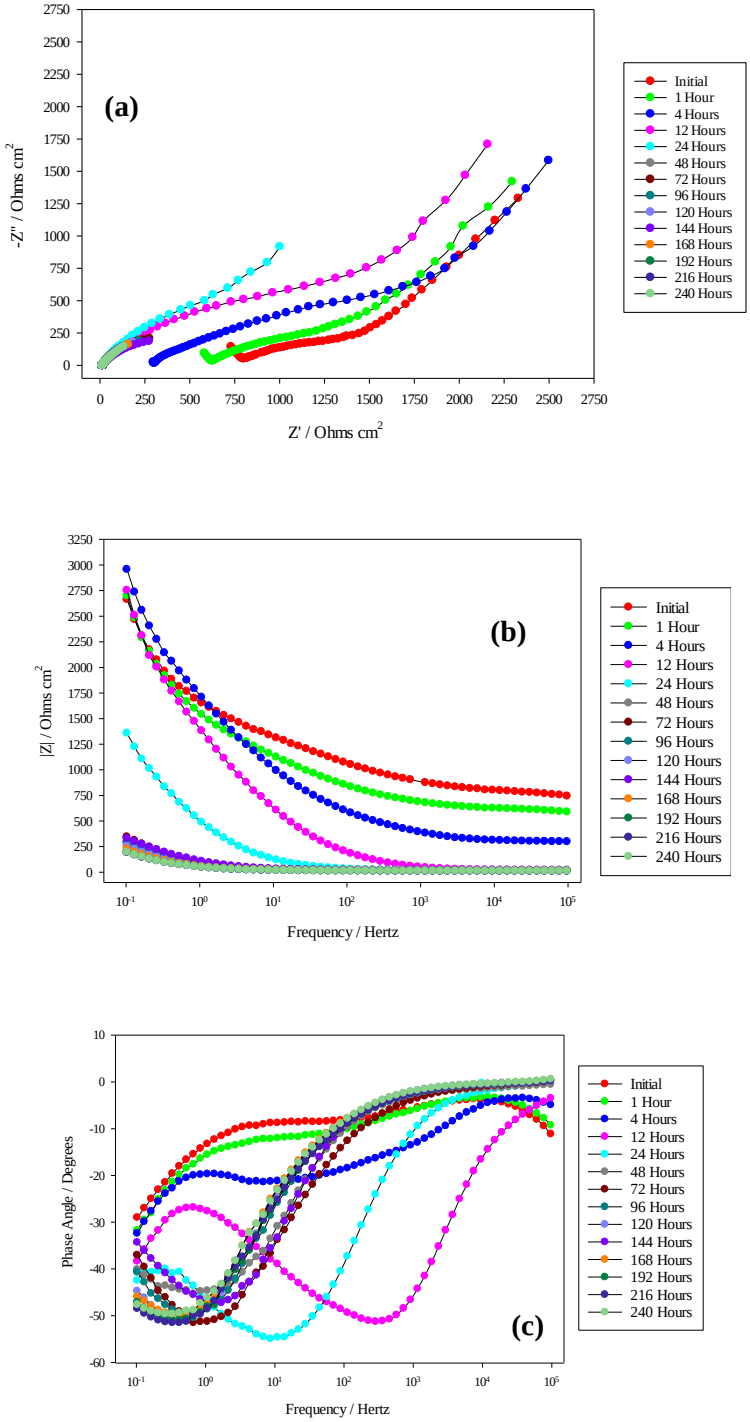

Figure 6.33 - (a) Nyquist, (b) Bode |Z| and (c) Bode phase angle plots for a scratch induced using a glass rod into a p-BQ- mediated PoDA coating deposited from a 2 mg mL^{-1} dopamine solution at 35°C.

The Nyquist plots for the initial 1 hour and 4-hour time points cannot be fitted by any conventional EIS circuit. When fitted to a Randles circuit that incorporates a diffusive element, the uncompensated resistance has fitted values of 800 Ω. Every other sample subjected to EIS testing in 3.5% NaCl solution throughout the project has had an uncompensated resistance of between 11 Ω and 20 Ω. This indicates that there is a chemical reaction occurring between some aspect of the coating and the exposed substrate that is detected at the higher frequencies of EIS testing (100,000 Hz – 50,000 Hz). In addition, the differences in impedance magnitude between intact and glass-scratched p-BQ-mediated PoDA coatings are much smaller than for O_2-mediated PoDA indicating that the protective capabilities of p-BQ are not only the result of improved barrier properties. However, the protective effect of a scratched coating is not maintained for as long a time period as for an intact coating, which is to be expected as the bare substrate has been exposed allowing corrosive species from the surrounding media to attack the substrate and initiate corrosion.

By the 12-hour time point, the high frequency resistance measurement returned to expected levels after gradually decreasing in magnitude over the 12-hour period. This indicates that the species involved in the reaction between coating and substrate have been consumed and that their protective effect has been lost.

Metal rod induced scratch

The larger size of the metal induced scratch (compared to the size of the glass induced scratch) has resulted in a significant drop in initial impedance and the protective capabilities are only present for the first hour of exposure. This indicates that the protective capabilities of p-BQ mediated PoDA only extend over very small areas of exposed substrate unlike those of polyaniline which can be extended over areas of up to 6 mm^2 [77]. It appears, therefore, that the protective capabilities of p-BQ mediated PoDA can be attributed to p-BQ acting as a corrosion inhibitor at a localised level.

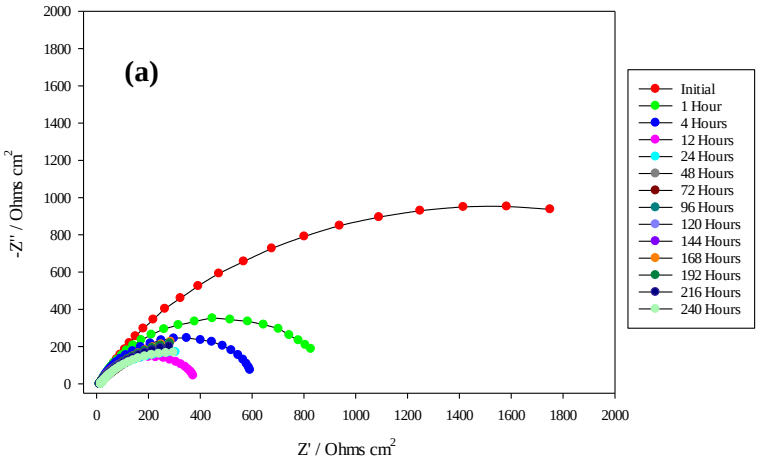

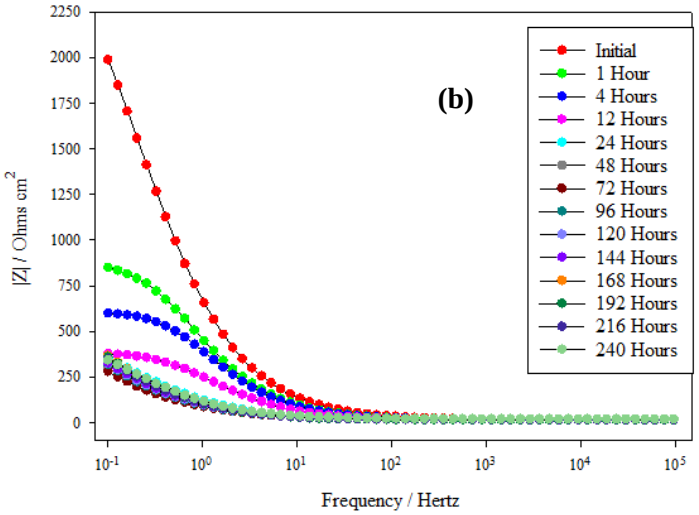

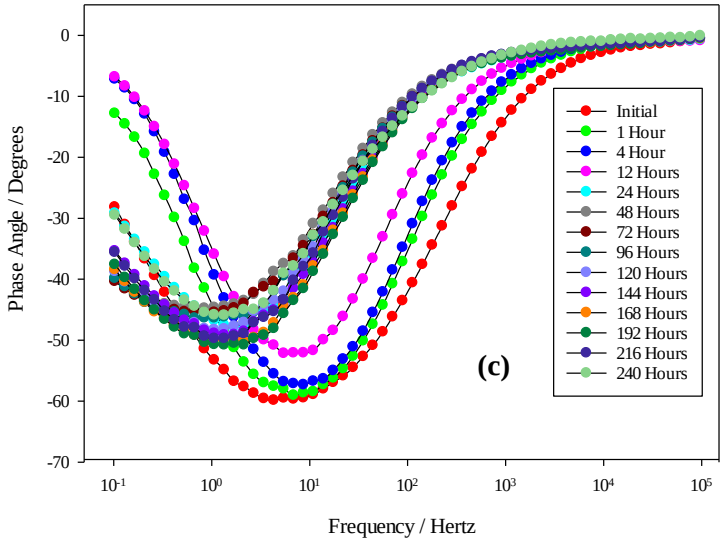

Figure 6.34 - (a) Nyquist, (b) Bode |Z| and (c) Bode phase angle plots for a scratch induced using a metal rod into a p-BQ-mediated PoDA coating deposited from a 2 mg mL^{-1} dopamine solution at 35°C. EIS was carried out in 3.5% NaCl

p- BQ monomer has been introduced as a corrosion inhibitor as monomer form. Rohm and Hass have filed two US patents for the use of p-BQ as a corrosion inhibitor in the distillation of alkanoic acids, such as for the highly corrosive formic acid [210]. Here p-BQ monomer was added to the distillation solution and was believed to act as an oxygen scavenger by reacting with oxygen-based radicals which inhibits the cathodic partial corrosion reaction and therefore limits the overall corrosion reaction.

Raicheva and Sokolova [211] undertook an extensive study into how the structure of organic corrosion inhibitors affects their ability to limit the corrosion of mild steel. Their study was conducted in acidic conditions, rather than the near-neutral conditions that a 3.5% NaCl solution provides. This means that the corrosion protection mechanism would be different, as the kinetics of the corrosion reaction of mild steel itself would be different from the mechanism in a near-neutral solution [180, 212] as they depend on the presence of H+ not present in near-neutral solutions. Following analysis of the adsorption energy of a layer of p-BQ, Raicheva and Sokolova concluded that its ability to protect against corrosion came as a result of repulsive forces in the adsorption layer, demonstrated by negative values measured for the adsorption energy. Because the authors considered many compounds, they do not consider p-BQ in much detail, and no EIS plots or XPS information are presented as they are for other compounds considered. However, the authors do make one important conclusion, namely that the presence of organic inhibitor in a thin film requires the use of a Randles circuit that incorporates a CPE in place of a capacitor, and also that a diffusive

element as the surface is not homogenous either in composition or behaviour, which concurs with the EIS data obtained for the p-BQ mediated PoDA coatings at a 0.5:1 ratio of p-BQ to dopamine.

Slavcheva et al. used p-benzoquinone, amongst other quinones, as a corrosion inhibitor for mild steel in near-neutral solutions [213, 214]. Their work was some of the first to use an organic molecule as a corrosion inhibitor in a neutral solution and they made the key identification that organic inhibitors can act at either: (a) the metal-film interface, (b) the film-solution interface or (c) the metal itself. The exact interaction would depend on whether the inhibitor remained in solution or was incorporated into the film. Slavcheva et al. [214] monitored the effect of temperature and concentration on the activity of the quinones, investigating the effect of the inhibitors in model cooling water, a near neutral solution containing $CaCl_2$, $MgSO_4$ and Na_2SO_4. These two studies demonstrated that when the inhibitor was added to the corrosive electrolyte, the inhibitor was adsorbed onto the substrate surface which blocked cathodic reactants from reaching the surface and thus impeded the cathodic reactants [214]. This could account for observations of the SKP testing where the secondary spreading was slowed but not completely inhibited.

6.1.4.4 Conclusions

Although the experiments undertaken with polydopamine have resulted in some improvements in the performance of the PoDA coatings with regards to corrosion protection, they are still inferior to the more established and widely studied polyaniline coatings. Furthermore, the fact that even the PoDA coatings produced when *p*-Benzoquinone was the oxidant are iridescent (Figure 6.35), suggests that they are still very thin films. The films are thin enough that grooves left after polishing can still be seen through the coatings.

Figure 6.35 – Iridescent PoDA coating formed from a solution of 2 mg mL^{-1} dopamine in 0.1M phosphate buffer containing a 0.5:1 molar ratio of *p*-Benzoquinone to dopamine at 25°C: the S275 steel disc is 15 mm in diameter

The steel substrate was not suitable for ellipsometry as it was too rough, even after polishing to a mirror finish, relative to the thickness of the coatings. Therefore, it has not been possible to determine the exact thickness of the films. Previous work undertaken with polydopamine has achieved a maximum film thickness of 90 nm [42]. It is unlikely, given the iridescence, that these films are much thicker than those achieved in previous work. Indeed, since this current work was undertaken, multiple studies have found that, regardless of the deposition conditions used, 100 nm appears to be the maximum film thickness which can be achieved by placing the substrate in a dopamine solution and allowing the dopamine to polymerise on the substrate [215-217].

Hulvat proposed that in order to successfully incorporate a mesoporous network into a coating, the coating would need to be at least 300 nm thick [128]. Therefore, it can be concluded that polydopamine coatings are not suitable for incorporating the porous network required in this project and so polyaniline is a more suitable alternative. The templating and self-healing aspects of the project will be developed using a polyaniline coating.

Chapter 7 Development of a polyaniline-based self-healing coating

The investigations into polydopamine coatings indicated that polydopamine was not a suitable basis for the self-healing coating and so the decision was made to use the more established and more-understood polyaniline (PANi) coating. It was hoped that the final coating would take the form represented in Figure 7.1 below. An epoxy top coat is often applied ballast tank coatings to increase the barrier protection of coating [12] and so such a top coat has been used in the studied coating. .

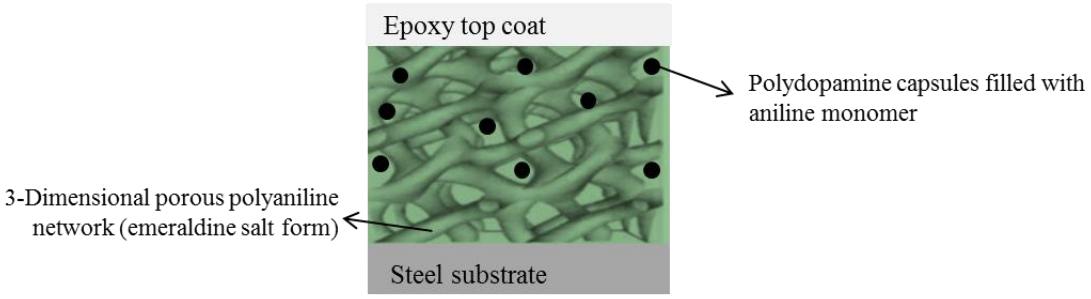

Figure 7.1 - Self-healing coating schematic

As discussed in section 3.2, the Emeraldine salt form of PANi (PANi-ES) is required as this is responsible for the protective mechanism of the polyaniline coatings. Because of the requirement for the coating to possess a 3-D structure, the polyaniline coating will need to be formed around a template. A “soft” liquid crystal-based template was selected as the best option because “hard” porous silica templates require hydrofluoric acid to remove them and are expensive to produce. The liquid-crystal templates can be removed with distilled water and the polyoxyethylene surfactants used to produce the liquid crystal phases are very cheap. Previous work at nCATS in Southampton identified that a bi-continuous cubic liquid crystal mesophase phase would provide the required 3-D structure [2]. There are existing mesophase diagrams for a large number of surfactants and water. However, the deposition of aniline requires an acidic media. As discussed in section 3.2.3.2, the chosen acid is oxalic acid, as the results from the existing literature demonstrate that oxalic acid provides coatings of good thickness and adherence without using the harsh conditions of sulphuric or hydrochloric acid. Therefore, new phase diagrams needed to be produced for 0.3M oxalic acid and each of the tested surfactants.

The use of a soft template requires the PANi-ES to be deposited electrochemically. There are several known procedures for the electrochemical deposition of PANi-ES but it was not known how the conditions would be affected by the inclusion of the liquid crystal template into the deposition medium and so the precise conditions for deposition needed to be determined by experimentation.

7.1 Production of phase diagrams

The first stage of producing a templated porous polymer was the production of binary phase diagrams for the aqueous polymerisation medium (oxalic acid) and the templating surfactant.

The phase diagrams were produced following the evaluation of polarising microscopy images and viscosity testing of the mesophases which appeared isotropic under polarised light. The mesophases which are anisotropic with respect to cross-polarised light possess distinct textures as a result of the geometry of the packing of micelles within the mesophase. It was not possible to obtain microscopy images for those areas of the phase diagram which present as a distinct phase separation. Relevant microscopy images have been included in the discussion below, but the full collection of images is presented in Appendix A.

7.1.1 Brij L4

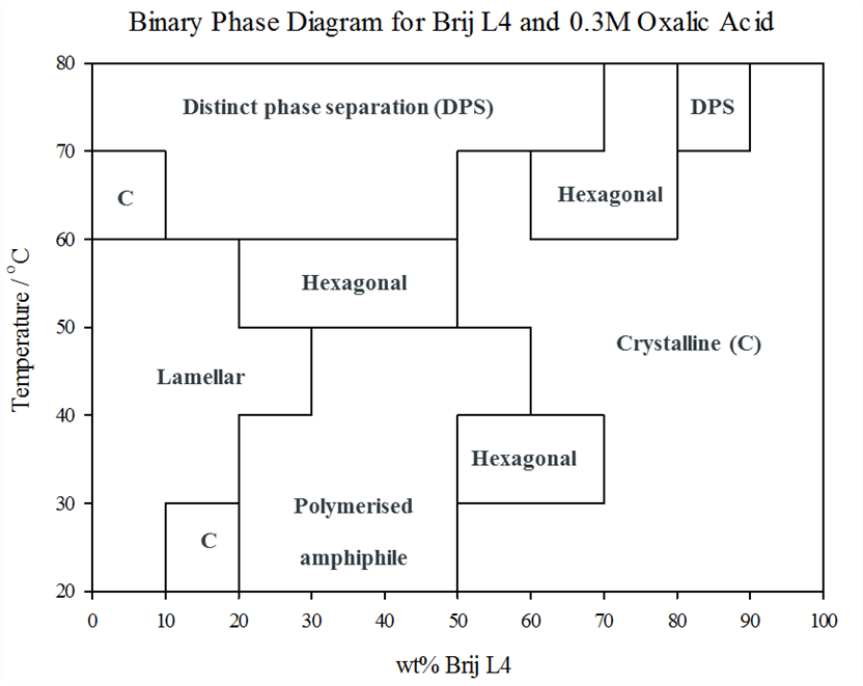

Figure 7.2 – Binary phase diagram for Brij L4 and 0.3M oxalic acid

As can be seen from Figure 7.2, the binary mixture of Brij L4 and 0.3M oxalic acid does not produce a cubic phase at any wt% of Brij L4 or at any of the tested temperatures. Above 50 wt%, the most prominent mesophase is crystalline; here the surfactant begins to form crystals (as shown in Figure 7.3 below).

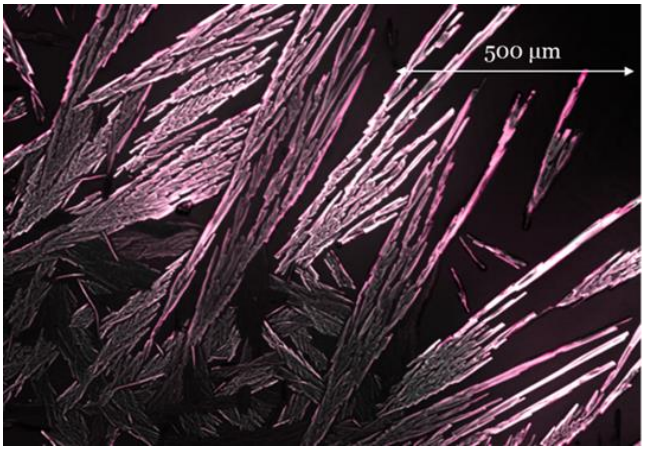

Figure 7.3 - Brij L4 crystals as observed using polarised light microscopy: the sample was 80 wt% of Brij L4 incubated at 50°C.

At higher temperatures, there is a distinct phase separation between the surfactant and the aqueous phase. This occurs because polyethyoxylate surfactants are unusual in that their solubility decreases as the temperature increases [126]. Therefore above 60°C, the Brij L4 ceases to be soluble in the aqueous phase and forms crystals instead. Because of the phase separation, it is not possible to obtain microscopy images for these samples.

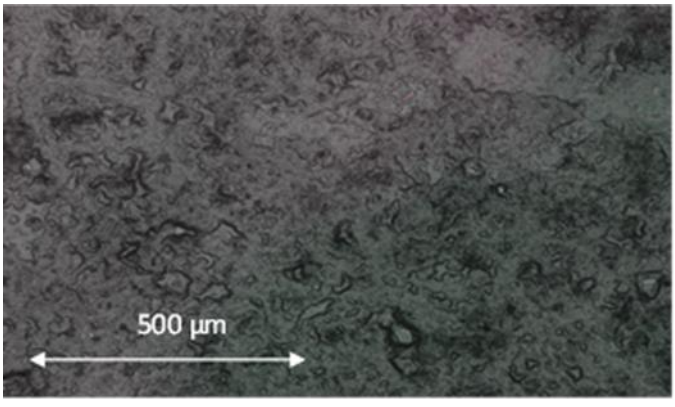

Figure 7.4 - Polymerised surfactant in a binary mixture of Brij L4 and 0.3M oxalic acid as viewed under polarised light: the sample was 40 wt% Brij L4 and incubated at 30°C

At lower temperatures, the lamellar phases form or the amphiphillic component of the mixture (the Brij L4) begins to polymerise to form an amorphous gel as shown in Figure 7.4 above [20]. Although the polymerised surfactant is anisotropic with respect to polarised light, it does not

possess the characteristic textures of the mesophases; the micelles have polymerised and so the packing geometry no longer exists.

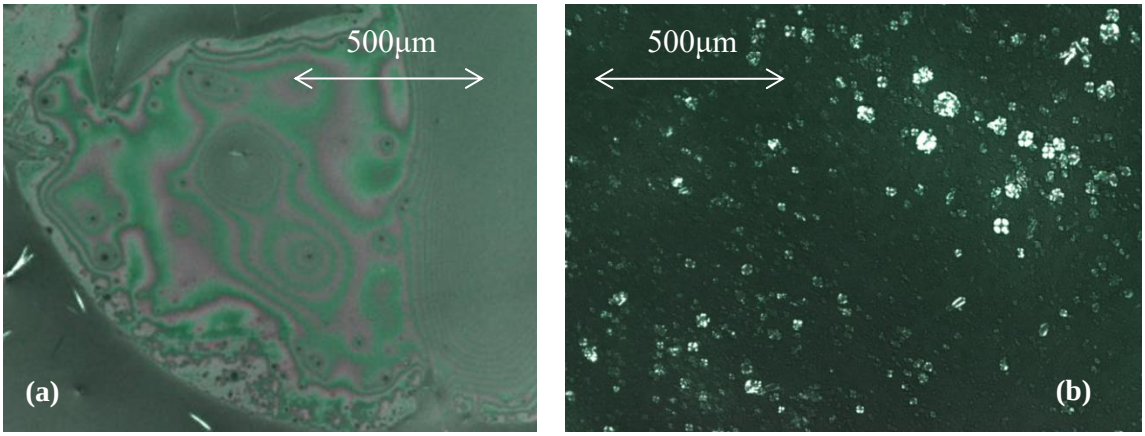

Figure 7.5 - The lamellar phases formed from mixtures of Brij L4 and 0.3M Oxalic acid (a) the "streaky" or "oil slick texture" (20 wt% Brij L4 at 40°C) and (b) the mosaic texture (10 wt% Brij L4 at 50°C).

The formation of the lamellar phase at lower weight percentages of Brij L4 is typical for such a short chained surfactant because the simple 1-Dimensional bilayer arrangement is the most energy efficient mesophase for short chained surfactants to adopt even at low concentrations [121]. As the concentration of Brij L4 increases, the lamellar phase is no longer the most stable configuration and so the bilayer arrangement collapses. The "streaky" texture of Figure 7.5a occurs when the lamellar phase is in the flat bilayer arrangement. The mosaic texture of Figure 7.5 b forms because the bilayer folds into vesicles [118] leading to a spherical geometry.

7.1.2 Brij C10

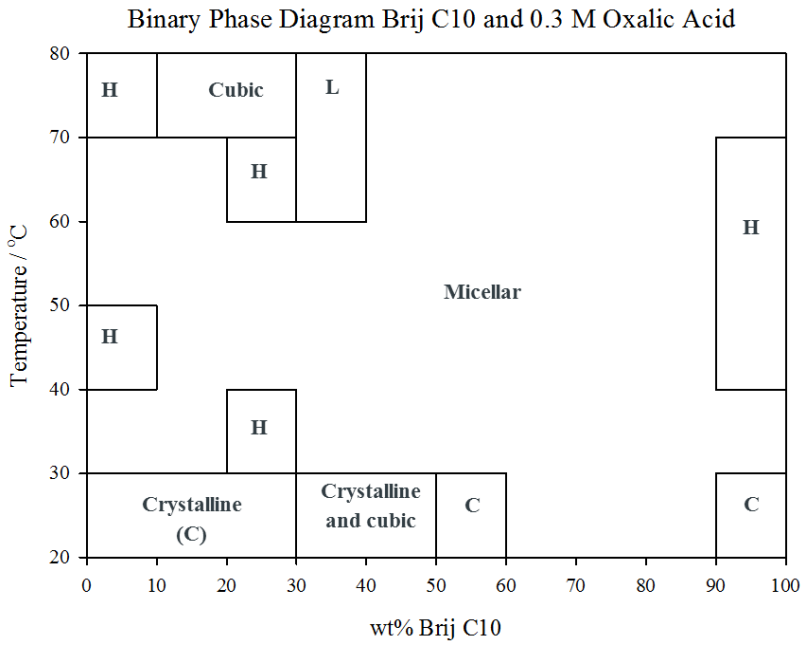

Figure 7.6 - Binary phase diagram for Brij C10 and 0.3M oxalic acid. H represents a hexagonal phase and L is a lamellar phase

Figure 7.6 demonstrates that a cubic phase is produced when Brij C10 is used a surfactant. The longer amphiphillic chain (compared with that of Brij L4) increases the forces between the surfactant head (hydrophilic) and the chain (hydrophobic) during micelle packing which allows a greater concentration of micelles to form and subsequently the micelles are able to self-assemble into more complex mesophases [218]. The isotropic cubic phase is shown in Figure 7.7.

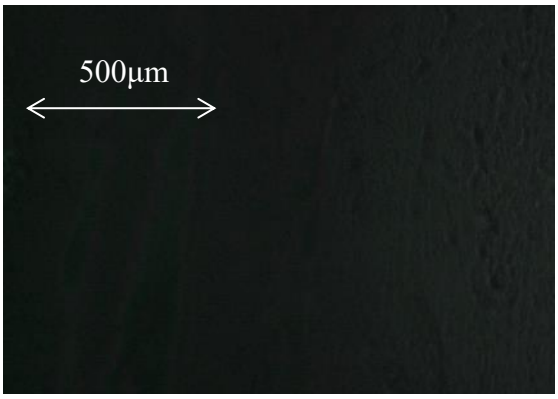

Figure 7.7 - Isotropic cubic phase formed from mixtures of Brij C10 and 0.3M oxalic acid: the sample was 20 wt% Brij C10 and the temperature was 70°C.

7.1.3 Brij O20

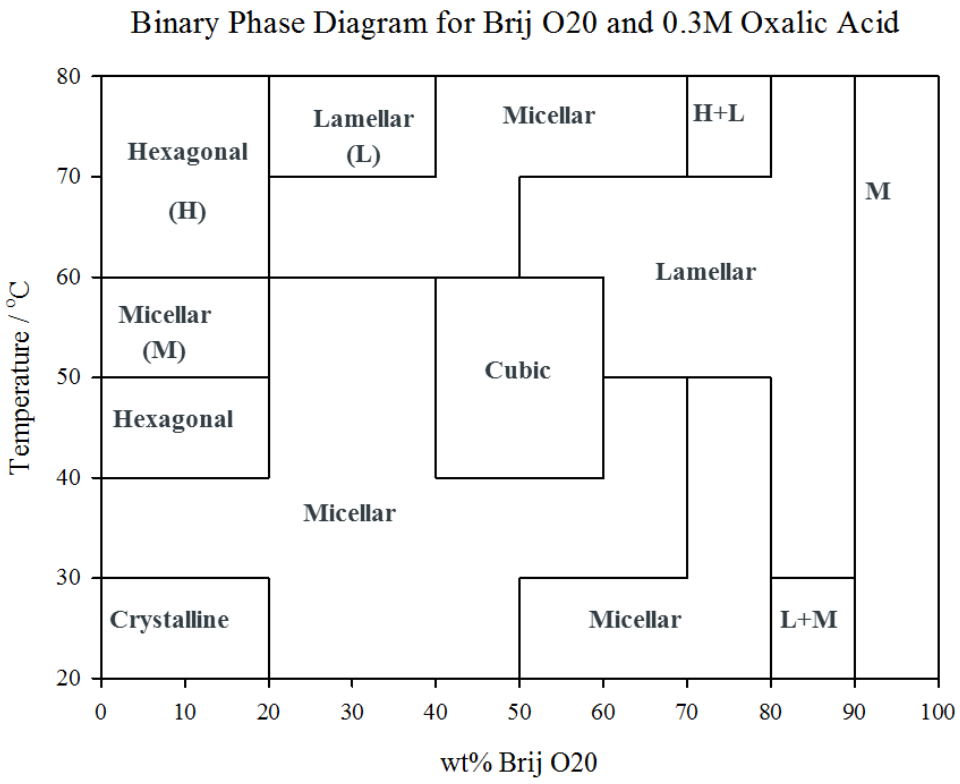

Figure 7.8 - Binary phase diagram for Brij O20 and 0.3M oxalic acid. H represents a hexagonal phase and L is a lamellar phase

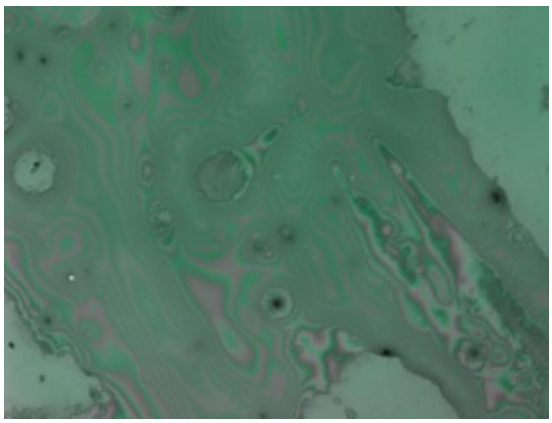

Figure 7.9 - The characteristic "oil slick" or "streaky" texture of a lamellar phase formed from a binary mixture of Brij O20 and 0.3M oxalic acid: The sample was 30 wt% Brij O20 and the sample was incubated at 70°C

In longer-chain surfactants, the lamellar phase (Figure 7.9) does not usually exist at below 50 wt% of surfactant. This is because increasing surfactant concentration is required for the elongation of

the micelle when initially spherical mesophase transforms into a rod-shaped micelle. The rod-shaped micelle then requires further elongation, as a result of increased surfactant concentration, to form a lamellar phase [119, 126]. However, the presence of other organic moieties, namely the oxalic acid present in the mesophase, will disrupt the packing of the micelles with the result that lower concentrations of surfactant are required for the previously spherical micelles to elongate and form cylindrical or rod-shaped micelles (which can then form into the hexagonal phase) then further elongate until a single lamellar bilayer is formed [118, 132]. This explains why lamellar and hexagonal phases have formed in samples with only 10 wt% of surfactant.

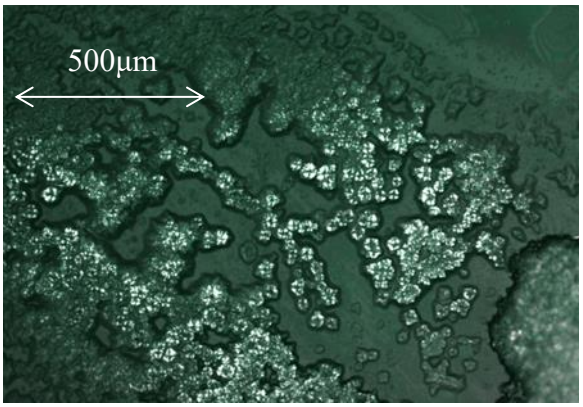

Figure 7.10 - The "mosaic" texture of the lamellar phase formed from a binary mixture of Brij O20 and 0.3M oxalic acid; the sample was 70 wt% Brij O20 and the temperature was 60°C

Figure 7.10 shows the mosaic lamellar texture. The mosaic texture forms at higher surfactant concentrations than the “streaky” texture because the greater the concentration of surfactant, the greater the degree of curvature that will be present in the mesophase and the greater the likelihood is that the lamellar bilayers will curve into vesicles [219].

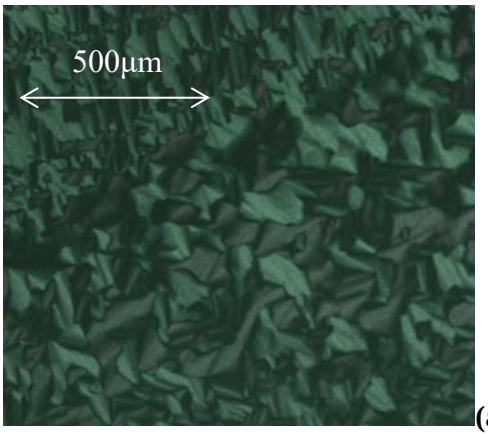

(a)

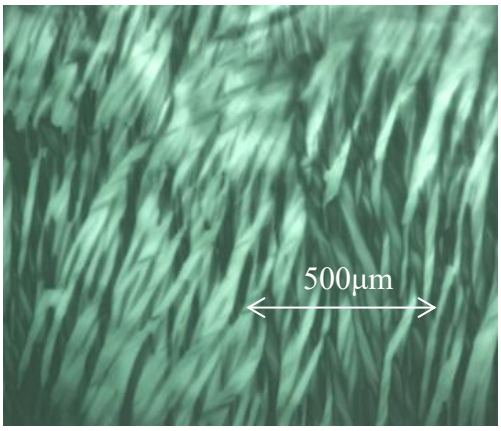

(b)

Figure 7.11 – The characteristic fan texture of the hexagonal phase: sample (a) was 10wt% Brij O20 at 70C and sample (b) was 10 wt% at 40°C

As previously discussed, the hexagonal phases (Figure 7.11) have formed at lower concentrations than would generally be expected because of the presence of oxalic acid in the aqueous region of the mesophase. The position of the mesophase indicates that the hexagonal phase is a normal rather than a reverse phase; reverse phases require higher surfactant concentrations.

The isotropic cubic phase appears in the middle of the surfactant phase. The sample that represented by Figure 7.12 was almost solid at 50°C which indicates that the sample is a bi-continuous cubic phase rather than the micellar cubic phase. The body centred cubic phase generally occurs between the micellar solution and normal hexagonal phases (normal micellar cubic) and the micellar solution and reverse hexagonal phase (reverse micellar cubic). The bicontinuous cubic mesophase usually appears between the lamellar and normal hexagonal phase (normal cubic phase) or the lamellar phase and reverse hexagonal phase (reverse cubic phase) [132].

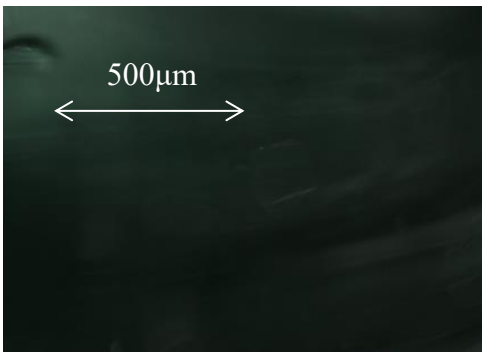

Figure 7.12 - The isotropic cubic phase, the sample was 50wt% Brij O20 and the temperature was 50°C.

7.1.4 Brij S100

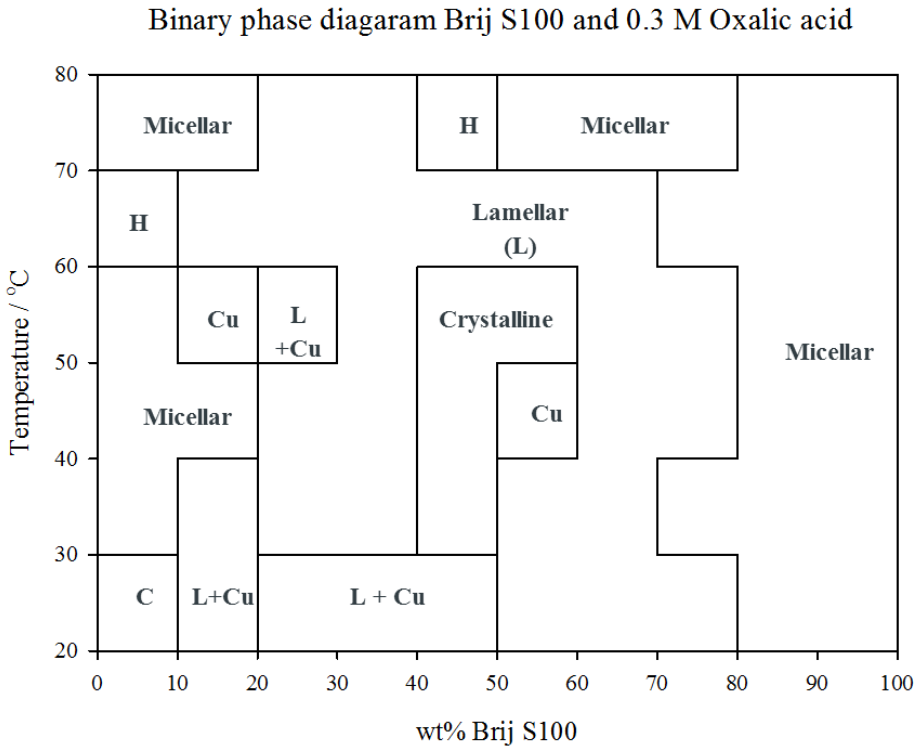

Figure 7.13 - Binary phase diagram for Brij S100 and 0.3M oxalic acid. H is a hexagonal phase, Cu is a cubic phase and C is a crystalline phase

Figure 7.14 shows the cubic phase formed using 50 wt% Brij S100 surfactant and 50 wt% 0.3 M oxalic acid. Figure 7.15 shows a sample which has cubic mesophase regions and also lamellar mesophase regions. The lamellar mesophase is identified by the characteristic “maltese cross” texture.

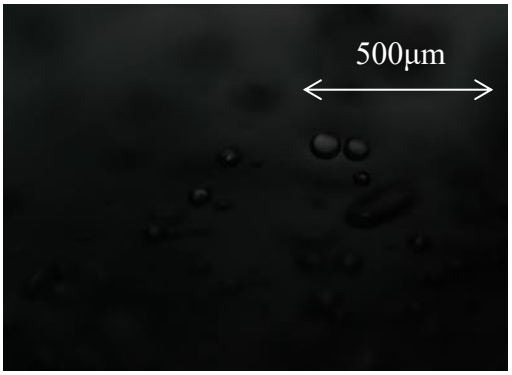

Figure 7.14 – The isotropic cubic phase; the sample was 50wt% surfactant and the temperature was 50°C

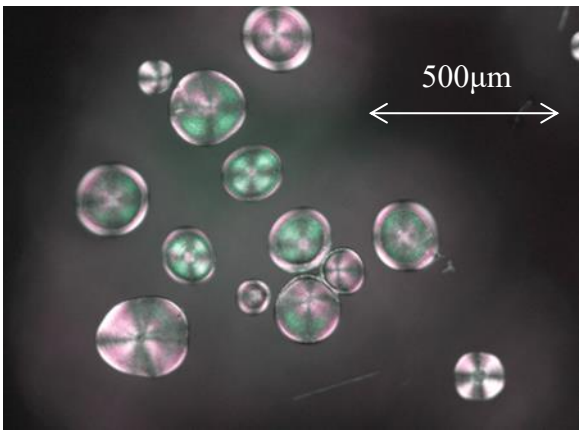

Figure 7.15 - The co-occurrence of a cubic (dark area) and lamellar phase, the lamellar phase is identified by the characteristic "maltese cross" texture; the sample was 50 wt% surfactant and the temperature was 30°C

7.1.5 Viscosity measurements

In order to differentiate between the micellar cubic and bi-continuous cubic phases, viscosity measurements were performed on the samples which presented as isotropic with respect to polarised light. The viscosity of the micellar cubic phases is lower than the bi-continuous because the micelles are capable of gliding over one another whereas the bi-continuous layers are not.

Table 7.1– Measured viscosities of isotropic liquid crystal mesophases: viscosities were measured on a Brookfield CAP 2000+ viscometer using the heated stage and cone 2 at 100 rpm

Sample	Surfactant	Wt% surfactant	Temperature / °C	Viscosity/ mPa-s	Nature of cubic phase
1	Brij C10	10	70	1547	Micellar
2	Brij C10	10	80	1968	Micellar
3	Brij C10	20	70	2568	Micellar
4	Brij C10	20	80	2478	Micellar
5	Brij C10	30	70	7485	Micellar
6	Brij C10	30	80	6599	Micellar
7	Brij O20	40	40	12549	Micellar
8	Brij O20	40	50	11468	Micellar
9	Brij O20	40	60	13568	Micellar
10	Brij O20	50	40	<100,000	Bi-continuous
11	Brij O20	50	50	<100,000	Bi-continuous
12	Brij O20	50	60	<100,000	Bi-continuous
13	Brij O20	60	40	45875	Micellar
14	Brij O20	60	50	57496	Micellar
15	Brij O20	60	60	56611	Micella
16	Brij S100	10	50	2563	Micellar
17	Brij S100	10	60	2748	Micellar
18	Brij S100	20	50	3658	Micellar
19	Brij S100	20	60	5248	Micellar
20	Brij S100	50	50	<100,000	Bi-continuous

21	Brij S100	50	60	<100,000	Bi-continuous
22	Brij S100	60	50	33695	Micellar
23	Brij S100	60	60	33578	Micellar

Samples 10-12 and 20-21 were all too viscous to produce viscosity readings and so these were designated as the bi-continuous cubic mesophases because of their almost solid appearance even at 50°C temperatures. Table 7.1 demonstrates that only Brij O20 and Brij S100 produced mesophases which were classified as bi-continuous cubic mesophases. This can be attributed to their longer chain lengths (20 and 100 polyoxyethylene units respectively) because the increased size of the hydrophobic element of the surfactant relative to the hydrophilic element results in increased geometric frustration which leads to the formation of a continuous bi-layer [218, 219].

Samples 10, 11, 12, 20 and 21 were re-tested after 24 hours to determine their stability in the bulk phase over time. Only the sample of 50wt% Brij S100 surfactant remained stable (Figure 7.16); the other samples all collapsed into micellar solutions. As a result, the chosen mesophase for templating was the 50/50 wt% mixture of Brij S100 and 0.3M oxalic acid.

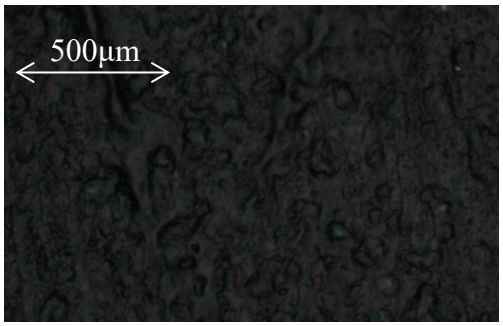

Figure 7.16 – Sample consisting of 50 wt% Brij S100 at 50°C re-tested after 24 hours

7.2 Templating of polyaniline

The procedure and conditions for the electrodeposition of conducting polyaniline (PANi) on to steel are well established in the prior art [77, 83, 89, 90, 92, 191, 220, 221] but the deposition of porous PANi using a cubic liquid crystal template has not yet been performed. Because the deposition medium for templated PANi is a very viscous gel rather than the liquid medium used for non-templated PANi, the deposition conditions for templated PANi using cyclic voltammetry. The monomer was dispersed in the aqueous phase of a cubic mesophase formed from 50/50 wt% mixture of Brij S100 and 0.3M oxalic acid. Initially the performance was evaluated by the physical appearance of the steel plate after the experiment had been performed; the most conducting form of PANi and the desired product of this investigation, is acid doped Emeraldine salt which is bright green and easily identifiable [74]. Oxalic acid was chosen as the deposition medium because various studies [90, 91, 222] have shown that only dibasic acids, such as oxalic acid, provide adequate adhesion of PANi to iron containing substrates; mineral acids such as hydrochloric and sulphuric acids result in PANi coatings that readily delaminate from the underlying substrate [94, 223].

Table 7.2 presents the results of the experiments undertaken to determine the optimum scanning range for the deposition of polyaniline. The starting point for the experiments was a 1.0V highest scan point and -1.0V (both vs Ag/AgCl) lowest scan point as this resulted in an Emeraldine coating when used for a non-templated PANi deposition. The scan rate and number of cycles performed were kept constant for all of the experiments.

Table 7.2 - Results of scan range experiments

Sample number	Lowest scan point/ V(vs Ag/AgCl)	Highest scan point/ V(vs Ag/AgCl)	Scan rate/ mVs^{-1}	Number of cycles performed	Appearance
1	-1.0	1.0	50	25	Grey - iron oxalate
2	-1.0	1.5	50	25	Grey - iron oxalate
3	-1.0	2.0	50	25	Green - Emeraldine (acid doped)
4	-1.0	2.5	50	25	Black/purple (Pernigraniline)
5	-1.0	2.1	50	25	Black/purple (Pernigraniline)
6	-1.0	2.2	50	25	Black/purple (Pernigraniline)
7	-1.0	2.3	50	25	Black/purple (Pernigraniline)
8	-1.0	2.4	50	25	Black/purple (Pernigraniline)
9	-0.9	2.0	50	25	Green - Emeraldine (acid doped)
10	-0.8	2.0	50	25	Green - Emeraldine (acid doped)
11	-0.7	2.0	50	25	Patchy green coating
12	-0.6	2.0	50	25	Grey - iron oxalate
13	-0.5	2.0	50	25	Grey - iron oxalate
14	-0.4	2.0	50	25	Grey - iron oxalate
15	-0.3	2.0	50	25	Grey - iron oxalate
16	-0.2	2.0	50	25	Grey - iron oxalate
17	-0.1	2.0	50	25	Grey - iron oxalate
18	0.0	2.0	50	25	Grey - iron oxalate

Samples one and two failed to produce a successful emeraldine coating because the +1.0V and +1.5V (vs Ag/AgCl) final potential was too low for the oxidation of aniline monomer to polyaniline. Although the -1.0V to +1.0V (vs Ag/AgCl) range worked when the aniline in oxalic acid solution was in liquid form, the greatly increased viscosity if the cubic mesophase restricts the diffusion of the aniline monomer.

The purple coating produced on samples 4-8 is Pernigraniline, the most oxidised form of polyaniline [74]. The higher oxidation potentials which were applied to these samples forced the over-oxidation of the aniline monomer to the less conducting pernigraniline form of PANi. Of all the forms of PANi, emeraldine provides the best protection against corrosion. The protection mechanism relies on the interaction between the acid doped emeraldine and the underlying steel substrate [77]. As a result, pernigraniline is not suitable for use in the current coating system [221].

Samples 12-18 failed to produce a coating because the lower scan point was too high to force the reduction of Fe^{3+} to Fe^{2+}.It has been found in several previous studies of the deposition of PANi from acidic media onto steel or iron substrates that the iron reduction reaction is essential for the passivation of the steel substrate which, in turn, is necessary for the good adhesion of the deposited PANi coating [92] [89] [71]. The conditions used for sample 11 resulted in a patchy coating because the lower scan point pf -0.7 V was sufficient to reduce the iron in the steel substrate across only parts of the substrate surface hence the deposited PANi could successfully adhere to these portions but not the rest of the substrate.

Samples 3, 9 and 10 produced a complete green coating. The conditions used for these samples used lowest scan points which were sufficiently reducing to allow the reduction of Fe^{3+} to Fe^{2+} across the surface of the substrate and the highest scan point was oxidising enough to ensure the successful oxidation of aniline monomer to polyaniline.

These conditions were tested again in order to determine the thickness of the coating been deposited. These results are presented in Table 7.3 below.

Table 7.3 - Coating thicknesses produced by best conditions

Sample number	Mass of steel plate before deposition/ g	Mass of steel plate following coating deposition and drying/g	Area covered by coating/ cm^2	Calculated thickness of coating/ µm
3	795.63	797.32	45.12	0.35
9	802.76	805.17	44.93	0.49
10	799.52	801.48	45.78	0.39

The conditions used for sample 9 resulted in the thickest coatings and so these scan points were used for further experiments which altered the scan rate.

Table 7.4 - Results of scan rate variation experiments for the deposition of PANi

Lowest scan point/ V(vs Ag/AgCl)	Highest scan point/ V (vs Ag/AgCl)	Scan rate/ mVs^{-1}	Number of cycles performed	Mass of steel plate before deposition/ g	Mass of steel plate following coating deposition and drying/g	Area covered by coating/ cm^2	Calculated thickness of coating/ µm
-0.9	2.0	10	25	801.47	801.99	44.78	0.11
-0.9	2.0	20	25	798.25	799.65	43.65	0.30
-0.9	2.0	30	25	800.32	802.14	46.52	0.36
-0.9	2.0	40	25	799.24	801.27	45.37	0.41
-0.9	2.0	75	25	796.74	799.04	44.36	0.48
-0.9	2.0	100	25	797.14	799.49	44.69	0.49

The results presented in Table 7.4 show that the thickness of the deposited coating increased with increasing scan rate. Martyak et al. found that the passivation layer of iron oxalate did not form at scan rates above 25 mVs^{-1} and no PANi layer was deposited [92]. The results presented in Table 7.4 directly contradict this in that increasing scan rate increases the thickness of the deposited coating.

Increasing the scan rate also increases the current. Hulvat et al.[128] [124]and Bender et al. [125] each found that a liquid crystal template inhibited the deposition of a conducting polymer. For the successful deposition of a templated polymer to take place, the current of the deposition had to be increased greatly relative to a non-templated deposition. The templated polymerisation of aniline monomer is a under diffusion control because the availability of aniline monomer for polymerisation onto the steel working electrode is dependent on its diffusion through the deposition media. In the liquid media used for deposition of non-templated PANi, diffusion is relatively facile but in the solid template, the aniline monomer cannot readily diffuse through the template. At lower scan rates, the oxidising potential is applied slowly enough that the monomer may diffuse away from the electrode surface before it can be oxidised. This results in the deposition of thinner films.

Table 7.5 - Coating thicknesses resulting from the variation of the number of deposition cycles performed

Lowest scan point/ V (vs Ag/AgCl)	Highest scan point/ V (vs Ag/AgCl)	Scan rate/ mVs^{-1}	Number of cycles performed	Mass of steel plate before deposition/ g	Mass of steel plate following coating deposition and drying/g	Area covered by coating/ cm^2	Calculated thickness of coating/ µm
-0.9	2.0	50	30	801.58	804.13	46.12	0.51
-0.9	2.0	50	40	798.63	801.05	43.25	0.52
-0.9	2.0	50	50	800.47	803.22	44.89	0.56
-0.9	2.0	50	60	803.89	806.78	44.78	0.59
-0.9	2.0	50	80	804.82	807.86	45.32	0.61
-0.9	2.0	50	90	796.2	799.28	45.41	0.63
-0.9	2.0	50	100	804.36	807.64	44.52	0.67

Table 7.5 shows that the thickness of the deposited coating increases with an increased number of performed cycles. This concurs with the findings of Hulvat et al whose templating methods required considerably longer than a non-templated deposition because the film growth is under diffusion-limited control as a result of the monomer becoming trapped within the hydrophobic domains of the template [128].

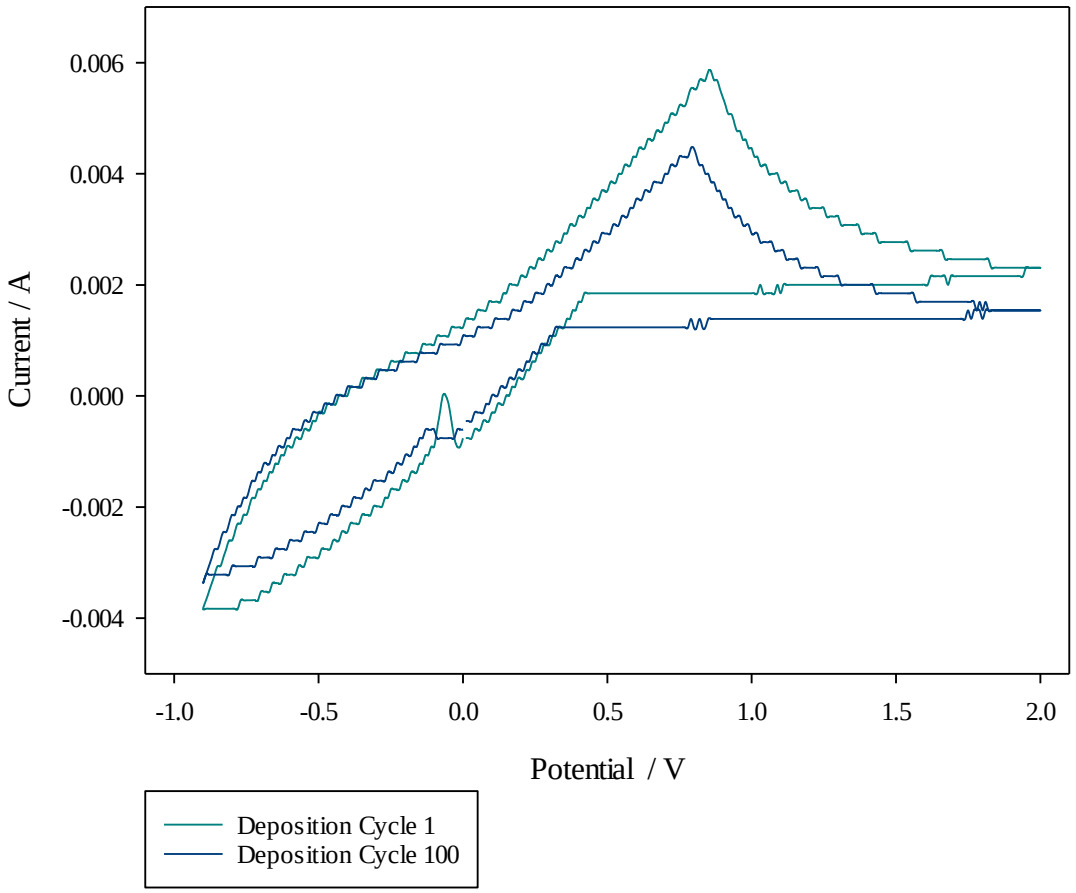

Figure 7.17 – Cyclic voltammograms produced by the deposition polyaniline by the electrochemical oxidation of aniline monomer: black trace is the 1st deposition cycle and the purple trace is the 100th deposition cycle

Camalet et al. [224] and Sazou et al.[223] independently determined that passivation of the steel is necessary for the successful adhesion of a deposited PANi coating to an iron containing substrate. They both suggested that the steel be passivated in the acidic deposition medium without the presence of the aniline monomer. The results of these experiments indicate that such prior passivation is not necessary when the aniline is deposited using a template. Figure 7.17 shows the voltammograms resulting from the deposition of PANi, The large peak at +0.82 V (vs Ag/AgCl) occurs because of the oxidation of aniline monomer; the breadth of the peak occurs because a non-reversible chemical reaction (the oxidation of aniline monomer) is taking place alongside the redox behaviour of the already deposited PANi coating which results in non-Nernstian behaviour.

Table 7.6 - Effect of molar concentration of aniline on coating thickness

Molar concentration of aniline solution/ M	Mass of steel plate before deposition/ g	Mass of steel plate following coating deposition and drying/g	Area covered by coating/ cm^2	Calculated thickness of coating/ µm
0.1	783.43	799.56	46.53	0.54
0.2	795.21	793.68	45.45	0.88
0.3	789.71	808.45	44.1	0.84
0.4	803.84	795.36	46.06	0.92
0.5	791.28	785.27	46.69	0.81
0.6	781.08	777.16	47.06	0.84
0.7	772.44	797.31	45.77	0.98
0.8	792.07	805.87	44.63	1.09
0.9	798.35	804.74	45.01	1.54
1.0	802.61	799.56	45.59	0.65
1.1	White precipitate which resulted from the addition of aniline to oxalic acid did not dissolve			
1.2	White precipitate which resulted from the addition of aniline to oxalic acid did not dissolve			

Table 7.6 demonstrates that a 0.9M concentration of aniline monomer in 0.3M oxalic acid results in the thickest coating. The highly viscous and gelatinous nature of the liquid crystal mesophase template means that aniline monomer cannot readily diffuse through the deposition medium in the same way that it can through the liquid oxalic acid medium and is liable to become trapped within the hydrophobic regions of the mesophase [128]. Therefore, having a higher concentration of monomer present in the mesophase gel template which is in contact with the working electrode i.e. the substrate to be coated, means that more monomer is readily available for deposition onto the substrate. The 1.1 M and 1.2 M aniline samples were not tested for weight and subsequent coating thickness because the precipitate which formed during the addition of aniline to oxalic acid did not dissolve and its presence in the template medium disrupted the coating formation. The 1.0 M sample resulted in a thinner coating because, although the white precipitate dissolved before the aniline/oxalic acid solution was combined with the surfactant, it had precipitated out when the mesophase sample was removed from the heating period. Although the presence of the precipitate

did not affect the formation of the coating, it meant that less aniline monomer was available for polymerisation and so a thinner coating was produced.

Scanning electron microscopy (SEM) images were obtained for the best performing coating deposition parameters.

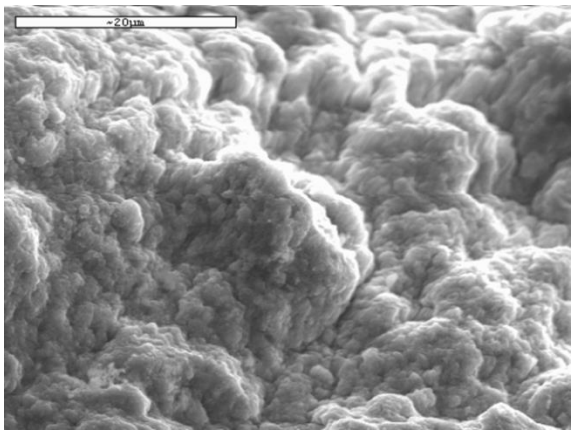

Figure 7.18 - SEM image of a templated Emeraldine salt coating deposited on an S275 steel substrate from a solution of 0.9M of aniline in 0.3M oxalic acid. Deposition was undertaken using cyclic voltammetry between -0.9V and 2.0V (vs Ag/AgCl) using a scan rate of 100 mVs^{-1} and 100 deposition cycles

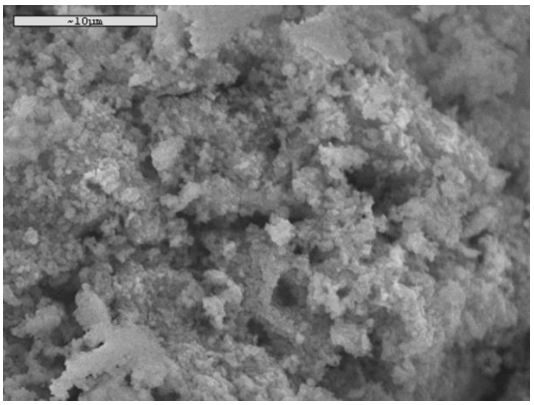

Figure 7.19 - SEM image of a templated Emeraldine-salt coating deposited on an S275 steel substrate from a solution of 0.9M of aniline in 0.3M oxalic acid. Deposition was undertaken using cyclic voltammetry between -0.9V and 2.0V (vs Ag/AgCl) using a scan rate of 100 mVs^{-1} and 100 deposition cycles

Figure 7.18 and Figure 7.19 both demonstrate that the deposited coating has been deposited with a porous internal structure. However, hexagonal mesophase template s would also result in the deposition of porous coatings; the existing investigations into the templating of porous polymers have all used hexagonal mesophases as the template [124, 125, 128]. Therefore the deposited coating was subjected to polarised light microscopy to determine whether the coating was anisotropic or isotropic with respect to polarised light.

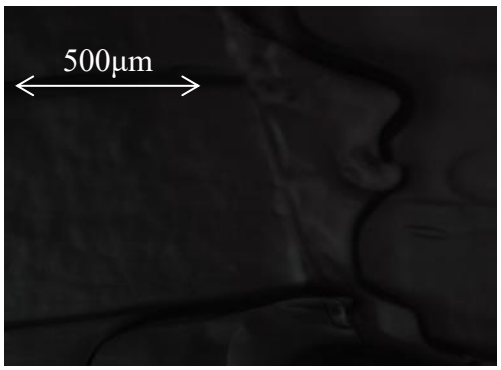

Figure 7.20 - Optical micrograph obtained under polarised light of the templated PANi coating deposited using the optimum conditions

Figure 7.20 demonstrates that the coating is isotropic with respect to polarised light which shows that the coating has retained the optical properties of the mesoporous template; the viscosity of the templating media shows that the template was cubic and the polarised light microscopy confirms that the cubic properties of the template have been transferred to the coating.

7.3 Evaluation of the self-healing coating

Once the porous polyaniline coatings had been successfully deposited, the next stage was to produce the polydopamine capsules which would hold the aniline monomer required for self-healing. The method for producing these capsules and forming them round a liquid so that the liquid remains encased in the capsule is known in the art and the incorporation of aniline as the liquid cargo proved facile. Therefore, no development work was required for the making of the capsules.

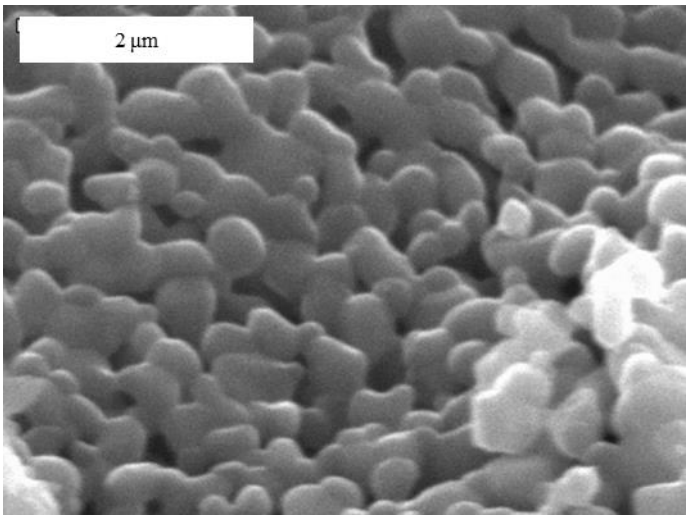

Figure 7.21 – SEM image of aniline monomer encapsulated in polydopamine capsules

Figure 7.21 shows aniline encapsulated in polydopamine nanocapsules made by the modified Cui method [1] (section 5.4). The capsules were shown to be approximately 500 nm in diameter and so are easily able to incorporate into a templated polyaniline film.

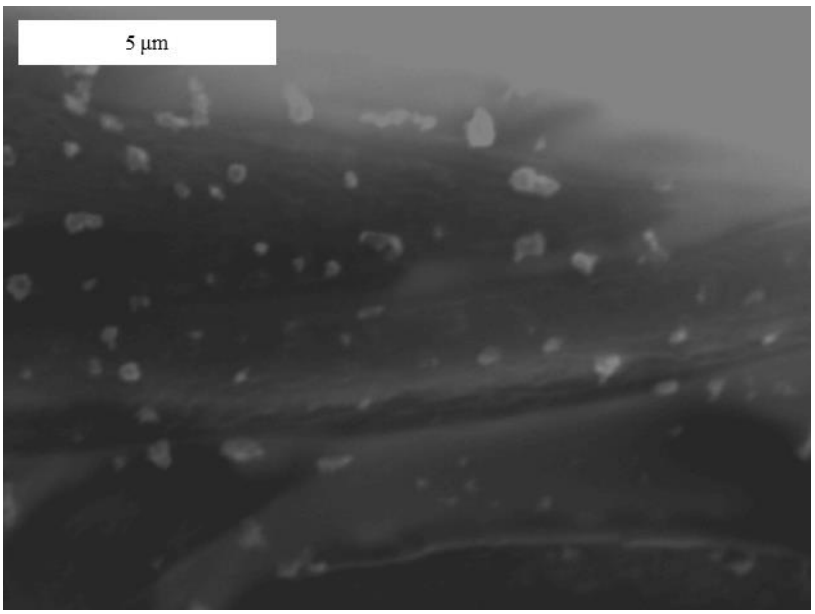

Figure 7.22 - SEM image of a porous templated polyaniline coating; the lighter patches are the polydopamine capsules containing aniline monomer and an epoxy top-coat was applied over the polyaniline

Once the capsules had been successfully manufactured, the next stage was to build the self-healing coating. The coating system was assembled by first depositing a layer of templated polyaniline onto S275 steel using the optimum deposition conditions that had been determined. The template was removed with an ethanol wash for 24 hours. Once the template was removed and the deposited coating dried, previously prepared polydopamine capsules (section 5.4), which had been loaded with aniline, were distributed over the coating surface and an epoxy top coat was applied on top. SEM images were taken of the assembled coating system, as shown in Figure 7.22 above.

Following the assembly of the coatings, the self-healing capabilities of the coating were examined by EIS spectroscopy.

Once the epoxy had cured, a 3cm length cut into the coating system was made with a scalpel blade and the coating was immediately immersed in 3.5% NaCl solution. A cyclic voltametric sweep was applied to the sample using a -1.0V to +1.0V (vs Ag/AgCl) range and a scan rate of 25mVs^{-1} to allow the released aniline monomer to polymerise. The sample was also subjected to periodic EIS testing.

The Nyquist plots recorded at selected time points are shown in Figure 7.23 and Figure 7.25 below. The Nyquist plots recorded for the first four time points have been presented separately to allow their different behaviour to be shown to its best advantage. Figure 7.24 shows a close-up of the high frequency end of the Nyquist plot.

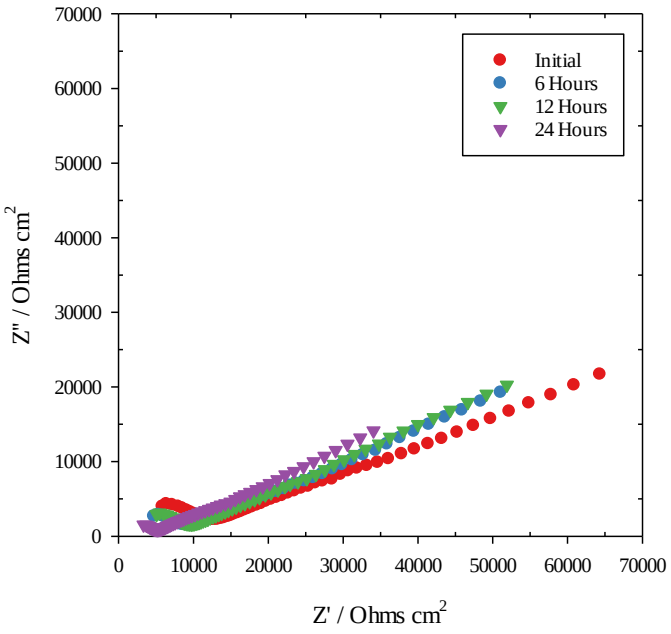

Figure 7.23 - Nyquist plots of a porous templated polyaniline coating incorporating aniline filled microcapsules and finished with an epoxy top-coat; a 3cm defect was induced into the coating system by scoring the coating with a scalpel blade

Figure 7.23 shows that the impedances of the coating system are high compared with the impedances seen for polydopamine coatings. The complete absence of a conductive semi-circle indicates that the coating system overall is an insulator rather than an electo-active coating. This is due to the presence of the epoxy coating which will also provide good barrier properties in an intact coting system [197]. The 45° angle of the low frequency end of the Nyquist plot can be attributed

to diffusion within the coating itself. This is thought to be diffusion of the capsules throughout the coating.

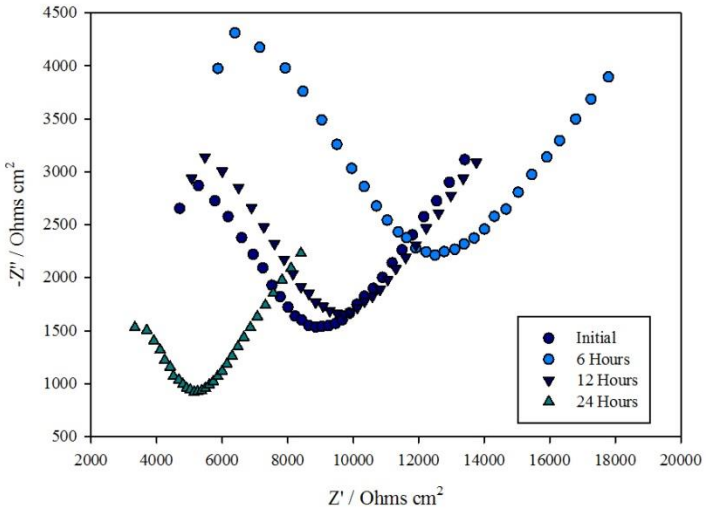

Figure 7.24 –High frequency region of the Nyquist plots of a porous templated polyaniline coating incorporating aniline filled microcapsules and finished with an epoxy top-coat; a 3cm defect was induced into the coating system by scoring the coating with a scalpel blade

The tails shown in Figure 7.24 are similar to those which appear at the low frequency end of the Nyquist plots produced when scratches were induced into *p*-benzoquinone-mediated polydopamine coatings (Figure 6.33). The tails can be attributed to the diffusion of the aniline monomer from the ruptured capsules to the defect site and the subsequent polymerisation of aniline monomer by electrochemical oxidation.

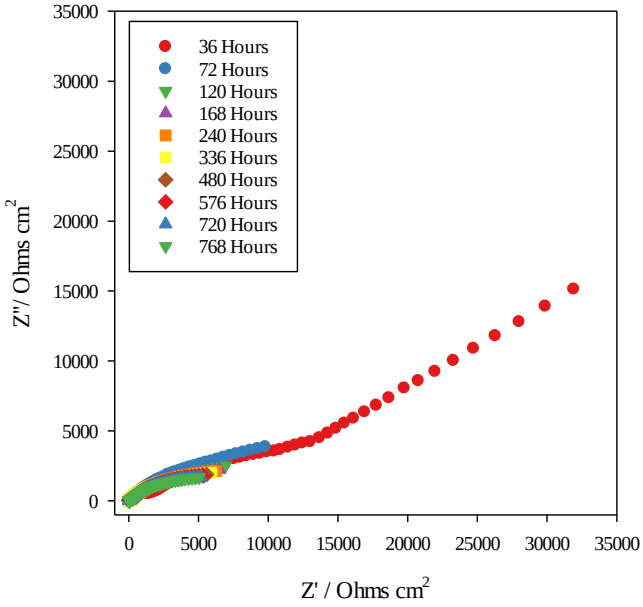

Figure 7.25 – Nyquist plots of a porous templated polyaniline coating incorporating aniline filled microcapsules and finished with an epoxy top-coat; a 3cm defect was induced into the coating system by scoring the coating with a scalpel blade

Figure 7.25 demonstrates that by 36 hours, the self-healing process is complete; the oxidation of aniline monomer is complete, and the coating has completed itself. After 120 hours, there is no further variation in the Nyquist plot which shows that the self-healing process results in the production of a protective coating and the underlying steel substrate ceases to be in contact with the 3.5% NaCl test solution. Figure 7.26 below shows the same Nyquist plots but without the 36-hour plot so that the lower frequency region of the other plots can be better seen.

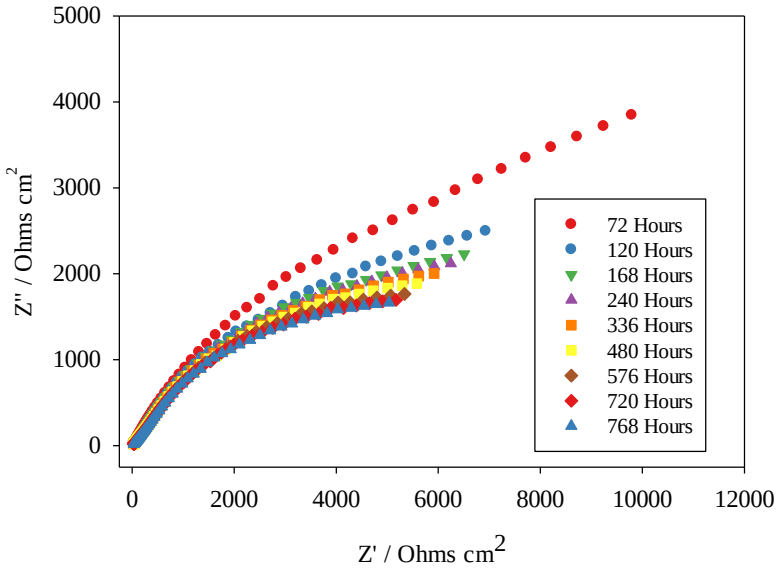

Figure 7.26 - Nyquist plots of a porous templated polyaniline coating incorporating aniline filled microcapsules and finished with an epoxy top-coat; a 3cm defect was induced into the coating system by scoring the coating with a scalpel blade

Figure 7.26 shows that the diffusion process associated with self-healing process has largely diminished. However, there is still diffusion occurring and this can be attributed to the diffusive processes often seen in conductive coatings [223]. The fact that there is no further behavioural change in the complete coating system after 120 hours indicates that the defect has healed with stable polymer rather than friable and permeable corrosion products [225].

Initially, the coating surrounding the defect was bright green which is indicative of the conducting Emeraldine salt form of the polyaniline (PANi-ES). Following the healing of the defect, by 768 hours after initial immersion, the defect site had become a blue colour but the area surrounding the defect site was still green. The blue defect site occurs because there is no suitable dopant present in solution to enable the healed coating to adopt the salt form of Emeraldine and instead, the Emeraldine base form is adopted. Green colour around the defect indicated that the rest of the coating had not yet been fully reduced to the Emeraldine base form. The full reduction of PANi-ES to PANi-EB has been observed, using the distinct colour change by several studies [99] [100] over shorter time periods than have been examined here. These studies were conducted under atmospheric corrosion conditions but Rohwerder et al. [101] have suggested that the protection mechanism of PANi-ES is more effective under immersion conditions than under atmospheric conditions as in immersion; the whole PANi-ES surface is active and able to take part in passivating the metal substrate. It is also possible that the healing of the defect with PANi-EB meant that the protective mechanism of PANi was not required.

In order to isolate the effects of self-healing, the same procedure was repeated with the templated PANi-ES coating and an epoxy top-coat but no aniline-filled capsules were incorporated and the cyclic sweep was not applied. The results are shown in Figure 7.27 in the form of the Nyquist plots. Another plot has been produced (Figure 7.28) which shows the 1-768 hour plots only, allowing the detail of the lower frequency region to be seen.

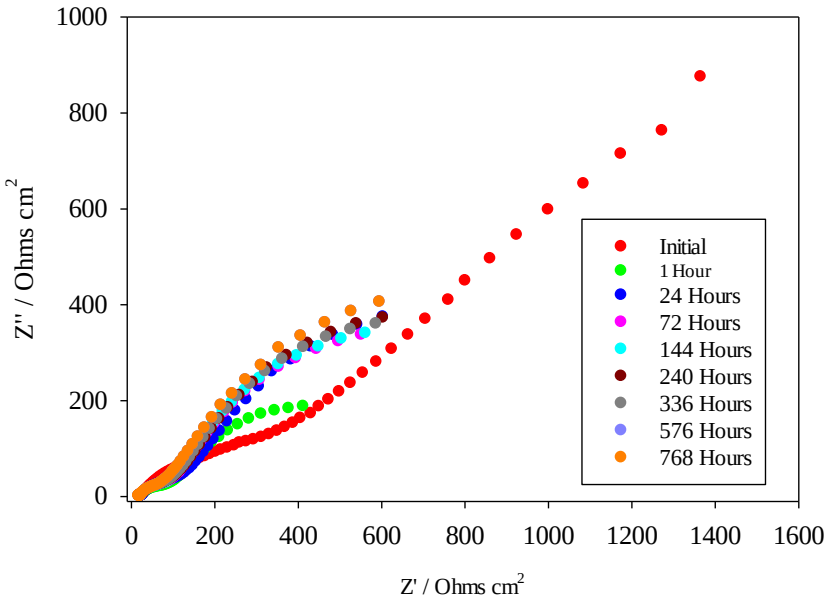

Figure 7.27 - Nyquist plots of a porous templated polyaniline coating finished with an epoxy top-coat; a 3cm defect was induced into the coating system by scoring the coating with a scalpel blade

Figure 7.27 shows that after being immersed in 3.5%NaCl for an hour, two distinct regions are present at all time points and that both regions incorporate a diffusive process. The initial time point shows a single semi-circle with a diffusive process line adjacent to it. This would be expected for an electroactive coating with an induced defect because the diffusion controlled passivation of iron [221, 226] is occurring at the defect site. After being immersed for an hour, the porous coating has effectively failed and this is demonstrated by the appearance of the second region at the higher frequencies. Give the porous nature of the coating, this is not entirely surprising as electrolyte will readily be able to diffuse through the pores in the coating and reach the electrolyte and allow delamination to occur. The porous nature of the coating may well increase the ability of cathodic delamination to take place. After an hour, the area around the defect site was blue indicating that the alkalinity of the defect site had reduced all the surrounding PANi-ES to the PANi-EB form.

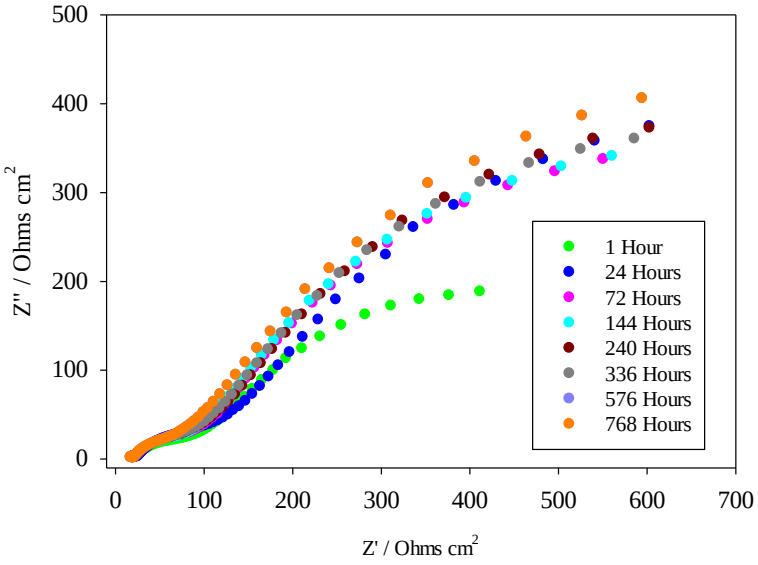

Figure 7.28 - Nyquist plots of a porous templated polyaniline finished with an epoxy top-coat; a 3cm defect was induced into the coating system by scoring the coating with a scalpel blade

The lack of visible corrosion products indicted that the delamination was taking place between the epoxy topcoat and the PANi-ES under layer rather than at the coating/metal interface. This would account for the diffusive elements present in both time constants. In the PANi layer, the diffusion-controlled passivation of the iron substrate will be taking place as well as electrolyte diffusing through the pores in the PANI-ES layer to enable the anodic dissolution of iron. Diffusion will also be taking place at the defect site in the epoxy coating as this will be the most facile route for electrolyte to take through the coating.

These results highlight that the inclusion of the aniline-containing capsules is crucial as the speedy healing of the defect site prevents diffusion of electrolyte through the coating and subsequent separation of the epoxy and PANi-ES layers.

In order to compare the system with the well-known electrodeposited PANI coatings which have been well studied in the literature, the procedure was repeated with a non-templated coating.

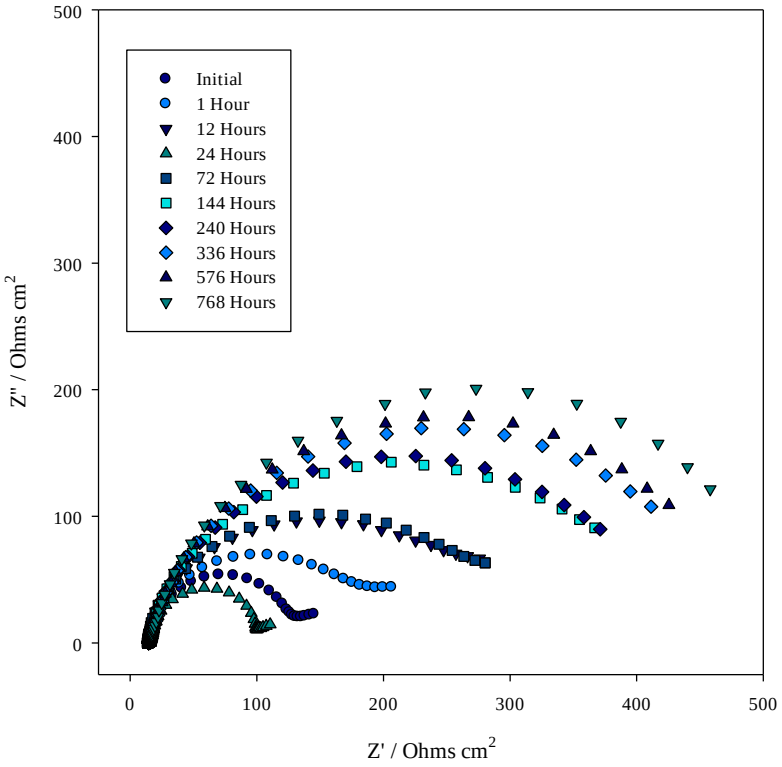

Figure 7.29 - Nyquist plots of a non-templated polyaniline coating finished with an epoxy top-coat; a 3cm defect was induced into the coating system by scoring the coating with a scalpel blade

Figure 7.29 shows the variation of the Nyquist plot over time for a sample of polyaniline with an epoxy topcoat and a defect induced into the coating. The initial time point shows fits to a Randles circuit that incorporates a Warburg diffusive element. The as well as the intrinsic corrosion protection capabilities of the PANi coating .Previous studies that have investigated polyaniline coatings using EIS found that the diffusive elements were less pronounced and an order of magnitude smaller than those of the templated polyaniline coating [76, 82]. The previously deposited coatings were considered to be slightly porous but not to the extent of the deliberately induced porous network found in these coatings. This results in higher impedances and a larger diffusive element in the templated coating. The impedance of the coating increases with time because the defect becomes “plugged” with corrosion products [227]. The impedance of the coating containing microcapsules decreases with time, because no further diffusion of aniline monomer occurs, until 120 hours after which

point the behaviour of the coating remains stable. After 72 hours, the whole coating, previously green, had become blue, indicating that the whole coating had been reduced to PANi-EB. Figure 7.29 only shows a single time constant unlike Figure 7.27 and Figure 7.28. This is because the less porous nature of the non-templated PANi coating facilitates diffusion of the electrolyte through the coating.

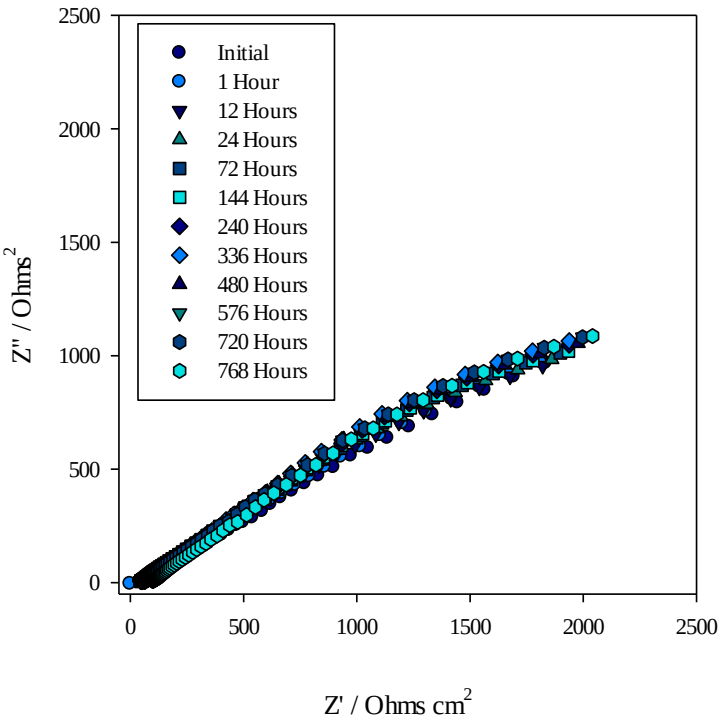

Figure 7.30 - Nyquist plot of a templated polyaniline coating that contains polyaniline filled microcapsules with an epoxy top-coat

Figure 7.30 shows that if no defect was induced then the Nyquist plot did not change over the whole of the 768 hour period, indicating that the intact coating provided good protection for the steel substrate against 3.5% NaCl even when the self-healing capability was not employed. This is most likely due to the epoxy top-coat as previous studies have shown that polyaniline coatings with no topcoat fail within 24 hours.

In conclusion, phase diagrams have been produced for mixtures of four different polyethylene surfactants. This has allowed successful identification of a bi-continuous cubic phase. The mesophase was subsequently used as a template for electrodeposited PANi-ES. The deposition conditions for the templated PANi-ES have been determined. Polydopamine microcapsules filled with aniline have been produced and these have been incorporated into a coating system which comprises an electrodeposited PANI-ES base, the microcapsules and then an epoxy top-coat. The self-healing properties of the coating were tested by deliberately inducing defects into the coating and applying a potential to force the oxidation of aniline. The lack of a suitable dopant meant that the PANi-EB form was deposited, rather than the PANi-ES form. EIS studies of deliberately damaged coatings have highlighted the importance of the inclusion of the capsules, as the porous nature of the templated PANi-appears to accelerate the failure of the damaged coating.

Chapter 8 Conclusions and Future Work

8.1 Conclusions

The first part of this thesis was devoted to furthering the development of polydopamine (PoDA) coatings and exploring their use as corrosion protection measures. It has been shown that the coatings produced with the alternative oxidants, especially *p*- benzoquinone, are better at protecting mild steel substrates from the effects of corrosion than the original autoxidated PoDA coatings. Following the refinement of deposition parameters, it became apparent that the best combination of conditions for successful coating PoDA coatings was to use a 2 mg mL^{-1} dopamine solution of dopamine and a 0.5:1 molar ratio of *p*-BQ to dopamine at a deposition temperature of 35°C.

Following this finding, it became apparent that more information was required about the properties of the deposited PoDA based coating. X-ray photoelectron spectroscopy was used to determine the composition of deposited polymer with the aim of identifying whether *p*-BQ had been incorporated into the deposited PoDA polymer. The XPS study revealed that dopamine monomer was present in the autoxidated PoDA coating but was absent from the *p*-BQ oxidised PoDA, indicating that *p*-BQ was acting as a more effective oxidant than atmospheric oxygen. It was hoped that XPS would allow the identification of one of the following outcomes:

1. *p*-BQ was acting as a more effective oxidant producing a coating that possesses better barrier properties and therefore increased protection against corrosion.
2. *p*-BQ monomer had been incorporated into the deposited PoDA coating and acts as a corrosion inhibitor
3. A co-polymer had formed between the amine groups of the dopamine monomer and the quinone functional group of the *p*-BQ monomer. Such poly(aminoquinones) had been identified in the literature.
4. *p*-BQ undergoes autoxidation to form protecting polymers.

However, as the functional groups identified from the XPS surveys would be present in the coatings that would result from any of the identified outcomes, further analysis was required to determine the nature of the deposited polymer.

SKP was used to try and identify the corrosion protection mechanism of the *p*-BQ mediated PoDA. The *p*-BQ polymers and the poly(aminoquinones) have a corrosion protection mechanism akin to that of polyaniline which undergoes red-ox reactions with the metal substrate to provide protection against the anodic and cathodic reactions. Such a protective mechanism would have

manifested itself on the SKP plots as an absence of the secondary spreading. However, whilst the *p*-BQ oxidised PoDA minimised the secondary spreading, it did not inhibit it. It can be concluded, therefore, that the protection mechanism of the *p*-BQ oxidised PoDA does not rely on red-ox reactions between the deposited polymer and the underlying substrate and therefore, the polymer is unlikely to be either a polymer comprising solely *p*-BQ monomers or a member of the poly(aminoquinone) class. However, in order to be certain, further structural analysis in the form of TOF-SIMS is required to confirm the structure of the deposited polymer. TOF-SIMS analysis will also indicate whether *p*-BQ is present in monomeric form in the deposited coating which will either confirm or deny whether the proposed protection mechanism of *p*-BQ acting as a corrosion inhibitor is a valid proposition.

Regardless of protection mechanism confirmation, it has been confirmed that, even after extensive attempts to use alternative oxidants, PoDA coatings cannot be made sufficiently thick to act as protective coating. The thinness of the current coating would make the incorporation of a porous network and microcapsules impossible as both capsules and pores would be greater in diameter than the thickness of the coating. In addition, the coating needs to be robust enough to survive in a harsh environment i.e. a naval ballast tank which is not the case with the PoDA coatings.

Therefore, polyaniline was used as the basis for the smart self-healing coating. Polyaniline is capable of protecting mild steel against corrosion, including in chloride containing solutions, providing the correct deposition conditions are selected. Whilst PANi has established and proven corrosion prevention capabilities, it has not been used as the basis for a self-healing polymer nor has it been templated using a liquid-crystal based soft template so the outcome of the project can still be considered a novel system. It is relatively facile to deposit micrometre thick coatings of PANi in a few hours when electropolymerisation is used.

In order to determine which liquid crystal mesophase would provide the most suitable template for the deposition of a porous polyaniline coating, phase diagrams were created for various surfactants and from these it was concluded that a 50/50 wt% mix of Brij S100 surfactant and 0.3 M oxalic acid produced a bi-continuous cubic mesophase that was stable for 24 hours.

The template was then used as the basis for the production of porous (templated) polyaniline. A series of experiments and optimisations were undertaken in order to produce the thickest possible templated coating. The conditions required for templated deposition of polyaniline differed greatly to those required for the deposition of non-templated PANi. This was attributed to the highly viscous nature of the liquid crystal template when compared to the more established liquid

deposition media. The presence of the template hindered the diffusion of the aniline monomer, dispersed throughout the template, to the electrode surface. When compared to polyaniline coatings deposited from an aqueous solution, as per the existing prior art, higher concentrations of aniline monomer were required to form templated coatings of similar thickness and uniformity of coverage.

Polydopamine capsules filled with aniline monomer were created using an established method, although the encapsulation of aniline is novel. The capsules were then added to a deposited polyaniline coating and an epoxy top coat was applied. The self-healing capabilities of the system were tested by deliberately inducing a defect into the coating system and then observing the EIS behaviour of the coating. It was found that diffusion controlled chemical reactions too place over the first 24 hours after the defect was introduced. After 72 hours, the coating had achieved a state of equilibrium and no further change to its impedance or electrochemical behaviour was observed until the test was stopped after 728 hours. This indicated that the defect had healed by the formation of polyaniline in-situ and that subsequently, no further corrosion could occur.

The results presented here demonstrate that the stated aims of the project have been met. A 3-Dimensional porous network has been incorporated into the emeraldine (conducting) form of polyaniline. Aniline monomer has been encapsulated into polydopamine microcapsules and the microcapsules added to the coating; the monomer has subsequently been used to repair a defect that was deliberately induced into the coating. In this respect the coating system can be said to be self-healing. However an external stimulus in the form of an applied voltage was required in order to oxidise the aniline monomer to form polyaniline. In this respect the self-healing aspect of the coating has only been partially successful.

8.2 Future Work

The self-healing nature of the coating system has only been demonstrated using electrochemical oxidation of the released monomer. Such a system is not necessarily practical and so the coating system could be developed further through the encapsulation of oxidation agents. Assuming the aniline containing capsules and the oxidant containing capsules can be evenly mixed and distributed throughout the porous coating, damage to the coating would rupture equal quantities of oxidant and oxidative chemical polymerisation of aniline would occur and the formed polymer would “heal” the defect.

The effectiveness of the coating may be further improved by the optimisation of the size of the pores in the polyaniline coating and by altering the size of the polydopamine capsules. Smaller

capsules in larger pores would allow the capsules to travel further into the coating which could increase the efficiency of the coating, and also allow more substantial defects to be healed. Scanning kelvin probe investigations may provide more information as to the exact mode of protection of the self-healing system.

It may also be beneficial to incorporate a sensing network into the coating to allow remote monitoring of the coating and detection of defects. Localised electrochemical impedance spectroscopy has been used as a successful means of remotely detecting corrosion in pipelines [228-230].

Further long-term testing is needed to ensure that the coating is stable for periods of longer than one month (the longest tested period so far).

List of References

[1] J. Cui, Y. Wang, A. Postma, J. Hao, L. Hosta-Rigau, and F. Caruso, "Monodisperse Polymer Capsules: tailoring Size, Shell Thickness and Hydrophobic Cargo Loading via Emulsion Templating," *Adv. Funct. Mater.*, vol. 20, pp. 1625-1631, 2010.

[2] M. Nie, "Deliverable 4 and Final Report," in "New Coating Systems for Protection of Critical Areas " University of Southampton / Centre for Defence Enterprise, Southampton2012.

[3] C. o. S. B. O. M. B. C. o. E. a. T. S. N. R. Council *et al.*, "Ballast water and Ships," in *Stemming The Tide. Controlling Introductions of Nonindigenous Species by Ship's Ballast Water*, N. A. o. Sciences, Ed. Washington DC: National Academy Press, 1996, pp. 22-31.

[4] G. Tourret, J.-L. Guibert, D. Drevet, B. Parizot, Y. H. D. Fretay, and B. Lion, "Report of the Enquiry into the Sinking of the Erika Off the Coasts of Brittany on 12 December 1999," Bureau d'enquetes sur les evenements de mer (BEAmer), La Defense, Paris2000.

[5] M. Pourbaix, *Atlas of Electrochemical Equilibria in Aqueous Solutions*, 2nd ed. NACE International, 1974.

[6] R. W. R. a. H. H. Uhlig, *Corrosion and Corrosion control*. John Wiley & Sons Inc. , 2008.

[7] A. Cook, A. Gabriel, and N. Laycock, "On the Mechanism of Corrosion Protection of Mild steel with Polyaniline," *J. Electrochem. Soc.*, vol. 151, pp. B529-B535, 2004.

[8] W. G. Characklis and K. C. Marshall, "Biofilms: A Basis For an Interdisciplinary Approach," in *Biofilms*, W. G. Characklis and K. C. Marshall, Eds. New York: Wiley, 1990, p. 4.

[9] W. Hamilton, "Sulphate-Reducing Bacteria and Anaerobic Corrosion," *Annu. Rev. Microbiol. ,* vol. 39, pp. 195-217, 1985.

[10] A. G. Wikjord, T. E. Rummery, F. E. Doern, and D. G. Owen, "Corrosion and Deposition During the Exposure of Carbon Steel to Hydrogen Sulphide Water Solutions," *Corros. Sci.*, vol. 20, pp. 651-671, 1980.

[11] K. J. Rawson and E. C. Tupper, "Flotation and Trim," in *Basic Ship Theory*, vol. 1Fifth ed. Oxford, UK: Butterworth-Heineman, 2001.

[12] A. Hayer, D. D'Souza, C. F. L. Morales, G. Ferrari, J. M. C. Mol, and J. H. W. d. Wit, "Ship Ballast tanks a Review From Microbial Corrosion and Electrochemical Point of View," *Ocean Engineering,* vol. 70, pp. 188-200, 2013.

[13] G. Ferrari *et al.*, "Susceptibility of Epoxy Coatings To Microbial Influenced Degradation," presented at the Eurocorr 2010, Moscow, Russia, 2010.

[14] B. Little, R. Ray, P. Wagner, J. Jones-Mehan, C. Lee, and F. Mansfield, "Spatial Relationships Between Marine Bacterial and Localised Corrosion," *Biofouling*, vol. 13, pp. 301-321, 1999.

[15] G. Loget, J. B. Wood, K. Cho, A. R. Halpern, and R. M. Corn, "Electrodeposition of Polydopamine Thin Films for DNA Patterning and Microarrays," *Anal. Chem.*, vol. 85, pp. 9991-9995, 2013.

[16] F. Bernsmann, J.-C. Voegel, and V. Ball, "Different Synthesis Methods Allow to Tune the Permeability and Permselectivity of Dopamine-Melanin Films to Electrochemical Probes," *Electrochim. Acta*, vol. 56, pp. 3914-3919, 2011.

[17] Y. Li, M. Liu, C. Xiang, Q. Xie, and S. Yao, "Electrochemical Quartz Crystal Microbalance Study on Growth and Property of the Polymer Deposit at Gold Electrodes During Oxidation of Dopamine in Aqueous Solutions " *Thin Solid Films*, vol. 2006, pp. 270-278, 2006.

[18] H. S. Raper, "The Tyrosinase-Tyrosine Reaction," *Biochem. J.*, vol. 21, pp. 89-96, 1927.

[19] A. B. Barron, E. Sovik, and J. L. Cornish, "The Roles of Dopamine and Related Compounds in Reward-seeking Behaviour Across Animal Pyla. ," *Front. Behav. Neurosci.* , vol. 4, pp. 1-9, 2010.

[20] J. H. Waite, "Mussel Power," *Nature Materials*, vol. 7, pp. 8-9, 2008.

[21] G. Anderson. (2003, 19 July 2014). *http://www.marinebio.net/marinescience/03ecology/tphi.htm* *The High Tide Zone*.

[22] H. Lee, N. F. Scherer, and P. B. Messersmith, "Single-Molecule Mechanics of Mussel Adhesion," *PNAS*, vol. 103, no. 35, pp. 12999-13003, 2006.

[23] J. Purdue. (19 July 2014). *http://www.chem.purdue.edu/wilker/Research/Characterization%20of%20Biological%20Materials.html*.

[24] M. Yu, J. Hwang, and T. J. Deming, "Role of L-3,4-Dihydroxyphenylanaline in Mussel Adhesive Proteins," *J. Am. Chem. Soc*, vol. 121, pp. 5825-5826, 1999.

[25] J. H. Waite, "Adhesion a la Moule," *Integr. Comp. Biol*, vol. 42, pp. 1172-1180, 2002.

[26] B. P. Lee, P. B. Messersmith, J. N. Israelachvili, and J. H. Waite, "Mussel-Inspired Adhesives and Coatings," *Annu. Rev. Mater. Res.* , vol. 41, pp. 99-132, 2011.

[27] F. Yu, Y. Chen, H. Li, L. Yang, Y. Chen, and Y. Yin, "Experimental and Theoretical Analysis of Polymerization Reaction process on the Polydopamine Membranes and its Corrosion Protection Properties for 304 Stainless Steel," *J. Mol. Struc.*, vol. 982, pp. 152-161, 2010.

[28] F. Bernsmann *et al.*, "Characterisation of Dopamine-Melanin Growth on Silicon Oxide," *J. Phys. Chem. C*, vol. 113, pp. 8234-8242, 2009.

[29] F. Cataldo, "On the Structure of Macromolecules Obtained by Oxidative Polymerisation of Polyhydroxyphenols and Quinones " *Polym. Int.* , vol. 46, pp. 263-268, 1998.

[30] A. Pezzella, L. Panzella, A. Natangelo, A. Arzillo, A. Napolitano, and M. d'Ischia, "5,6-Dihyroxyindole tetramers with "Anomalous" Interunit Bonding Patterns by Oxidative Coupling of 5,5',6,6'-Tetrahydroxy-2,7'-biindolyl: Emerging Complexities on the way Toward an Improved Model of Eumelanin Buildup," *J. Org. Chem.*, vol. 72, pp. 9225-9230, 2007.

[31] M. d'Ischia, A. Napolitano, A. Pezzella, P. Meredith, and T. Sarna, "Chemical and Structural Diversity in Eumelanins: Unexplored Bio-Optoelectronic Materials," *Angew. Chem. Int. Ed.*, vol. 48, pp. 3914-3921, 2009.

[32] A. Lerner and T. B. Fitzpatrick, "Biochemistry of Melanin Formation," *Physiological Rev.* , vol. 30, pp. 91-126, 1950.

[33] F. Binns *et al.*, "Studies Related to the Chemistry of Melanins. Part XIII. Studies on the Structure of Dopamine-Melanin," *J. Chem. Soc. C*, vol. 1970, pp. 2063-2070, 1970.

[34] D. R. Dreyer, D. J. Miller, B. D. Freeman, D. R. Paul, and C. W. Bielawski, "Perspectives on poly(dopamine)," *Chem. Sci*, vol. 4, pp. 3796-3802, 2013.

[35] D. R. Dreyer, D. J. Miller, B. D. Freeman, D. R. Paul, and C. W. Bielawski, "Elucidating the Structure of Poly(dopamine)," *Langmuir*, vol. 28, pp. 6428-6435, 2012.

[36] E. Herlinger, R. F. Jameson, and W. Linert, "Spontaneous Autoxidation of Dopamine," *J. Chem. Soc. Perkin Trans. 2*, vol. 1995, pp. 259-263, 1995.

[37] H. Lee, S. M. Dellatore, W. M. Miller, and P. B. Messersmith, "Mussel-Inspired Surface Chemistry for Multifunctional Coatings " *Science*, vol. 426, pp. 426-430, 2007.

[38] Q. Wei, F. Zhang, J. Li, and C. Zhao, "Oxidant-Induced Dopamine Polymerization for Multifunctional Coatings," *Polym. Chem.* , vol. 1, pp. 1430-1433, 2010.

[39] A. Postma, Y. Yan, Y. Wang, A. N. Zelikin, E. Tjipto, and F. Caruso, "Self-Polymerisation of Dopamine as Versatile and Robust Technique to Prepare Polymer Capsules," *Chem. Mater.*, vol. 21, pp. 3042-3044, 2009.

[40] B. Yu, D. A. Wang, Q. Ye, F. Zhou, and W. Liu, "Robust Polydopamine Nano/microcapsules and Their Loading and Release Behaviour," *Chem. Commun.*, vol. 6789-6791, 2009.

[41] J. Liebscher *et al.*, "Structure of Polydopamine: A Never-Ending Story," *Langmuir*, vol. 29, pp. 10539-10548, 2013.

[42] V. Ball, "Impedance Spectroscopy and Zeta Potential Titration of Dopa-Melanin Films Produced by Oxidation of Dopamine " *Colloids and Surfaces A: Physicochem. Eng. Aspects*, vol. 363, pp. 92-97, 2010.

[43] V. Ball, D. D. Frari, V. Toniazzo, and D. Ruch, "Kinetics of Polydopamine Film Deposition as a Function of pH and Dopamine Concentration: Insights in the Polydopamine Deposition Mechanism," *J. Colloid Interfac. Sci.* , vol. 386, pp. 366-372, 2012.

[44] R. Mrowczynski, R. Turcu, C. Leostan, H. A. Scheidt, and J. Liebscher, "New Versatile Polydopamine Coated Functionalised Magnetic Nanoparticles," *Mat. Chem. Phys.*, vol. 138, pp. 295-302, 2013.

[45] E. Kaxiras, A. Tsolakidis, G. Zonios, and S. Meng, "Sructural Model of Eumelanin," *Phys. Rev. Lett*, vol. 97, no. 218102, pp. 1-4, 2006.

[46] H. W. Kim *et al.*, "Oxygen Concentration Control of Dopamine-Induced High Uniformity Surface Coating Chemistry," *Appl. Mater. Interfaces*, vol. 5, pp. 233-238 2013.

[47] S. Hong, Y. S. Na, S. Choi, I. T. Song, W. Y. Kim, and H. Lee, "Non-Covalent Self-Assembly and Covalent Polymerization Co-Contribute to Polydopamine Formation," *Adv. Funct. Mater.*, vol. 22, pp. 4711-4717, 2012.

[48] N. F. d. Vecchia, R. Avolio, M. Alfe, M. E. Errico, A. Napolitano, and M. d'Ischia, "Building-Block Diversity in Polydopamine Underpins a Multifunctional Eumelanin-Type Platform Tunable Through a Quinone Control Point," *Adv. Funct. Mater.*, vol. 23, pp. 1331-1340, 2013.

[49] F. Bernsmann *et al.*, "Dopamine-Melanin Film Deposition Depends on the Used Oxidant and Buffer Solution," *Langmuir*, vol. 27, pp. 2819-2825 2011.

[50] J. Jiang, L. Zhu, L. Zhu, B. Zhu, and Y. Xu, "Surface Characteristics of a Self-Polymerized Dopamine Coating Deposited on Hydrophobic Polymer Films," *Langmuir*, vol. 27, pp. 14180-14187, 2011.

[51] H. Wei, J. Ren, B. Han, L. Xu, L. Han, and L. Jia, "Stability of polydopamine and poly(DOPA) melanin-like films on the surface of polymer membranes under strongly acidic and alkaline conditions," *Colloids and Surfaces B: Biointerfaces*, vol. 110, pp. 22-28, 2013.

[52] A. V. Ragimov, S. S. Suleimanova, and S. I. Sadykh-Zade, *Azerb. Khim. Zh.* , vol. 6, 1971.

[53] Y. V. Medvedev, N. V. Sidorkina, A. I. Koltsov, A. V. Purkina, and M. M. Koton, "Potentiometric Study of p-Benzoquinone Polymerisation and the Structure of the Polymer," *Vysokomol. Soyed.*, vol. A17, pp. 557-563, 1975.

[54] A. Furlani, M. V. Russo, and F. Cataldo, "Oxidative Polymerisation of p-Benzoquinone and Hydroquinone. Conductivity of Doped and Undoped Polymerisation Products," *Synth. Met.*, vol. 29, pp. E507-E510, 1989.

[55] E. Berliner, "A Relation Between the Oxidation-Reduction Potentials of Quinones and the Resoance Energies of Quinones and Hydroquinones," *J. Am. Chem. Soc.*, vol. 68, pp. 49-51, 1946.

[56] J. Stejskal and M. Trchova, "Aniline oligomers *versus* polyaniline," *Polym. Int.,* vol. 2012, pp. 240-251, 2014.

[57] E. C. Venancio, P.-C. Wang, and A. G. McDiarmid, "The azanes: A class of materal incorporating nano/micro self-assembled hollow spheres obtained by aqueous oxidative polymerisation of aniline," *Synth. Met.,* vol. 156, p. 357, 2006.

[58] S. P. Surwade, V. Dua, N. Manohar, S. K. Manohar, E. beck, and J. P. Ferraris, "Oligoaniline Intermediates in the Aniline-Peroxydisulfate System," *Synth. Met.,* vol. 159, pp. 445-455, 2009.

[59] J. Kriz, L. Starovoytova, M. Trchova, E. N. Konyushenko, and J. Stejskal, "NMR investigation of Aniline Oligomers Produced in the Early Stages of Oxidative POlymerisation of Aniline," *J. Phys. Chem. B,* vol. 113, pp. 6666-6673, 2009.

[60] Z. D. Zujovic *et al.*, "Role of Aniline Oligomeric Nanosheets in the Formation of Polyaniline Nanotubes," *Macromolecules,* vol. 43, pp. 662-670, 2009.

[61] S. Muralidharan, K. L. N. Phani, S. pitchumani, S. Ravichandran, and S. V. K. Lyer, "Polyamino-Benzoquinone Polymers: A new Class of Corrosion Inhibitors for Mild Steel " *J. Electrochem. Soc.,* vol. 142, pp. 1478-1483, 1995.

[62] E. Vaccaro, C. D. Simone, and D. A. Scola, "Amino-p-benzoquinone Adducts and Polymers as Adhesion Promoters for Steel," *J. Adhes,* vol. 72, pp. 157-176, 2006.

[63] K. Kaleem, F. Chertok, and S. Erhan, "A novel coating based on Poly(etheramine-quinone) polymers," *Prog. Org. Coat,* vol. 15, pp. 63-71, 1987.

[64] K. L. N. Phani, S. Pitchumani, S. Muralidharan, S. Ravichandaran, and S. V. K. Iyer, "Electrosynthesis of Polyamino-benzoquinone (PAQ) polymers," *J. Electroanal. Chem.,* vol. 353, pp. 315-322, 1993.

[65] J. Stejskal, P. Bober, M. Trchova, J. Horsky, and Z. Walterova, "The Oxidation of Aniline with *p*-Benzoquinone and its Impact on the Preparation of the Conducting Polymer, Polyaniline," *Synth. Met.,* vol. 192, pp. 66-73, 2014.

[66] B. D. Mather, K. Viswanathan, K. M. Miller, and T. E. Long, "Michael Addition Reactions in Macromolecular Design for Emerging Technologies," *Prog. Poly. Sci.,* vol. 31, pp. 487-531, 2006.

[67] C. Jeyaprabha, S. Sathiyanarayanan, K. L. N. Phani, and G. Venkatachari, "Influence of Poly(aminoquinone) on Corrosion Inhibition of Iron in Acid Media," *Appl. Surf. Sci.,* vol. 252, pp. 966-975, 2005.

[68] R. A. Zangmeister, T. A. Morris, and M. J. Tarlov, "Characterisation of Polydopamine Thin Films Deposited at Short Times by Autoxidation of Dopamine," *Langmuir,* vol. 29, pp. 8619-8628, 2013.

[69] R. Battino, T. R. Rettich, and T. T, "The Solubility of Oxygen and Ozone in Liquids," *J. Phys. Chem. Ref. Data,* vol. 12, no. 2, pp. 163-178, 1983.

[70] V. Ball *et al.*, "Deposition Mechanism and Properties of Thin Polydopamine Films for High Added Value Applications In Surface Science at the Nanoscale," *BioNanoSci*, vol. 2, pp. 16-34, 2012.

[71] T. K. Rout, G. Jha, A. K. Singh, N. Brandyopadhyay, and O. N. Mohanty, "Development of Conducting Polyaniline Coating: a Novel Approach to Superior Corrosion Resistance," vol. 2003, pp. 16-24, 2003.

[72] I. Sapurina and J. Stejskal, "The Mechanism of the Oxidative Polymerization of Aniline and the Formation of Supramolecular Polyaniline Structures " *Polym. Int.*, vol. 57, pp. 1295-1325, 2008.

[73] F. Bernsmann *et al.*, "Use of Dopamine Polymerisation to Produce Free-Standing Membranes From (PLL-HA)n Exponentially Growing Multilayer Films," *Soft Matter*, vol. 4, pp. 1621-1624, 2008.

[74] A. G. MacDiarmid and A. J. Epstein, "Polyanilines: A Novel Class of Conducting Polymers," *Faraday Discuss. Chem. Soc.* , vol. 88, pp. 317-332, 1989.

[75] B. Wessling, "Scientific and Commercial Breakthrough for Organic Metals," *Synth. Met.*, vol. 85, pp. 1313-1318, 1997.

[76] A. Talo, P. Passiniemi, O. Forsen, and S. Ylasaari, "Polyaniline/Epoxy Coatings with Good Anti-Corrosion Properties," *Synth. Met.*, vol. 85, pp. 1333-1334, 1997.

[77] D. E. Tallman, Y. Pae, and G. P. Bierwagen, "Conducting Polymers and Corrosion: Polyaniline on Steel," *Corrosion*, vol. 55, pp. 779-786, 1999.

[78] T. P. McAndrew, *Trends Polym. Sci.*, vol. 5, pp. 7-12, 1997.

[79] L. Y. O. Wang, C. Chang, S. Liu, C. Wu, and S. L. Yau, "Direct Visualization of an Aniline Admolecule and Its Electropolymerization on Au(111) with in Situ Scanning Tunneling Microscope," *J. Am. Chem. Soc.*, vol. 129, pp. 8076-8077, 2007.

[80] I. Sapurina and J. Stejskal, "Oxidation of Aniline with Strong and Weak Oxidants," *Russian. J. General Chem.*, vol. 82, pp. 256-276, 2012.

[81] S. R. Moraes, D. Huerta-Vilca, and A. J. Motheo, "Corrosion Protection of Stainless Steel by Polyaniline Electrosynthesised From Phosphate Buffer Solutions," *Prog. Org. Coat*, vol. 48, pp. 28-33, 2003.

[82] T. Pan and Z. Wang, "A Polyaniline Based Intrinsically Conducting Coating for Corrosion Protection of Structural Steels," *Micros. Res. Techniq.* , vol. 76, pp. 1186-1195, 2013.

[83] W.-K. Lu, R. L. Elsenbaumer, and B. Wessling, "Corrosion Protection of Mild Steel by Coatings Containing Polyaniline," *Synth. Met.*, vol. 71, pp. 2163-2166, 1995.

[84] R. Vera, R. Schrebler, P. Cury, R. D. Rio, and H. Romero, "Corrosion Protection of Carbon Steel and Copper by Polyaniline and Poly(ortho-methoxyaniline) Films in Sodium

Chloride Medium. Electrochemical and Morphological Study. ," *J. Appl. Electrochem.*, vol. 37, pp. 519-525, 2007.

[85] A. R. Elkais, M. M. Gvozdenovic, B. Z. Jugovic, J. S. Stevanovic, N. D. Nikolic, and B. N. Grgur, "Electrochemical synthesis and characterization of polyaniline thin film and polyaniline powder," *Prog. Org. Coat,* vol. 71, pp. 32-35, 2011.

[86] S. Biallozor and A. Kupniewska, "Conducting Polymers Electodeposited on Active Metals," *Synth. Met.*, vol. 155, pp. 443-449, 2005.

[87] T. D. Nguyen, J.-L. Camalet, J.-C. Lacroix, S. Aeiyach, M. C. Pham, and P.-C. Lacaze, "Polyaniline Electrodeposition from Neutral Aqueous Media: Application to the Deposition on Oxidizable Metals," *Synth. Met.*, vol. 102, pp. 1388-1389, 1999.

[88] J.-L. Camalet *et al.*, "Aniline Electropolymerisation on Platinum and Mild Steel From Neutral Aqueous Media," *J. Electroanal. Chem.*, vol. 485, pp. 13-20, 2000.

[89] C. B. Breslin, A. M. Fenelon, and K. G. Conroy, "Surface Engineering: Corrosion protection using conducting polymers," *Materials and Design* vol. 26, pp. 233-237, 2005.

[90] A. M. Fenelon and C. B. Breslin, "An Investigation into the degradation of polyaniline films grownon iron from oxalic acid," *Synth. Met.*, vol. 144, pp. 125-131, 2004.

[91] N. M. Martyak, "Chronoamperiteric Studies During the Polymerisation of Aniline from an Oxalic Acid Solution," *Mat. Chem. Phys,* vol. 81, pp. 143-151, 2003.

[92] N. M. Martyak, P. McAndrew, J. E. McCaskie, and J. Dijon, "Electrochemical polymerisation of aniline from an oxalic acid medium," *Prog. Org. Coat,* vol. 45, pp. 23-32, 2002.

[93] R. A. Dickie and F. L. Floyd, "Polymeric Materials for Corrosion Control: An Overview," *ACS Symposium Series,* vol. 1986, pp. 1-16, 1986.

[94] R. Gasparac and C. R. Martin, "Investigations of the Mechanism of Corrosion Inhibition by Polyaniline. Polyaniline-Coated Stainless Steel in Sulfuric Acid Solution " *J. Electrochem. Soc.*, vol. 148, pp. B138-B145, 2004.

[95] M. Fahlman, S. Jasty, and A. J. Epstein, "Corrosion Protection of Iron/Steel by Emeraldine Base Polyaniline: an X-Ray Photoelectron Spectroscopy Study," *Synth. Met.*, vol. 85, pp. 1323-1326, 1997.

[96] W. S. Araujo, I. C. P. Margarit, M. Ferreira, O. R. Mattos, and P. L. Neto, "Undoped Polyaniline Anticorrosive Properties," *Electrochim. Acta,* vol. 46, pp. 1307-1312, 2001.

[97] B. Wessling, "Passivation of metals by coating with polyaniline: Corrosion potential shift and morphological changes," *Adv. Mater,* vol. 6, pp. 226-228, 1994.

[98] G. W. R. J. H. D. A. W. H. N. McMurray, "Inhibition of corrosion-driven organic coating delamination on zinc by polyaniline," *Electrochem. Commun. ,* vol. 6, pp. 549-555, 2004.

[99] R. J. H. G. W. D. A. W. a. H. N. McMurray, "Polyaniline Inhibition of Corrosion-Driven Organic Coating Cathodic Delamination on Iron," *J. Electrochem. Soc.*, vol. 152, pp. B73-B81, 2005.

[100] G. W. A. G. A. C. a. H. N. McMurray, "Dopant Effects in Polyaniline Inhibition of Corrosion-Driven Organic Coating Cathodic Delamination on Iron" *J. Electrochem. Soc.*, vol. 153, pp. B425-B433, 2006.

[101] M. R. A. Michalik, "Conducting polymers for corrosion protection: What makes the difference between failure and success?," *Electrochim. Acta*, vol. 53, pp. 1300-1313, 2007.

[102] M. Kraljic, Z. Mandic, and L. Duic, "Inhibition of Steel Corrosion by Polyaniline Coatings," *Corros. Sci.*, vol. 45, pp. 181-198, 2003.

[103] N. Ahmad and A. G. MacDiarmid, "Inhibiiton of Corrosion of Steelsa with the Exploitation of Conducting Polymers," *Synth. Met.*, vol. 78, pp. 103-110, 1996.

[104] A. Yagan, N. O. Pekmez, and A. Yildiz, "Inihibition of Corrosion of Mild Steel by Homopolymer and Bilayer Coatings of Polyaniline and Polypyrrole," *Prog. Org. Coat*, vol. 59, pp. 297-303, 2007.

[105] J. E. P. d. Silva, S. I. C. d. Torresi, and R. M. Torresi, "Polyaniline Acrylic Coatings for Corrosion Inhibition: The Role Played by Counter-Ions," *Corros. Sci.*, vol. 47, pp. 811-822, 2005.

[106] S. Sathiyanarayanan, S. Dev, and G. Venkatachari, "Corrosion Protection of Stainless Steel by Electropolymerised PANi Coating," *Prog. Org. Coat*, vol. 56, pp. 114-119, 2006.

[107] B. N. Grgur, M. M. Gvozdenovic, V. B. Miskovic-Stankovic, and Z. Kacarevic-Popovic, "Corrosion Behaviour and Thermal Stability of Electrodeposited PANI/Epoxy Coating System on Mild Steel in Sodium Chloride Solution," *Prog. Org. Coat*, vol. 56, pp. 214-219, 2006.

[108] K. G. Thompson and B. C. Benicewicz, "Corrosion-Protective Coatings from Electroactive Polymers," in *ACS Symposium Series 843*, vol. 843, P. Zarras, J. D. S. Smith, and Y. Wei, Eds. Washington DC: American Chemical Society, 2003, pp. 126-139.

[109] IUPAC, *IUPAC. Compendium of Chemical Terminology*, 2nd Edition ed. (1). Oxford: Blackwell Scientific Publications, 1997.

[110] S.-W. Kang, S.-H. Jin, L.-C. Chien, and S. Sprunt, "Spatial and Orientational Templating of Semiconducting Polymers in a Cholesteric Liquid Crystal," *Adv. Funct. Mater.*, vol. 14, pp. 329-334, 2004.

[111] M. H. Huang, A. Choudrey, and P. Yang, "Ag nanowire formation within mesoporous silica," *Chemical Communications*, 10.1039/B002549F no. 12, pp. 1063-1064, 2000.

[112] F. Kleitz, S. H. Choi, and R. Ryoo, "Cubic Ia3d Large Mesoporous Silica: Synthesis and Replication to Platinum Nanowires, Carbon Nanorods and Carbon Nanotubes," *Chem. Commun.* , vol. 2003, pp. 2136-2137, 2003.

[113] J. Y. Kim, S. B. Yoon, F. Kooli, and J.-S. Yu, "Synthesis of Highy Ordered Mesoporous Polymer Networks," *J. Mater. Chem.* , vol. 11, pp. 2912-2914, 2001.

[114] W. Li and D. Zhao, "An Overview of the Synthesis of Ordered Mesoporous Materials," *Chem. Commun.*, vol. 49, pp. 943-946, 2013.

[115] Y. Ren, Z. Ma, and P. G. Bruce, "Ordered mesoporous metal oxides: synthesis and applications," *Chem. Soc. Rev.*, vol. 41, pp. 4909-4927, 2012.

[116] S. A. Johnson, P. A. Ollivier, and T. E. Mallouk, "Ordered Mesoporous Polymers of Tunable Pore Size from Colloidal Silica Templates," *Science*, vol. 283, pp. 963-965, 1999.

[117] C.-G. Wu and T. Bein, "Conducting Polyaniline Filaments in a Mesoporous Channel Host," *Science*, vol. 264, pp. 1757-1759, 1994.

[118] S. T. Hyde, "Identification of Lyotropic Liquid Crystalline Mesophases," in *Handbook of Applied Surface and Colloid Chemistry*, K. Holmberg, Ed. 1st ed. Chichester, UK: John Wiley & Sons, Ltd, 2001, pp. 299-327.

[119] P. S. Pershan, "Lyotropic Liquid Crystals," *Physics Today*, vol. 34, pp. 34-39, 1982.

[120] J. W. Goodby and G. W. Gray, "Guide to the Noclamenture and Classification of Liquid Crystals," in *Handbook of Liquid Crystals*, vol. 1. Fundamentals D. Demus, J. Goodby, G. W. Gray, H.-W. Spiess, and V. Vill, Eds. Weinheim: Wiley-VCH Verlag GmbH, 1998, pp. 17-23.

[121] L. M. Blinov, "Liquid Crystal Phases," in *Structure and Properties of Liquid Crystals*, vol. 1, L. M. Blinov, Ed. First ed. Dordrecht: Springer, 2011, pp. 41-73.

[122] T. Kaasgaard and C. J. Drummond, "Ordered 2-D and 3-D Nanostructured Amphiphile Self-Assembly Materials Stable in Excess Solvent," *Phys. Chem. Chem. Phys.* , vol. 8, pp. 4957-4975, 2006.

[123] R. E. Raimondi and J. M. Seddon, "Liquid Crystal Templating of Porous Materials," *J. Liquid Crystals*, vol. 26, pp. 305-339, 1999.

[124] J. F. Hulvat and S. I. Stupp, "Anisotropic Properties of Conducting Polymers Prepared by Liquid Crystal Templating," *Adv. Mater*, vol. 16, pp. 589-592, 2004.

[125] F. Bender, T. C. Chilcott, H. G. L. Coster, D. B. Hibbert, and J. J. Gooding, "Characterisation of Mesoporous Polymer Films Deposited Using Lyotropic Liquid Crystal Templating," *Electrochim. Acta*, vol. 52, pp. 2640-2648, 2006.

[126] H. Kunieda, G. Umizu, and Y. Yamaguchi, "Mixing Effect of Polyoxyethylene-Type Nonionic Surfactants on the Liquid Crystalline Structures " *J. Coll. Inter. Sci.*, vol. 218, pp. 88-96, 1999.

[127] C. T. Kresge, M. E. Leonowicz, W. J. Roth, J. C. Vartuli, and J. S. Beck, "Ordered Mesoporous Molecular Sieve by a Liquid Crystal Templating Method," *Nature*, vol. 359, pp. 710-712, 1992.

[128] J. F. Hulvat and S. I. Stupp, "Liquid-Crystal Templating of Conducting Polymers," *Angew. Chem. Int. Ed.,* vol. 42, pp. 778-781, 2003.

[129] J. Jang and J. Bae, "Fabrication of Mesoporous Polymer Using Soft Template Method," *Chem. Commun.,* vol. 2005, pp. 1200-1202, 2005.

[130] A. J. Zarur and J. Y. Ying, "Reverse microemulsion synthesis of nanostructured complex oxides for catalytic combustion," *Nature,* 10.1038/47450 vol. 403, no. 6765, pp. 65-67, 01/06/print 2000.

[131] A. D. Roberts, X. Li, and H. Zhang, "Porous carbon spheres and monoliths: morphology control, pore size tuning and their applications as Li-ion battery anode materials," *Chemical Society Reviews,* 10.1039/C4CS00071D vol. 43, no. 13, pp. 4341-4356, 2014.

[132] D. J. Mitchell, G. J. T. Tiddy, L. Waring, T. Bostock, and M. P. McDonald, "Phase Behaviour of Polyoxyethylene Surfactants with Water," *J. Chem Soc., Faraday Trans. 1,*, vol. 79, pp. 975-1000, 1983.

[133] P. K. Dey, "An integrated assessment model for cross-country pipelines," *Environ. Assess. Rev,* vol. 22, pp. 703-721, 2002.

[134] Y. Zhang, A. A. Broekhuis, and F. Picchioni, "Thermally Self-Healing Polymeric Materials: The Next Step to Recycling Thermoset Polymers?," *Macromolecules,* vol. 42, pp. 1906-1912, 2009.

[135] S. K. Ghosh, *Functional Coatings by Polymer Microencapsulation*. Germany: Wiley-VCH Verlg, 2006.

[136] S. R. White *et al.,* "Autonomic healing of polymer composites," *Nature,* vol. 409, pp. 794-797, 2001.

[137] S. T. Nguyen, R. H. Grubbs, and J. W. Ziller, "Syntheses and activities of new single-component, ruthenium-based olefin metathesis catalysts," *Journal of the American Chemical Society,* vol. 115, no. 21, pp. 9858-9859, 1993/10/01 1993.

[138] S. H. Cho, H. M. Andersson, S. R. White, N. R. Sottos, and P. V. Braun, "Polydimethylsiloxane-Based Self-Healing Materials," *Adv. Mater,* vol. 18, pp. 997-1000, 2006.

[139] Z. Ma *et al.,* "Dual-Responsive Capsules with tunable Low Critical Solution Temperatures and Their Loading and Release Behaviour," *Langmuir,* vol. 29, pp. 5631-5637, 2013.

[140] Q. Liu, B. Yu, W. Ye, and F. Zhou, "Highly selective uptake and release of charged molecules by pH-responsive polydopamine microcapsules," *Macromol. Biosci.,* vol. 11, no. 1227-1234, 2011.

[141] H. Xu, X. Liu, and D. Wang, "Interfacial basicity-guided formation of polydopamine hollow capsules in pristine o/w emulsions - Toward understanding of emulsion template roles," *Chem. Mater.,* vol. 23, pp. 5105-5110, 2011.

[142] S. N. Shmakov, S. A. Dergunov, and E. Pinkhassik, "Ship-in-a-bottle Entrapment of Molecules in Porous Nanocapsules," *Chem. Commun.* , vol. 47, pp. 8223-8225, 2011.

[143] J. D. Rule, N. R. Sottos, and S. R. White, "Effect of Microcapsule Size on the Performance of Self-healing Polymers," *Polymer,* vol. 48, pp. 3520-3529, 2007.

[144] S. Mookhoek, "Novel routes to liquid-based self-healing polymer systems " PhD, Aerospace Engineering (Novel Aerospace Materials), Delft university of Technology, Delft, 2010.

[145] A. Kowalczuk, R. Trzcinska, B. Trzebicka, A. H. E. Muller, A. Dworak, and C. B. Tsvetanov, "Loading of Polymer Nanocarriers: Factors, Mechanisms and Applications," *Prog. Poly. Sci.*, vol. 39, pp. 43-86, 2014.

[146] M. Kohri *et al.*, "A Colourless Functional Polydopamine Thin Layer as a Basis for Polymer Capsules," *Polym. Chem.*, vol. 4, pp. 2696-2702, 2013.

[147] J. Cui *et al.*, "Immobilizatin and Intracellular Delivery of an Anticancer Drug using Mussel-Inspired Polydopamine Capsules," *Biomacromolecules,* vol. 13, pp. 2225-2228, 2012.

[148] B. Hilloulin, K. V. Tittelboom, E. Gruyaert, N. D. Belie, and A. Loukili, "Design of Polymeric Capsules for Self-healing Concrete," *Cement and Concrete Composites* vol. 55, pp. 298-307, 2015.

[149] J. P. Harmon and R. Bass, "Self-healing polycarbonate containing polyurethane nanotube composite," US Patent 8,846,801, 2010.

[150] D. J. Boday, J. Kuczynski, and J. T. Wertz, "Self-healing Material with Orthogonally Functional Capsules," US Patent 8,829,082, 2014.

[151] L. Guadagno *et al.*, "Process for preparing a self-healing composite material," US Patent 8,273,806, 2012.

[152] S. Sarangapani, A. Kumar, C. Thies, and L. D. Stephenson, "Self-healing coating and microcapsules to make same," US Patent 7,192,993, 2007.

[153] K. M. Harris and M. Rajagopalan, "Golf ball compositions with microencapsulated healing agent," US Patent 6,808,461, 2004.

[154] D. A. Hurley and D. R. Huston, "Coordinated Sensing and Active Repair for Self-Healing," *Smart Mater. Struct.* , vol. 20, no. 025010, pp. 1-7, 2011.

[155] K. A. Williams, A. J. Boydston, and C. W. Bielawski, "Towards electrically conductive, self-healing materials," *J. R. Soc. Interface,* vol. 22, pp. 359-362, 2006.

[156] J. A. Carlson, J. M. English, and D. J. Coe, "A flexible, self-healing sensor skin " *Smart Mater. Struc.* , vol. 15, p. N129, 2006.

[157] A. Amirudin and D. Thierry, "Application of Electrochemical Impedance Spectroscopy to Study the Degradation of Polymer-Coated Metals," *Prog. Org. Coat,* vol. 26, pp. 1-28, 1995.

[158] D. Loveday, P. Peterson, and B. Rodgers, "Evaluation Of Organic Coatings with Electrochemical Impedance Spectroscopy. Part 2: Application of EIS to Coatings," *J. Coat. Tech.,* vol. October 2004, pp. 88-93, 2004.

[159] H. P. Gavin, "The Levenberg-Marquardt Method for Nonlinear Least Squares Curve-Fitting Problems," Department of Civial and Environmental Engineering North Carolina2013.

[160] J. Pujol, "The Solution of Nonlinear Inverse Problems and the Levenberg-Marquardt Method," *Geophysics,* vol. 72, pp. W1-W15, 2007.

[161] P. R. Gill, W. Murray, and M. H. Wright, "The Levenberg-Marquardt Method," in *Practical Optimisation*First ed. London: Academic Press, 1981, pp. 136-137.

[162] M. S. A. L. W. F. H. S. H. Gehmecker; and K.-H. GroDe-Brinkhaus, "The scanning Kelvin probe; a new technique for the in situanalysis of the delamination of organic coatings," *Prog. Org. Coat,* vol. 27, pp. 261-267, 1996.

[163] A. Wiek and R. Holze, "Scanning Probe Methods," in *Encyclopedia of Applied Electrochemistry*, G. Kreysa, K.-i. Ota, and R. F. Savinell, Eds. New York, NY: Springer New York, 2014, pp. 1836-1851.

[164] A. K. Neufeld, I. S. Cole, A. M. Bond, and S. A. Furman, "The initiation mechanism of corrosion of zinc by sodium chloride particle deposition," *Corrosion Science,* vol. 44, no. 3, pp. 555-572, 2002/03/01/ 2002.

[165] A. L. H. S. M. Stratmann, "The delamination of polymeric coatings from steel [Part 1]: Calibration of the Kelvin probe and basic delamination mechanism," *Corros. Sci.,* vol. 41, pp. 547-578, 1999.

[166] A. L. H. S. M. Stratmann, "The delamination of polymeric coatings from steel [Part 2]: First stage of delamination, effect of type and concentration of cations on delamination, chemical analysis of the interface," *Corros. Sci.,* vol. 41, pp. 579-597, 1999.

[167] A. G. N. J. L. H. N. M. G. W. a. A. Cooka, "Inhibition by Polyaniline of Corrosion-Driven Coating Delamination on Carbon Steel: Aspects Regarding the Role of the Counter-anion," *ECS Transactions,* vol. 1, pp. 37-46, 2006.

[168] G. W. H. N. M. M. J. Loveridge, "Inhibition of corrosion-driven organic coating disbondment on galvanised steelby smart release group II and Zn(II)-exchanged bentonite pigments," *Electrochim. Acta,* vol. 55, pp. 1740-1748, 2010.

[169] G. W. H. N. McMurray, "Polyaniline inhibition of filiform corrosion on organic coated AA2024-T3," *Electrochim. Acta,* vol. 54, pp. 4245-4252, **2009**.

[170] A. C. A. G. D. S. N. Laycock, "Corrosion protection of low carbon steel with polyaniline: passivation or inhibition?," *Current Appl. Phys.*, vol. 4, pp. 133-136, 2004.

[171] M. R. L. M. D. A. Michalik, "In situ investigation of corrosion localised at the buried interface between metal and conducting polymer based composite coatings," *Electrochim. Acta*, vol. 54, pp. 6075-6081, 2009.

[172] A. M. M. U. a. M. Rohwerder, "The Protection Zone: A Long-Range Corrosion Protection Mechanism around Conducting Polymer Particles in Composite Coatings: Part I. Polyaniline and Polypyrrole," *J. Electrochem. Soc.*, vol. 166, pp. C304-C313, 2019.

[173] G. P.-P. M. S. M. Rohwerder and K. P.-K. Y. L. A. Z. P. H.-J. Adl, "On the development of polypyrrole coatings with self-healing properties for iron corrosion protection," *Corros. Sci.*, vol. 47, pp. 3216-3233, 2005.

[174] Y. L. A. V. X. W. M. Rohwerder, "Study of the buried interface between zinc and emeraldine base coating," *Electrochim. Acta*, vol. 161, pp. 10-16, 2015.

[175] G. Beamson and D. Briggs, *High resolution XPS of Organic Polymers*. Chichester UK: Wiley, 1992.

[176] J. Balla, T. Kiss, and R. F. Jameson, "Copper(II)-catalyzed oxidation of catechol by molecular oxygen in aqueous solution," *Inorg. Chem.* , vol. 31, pp. 58-62, 1992.

[177] V. Ball *et al.*, "Comparison of Synthetic Dopmine-Eumelanin Formed in the Presence of Oxygen and Cu^{2+} Cations as Oxidants," *Langmuir*, vol. 29, pp. 12754-12761, 2013.

[178] S. Arzola, M. E. Palomar-Pardave, and J. Genesca, "Effect of Resistivity on the Corrosion mechanism of Mild steel in Sodium Sulfate Solutions," *J. Appl. Electrochem.*, vol. 33, pp. 1233-1237, 2003.

[179] SigmaAldrich, "Copper (II) acetate MSDS," SigmaAldrich, Gillingham, Dorset28/11/2014 2014.

[180] K. R. Trethewey and J. Chamberlain, "15.1 Plain Carbon and Low Alloy Steels," in *Corrosion for Science and Engineering*2nd ed. Harlow, Essex: Longman Scientific & Technical, 1995, pp. 338-341.

[181] A. M. S. E. Din and L. Wang, "Mechanism of corrosion inhibition by sodium molybdate " *Desalination*, vol. 107, pp. 29-43, 1996.

[182] Y. Yao, Y. Zhou, and L. He, "Corrosion behavior of molybdate conversion coatings on AZ31 magnesium alloy in NaCl solution," *Anti-Corrosion Methods and Materials*, vol. 60, pp. 307-311, 2013.

[183] G. B. Reed, "The Measurement of Oxidation Potential and Its Significance in the Study of Oxidases," *Botanical Gazette*, vol. 61, p. 523.527, 1916.

[184] A. R. Katrizky, D. Fedoseyenko, P. P. Mohapatra, and P. J. Steel, "Reactions of p-Benzoquinone with S-Nucleophiles " *Synthesis*, vol. 5, pp. 777-786, 2008.

[185] *Electrochemical Impedance: Analysis and Interpretation* 1993.

[186] J. Kittel, N. Celati, M. Keddam, and H. Takenouti, "New Methods for the Study of Organic Coatings by EIS: New Insights into Attached and Free Films," *Prog. Org. Coat,* vol. 41, pp. 93-98, 2001.

[187] M. Ates, "Review study of electrochemical impedance spectroscopy and equivalent electrical circuits of conducting polymers on carbon surfaces," *Prog. Org. Coat,* vol. 71, pp. 1-10, 2011.

[188] J. M. McIntyre and H. Q. Pham, "Electrochemical Impednace spectroscopy; a Tool for Organic Coatings Optimization," *Prog. Org. Coat,* vol. 27, pp. 201-207, 1996.

[189] G. Bouvet, D. D. Nguyen, S. Mallarino, and S. Touzain, "Analysis of the non-ideal capacitive behaviour for high impedance organic coatings," *Prog. Org. Coat,* vol. 77, pp. 2045-2053, 2014.

[190] Y. Chen, X. H. Wang, J. Li, J. L. Lu, and F. S. Wang, "Long-Term Anticorrosion Behaviour of Polyaniline on Mild Steel," *Corros. Sci.,* vol. 49, pp. 3052-3063, 2007.

[191] A. T. Ozyilmaz, M. Erbil, and B. Yazici, "The electrochemical synthesis of polyaniline on stainless steel and its corrosion performance," *Current Appl. Phys. ,* vol. 6, pp. 1-9, 2006.

[192] N. J. W. Reuvers, H. P. Huinink, O. C. G. Adan, S. J. Garcia, and J. M. C. Mol, "Water Uptake in Thin Nylon 6 Films as Measured by Electrochemical Impedance Spectroscopy and Magnetic Resonance Imaging," *Electrochim. Acta,* vol. 94, pp. 219-228, 2013.

[193] U. Rammelt, P. T. Nguyen, and W. Plieth, "Corrosion Protection by Ultrathin Films of Conducting Polymers," *Electrochim. Acta,* vol. 48, pp. 1257-1262, 2003.

[194] A. Omrani, A. Alirostami, and M. Sharifirad, "Synthesize, Characterization, and Corrosion Inhibition of Polypyrrole Thin Films on Copper," *J. Macromol. Sci Part A: Pure Appl. Chem.,* vol. 50, pp. 513-521, 2013.

[195] K. C. Emregul and A. A. Aksut, "The Effect of Sodium Molybdate on the Pitting Corrosion of Aluminium," *Corros. Sci.,* vol. 45, pp. 2415-2433, 2003.

[196] R. Yildiz, "An Electrochemical and Theoretical Evaluation of 4,6-diamino-2-pyrimidinethiol as a Corrosion inhibitor for Mild Steel in HCl Solutions," *Corros. Sci.,* vol. 90, pp. 544-553, 2015.

[197] M. E. Orazem and B. Tribollet, *Electrochemical Impedance Spectroscopy*. Chichester, UK: John Wiley and Sons, 2011.

[198] D. H. Macdonald and M. C. H. McKubre, "4.4.8 Equivalent Circuit Analysis," in *Impedance Spectroscopy Theory, Experiment and Applications*, E. Barsoukov and J. R. Macdonald, Eds. 2nd ed. Hoboken, NJ: John Wiley and Sons, Inc., 2005.

[199] C. Gabrielli, "Use and Application of Electrochemical Impedance Techniques," Solartron Analytical, Farnborough1997.

[200] "Part I - Corrosion of Metals and Alloys," in *Handbook of Corrosion Data*, B. Craig and D. Anderson, Eds. Second ed. Materials park, Ohio: ASM International, 2002.

[201] V. Ball *et al.*, "Comparison of Synthetic Dopamine-Eumelanin Formed in the Presence of Oxygen and Cu^{2+} Cations as Oxidants," *Langmuir*, vol. 29, pp. 12754-12761, 2013.

[202] F. Ponzio *et al.*, "Polydopamine Films From the Forgotten Air/Water Interface," *J. Phys. Chem. Lett.*, vol. 5, pp. 3436-3440, 2014.

[203] F. Ponzio and V. Ball, "Persistenceof dopamine and small oxidation products thereof in oxygenated dopamine solutions and in "polydopamine" films," *Colloids and Surfaces A: Physicochem. Eng. Aspects*, vol. 443, pp. 540-543, 2014.

[204] M. W. Sabaa, T. M. Madkour, and A. A. Yassin, "Polymerization Products of *p*-Benzoquinone as Bound Antioxidants for SBR. Part II - The Antioxidizing Efficiency," *Polym. Deg. & Stab.*, vol. 22, pp. 205-222, 1988.

[205] M. W. Sabaa, T. M. Madkour, and A. A. Yassin, "Polymerisation Products of p-Benzoquinone as Bound Antioxidants for StyreneButadiene Rubber: Part I- Preparation of Quinone Polymers," *Polym. Deg. & Stab.*, vol. 22, pp. 195-203, 1988.

[206] I. S. C. T. H. M. S. A. F. N. W. A. Bradbury, "Products Formed during the Interaction of Seawater Droplets with Zinc Surfaces: I. Results from 1- and 2.5-Day Exposures," *J. Electrochem. Soc.*, vol. 155, 2008.

[207] M. S. V. I. S. C. B. Emmanuel, "Model for corrosion of metals covered with thin electrolyte layers: Pseudo-steady state diffusion of oxygen," *Electrochim. Acta*, vol. 56, pp. 7171-7179, 2011.

[208] I. S. C. D. L. F. C. D. A. Paterson, "Experimental studies of salts reoval from metal surfaces by wind and rain," *Corrosion Engineering,Science and Technology*, vol. 39, pp. 333-338, 2004.

[209] I. S. C. W. D. G. J. D. S. D. L. a. D. A. Paterson, "A Study of the Wetting of Metal Surfaces in Order to Understand the Processes Controlling Atmospheric Corrosion," *J. Electrochem. Soc.*, vol. 151, pp. B627-B635, 2004.

[210] J. S. Clovis and J. Dohling, "Quinones as Corrosion inhibitor in Distilling Alkanoic Acids," United States, 1974.

[211] S. N. Raicheva and E. I. Sokolova, "Influence of Inhibitor Structure and Metal/Solution Interface on the Corrosion Resistance of the Protected Metal," *Russ. J. Electrochem.*, vol. 42, pp. 1213-1223, 2006.

[212] J. Fang, K. Xu, L. Zhu, Z. Zhou, and H. Tang, "A Study on Mechanism of Corrosion Protection of Polyaniline Coating and its Failure," *Corros. Sci.*, vol. 49, pp. 4232-4242, 2007.

[213] E. Slavcheva, E. Sokolova, and S. Raicheva, "Corrosion Inhibition of Mild Steel in Neutral Solutions by Organic Compounds with Quinoid Structures," *Brit. Corros. J.* , vol. 28, pp. 125-129, 1993.

[214] E. Slavcheva, E. Sokolova, and S. Raicheva, "Temperature and Concentration Dependence of the Activity of Quinones of Presumed Inhibiting Action," *J. Electroanal. Chem.,* vol. 360, pp. 271-282, 1993.

[215] J. H. R. P. B. M. H. Lee, "Polydopamine Surface Chemistry: A Decade of Discovery," *ACS Appl. Mater. Interfaces,* vol. 10, pp. 7523-7540, 2018.

[216] F. P. J. B. J. B. M. M. P. H. B. J. Hemmerle, "Oxidant control of polydopamine surface chemistry in acids: a mechanism-based entry to superhydrophilic-superoleophobic coatings," *Chem. Mater.* , vol. 28, pp. 4697-4705, 2016.

[217] X. D. L. L. J. L. C. Y. N. F. A. Welle, "UV-triggered dopamine polymeization: control of polymerization, surface coating, and photoppaterning," *Adv. Mater.* , vol. 26, pp. 8029-8033, 2014.

[218] J. M. Seddon and R. H. Templer, "Cubic Phases of Self-Assembled Amphiphillic Aggregates," *Philos. T. Roy. Soc. A,* vol. 344, pp. 377-401, 1993.

[219] D. M. Anderson, S. M. Gruner, and S. Liebler, "Geometrical Aspects of the Frustration in the Cubic Phases of Lyotropic Liquid Crystals," *Proc. Natl. Acad. Sci. USA,* vol. 85, pp. 5364-5368, 1988.

[220] A. Eftekhari and R. Afshani, "Electrochemical Polymerization of Aniline in Phosphoric Acid," *J. Polym. Sci.: A Polym. Chem.* , vol. 44, pp. 3304-3311, 2006.

[221] A. Mirmohseni and A. Oladegaragoze, "Anti-corrosive Properties of Polyaniline Coatings on Iron," *Synth. Met.,* vol. 114, pp. 105-108, 2000.

[222] J.-L. Camalet, J.-C. Lacroix, S. Aeiyach, K. I. C. Ching, and P.-C. Lacaze, "Electrodeposition of Polyaniline on Mild Steel in a Two Step Process," *Synth. Met.,* vol. 102, pp. 1386-1387, 1999.

[223] D. Sazou and C. Georgolis, "Formation of conducting polyaniline coatings on iron surfaces by electropolymerisation of aniline in aqueous solutions," *J. Electroanal. Chem.,* vol. 429, pp. 81-93, 1997.

[224] J.-L. Camalet, J.-C. Lacroix, S. Aeiyach, K. Chane-Ching, and P.-C. Lacaze, *Synthetic Metals,* vol. 416, p. 179, 1996.

[225] P. P. Deshpande and D. Sazou, "Characterization of Anticorrosion Properties," in *Corrosion Protection of Metals by Intrinsically Conducting Polymers*Boca Raton, Fl: CRC Press, 2016.

[226] P. L. T. C. P. J. Y. Li, "Corrosion Protection of Mild Steel by electoactive Polyaniline Coatings," *Synth. Met.,* vol. 88, 1997.

[227] H. Yasuda, Q. S. Yu, and M. Chen, "Interfacial Factors in Corrosion Protection: an EIS Study of Model Systems," *Prog. Org. Coat*, vol. 41, pp. 273-279, 2001.

[228] Y. Yu, G. Qiao, and J. Ou, "Self-Powered Wireless Corrosion monitoring Sensors and Networks," *IEEE Sensors Journal*, vol. 10, pp. 1901-1902, 2010.

[229] M. J. D. Sloane, R. Betti, G. Marconi, A. L. Hong, and D. Khazem, "Experimental Analysis of a Nondestructive Corrosion Monitoring System for Main Cables of Suspension Bridges," *J. Bridge Eng.*, vol. 18, pp. 653-662, 2013.

[230] S.-G. Dong, C.-J. Lin, R.-G. Hu, L.-Q. Li, and R.-G. Du, "Effective Monitoring of Corrosion in Reinforcing Steel in Concrete Constructions by a Multifunctional Sensor," *Electrochim. Acta*, vol. 56, pp. 1881-1888, 2011.

Bibliography

P. P. Deshpande and D. Sazou, "Characterization of Anticorrosion Properties," in Corrosion Protection of Metals by Intrinsically Conducting PolymersBoca Raton, Fl: CRC Press, 2016.

J. W. Goodby and G. W. Gray, "Guide to the Noclamenture and Classification of Liquid Crystals," in Handbook of Liquid Crystals, vol. 1. Fundamentals D. Demus, J. Goodby, G. W. Gray, H.-W. Spiess, and V. Vill, Eds. Weinheim: Wiley-VCH Verlag GmbH, 1998

Appendix A: Phase diagram microscopy images

A.1 Brij L4

A.1.1 10 wt% surfactant

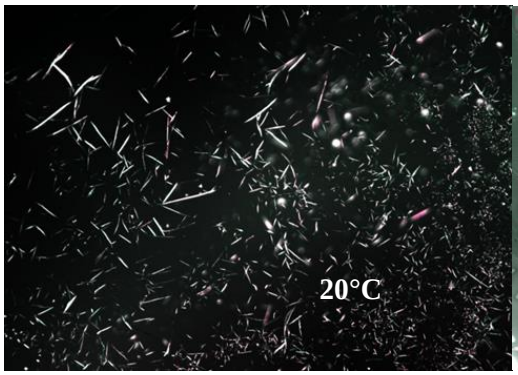

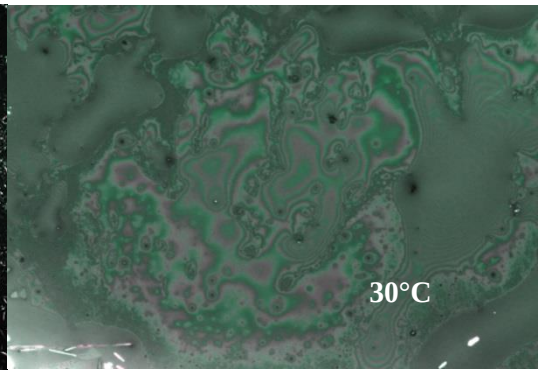

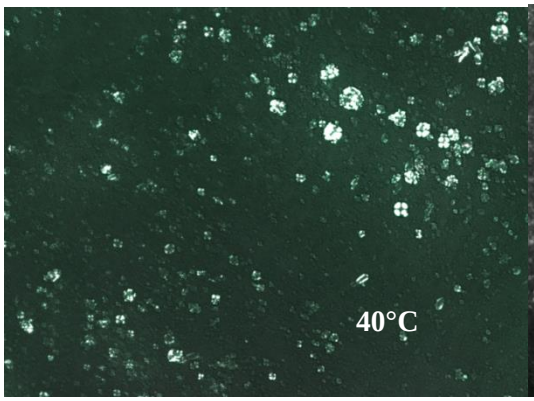

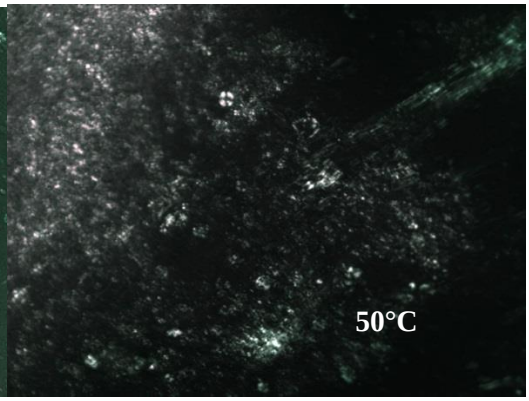

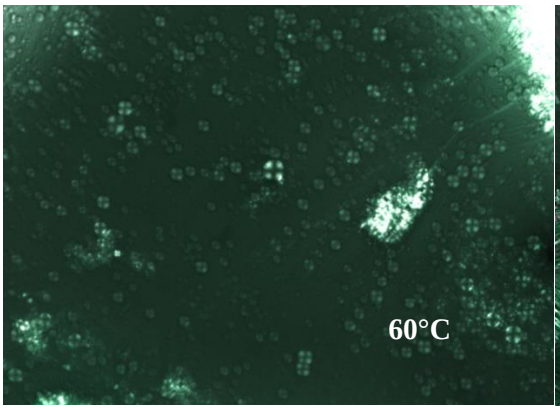

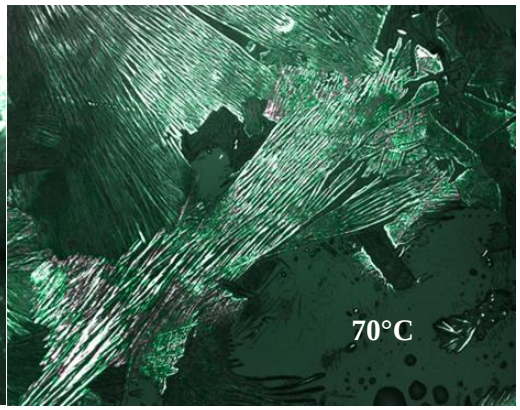

A.1.2 20 wt% surfactant

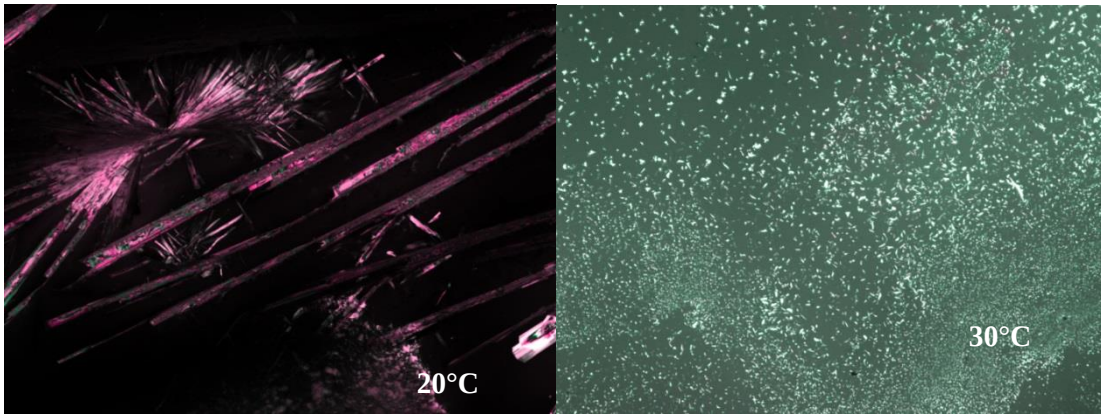

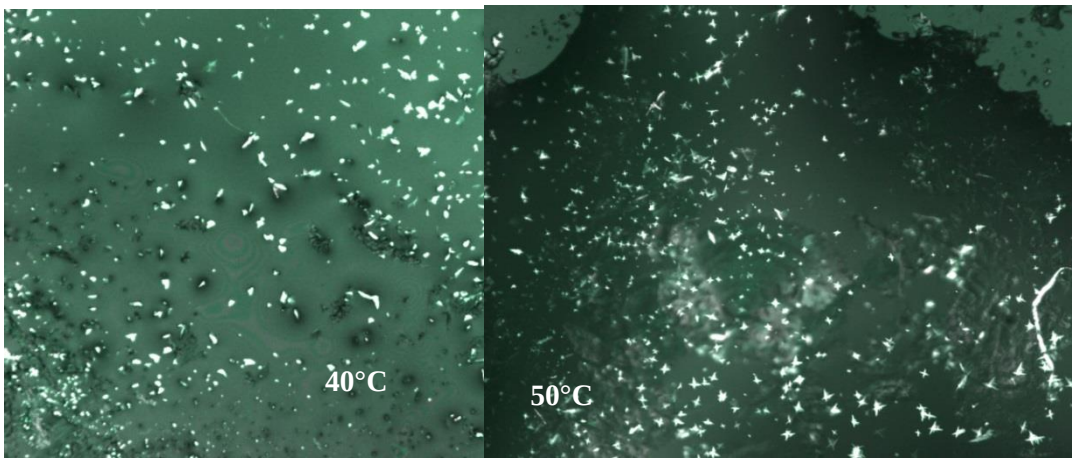

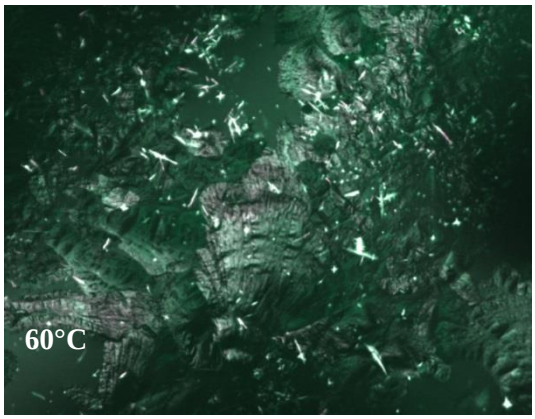

A.1.3 30 wt% surfactant

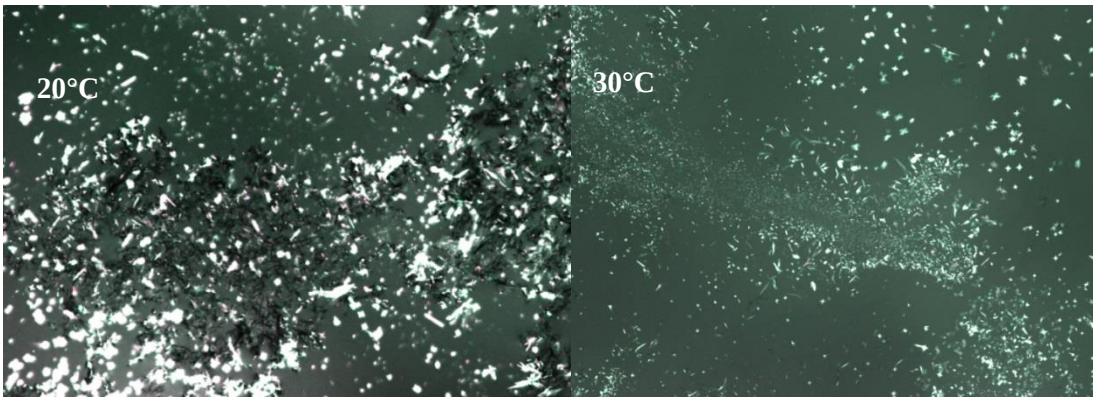

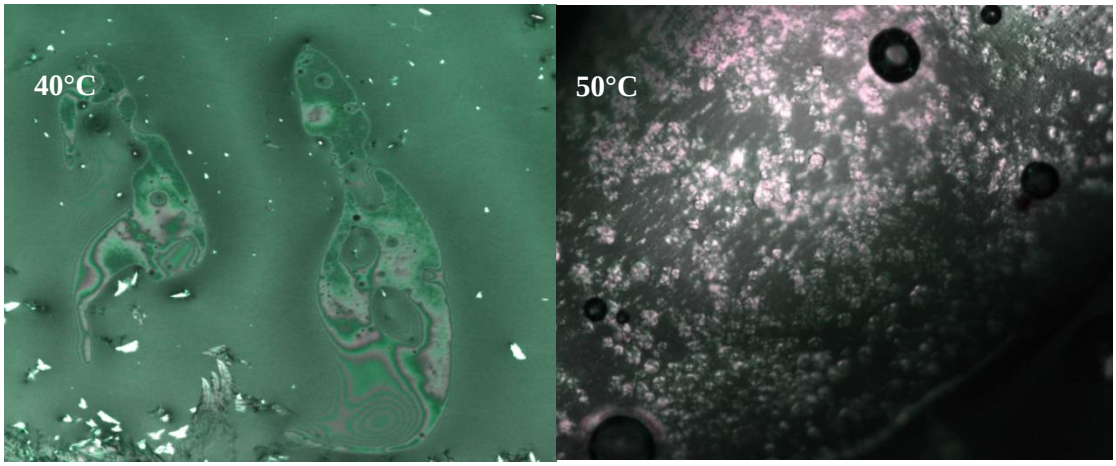

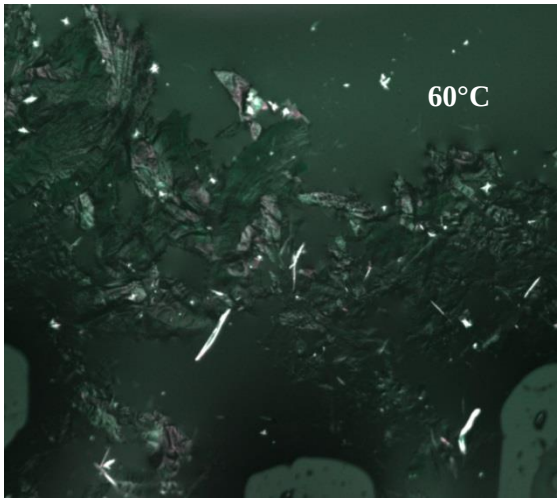

A.1.4 40 wt% surfactant

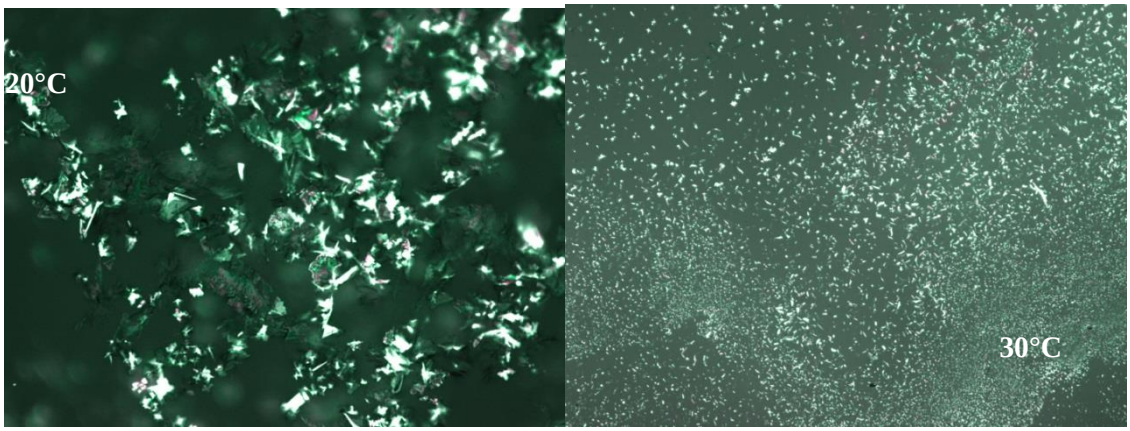

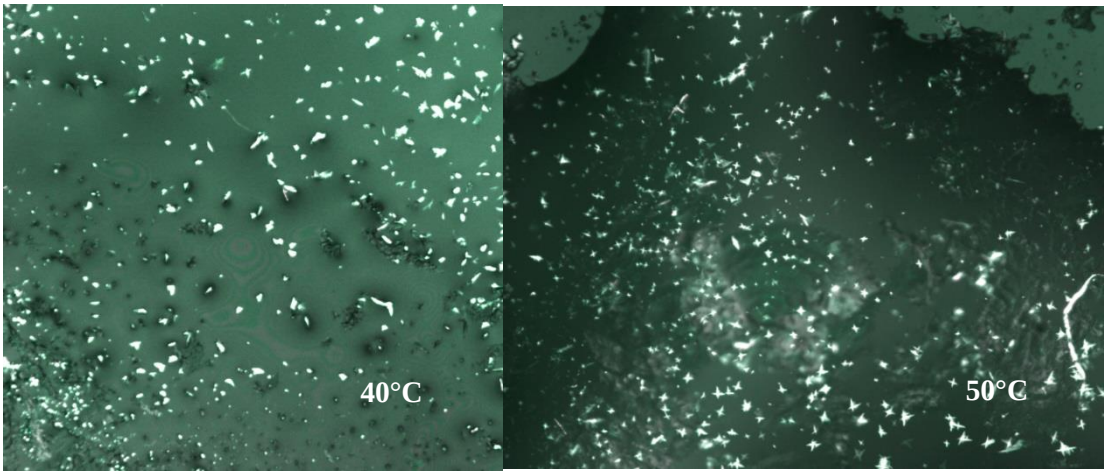

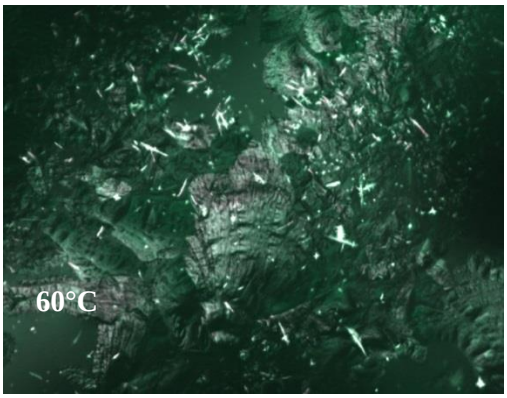

A.1.5 50 wt% surfactant

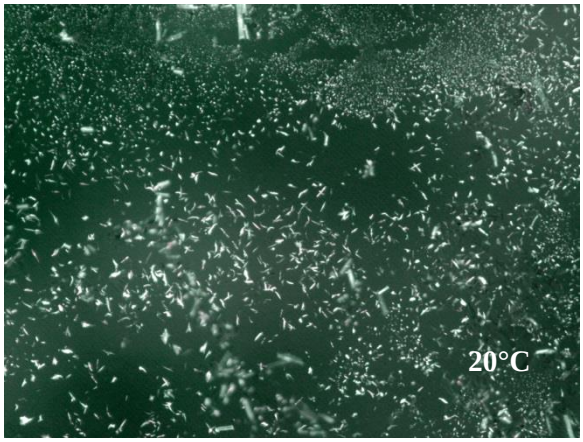

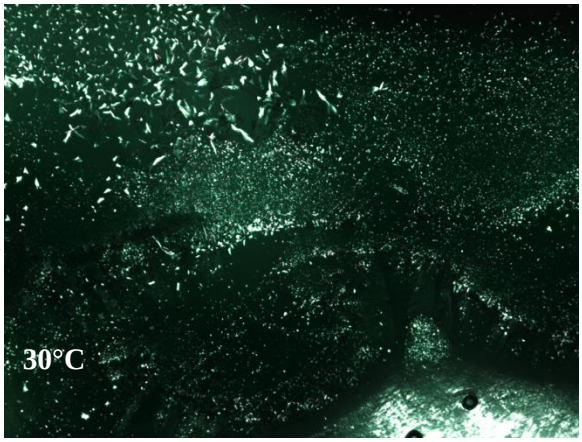

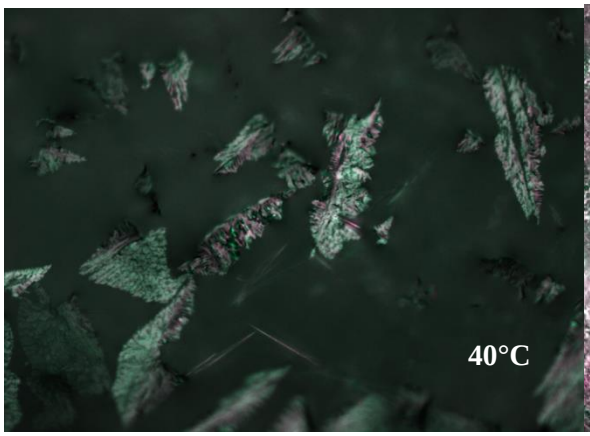

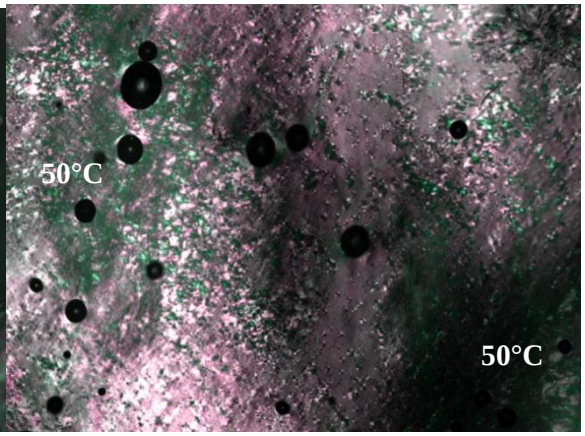

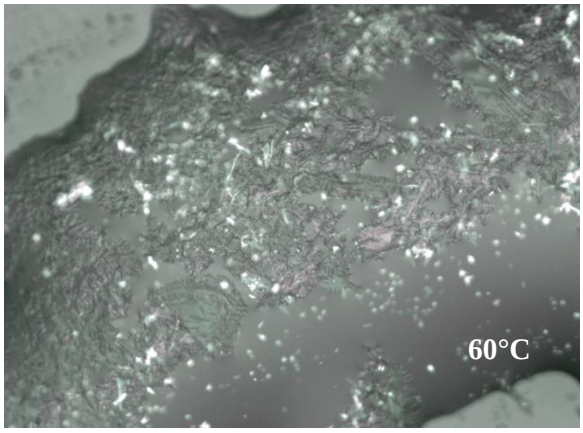

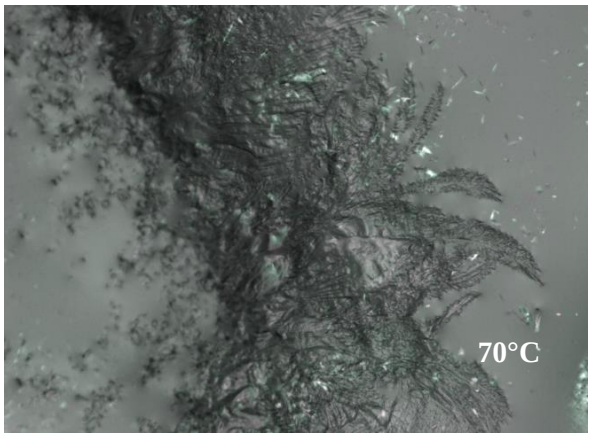

A.1.6 60 wt% surfactant

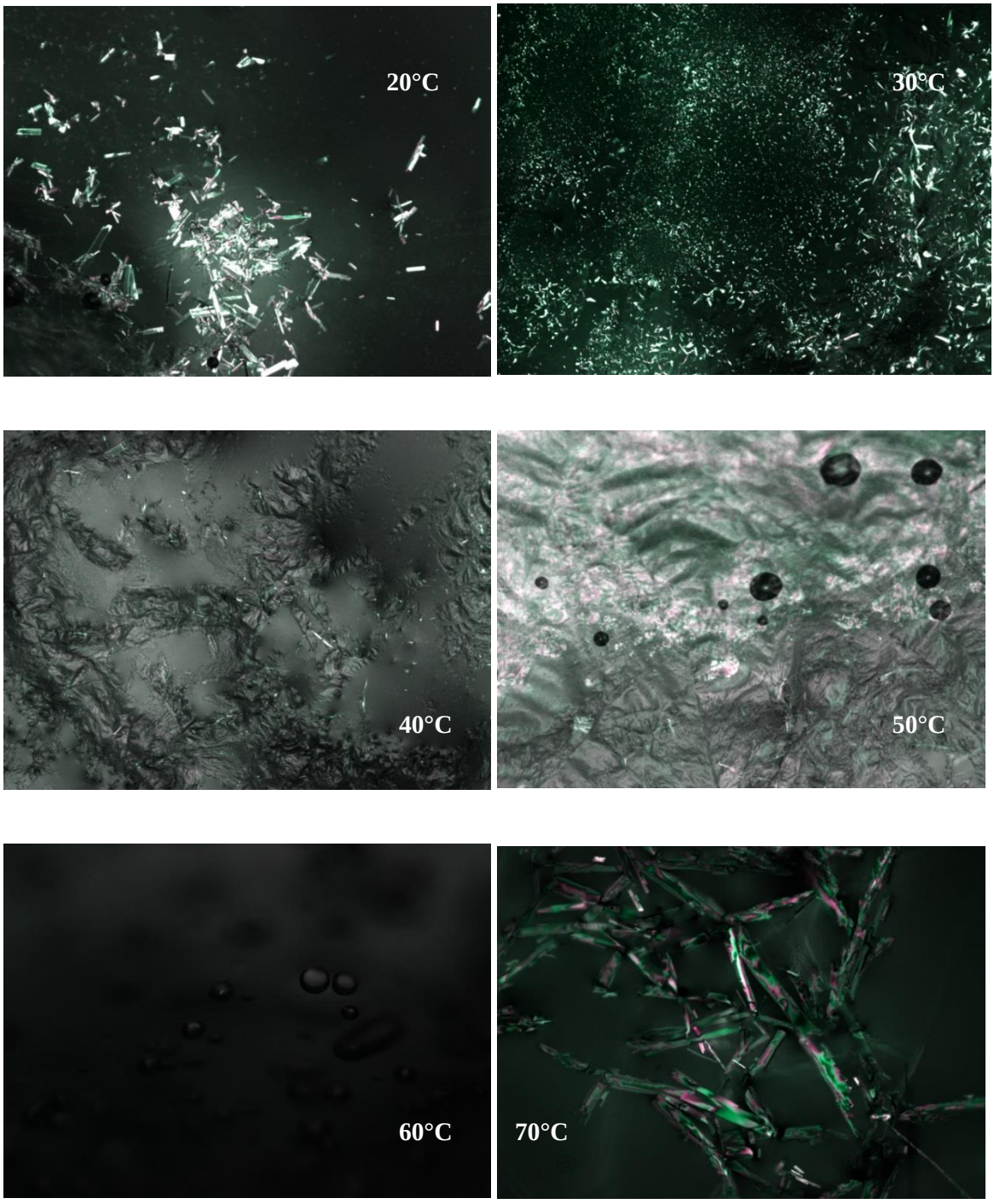

A.1.7 70 wt% surfactant

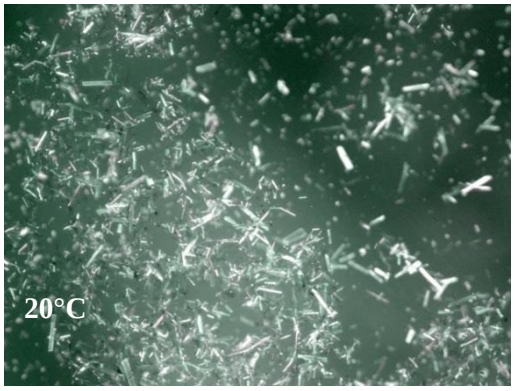

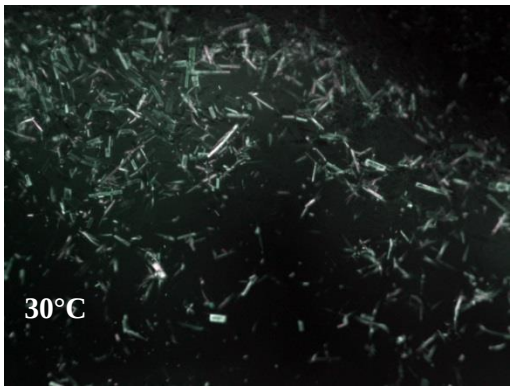

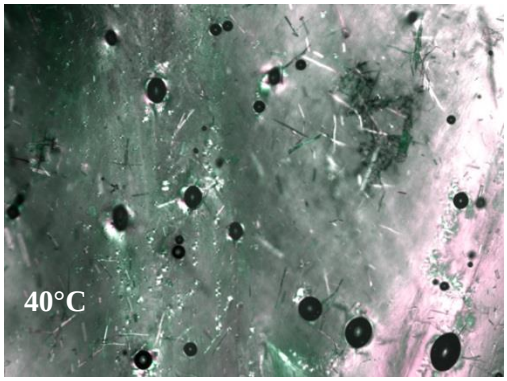

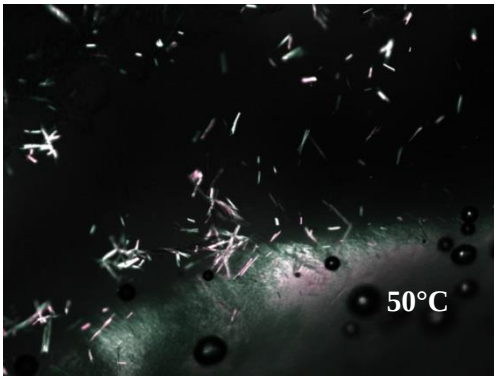

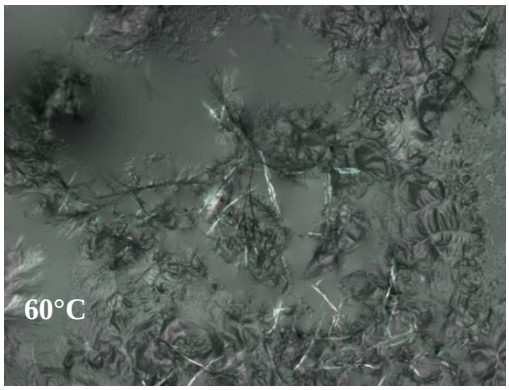

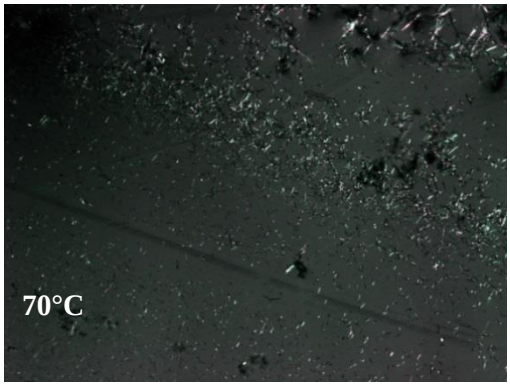

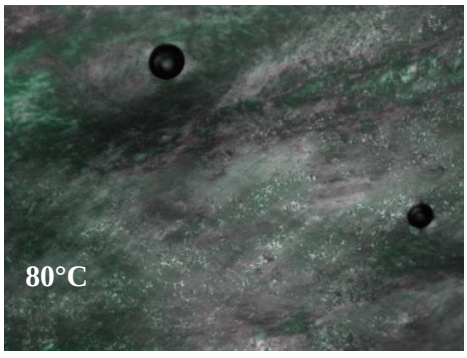

A.1.8 80 wt% surfactant

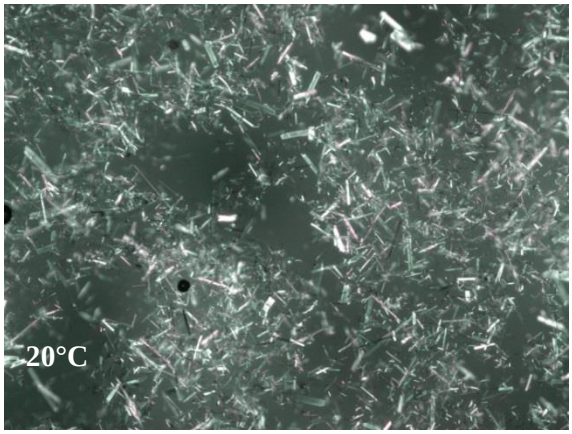

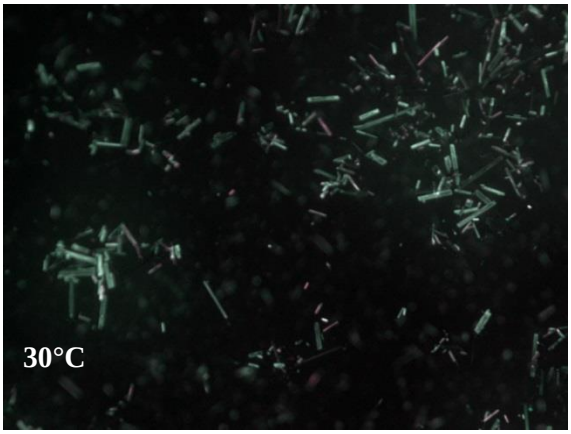

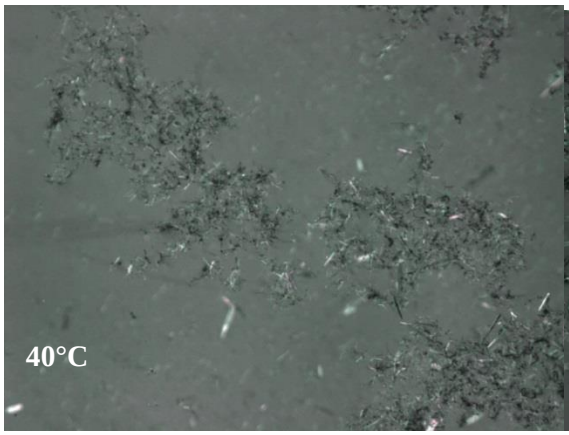

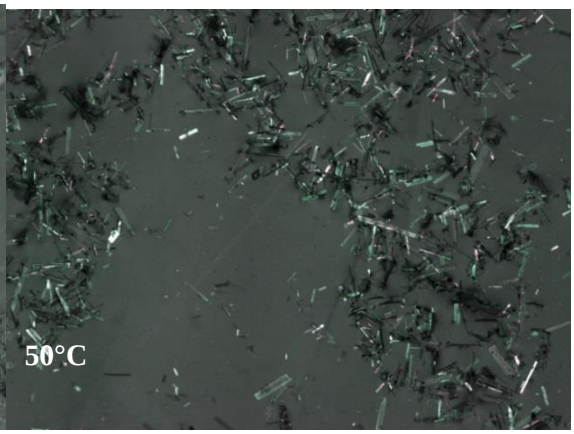

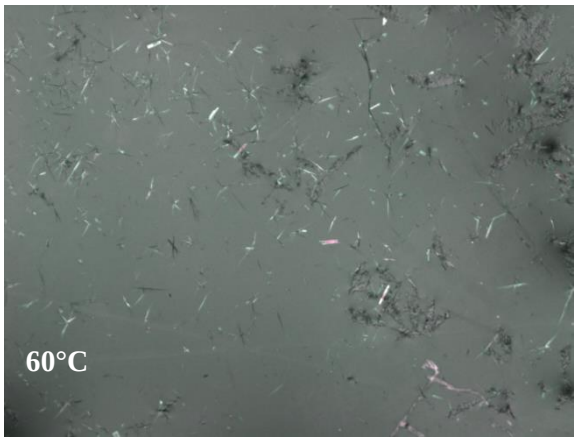

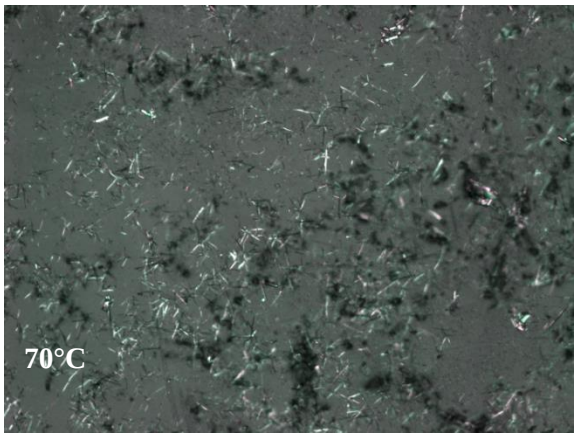

A.1.9 90 wt% surfactant

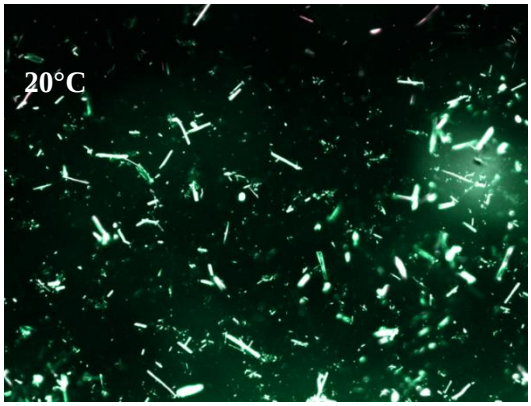

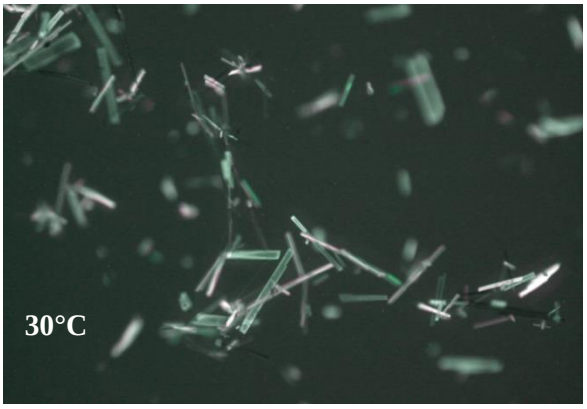

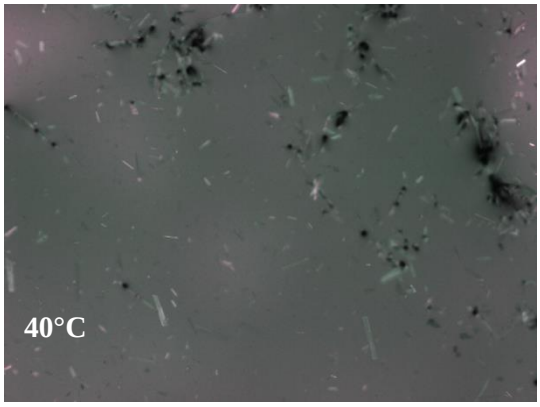

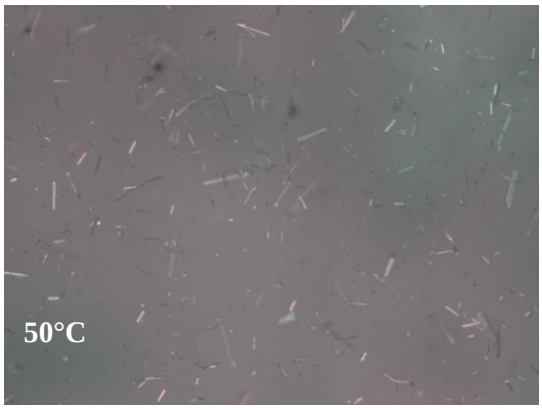

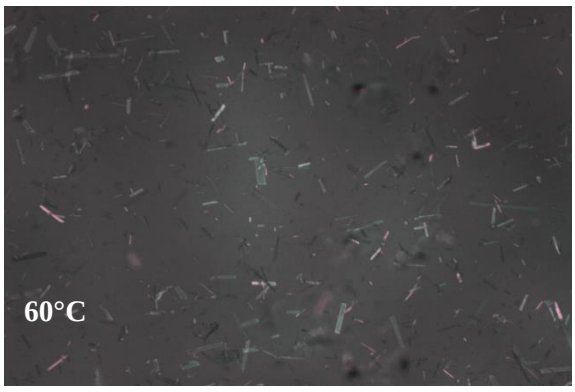

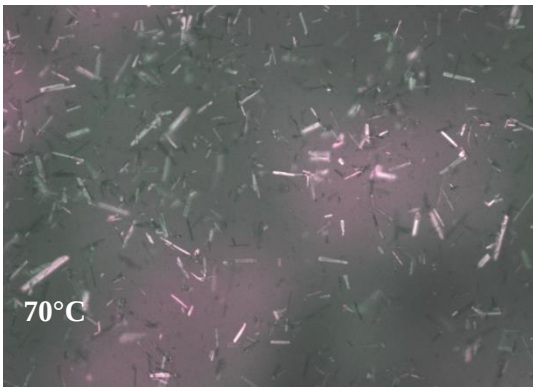

A.2 Brij C10

A.2.1 10 wt% surfactant

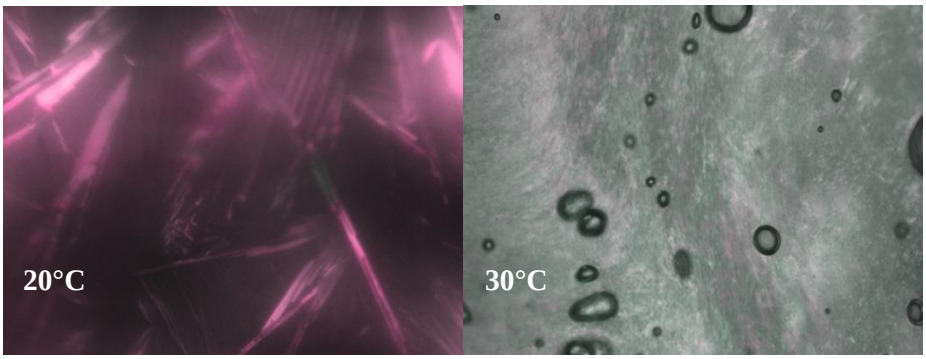

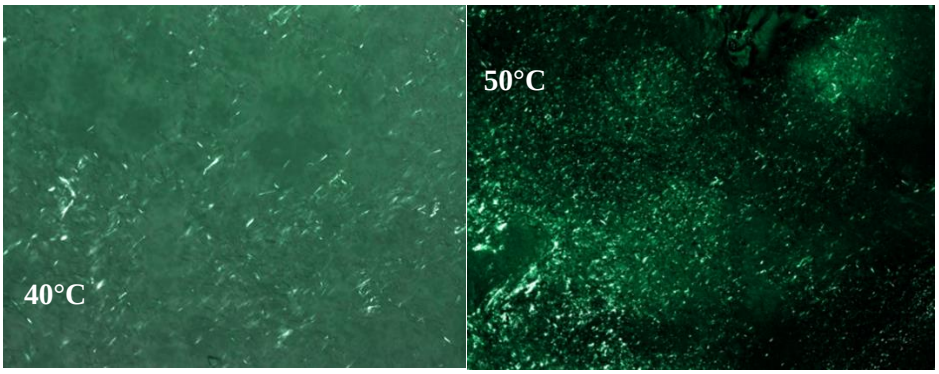

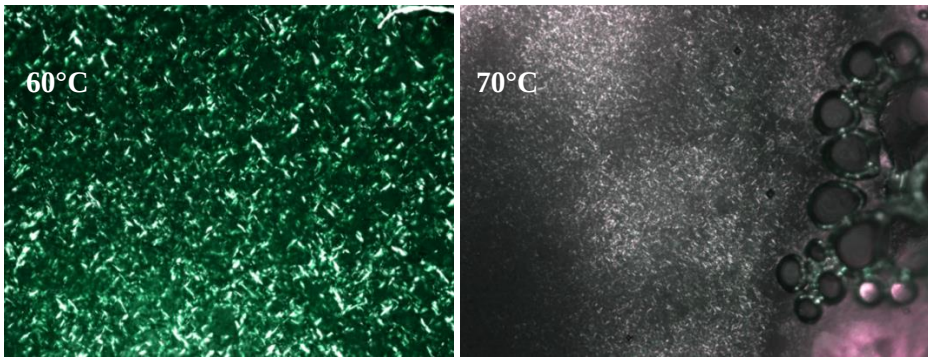

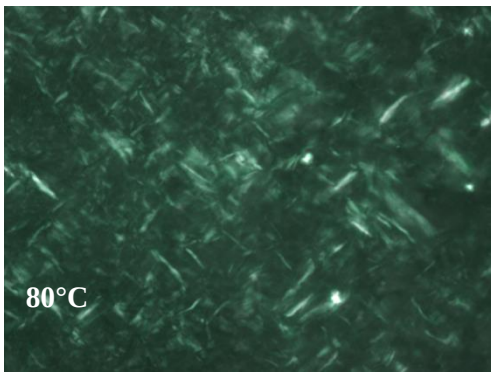

A.2.2 20 wt% surfactant

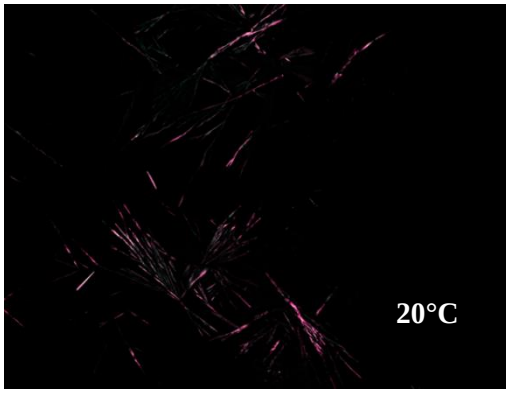

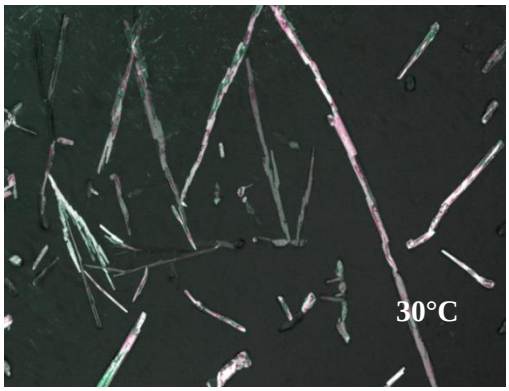

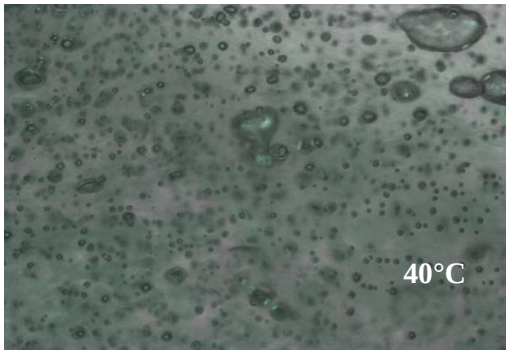

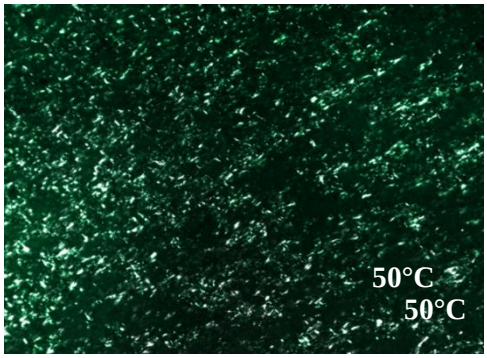

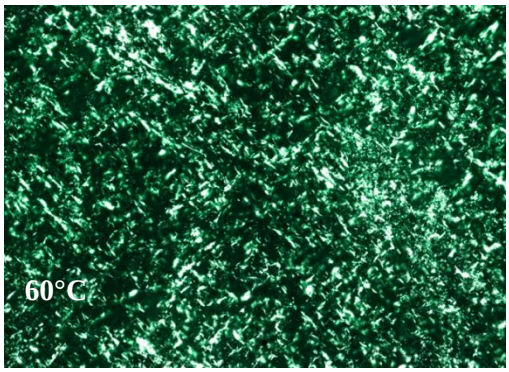

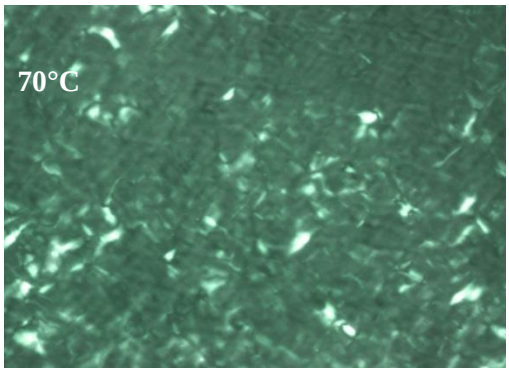

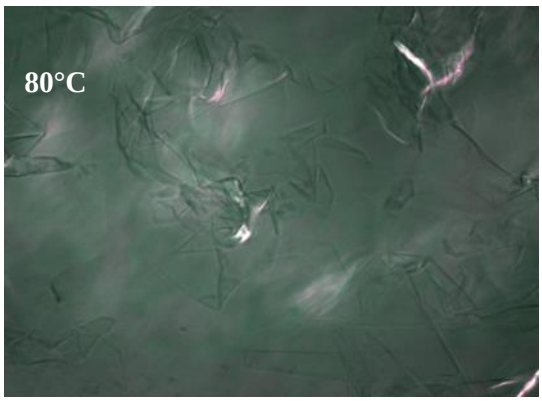

A.2.3 30 wt% surfactant

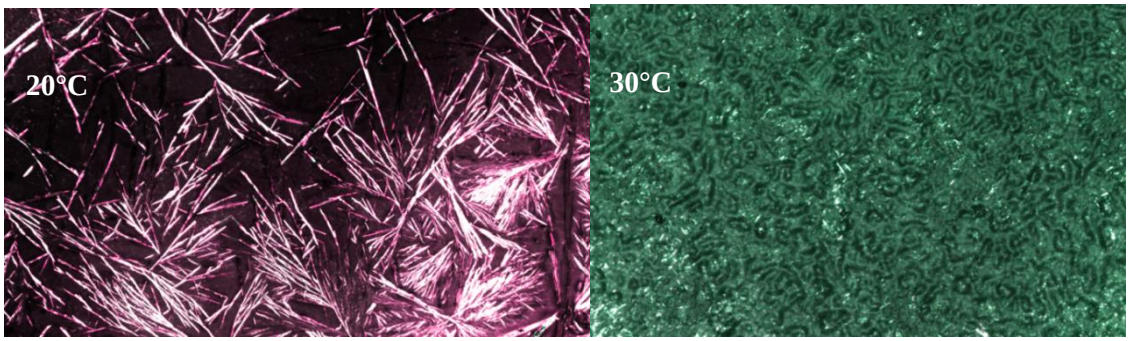

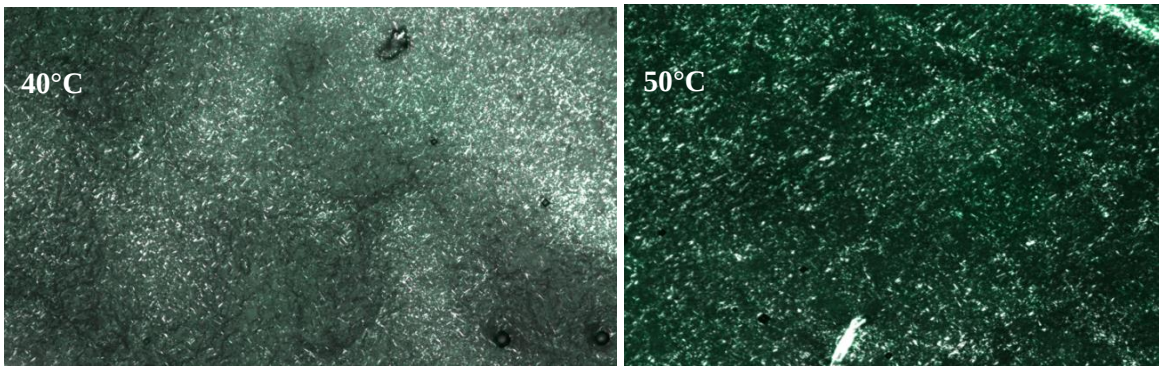

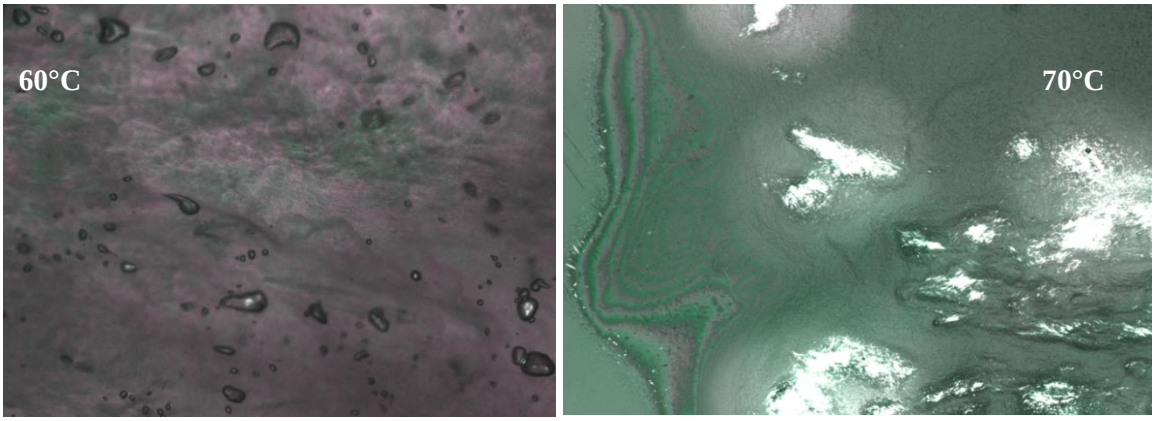

A.2.4 40 wt% surfactant

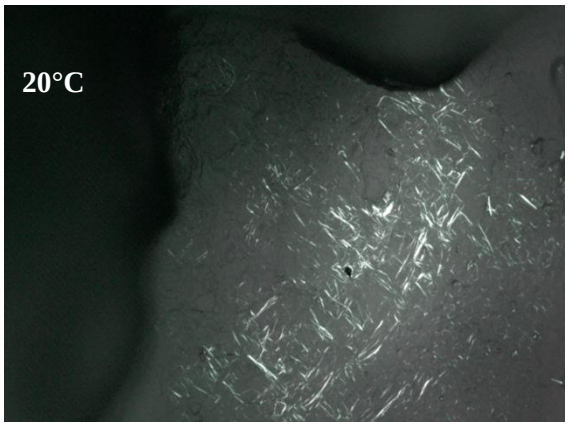

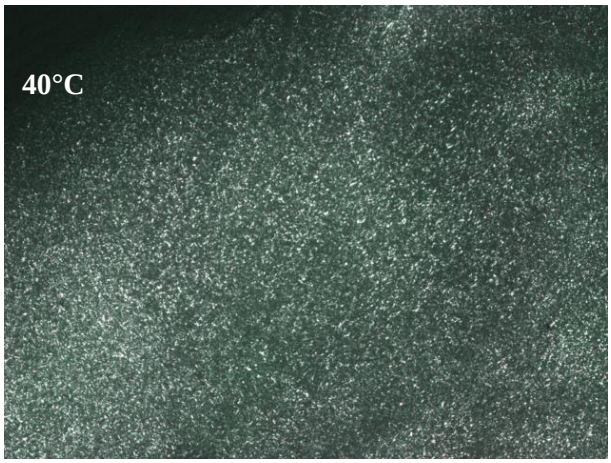

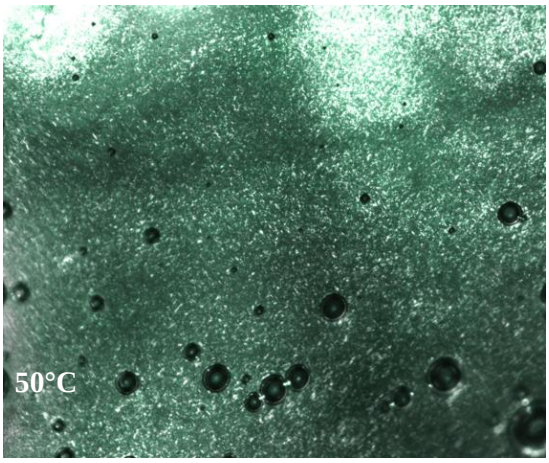

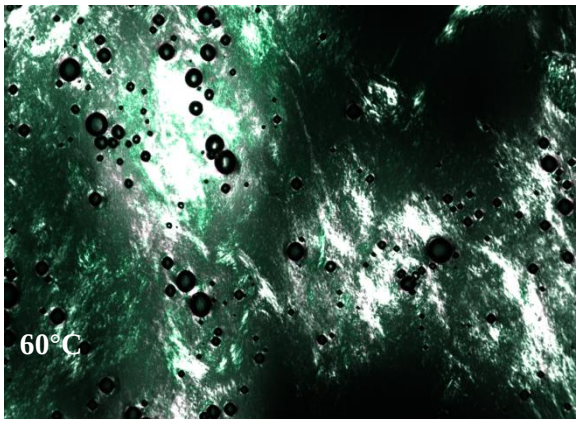

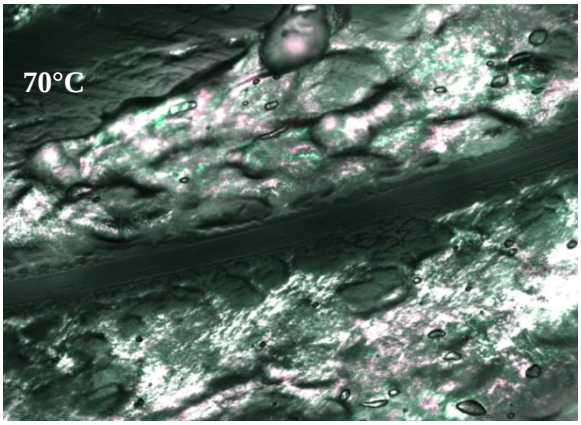

A.2.5 50 wt% surfactant

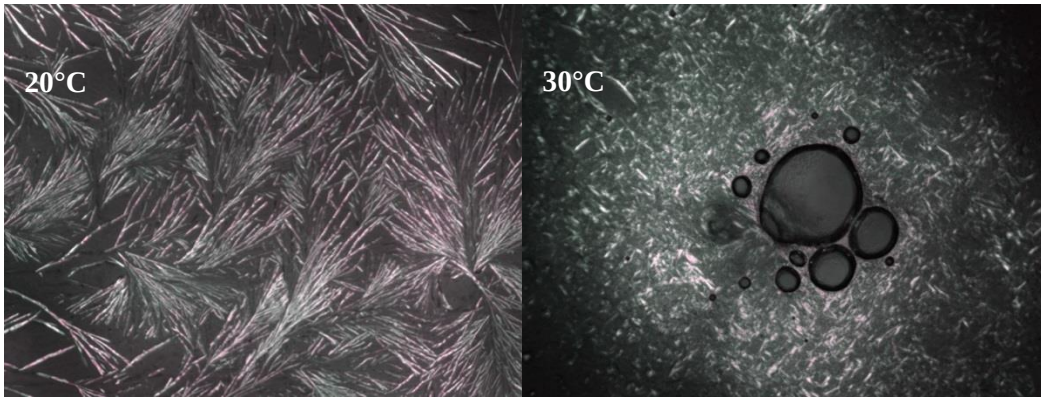

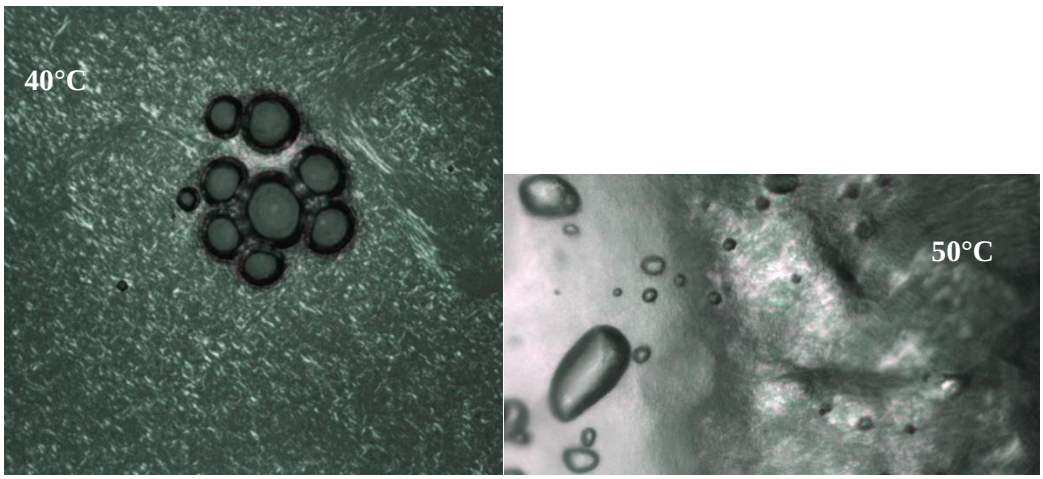

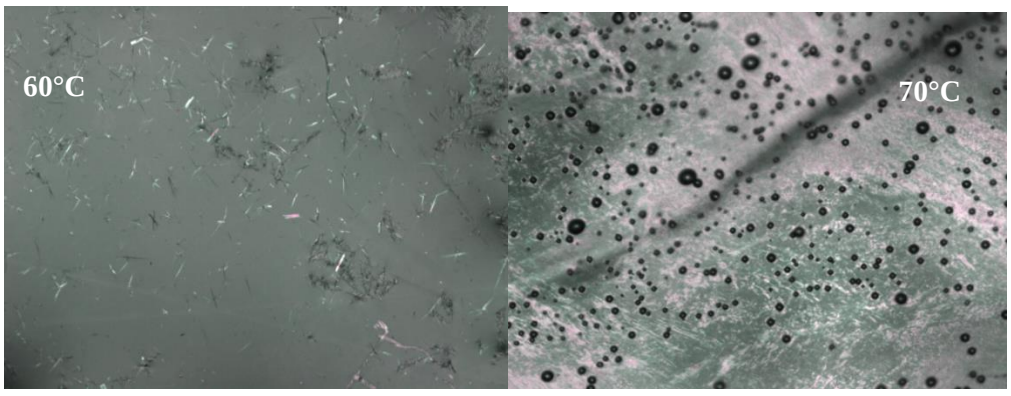

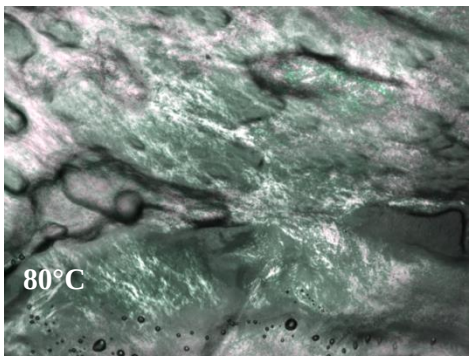

A.2.6 60 wt% surfactant

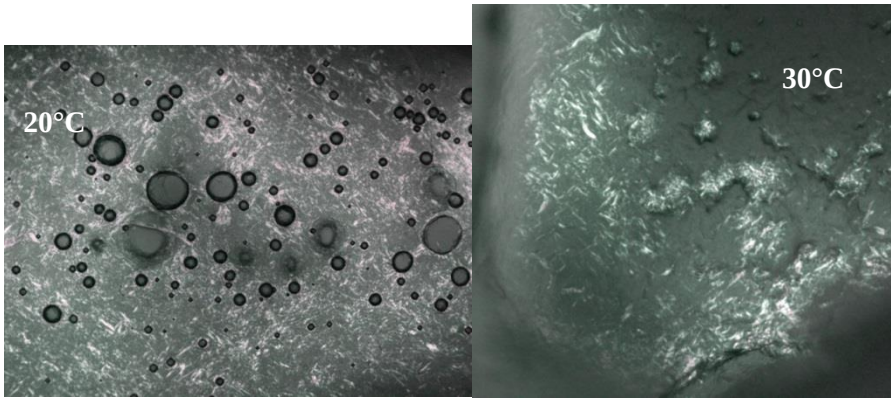

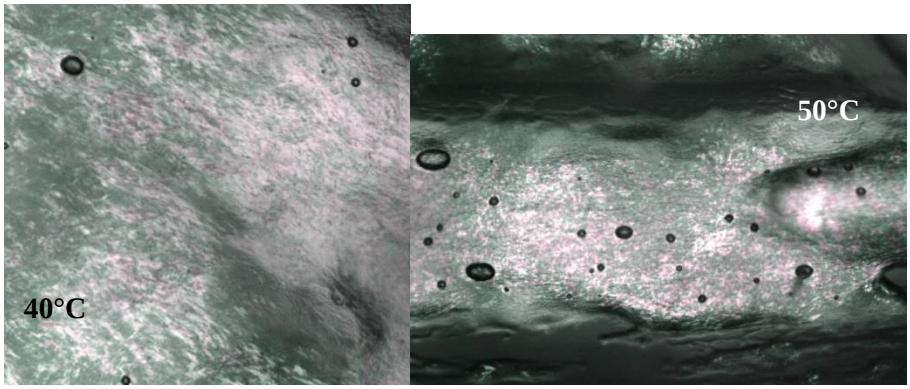

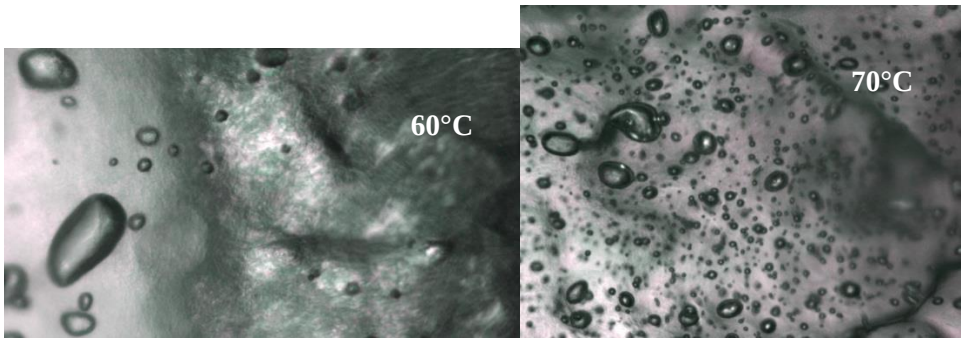

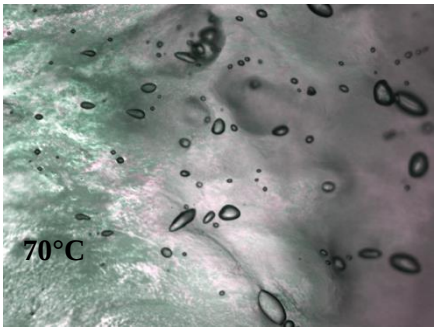

A.2.7 70 wt% surfactant

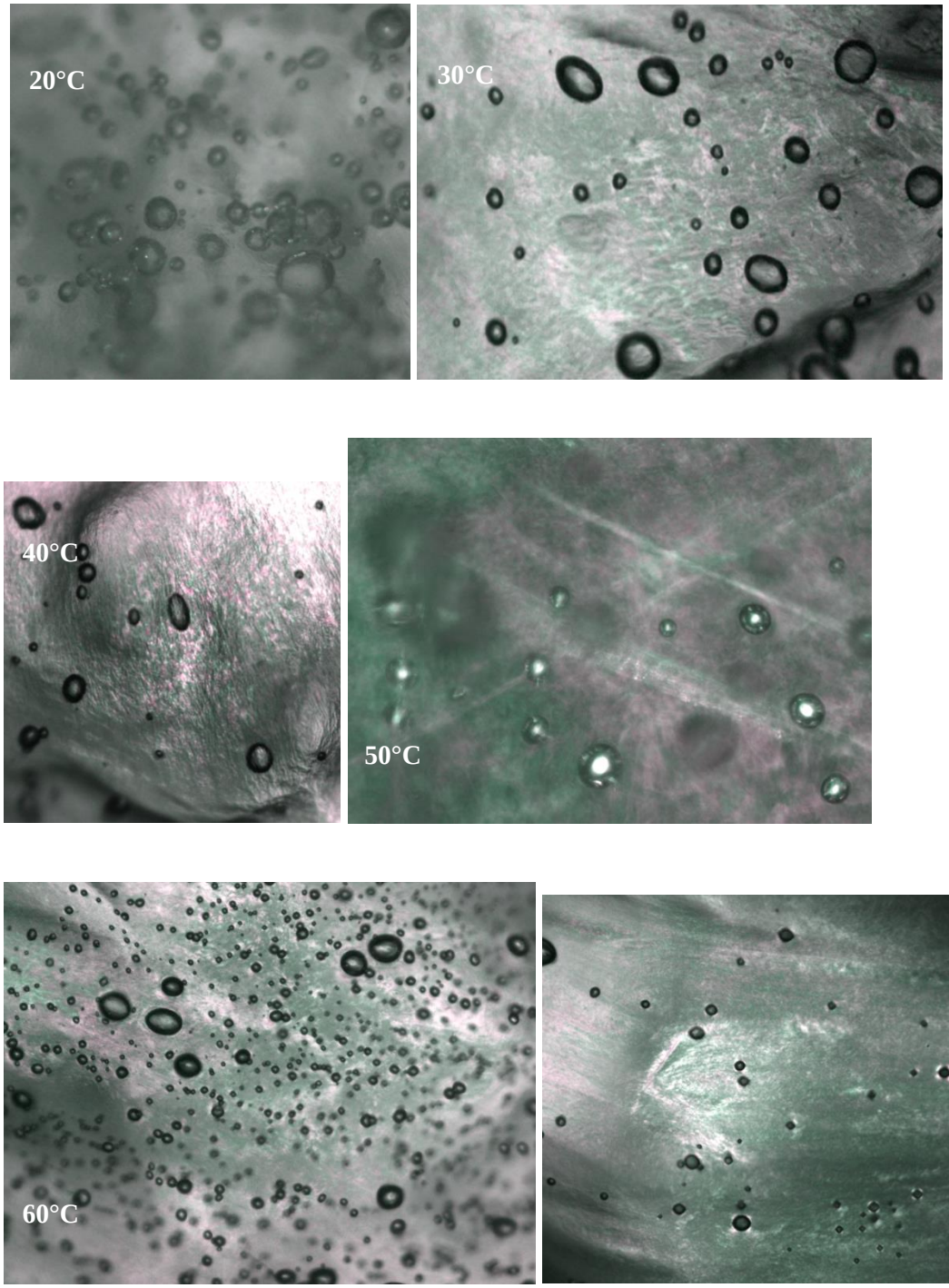

A.2.8 80 wt% surfactant

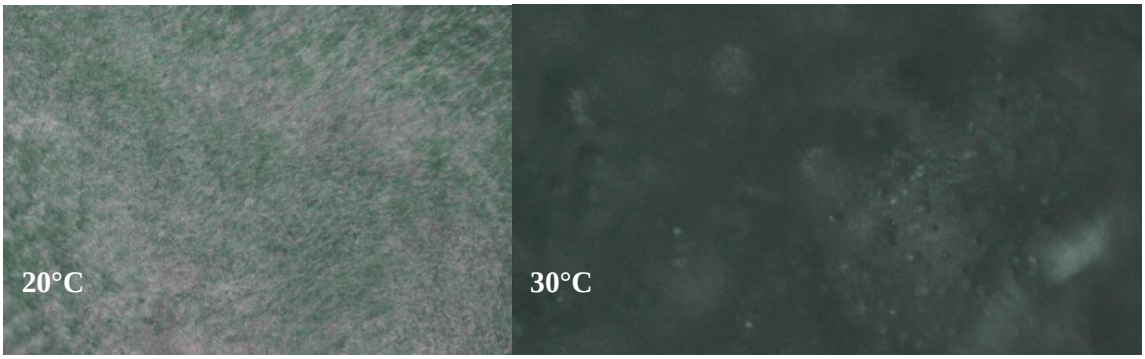

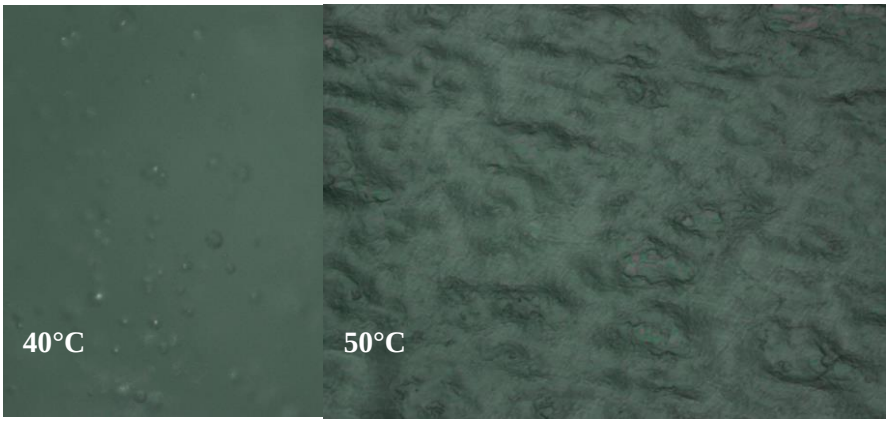

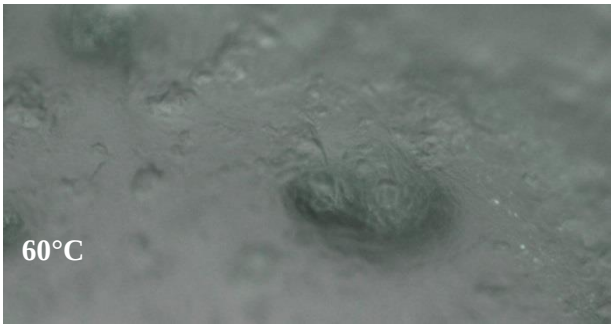

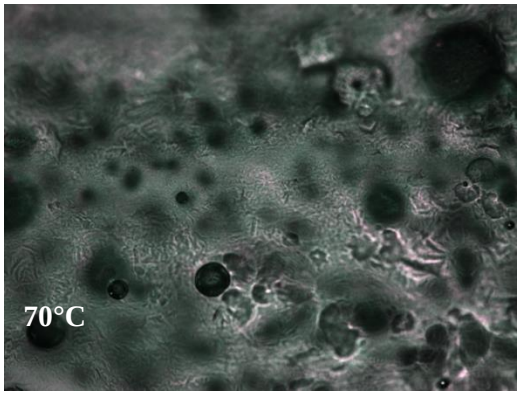

A.2.9 90 wt% surfactant

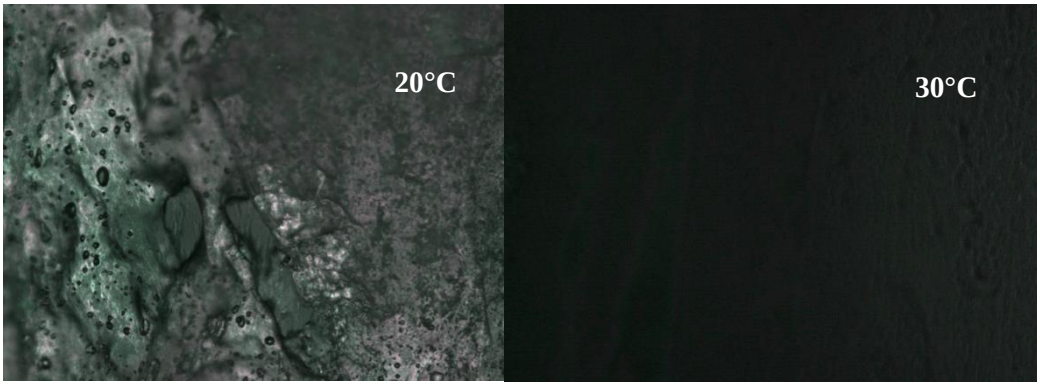

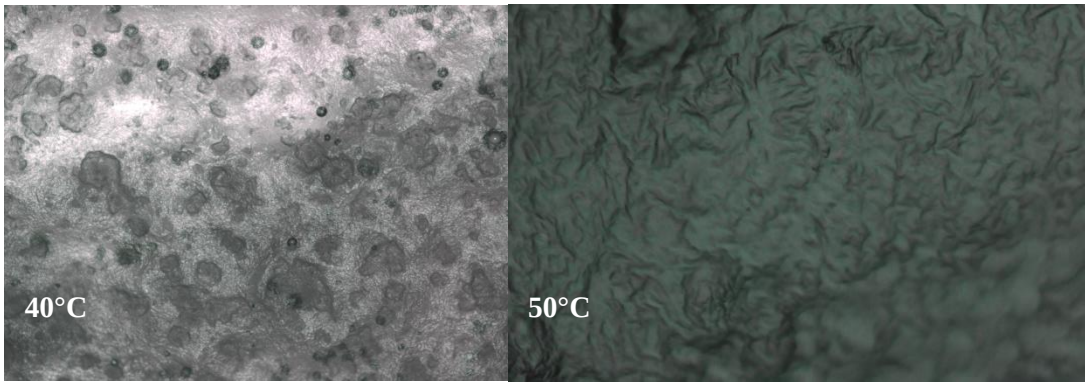

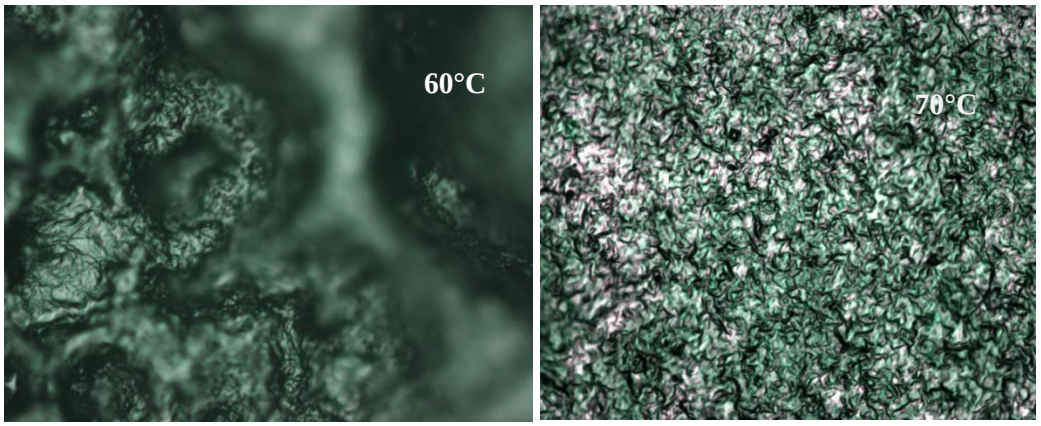

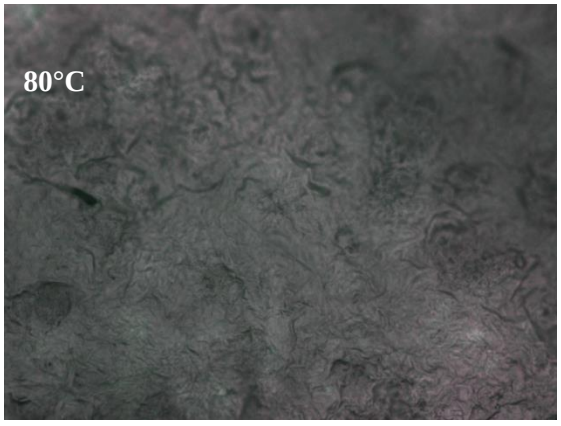

A.3 Brij O20

A.3.1 10 wt% surfactant

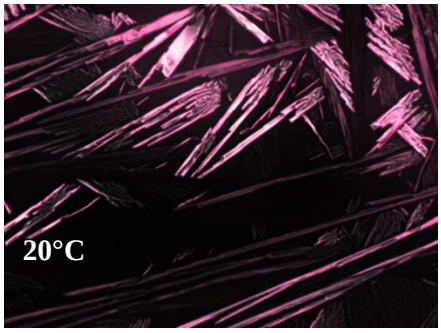

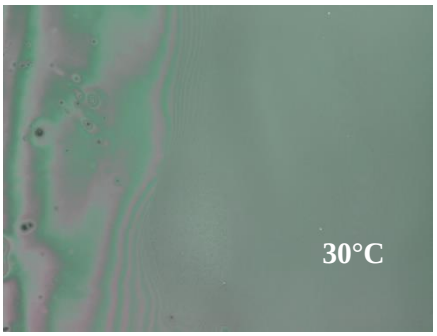

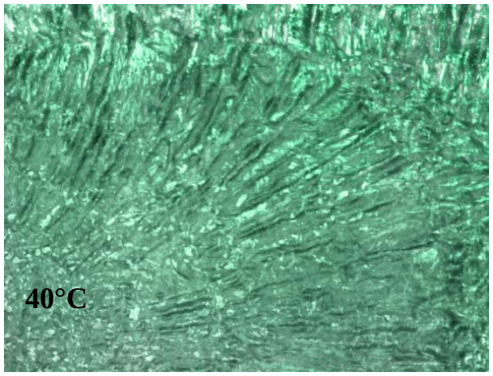

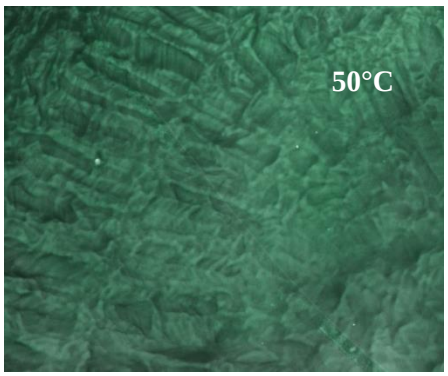

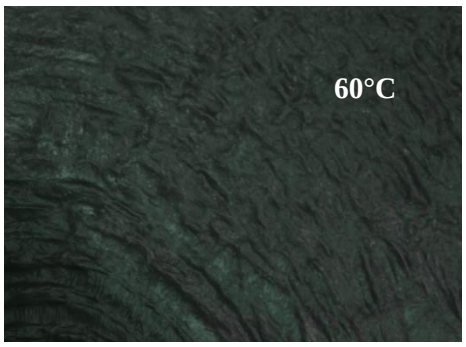

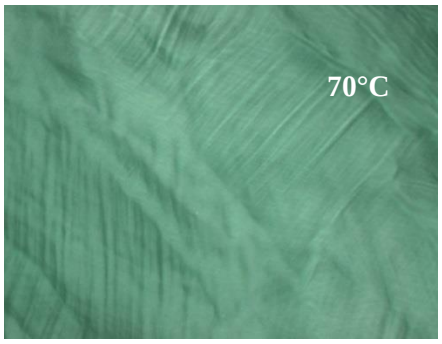

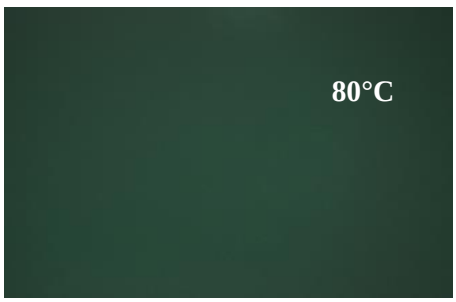

A.3.2 20 wt% surfactant

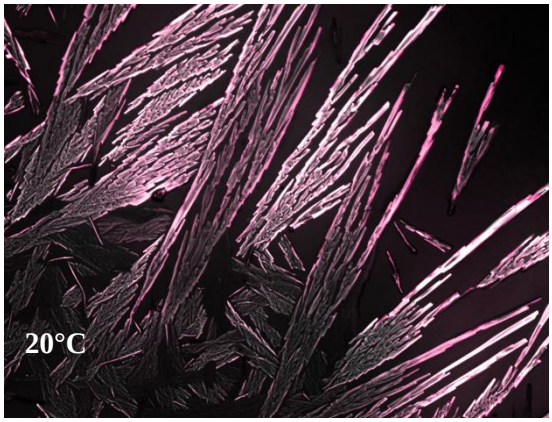

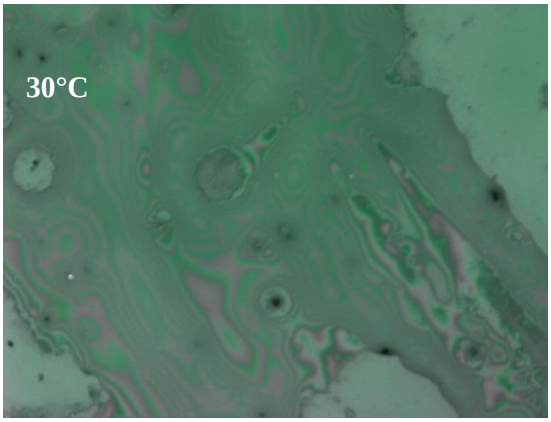

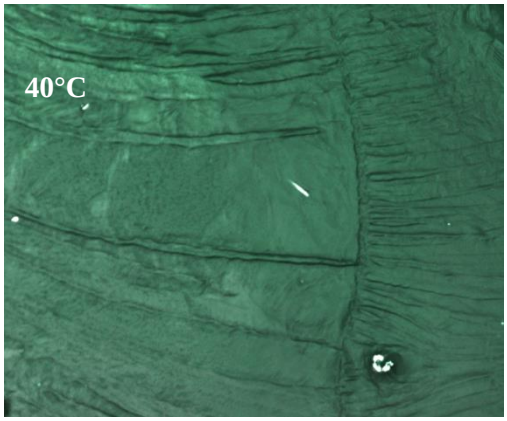

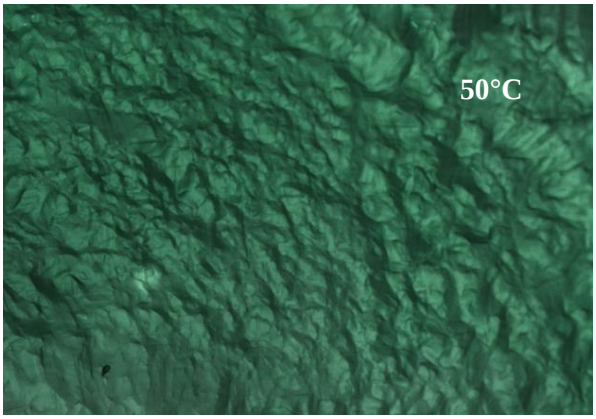

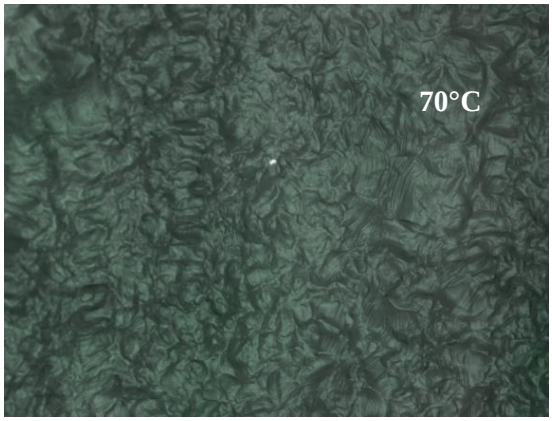

A.3.3 30 wt% surfactant

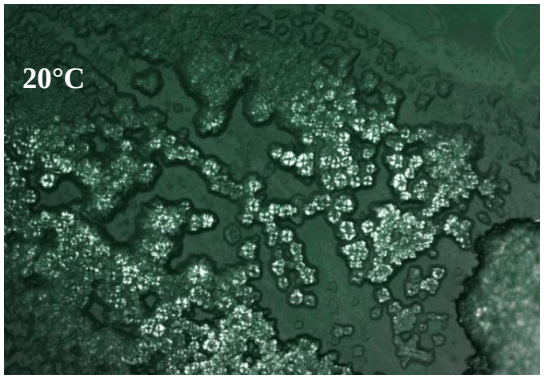

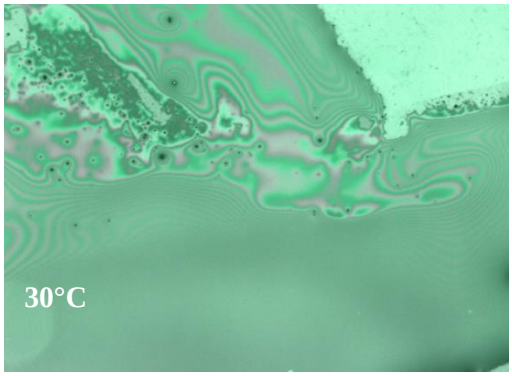

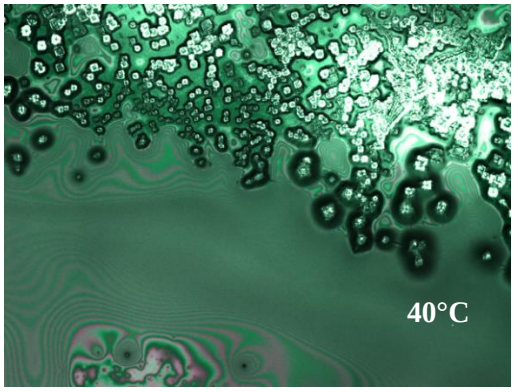

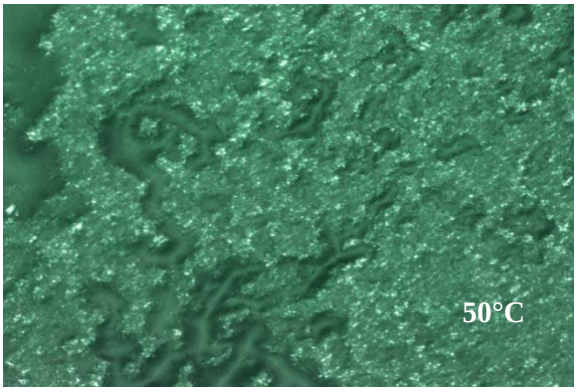

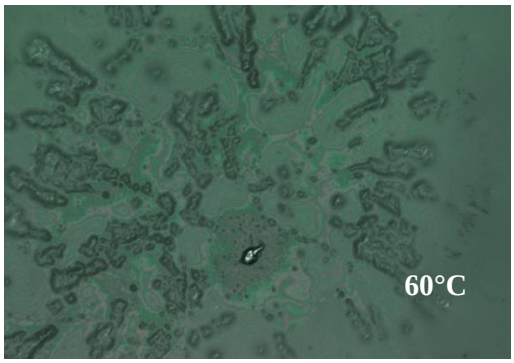

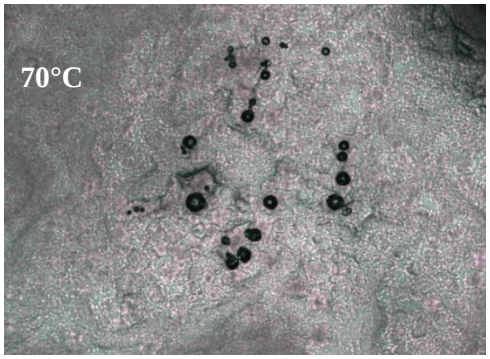

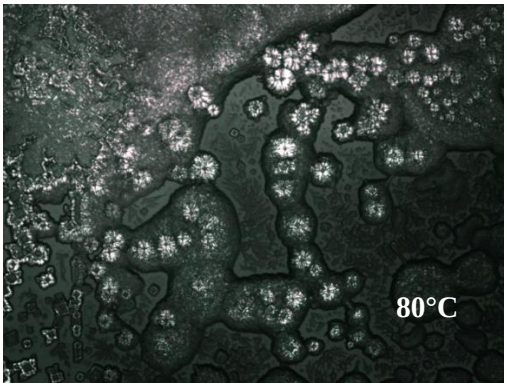

A.3.4 40 wt% surfactant

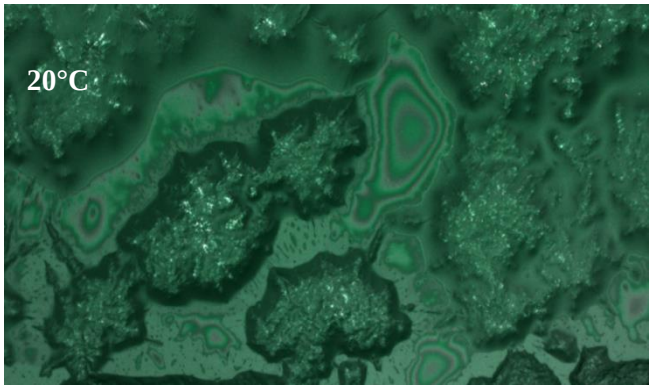

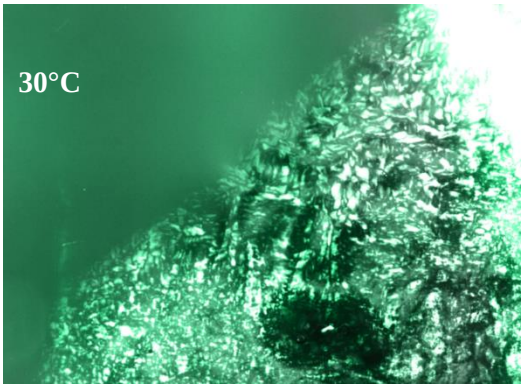

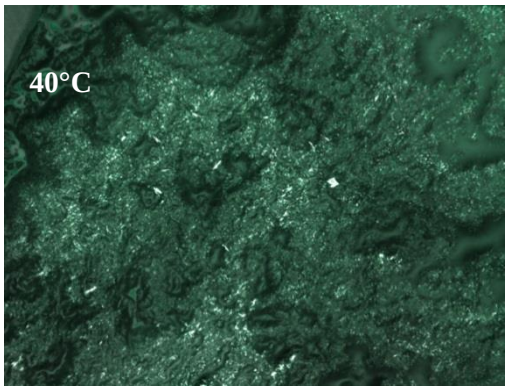

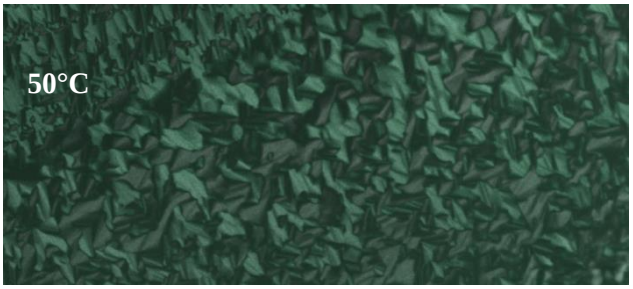

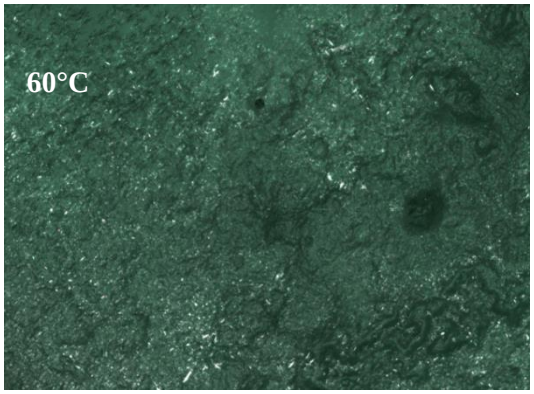

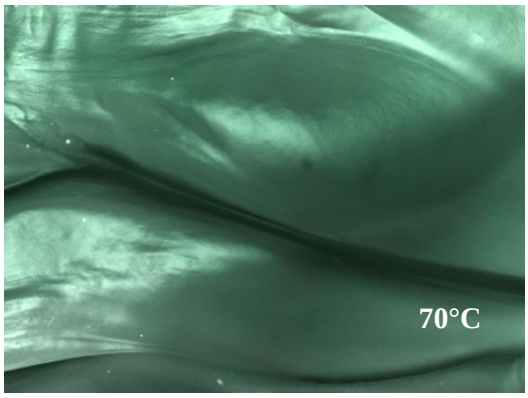

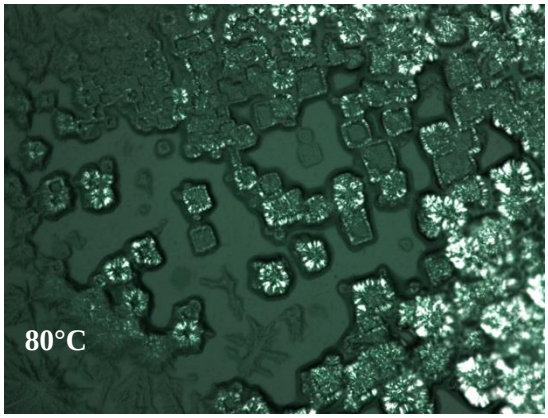

A.3.5 50 wt% surfactant

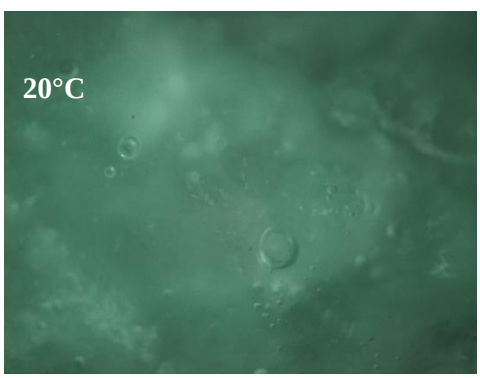

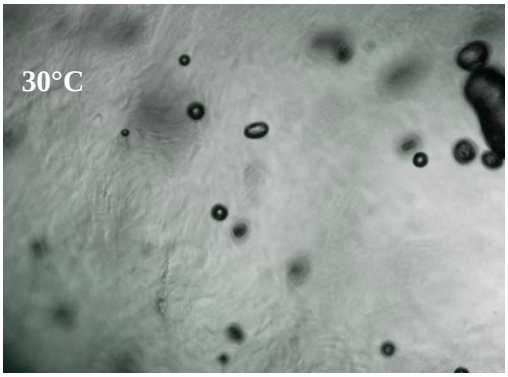

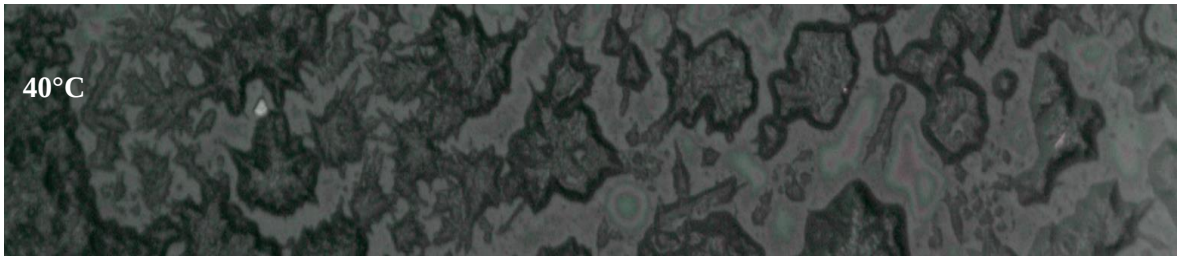

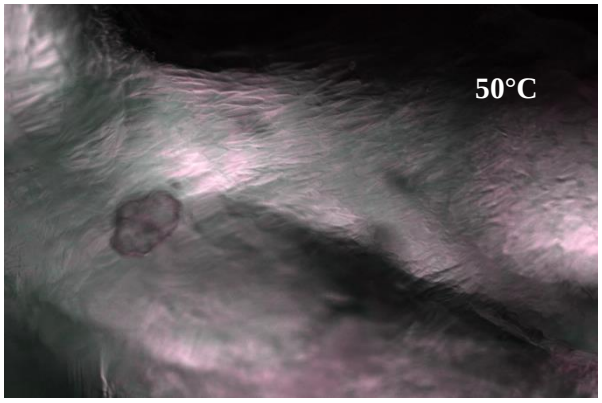

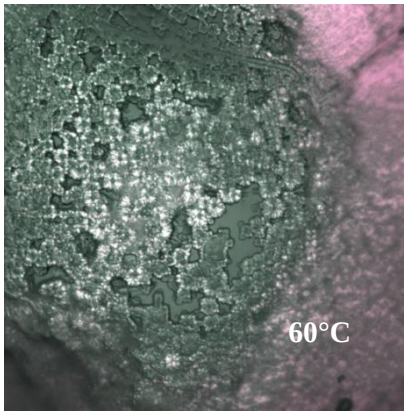

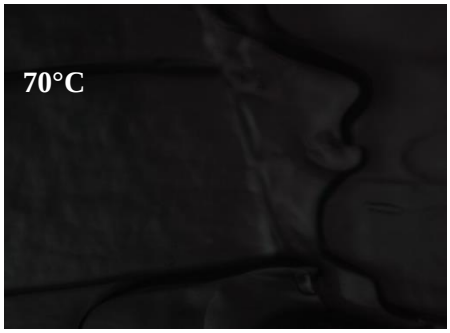

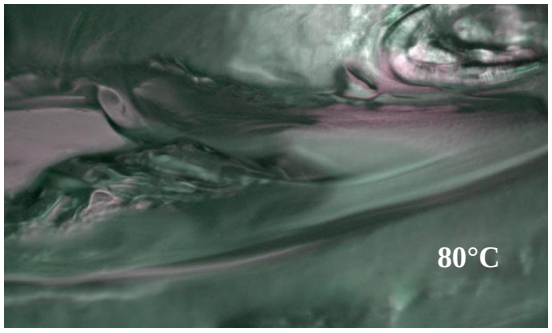

A.3.6 60 wt% surfactant

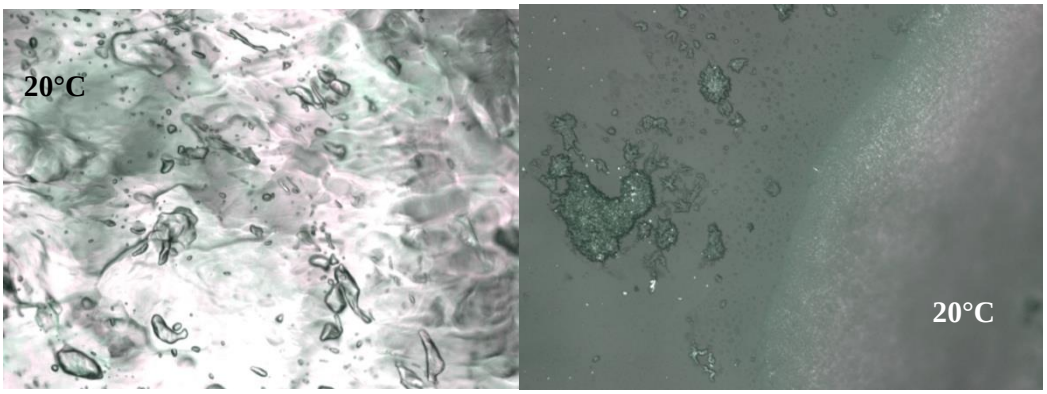

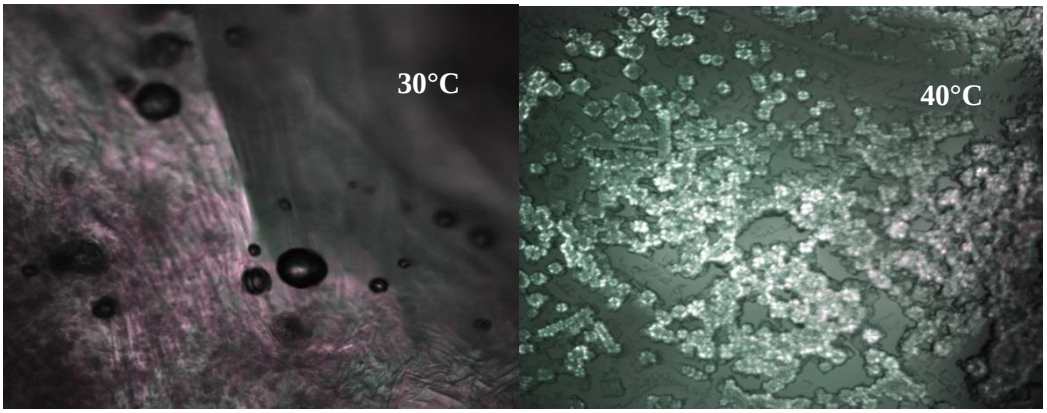

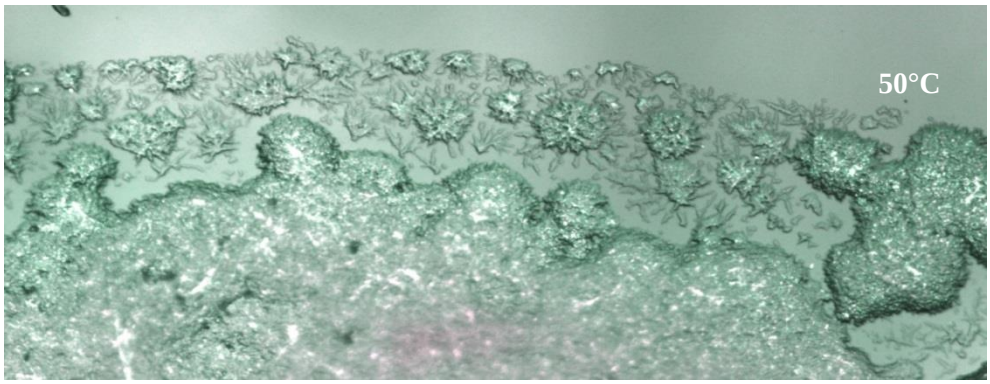

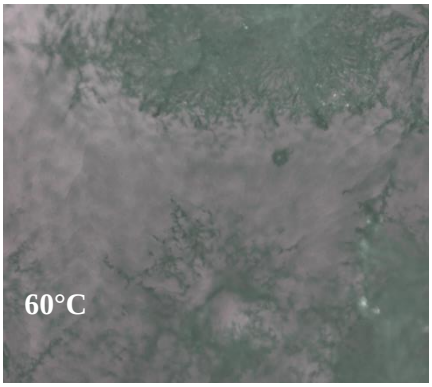

A.3.7 70 wt% surfactant

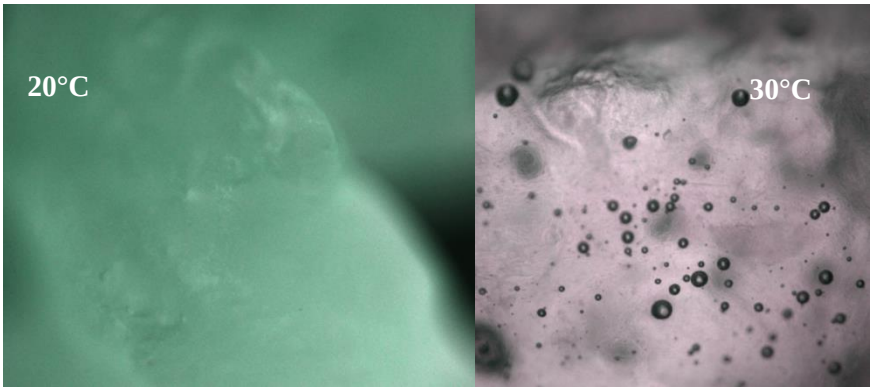

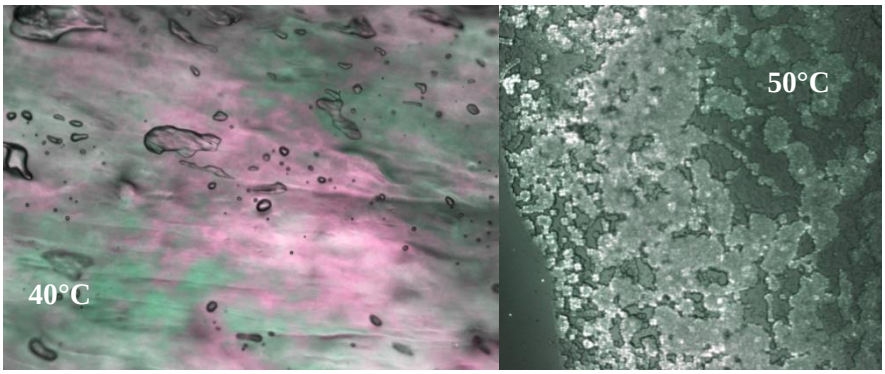

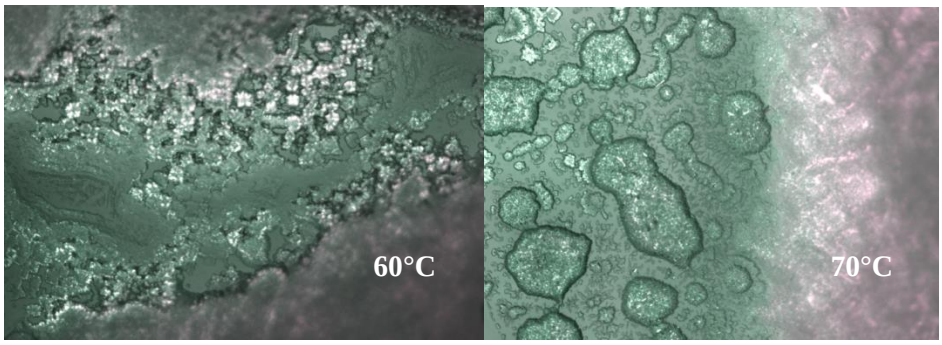

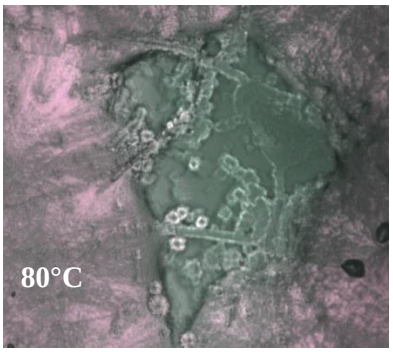

A.3.8 80 wt% surfactant

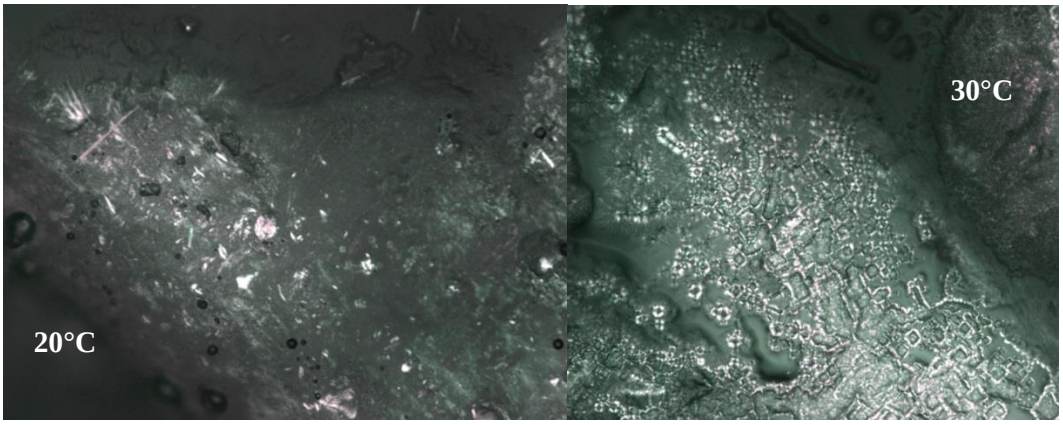

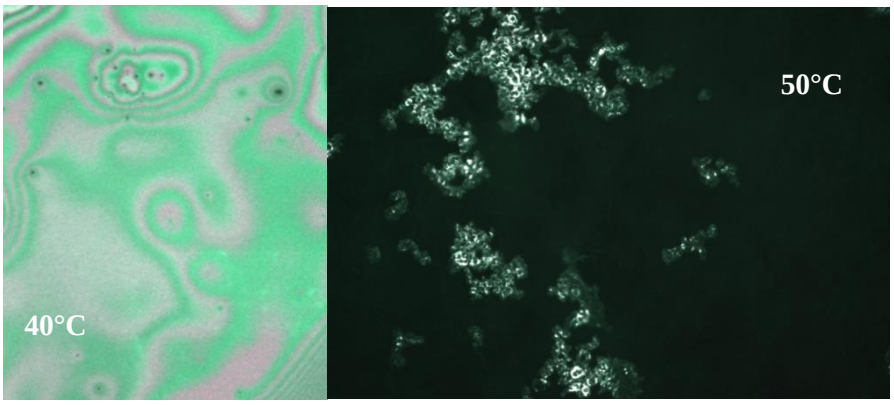

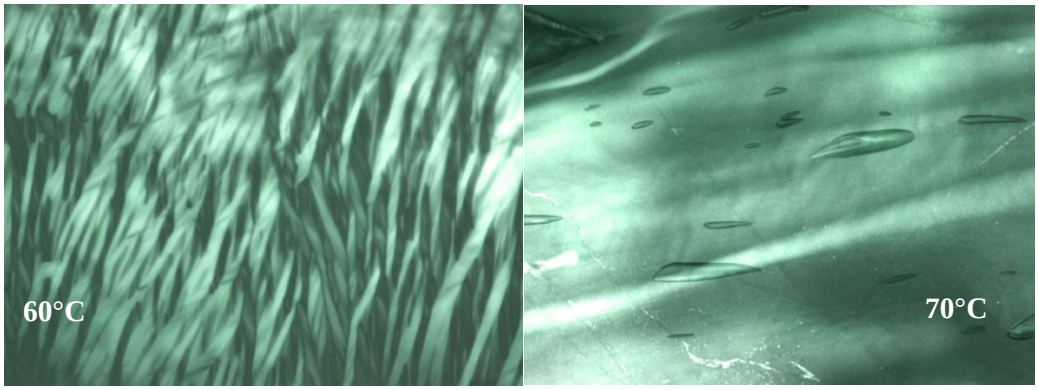

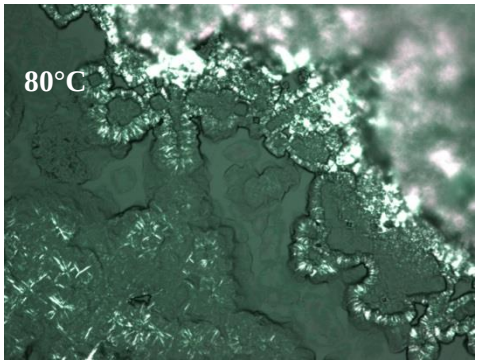

A.3.9 90 wt% surfactant

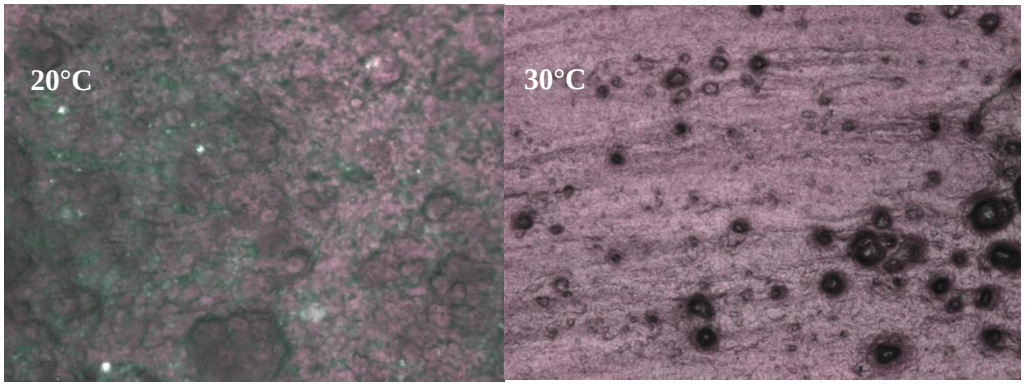

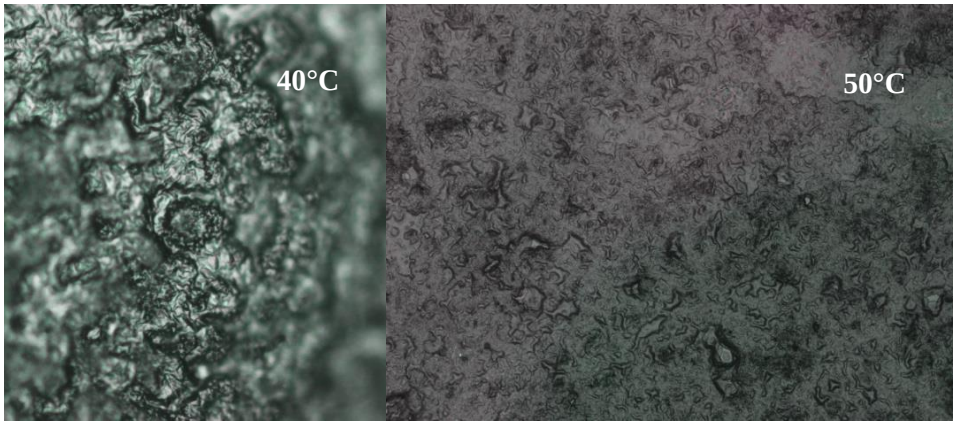

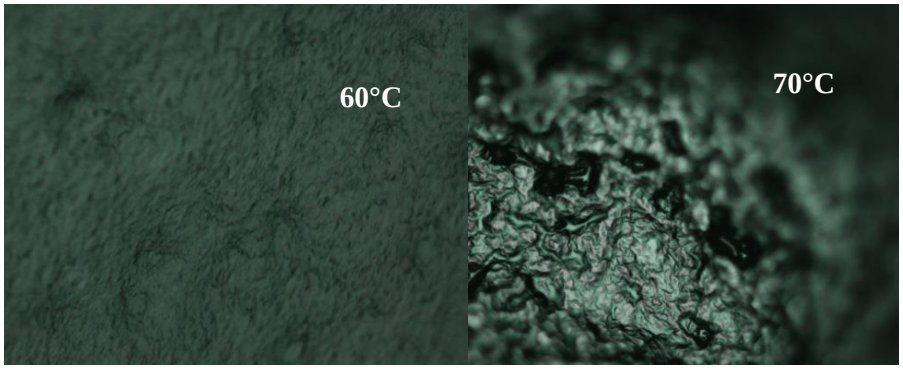

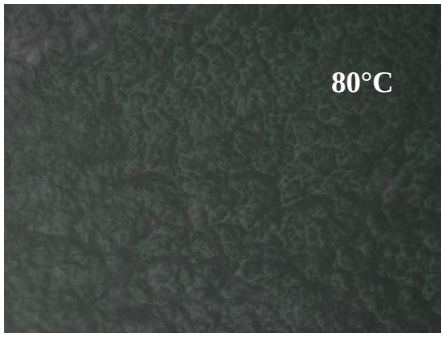

A.4 Brij S100

A.4.1 10 wt% surfactant

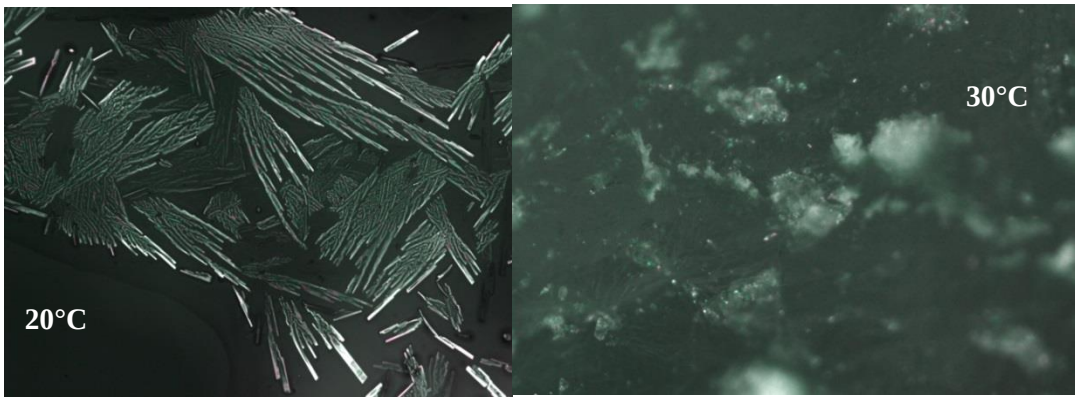

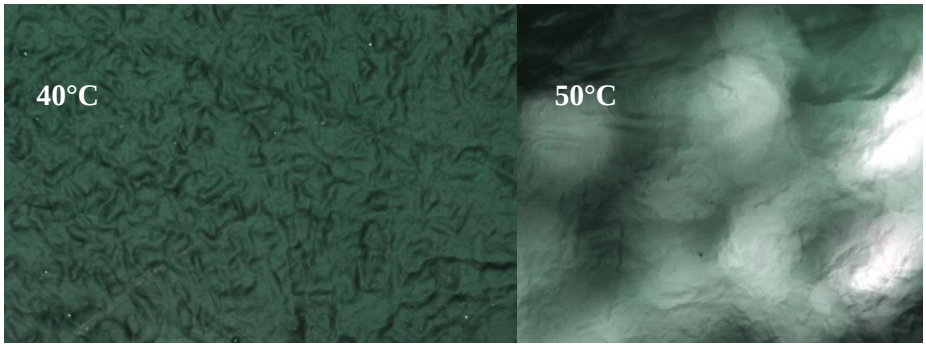

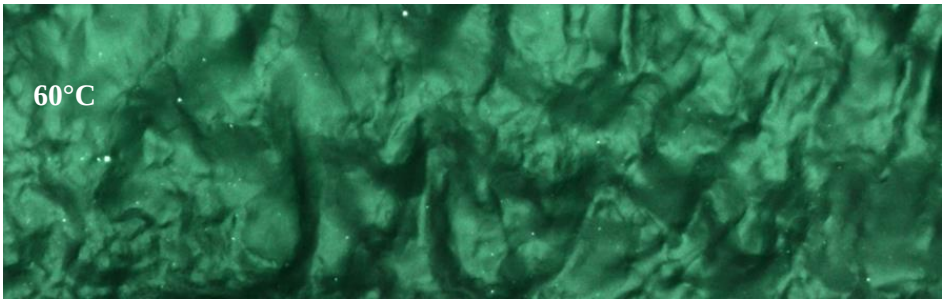

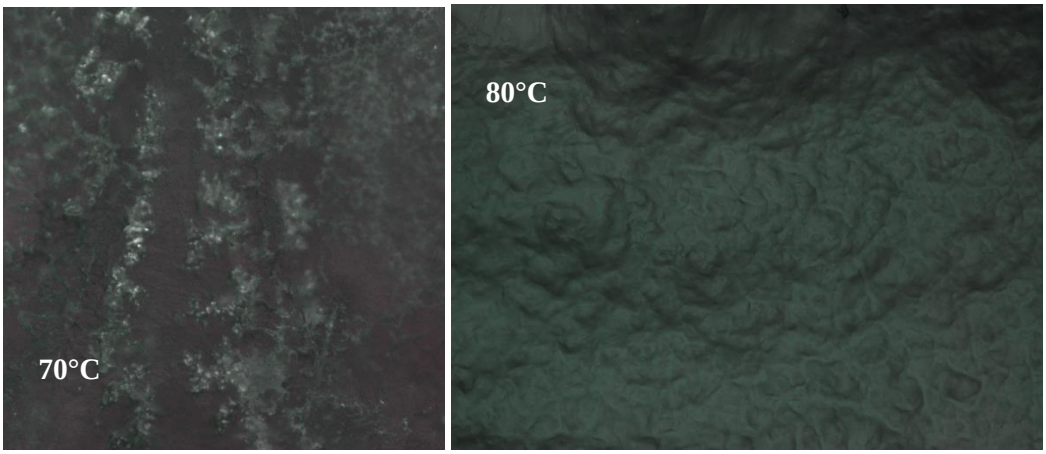

A.4.2 20 wt% surfactant

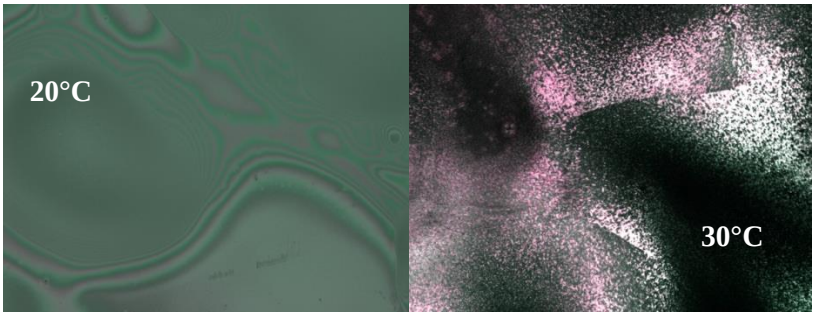

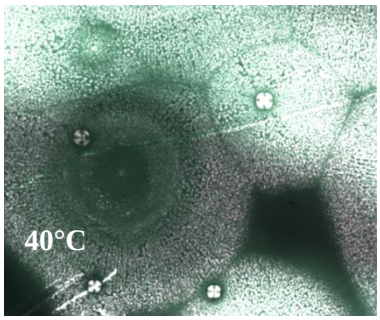

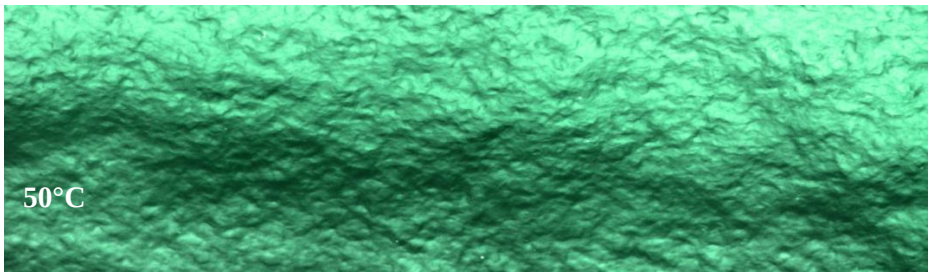

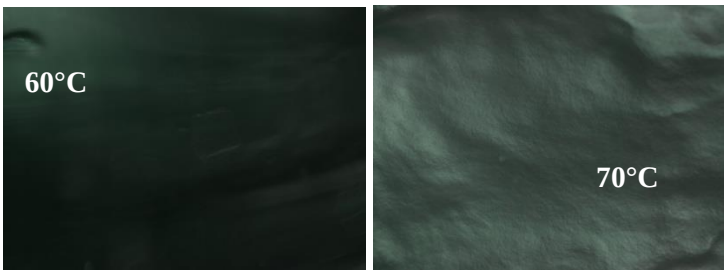

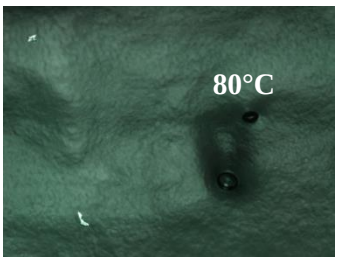

A.4.3 30 wt% surfactant

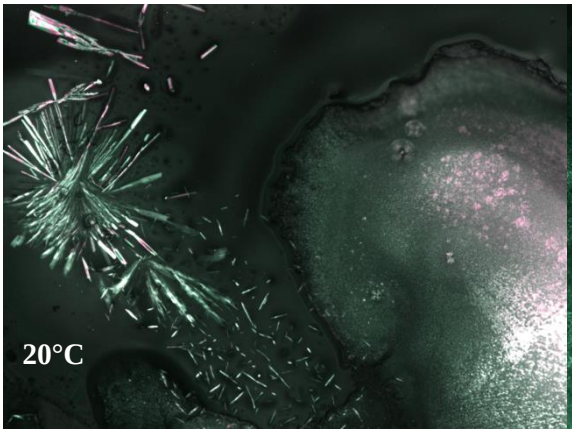

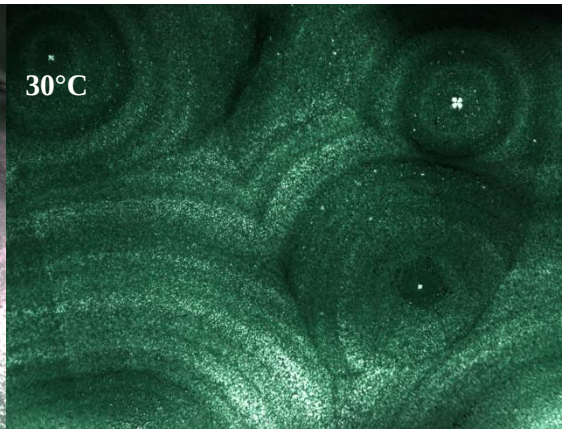

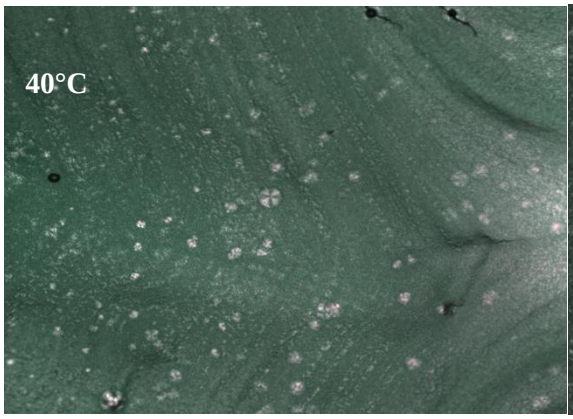

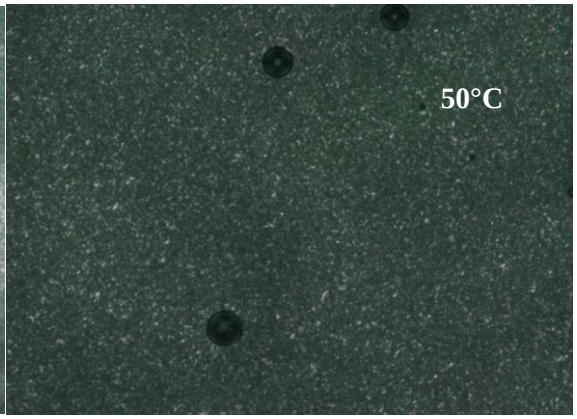

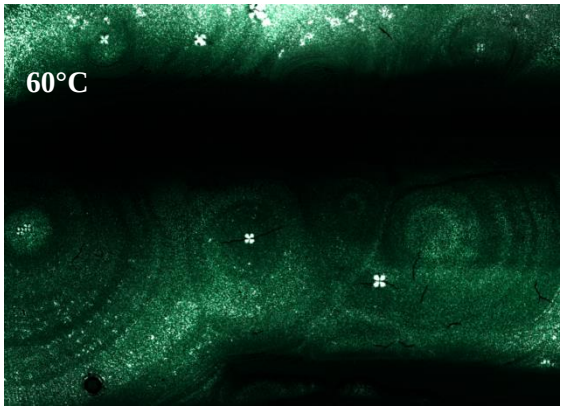

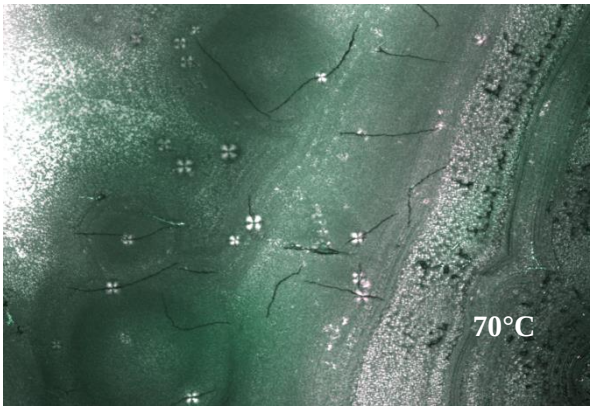

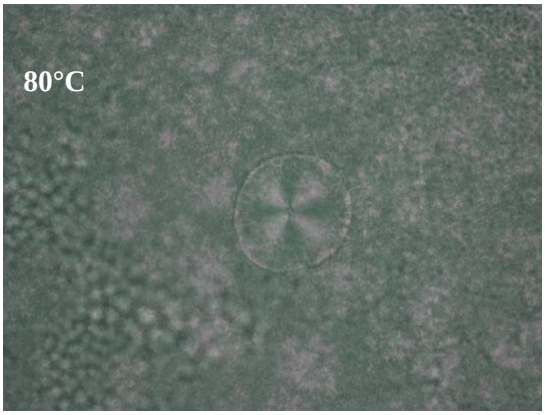

A.4.4 40 wt% surfactant

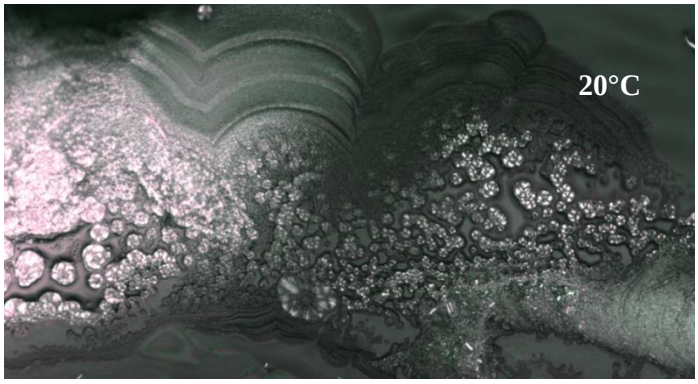

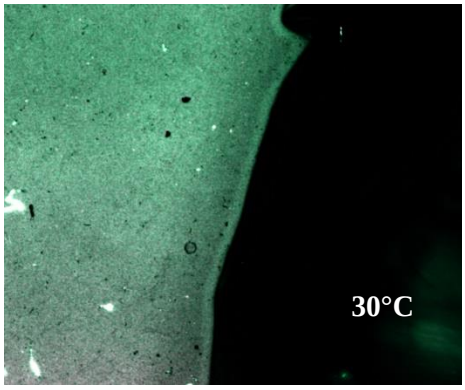

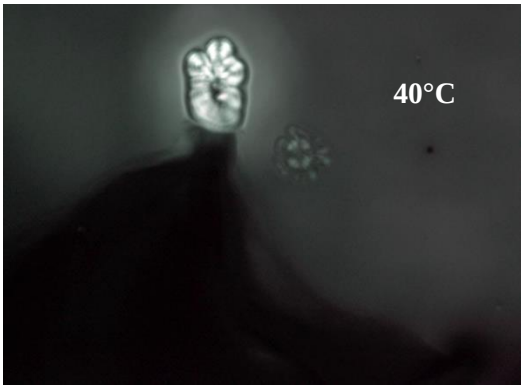

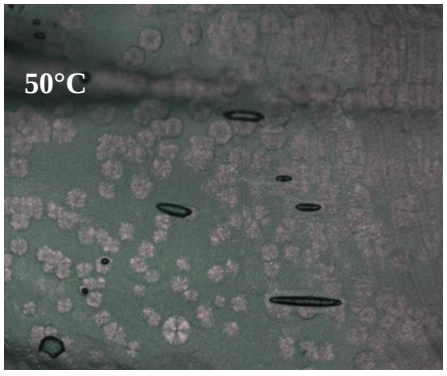

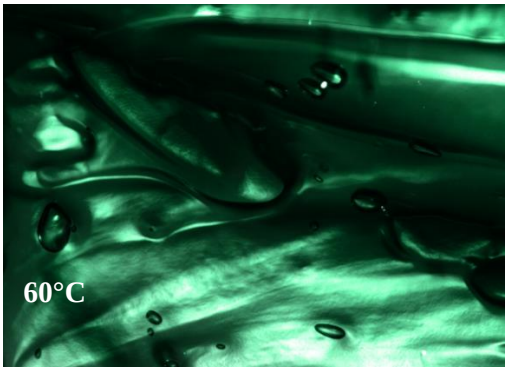

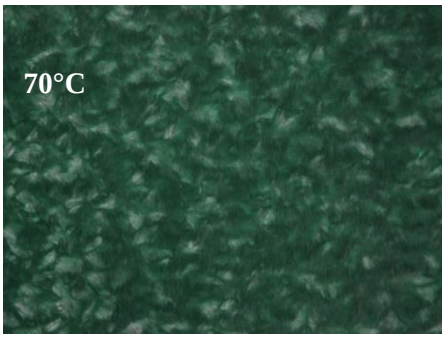

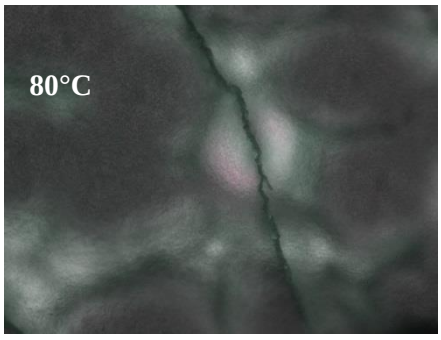

A.4.5 50 wt% surfactant

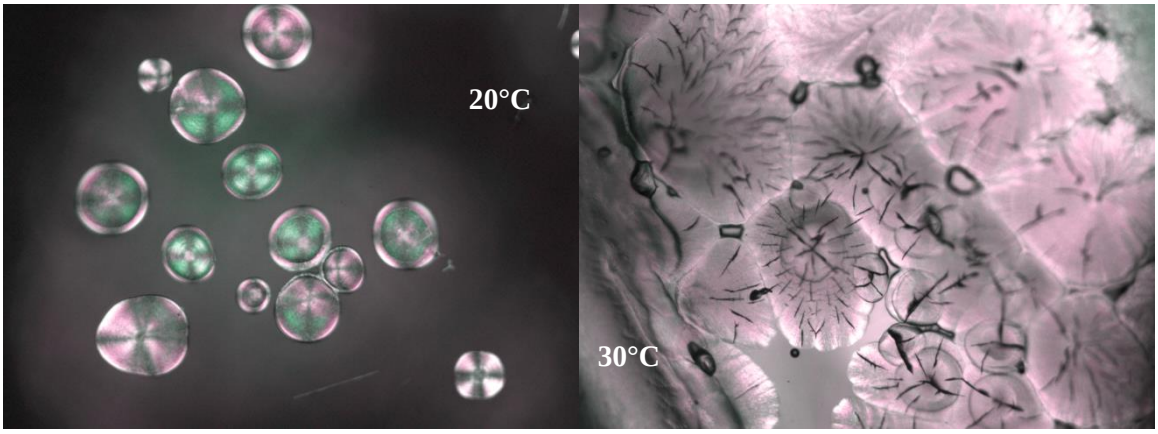

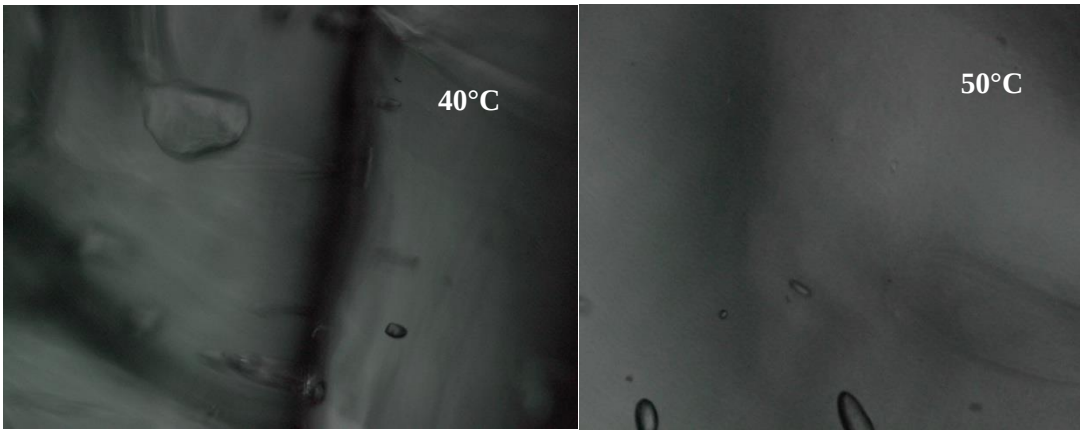

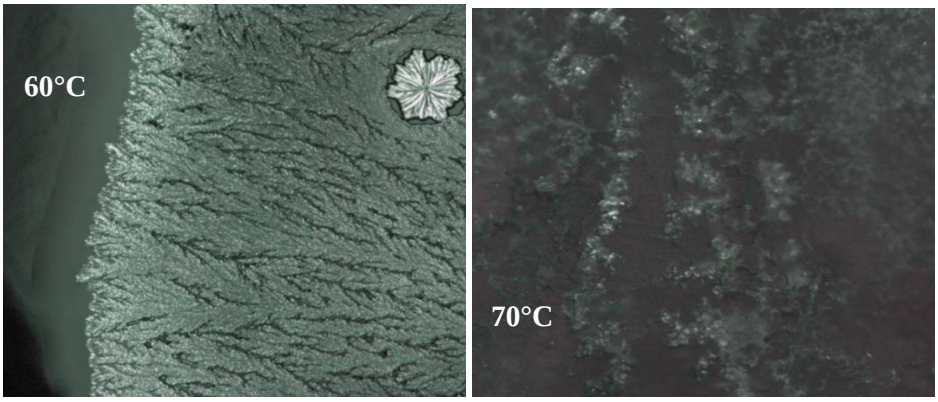

A.4.6 60 wt% surfactant

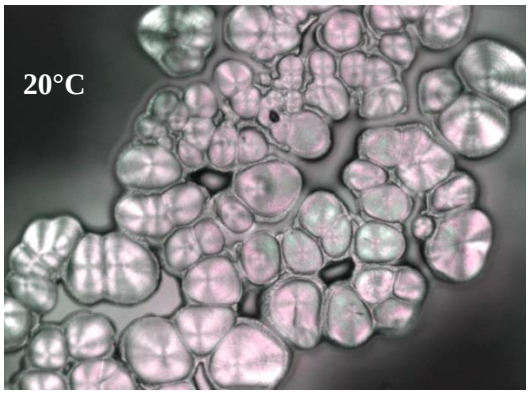

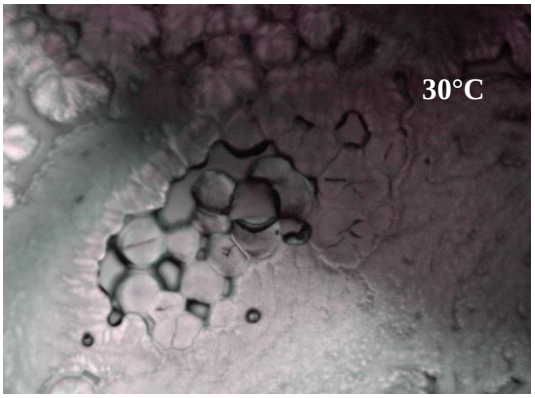

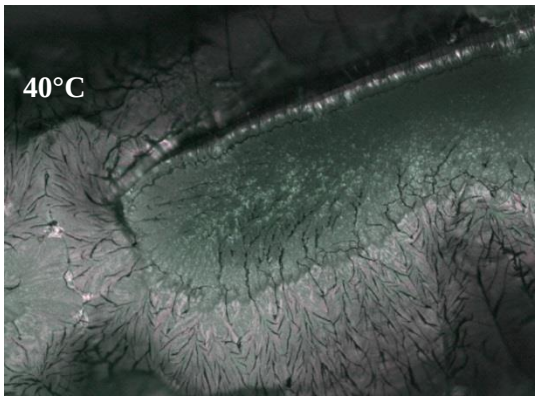

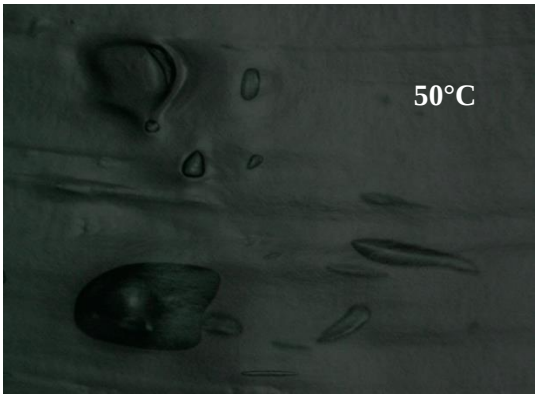

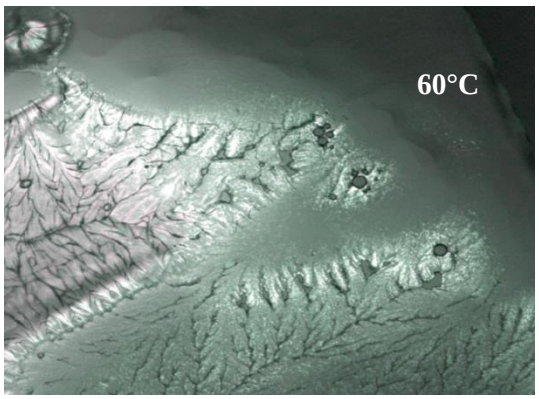

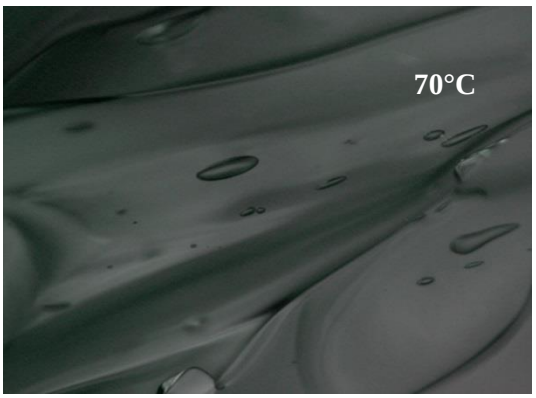

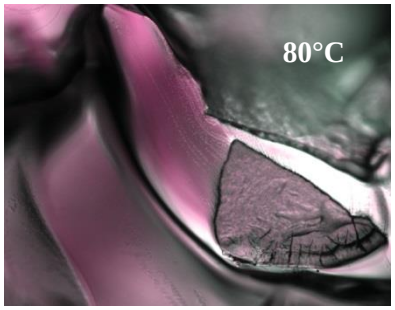

A.4.7 70 wt% surfactant

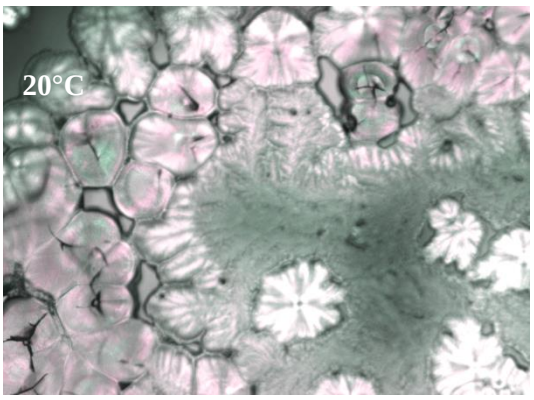

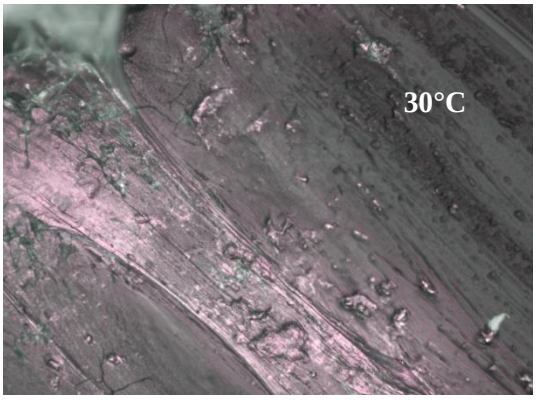

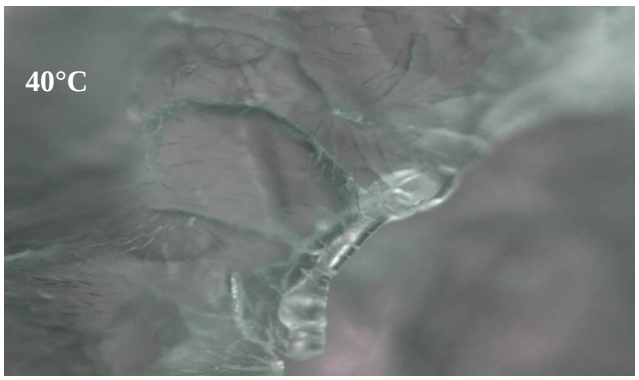

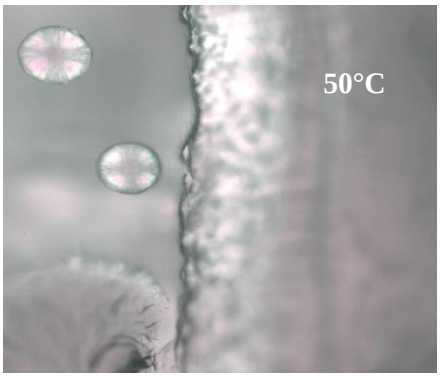

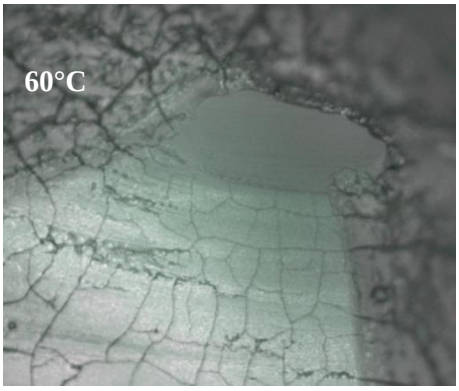

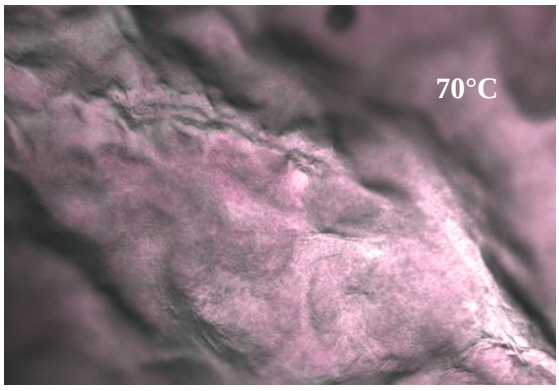

A.4.8 80 wt% surfactant

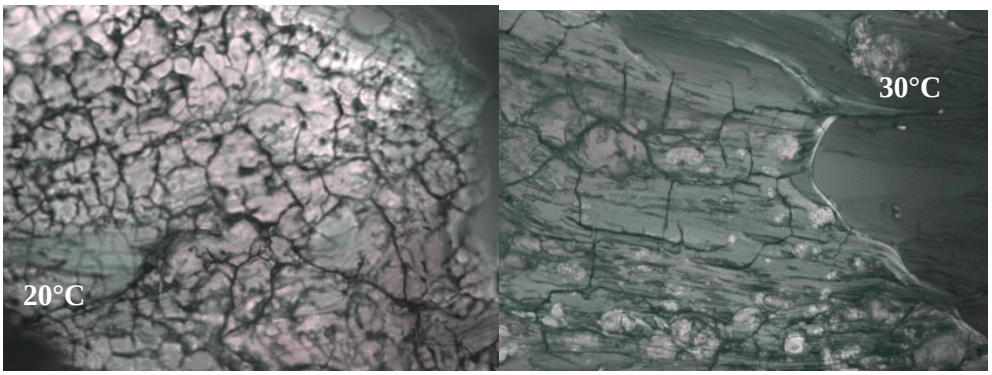

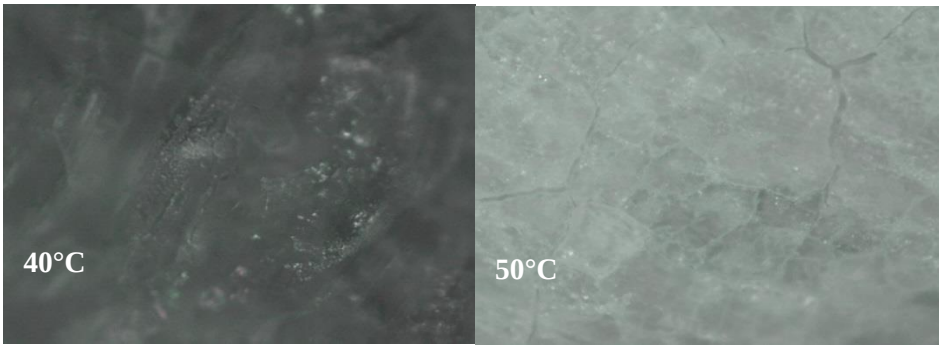

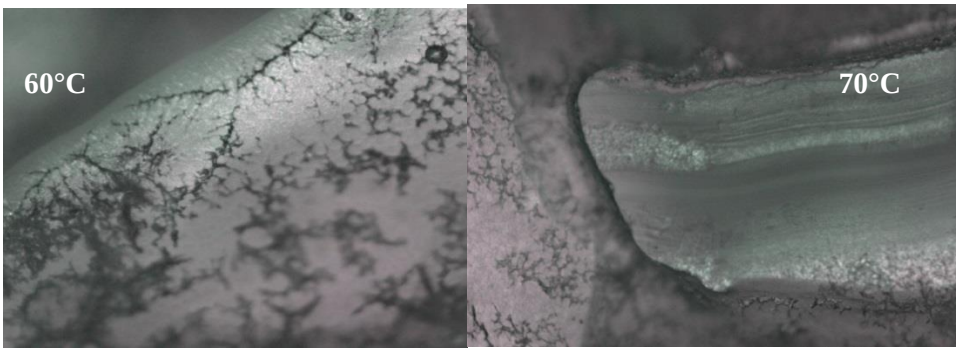

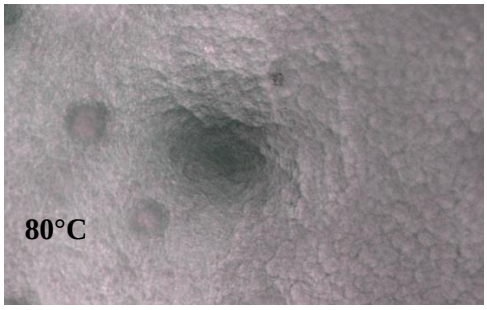

A.4.9 90 wt% surfactant

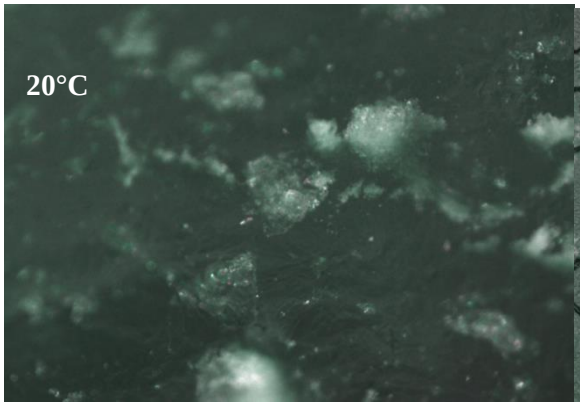

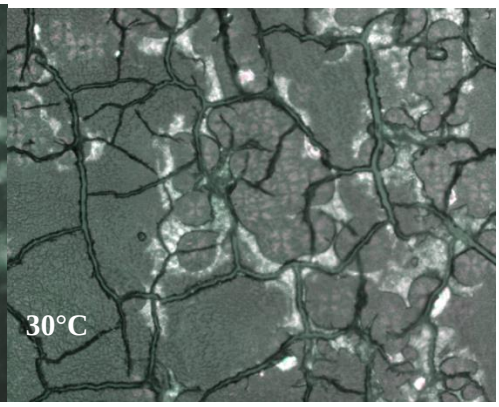

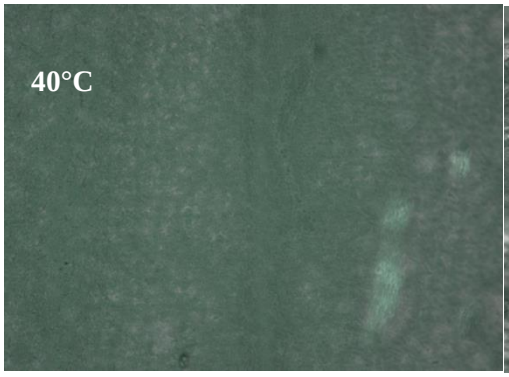

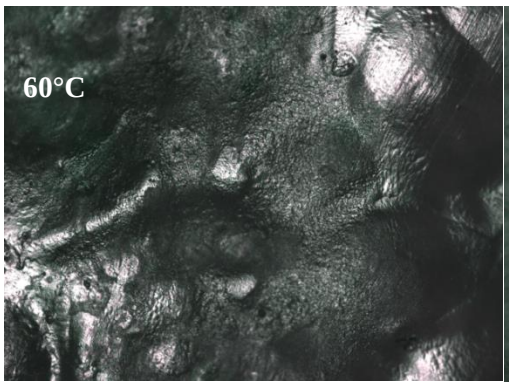

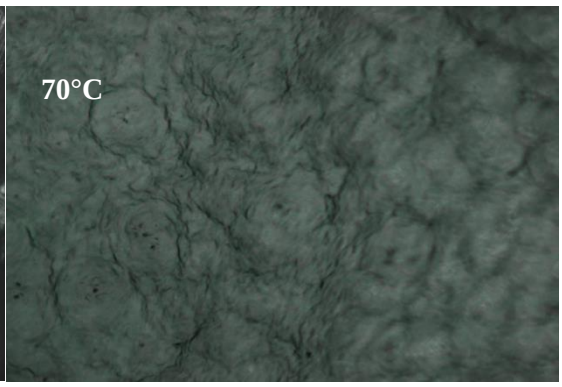

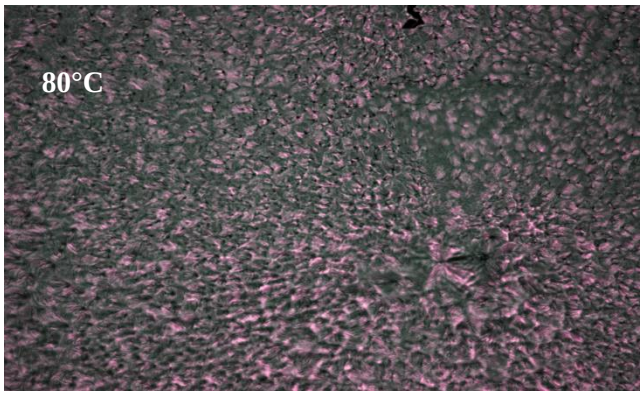

Appendix A: Phase diagram microscopy images